University of Oxford



Radcliffe Department of Medicine

Nuffield Department of Clinical Laboratory Sciences

Discovery of Molecular Signatures Underlying Angiogenic Versus Non Angiogenic Tumours

Alia Komsany
Linacre College

A thesis submitted for the degree of
Doctor of Philosophy

Michaelmas Term 2018

Table of contents ..... *i*

Table of figures ..... *vi*

Abstract ..... *vii*

Declaration ..... *x*

Acknowledgments ..... *xi*

Table of contents

Chapter 1 Introduction *1*

1.1Hallmarks of Cancer *1*

Sustaining proliferative growth and signalling *2*

DNA repair *7*

Apoptosis *9*

Autophagy *10*

Senescence *12*

Invasion and metastasis *14*

Metabolic rewiring *20*

Nutrient uptake *20*

Immune modulation *27*

1.2 Angiogenesis a hallmark of Cancer? *30*

Vascularisation *30*

Folkman's theory of angiogenesis *31*

The Angiogenic switch *31*

VEGF and angiogenesis *32*

Anti - angiogenic treatment *33*

Small compound-based anti – angiogenic drugs *35*

Non angiogenic growth in tumours and the case for co-option *36*

Co -option growth patterns in lung metastases *36*

Drug resistance in the context of anti-angiogenic therapy *39*

Co - option and its role in drug resistance *40*

Other alternate modes of angiogenesis *41*

Clinical pathology of angiogenesis *43*

The molecular characterization of non-angiogenic growth *44*

Gene expression profiling 46
The role of adhesion 47
Insights from primary brain tumours 49
Clinical trials for anti-angiogenic drugs 50
1.3 Transcriptional approaches to biomarker discovery 54
1.4 Metabolomics analysis for biomarker discovery 54
1.5 The role of proteomics in biomarker discovery 55
Label free quantification 55
Proteomic analysis of Laser Capture Micro dissescted tissue (FFPE) 56
Application of proteomics in understanding vascular states in cancer 56
1.6 Project objectives 56
Chapter 2 Experimental procedures 58
2.1 General reagents 58
2.2 General cell culture techniques 58
Cryo – conservation and thawing of cells 59
Preparation of cell lysates 59
2.3 mRNA preparation 60
2.4 Western blot and immunodetection of proteins 60
Antibodies 61
2.5 Metabolomics 62
Chemicals and metabolic standards 62
Metabolite extraction from tissue 63
Chemical derivatization 64
GCxGC -MS analysis 64
Data processing and analysis 65
2.6 Label free proteomics 66
In Solution digestion 66
Methanol/Chloroform Extraction. 66
SEP – PAK C18 purification 67
Filter-aided sample preparation (FASP) for tryptic digestion of tissues 67
2.7 LCM collection and Tissue lysis 69
Proteomic sample processing 69

LC-MS/MS. *70*

Data Analysis. *70*

2.8 Cellular assays *71*

Seahorse experiments *71*

MitoXpress intracellular probe to detect oxygen consumption rates *72*

Oxygen scale calibration..... *72*

2.9 Migration and intercalation experiments..... *74*

Isolation and culture of LMVEC's..... *74*

Tumour cell intercalation in static conditions..... *74*

Transwell migration andn invasion assay..... *75*

2.10 Immunostaining..... *75*

Preparation of LCM slides..... *76*

H & E Staining..... *77*

Chapter 3 Characterisation of cancer cells isolated from co option vs angiogenesis mouse models in vitro..... *78*

3.1 Introduction..... *78*

3.1.1 "In vitro work"versus animal model *78*

3.1.2 A model of vessel co option. *79*

3.2 Results..... *81*

3.2.1 Assessing the identity of the mother and daughter cell lines..... *81*

3.2.2 Investigating "In Vitro" growth patterns..... *82*

3.2.3 Characterisation oof the 786 and 6450 cell lines "Early" and "Late". *84*

3.2.4 Influence of acute starvation and low pH on cell growth *86*

3.2.5 Pilot proteomics study shows differential regulation of proteins in 786 vs 6450 cell lines..... *88*

3.2.6 Correlation analysis shows independent clustering of protein groups in 786 versus 6450..... *91*

3.2.7 Pathway analysis shows enrichment of well – known cancer pathways..... *94*

3.2.8 Western Blot validation shows differential expression of targets highlighted in proteomic pull down...... *95*

3.2.9 Metabolic profiling of 786 and 6450 cell lines..... *97*

3.2.10 Base line metabolic profiling shows differences in OCR and ECAR between cell lines..... *99*

3.2.11The effect of glucose starvation on metabolic status 786 versus 6450 (early passage)102

3.2.12 Fixing ambient oxygen to 5% influences the metabolic profiles of the cells.....104

3.2.13 The influence of glucose starvation and low pH on intracellular oxygen capacity...107

3.2.14 The influence of glutamine starvation on intracellular oxygen capacity..... 109

3.2.15 The effect of the electron transport chain inhibitors on intracellular oxygen levels..... 110

3.2.16 mRNA profiuling shows differential regulation of proteins in the 6450 cell line (early vs late passages). 110

3.2.17Downstream global analysis of the 6450 cell line highlights top variable pathways.....112

3.2.18 Characterisation of migration and invasion profiles between cell lines 135

3.2.19 Preliminary assessment of the intercalation capability of the cell lines..... 118

3.2.20 Discussion and limitations…… .121

Chapter 4 in vivo characterisation *131*

4.1 Introduction……..*131*

4.1.1 The in vivo model. *131*

4.1.2 Characterising vessel co- option in vivo *132*

4.1.3 Histopathology of vessel co - option. *133*

4.1.3 Results. *134*

4.1.5 Global tissue proteomic analysis (preliminary)..... *137*

4.1.6 Western blot validation highlights potential differentially expressed proteins..... *142*

4.1.7 COXIV and PKM2: energy metabolism *142*

4.1.8 L1CAM and Pan cadherin: adhesion receptor landscape..... *144*

4.1.9 SMAD4: TGF-β pathway..... *146*

4.1.10 TSP1 and ADAMTS2: angiogenesis and remodeling *148*

4.1.11 Ca2 and SLC9A1: pH regulation..... *150*

4.1.12 GSTP1:xenobiotic metabolism. *152*

4.1.13 Metabolomic analysis..... *153*

4.1.14 Pathway analysis of proteeomic pull down highlights role of metabolism..... *155*

4.1.15 Metabolomic analysis reveals differences in metabolites involved in cellular metabolic processes *157*

4.1.16 Laser capture microdissection...... *159*

4.1.17 Discussion and limitations 165

Chapter 5 Conclusions and future perspectives*.....172*

5.1 Future Directions*…… ..173*

Chapter 6 Appendix*……176*

Table of Figures

Figure 1: Hallmarks of Cancer..... 1
Figure 2: Alveolar and pushing growth patterns of human lung metastases 37
Figure 3: Sample Calibration Data..... 73
Figure 4: Mouse model of vessel co- option..... 79
Figure 5: In vivo mouse model vs tissue culture model..... 80
Figure 6: Representative images of cell morphology and confluency show differences in growth rates 84
Figure 7: Comparing growth curves in 786 vs 6450 cell lines (early vs late) reveals differences in growth rates 85
Figure 8: Growth rates under starvation conditions show no differences in growth between 786 early vs late passages 86
Figure 9: Growth rates under starvation conditions in 6450 cells reveal differences in growth between early vs late passages passages 87
Figure 10: Differential proteome analysis..... 91
Figure 11: Differential protein expression between cell lines 93
Figure 12: Pathway analysis highlights significant upregulated protein interactions 94
Figure 13: Validation of differential protein expression by western blot..... 95
Figure 14: Volcano plot showing upregulation of metabolic proteins in the 6450-cell line (early) vs 786 cell line..... 96
Figure 15: Metabolic profiling data output.....100
Figure 16: Metabolic profiling of early vs late passages show metabolic difference between cell lines 101
Figure 17: Metabolic profiling of the 786-cell line versus early 6450 passage under glucose starvation shows metabolic differences.....103
Figure 18: Metabolic profiles of 786 vs 6450 (early and late passages) in 5% oxygen environment show different metabolic signatures.....106
Figure 19: Metabolic profiles of 786 vs 6450 (early and late passages) in 5% oxygen environment show different metabolic signatures.....108
Figure 20: Influence of glutamine starvation on intracellular oxygen capacity..... 109
Figure 21: Treatment with electron chain inhibitors highlights differences in intracellular oxygen levels 110
Figure 22: Volcano plots showing differential regulation of genes between cell lines late vs early oxygen levels 111
Figure 23: Pathway analysis of mRNA protein profiles reveals upregulated molecular pathways in the 6450 cell lines…….....112
Figure 24: Canonical pathway analysis reveals upregulated hallmark signalling pathways in the 6450-cell line.....113
Figure 25: Characterisation of migration and invasion profiles between cell lines (early vs late) shows differences in invasion profiles…….....116
Figure 26: Visual differences in cell invasion between cell lines and before and after treatment with inhibitor…….....117
Figure 27: Measuring intercalation in the cell lines 786 vs 6450 (early vs late) highlights differences in intercalation capability…….....119
Figure 28: Visual representation of differences in intercalation between the cell lines 786 vs 6450 (early vs late)…….....120
Figure 29: Characterisation of the mouse in vivo model.....131

Figure 30: Summary of the in vivo studies carried out…….....132
Figure 31: Immunostaining validation of metastatic capability……..... 135
Figure 32: H &E staining of tissue representing subcutaneous injections highlights angiogenic features 136
Figure 33: Vessel co- option in growing lung metastasis.....137
Figure 34: Pilot proteomic experiment shows differential protein expression between 786 and 6450 cells injected IV 138
Figure 35: Preliminary label free proteomics reveals differential expression of proteins involved in metabolism and cell receptor signalling.....139
Figure 36: Top variable proteins across all tissue samples highlight key roles in metabolism and cell receptor signalling.....140
Figure 37: Comparison of 6450 co – option versus angiogenic phenotype reveals involvement of proteins associated with cell communication, metabolism and response to stress.....141
Figure 38: Western blot validation highlight potential role of metabolism in defining tumour phenotype 143
Figure 39: Western blot validation highlights the potential role of adhesion in defining tumour phenotype. 145
Figure 40: Western blot validation highlights the potential role of Smad 4.....147
Figure 41: Western blot validation highlights the potential role of Thrombospondin -1 (TSP1) and ADAMTS2 149
Figure 42: Western blot validation highlights the potential role of Carbonic anhydrase and SLC9A1 in defining tumour phenotype.....151
Figure 43: Western blot validation highlights the potential role of Glutahione S transferase pi in defining tumour phenotype 152
Figure 44: Comprehensive GCxGC- MS profiling of cancer cell extract.....153
Figure 45: Global metabolomic analysis highlights variable metabolite profile across tissue samples.....154
Figure 46: Pathway analysis reveals changes in enzymes involved in glycolysis and gluconeogenesis 156
Figure 47: Pathway analysis reveals changes in enzymes involved in oxidative phosphorylation.....157
Figure 48: GC-MS analysis across samples B-E show differences in metabolites involved in cellular metabolism 158
Figure 49: LCM workflow 160
Figure 50: LCM collection of tumour and vessel material.....161
Figure 51: Principal component analysis shows independent clustering of in vein versus subcutaneous injection and tissue versus tumour.. 162
Figure 52: Venn diagrams showing total number of proteins detected with percentage overlap between groups.....163
Figure 53: Volcano plot highlighting the upregulated proteins in vesseks B compared to Vessels E... 164

Discovery of molecular signatures underlying angiogenic versus non angiogenic tumours

Alia Komsany, Linacre college
D.Phil. Thesis, Michaelmas 2018

Abstract

Angiogenesis has long been considered an essential prerequisite for tumour growth and progression. However, this understanding is being overturned by studies showing that many human tumours can metastasise without angiogenesis, suggesting that their microcirculation may be provided by non – sprouting vessels. Vessel co-option, a mechanism whereby tumour cells may incorporate and or migrate along pre-existing vessels presents an alternative mode of tumour blood supply. Vessel co-option has been found to manifest in many malignancies, occurring with increased frequency in highly vascularised tissues, such as the brain, lung and liver. 10-30% of primary and metastatic lung cancer, in addition to liver metastasis originating from different primary sources, have been found to utilise this alternative mode of blood supply. Furthermore, owing to the fact anti angiogenic drugs were designed to target new blood vessel growth, co-option as a result has also been proposed as a mechanism that could drive drug resistance to anti - angiogenic therapy. However, vessel co-option in the context of lung metastases has not been investigated extensively and likewise it's potential to induce drug resistance in lung metastases is not well established.

The aim of the work described in this thesis was therefore to investigate and further understand the molecular underpinnings that determine whether a tumour will exhibit a co-optive phenotype or an angiogenic phenotype and thus shed light on co-optive drug resistance molecular mechanisms in the context of lung metastases. Using a lung metastasis mouse model of co-option established originally by Andy Reynolds at the ICR in London, a multi omics approach was utilised to profile the "in vitro" and in "vivo" settings and identify potential molecular candidates that discriminate between angiogenesis and vessel co - option.

These studies revealed the potential role the cellular microenvironment plays in dictating metastatic potential in addition to metabolic cellular profiles, ultimately driving the decision to co – opt existing vessels or promote angiogenesis. Moreover, preliminary proteomic and metabolomic data points towards potential differential regulation of metabolic pathways, cell signalling pathways and proteins involved in adhesion that show distinct profiles within tumour cells with different metastatic potential and tissues from co – opting versus angiogenic models. Of particular interest is the possible role of Carbonic anhydrase 2, the Na^+/H^+ exchanger protein family and pH regulation in general towards controlling the cellular tumorigenic potential and possibly the fate of angiogenic versus co optive tumours.

To further drill down on this, subsequent proteomic analysis carried out on laser capture micro dissected tumours and vessels have further confirmed the role of metabolism, with proteins involved in lipid metabolism and reactive oxidative species metabolism being found to be upregulated in co optive vessels when compared to their angiogenic counterparts. In addition to this, the differential abundance of Carbonic anhydrase 2 was similarly confirmed, as well as proteins implicated in both adhesion and migration processes.

In summary, these studies have contributed to paving the necessary groundwork in relation to understanding co-option in a pre-clinical model of lung metastases. They have not only confirmed what has been already noted in the literature but have also highlighted potential new molecular targets and pathways, worthy of further study and investigation.

Declaration

This thesis and the work presented in it were completed at the University of Oxford (Nuffield Department of Medicine) under supervision of Professor Benedikt M. Kessler and Professor Francesco Pezzella. Tissue samples and cell lines from the mouse model of co-option were provided by Dr Andrew R Reynolds who also acted as mentor throughout the project. Proteomics and metabolomic studies were carried out in the Kessler group (TDI mass Spectrometry Laboratory). All contributions made by others have been clearly stated in the text. This work has not been submitted in full or partial fulfilment of any other degree.

Oxford, 5th October 2018

Alia Komsany

Acknowledgements

I would like to express my appreciation and gratitude first and foremost to my supervisors Professor Benedikt Kessler and Professor Francesco Pezzella for providing me with the invaluable opportunity to undertake my doctoral research under their supervision. I am very grateful for all their support, scientific input and guidance throughout the course of my studies, which undoubtedly has contributed greatly to the development of my decision making, and scientific reasoning skills.

I would also like to thank Dr Andrew Reynolds for providing me with additional mentoring, feedback and encouragement.

A very special thanks goes to all members of the Kessler group, especially Dr Darragh O Brien and Adam Thorne for providing such a friendly, helpful and motivating environment. In particular I would like to thank Simon Davis who has been an immense source of help. I am truly grateful for him sharing his wealth of experience in relation to proteomic analysis, processing of samples, in addition to his invaluable help with the laser capture microdissection setup and use.

I would also like to thank Dr Honglei Huang and Dr Adan Pinto Fernandez for their help, advise and willingness to impart knowledge and assistance when required.

I also would like to extend my appreciation to former members of the Kessler group Dr Rebecca Konietzny, Ms Marie-L. Thezenas and Dr Mikael Altun for their immense support and encouragement during my time at the Kessler laboratory and in the follow up to starting my D.Phil. studies at Oxford.

A special thanks goes to Dr Serena Lucotti, who dedicated her time, effort and expertise in helping me setup the intercalation and migration assays and who was a great source of encouragement providing me with invaluable help and assistance at a much-needed time.

I would also like to thank Connor Scott for all his help with immunohistochemistry staining and laser microdissection setup and use.

In addition to this I would like to thank members of the Harris group for their help, especially Dr Laurel T. Bate-Eya who shared her expertise and experience regarding mRNA isolation from tissues.

I would also like to thank Dr Karl Morten and Dr Michelle Potter for all their help and their expertise, setting up the cellular metabolic assays.

Finally, I would like to express my sincere gratitude to my family for their constant support, encouragement and understanding throughout my studies. I would like to extend a special thank you to my brother in particular, for being an inspirational figure in my life and encouraging me to aim high in my academic and non-academic pursuits and endeavours, always leading by example. I would also like to dedicate a very special thank you to my husband, who has been immensely supportive, understanding and patient. I could not have come this far without him by my side.

Chapter 1

1. Introduction

1.1 Hallmarks of Cancer

In order to gain a comprehensive understanding of cancer in its complexity and diversity, it's often useful to identify the common traits that are shared and acquired during the multistep process of human tumourgenesis [1] [2].

Our current understanding is that a vast catalogue of cancer cell genotypes can arise because of manifestations in a number of essential alterations in cell physiology, that collectively dictate malignant growth. These alterations are known as the hallmarks of cancer.

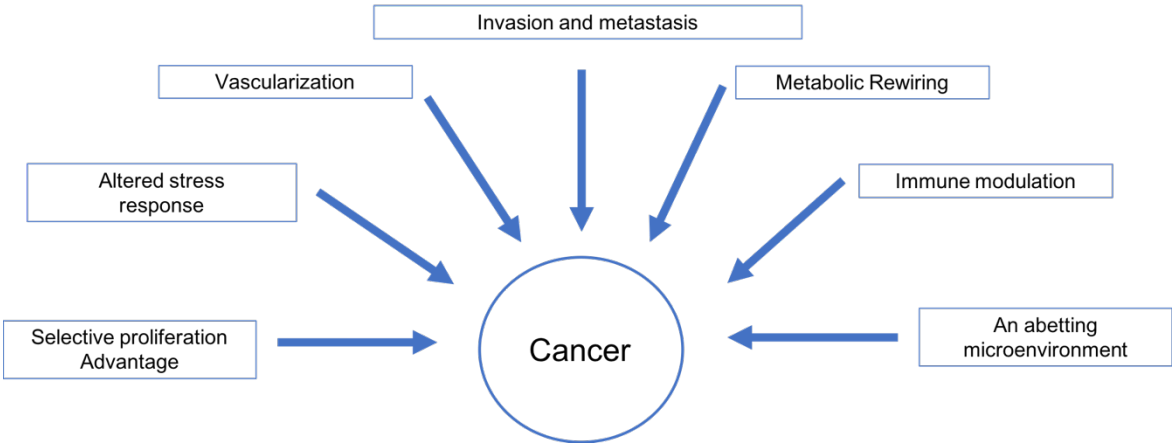


Figure 1: Hallmarks of Cancer: Schematic showing the hallmarks of cancer.

One of the most widely cited publications in the field of oncology is a paper by Hanahan and Weinburg entitled the hallmarks of cancer; an influential review that provided the framework to our understanding of cancer, and also provided the rationale for cancer drug design [3].

Originally published in 2000, the paper attempted to address the complexity of neoplastic diseases by categorising cancer biology into six major hallmarks, a decade later this was subsequently updated to include a further two emerging hallmarks [3]. More recently however, these hallmarks have undergone much critisism, and with advancements in the field of cancer research, our understanding of the various aspects of tumourgenesis, has evolved. As a result, the hallmarks of cancer, as first proposed by Hanahan and weinburg have been updated, revised and re approached alongwith considerations for the future of the field.

Sustaining proliferative growth and signalling

The first hallmark and arguably the most fundemental trait is the ability for a tumour to sustain chronic proliferation [1 4].

In normal tissues, progression of cells through cell growth and division cycles is carefully monitored and controlled by the release of cell growth promoting signals [5 1]. These signals act to maintain cell number, proliferation, and architecture of normal tissue [1].

This homeostasis is disregulated in cancer cells, with these cells acquiring the ability to overcome signalling pathways, in a variety of ways [6].

It is currently understood that cancer cells can employ one or more drivers of growth and proliferation within their compartments, thus confering a selective growth advantage [3 7]. These compartments constitute growth factor ligands, their receptors and cytosolic signalling molecules [3].

Cancer cell growth autonomy is often categorised as either growth promoting involving an increase in growth ligand production by epithelial or stromal cells acting in a autocrine or paracrine fashion or alternatively growth inhibiting, where in which the tumour is able to escape inhibitory signals [3].

One way this can be achieved is by the production of growth factor ligands, which results in proliferative stimulation [1].

Alternatively cancer cells can stimulate normal cells in the surrounding tumour associated stroma, which respond by supplying the cancer cells with a variety of growth factors, facilitating increased proliferation and tumour growth [8].

In addition to stimulating proliferation and subsequently growth, tumour cells can also deregulate receptor signalling by raising the level of receptor proteins present on the cancer cell surface, thus resulting in these cells becoming hyperresponsive to the already reduced amount of growth factor ligand [9].

A similar response can be achieved by inducing structural changes to the receptor molecules, facilitating ligand independent firing [1 10].

Similarly, cancer cells can activate downstream signalling pathways, thus eliminating the need for ligand mediated receptor signalling [1 9].

Although these signalling processes are often described as being either stimulatory or inhibitory in relation to proliferation and growth, growth ligands have been observed to act in a pleiotrophic manner [11].

For example, transforming growth factor TGF-β is conventionally known to be an anti growth ligand but it has also been implicated in tumour progression by stimulating cancer cell de differentiation and reshaping the tumour micro environment [12].

This less than straight forward type of signalling demonstrates the selective survival pressure on tumours to find the right balance of growth ligands, the expression of which being specifically tailored to each stage of tumorgenesis and adaptable depending on the tumour microenvironment [11].

In addition to receptor overexpression by gene amplication, there are various other mechanisms that result in alterations to ligand binding receptors such as somatic mutations that can result in constitutive receptor activation, chromosomal translocations which may lead to fusion proteins and irregular receptor activation as well as impairment of receptor recycling and degredation machinary [7] [13].

Disruption in growth dependant signalling pathways are complex and are still under investigation. Although this disruption can be found in both upstream and downstream compartments, the deregulation of downstream signalling networks, tends to be more common.

An illustrative example of this is the RAS protein, a small GTPase which is at the cross – road of a number of key regulatory signalling pathways [3]. Mutations in the RAS gene family of proto-oncogenes are very common, being found in 20% to 30% of cancers and in over 90% of pancreatic cancers [14].

Despite our knowledge of the mechanisms behind the regulation of RAS activity, namely that it is often caused by a missense mutation in its gene or an inactivating mutation in one of its key negative regulators e.g. NF1 [15] [16] many of the anti RAS cancer based therapeutic interventions have been found to be less than satisfactory [17].

In addition to this, components of prominent signalling networks such as the RAF – MEK – ERK and the PI3K – AKT – MTOR pathways which are implicated in the RAS downstream signalling cascade and consequently in the mediation of RAS function, can undergo independent mutation in a variety of cancers [18].

Irrespective of whether it's a mutation in RAS, its key regulatory proteins or its downstream networks, the resultant effect has been found to extend beyond enhanced proliferation and growth and can in fact include growth suppression, apoptosis, metabolic rewiring, the promotion of vascularisation and immune evasion [14].

This highlights the increasingly acknowledged fact that a single signalling cascade can be associated with a myriad of different cellular processes which can be categorised into multiple hallmarks of cancer. [19].

Even in the presence of growth signalling, cell cycle regulatory proteins play a crucial role in keeping cell division in check. These regulatory proteins are commonly inactivated in a number of malignancies and like growth signals are implicated in a multitude of cellular processes beyond enhanced growth and proliferative control [20].

The retinoblastoma protein (RB) is an example of one of these key regulatory proteins that is commonly inactivated in a number of malignancies [21] [22].

Much like the RAS protein, RB is not only associated with proliferative control, and has been shown to be implicated in a variety of roles characteristic to a number of cancer hallmarks. These include cell metabolism, maintenance of genomic stability, regulation of apoptosis, senescence, angiogenesis and suppression of invasion and metastasis [22] [3].

The tumour suppressor protein, p53 is another key regulator, functioning as stress detector and responder, expressing sensitivity to a variety of stresses which include genotoxic stress, excessive signalling, nutrient deprivation and hypoxia [3].

Similarly, the p53 gene is commonly found to be mutated in over 50% of sequenced tumours and has been found to not only be involved in arresting enhanced proliferation, inducing repair mechanisms and cell death, but has also been implicated in metabolic rewiring, regulation of autophagy and redox homeostasis. [3] [23].

In an attempt to simplify matters, it can be become very tempting once again to categorise cancer cellular components as either growth promoting, involving the activation of tumour oncogenes or growth inhibiting involving the activation of tumour suppressor genes.

Despite this, it has been observed that a collaboration of both growth promoting and restricting mechanisms are required for tumour progression, this too however is not entirely representative, nor does it give the full picture.

In the case of some cancer types, pancreatic adenocarcinoma for example, a large percentage of driving mutations can be found in the labelled oncogene compartment alone [3].

However, such labelling is perceived to be somewhat artificial, in reality a context dependant interchange of functions is observed at different stages of tumour development and in different settings [3] [24] [25] [26].

As a tumour progresses through towards full scale malignancy, cancer cells face a multitude of stresses, ranging from excessive signalling, DNA damage, hypoxia, nutrient depletion and scarcity and even anti-cancer therapy [27] [3].

Where possible cells adopt a variety of physiological responses to stress and in the face of overwhelming stress, cells altruistically eliminate themselves for the sake of healthy tissue.

In a cancer setting, these mechanisms are subverted for the outcome of overall survival and propagation [27].

DNA repair

Cells employ a number of repair pathways, each consisting of a variety of molecules that work in collaboration to restore a specific type of DNA lesion.

Different types of DNA damage elicit specific DNA damage mechanisms and repair signalling pathways [28].

In the case where a repair pathway is defective but not entirely redundant, different alternate pathways will usually compete, compensate, and work in its place [29] [30].

Cancer has its origin in DNA mutation, and for this reason it is often considered to be a disease of DNA repair. In order for cancer cells to replicate their DNA, proliferate and ultimately survive they need to be able to exploit a number of repair pathways [31].

Since the original mutated repair pathway that lead to the cancer in the first place is often defective, cancer cells as a result usually become heavily reliant on other repair pathways [32].

Consequently, these pathways are often targeted therapeutically impairing the repair of intrinsic damage that occurs during DNA replication and can also add to the DNA damaging effect of chemotherapy [33] [34].

Therapeutic exploitation of the ability of the cancer cells to become somewhat solely dependent on one specific repair pathway is based on the concept that the presence of a mutation in cancer cells often gives rise to a new vulnerability that can be targeted, a notion termed as "synthetic lethality" [35].

For tumour growth to progress, a culmination of unrepaired, persistent mutations is required. This alongside the already unstable genetic makeup of most tumours alludes to defects in essential repair machinery throughout the process of tumorigenesis [3] [34].

Some of the most notable cancer syndromes involve germline mutations in the genes that code for DNA repair pathways, in addition to acquired cancers which have been shown to exhibit defects in repair pathways as they evolve, with polymorphisms in repair genes being correlated to cancer risk as well [36] [37].

As a result, increased variability can be seen when it comes to therapeutic response as the majority of anti-cancer interventions work by eliciting DNA damage [36] [37].

It is also worth noting that in many tumours, overexpression of repair proteins has been observed, for example RAD51 is commonly overexpressed in pancreatic cancers, breast cancer and leukaemia [38] [39]. This upregulation has been linked with therapeutic resistance and post treatment relapse [3].

Thus, in the context of cancer, it can be concluded that DNA repair pathways are multidimensional regulators, the dysregulation of which (defects in one pathway which leads to an increased and over dependence on another) serves to ultimately enable tumours to survive and progress. DNA repair pathways also present a viable therapeutic window that can be exploited [33] [3].

Apoptosis

In addition to irreparable DNA damage, uncontrolled proliferation and loss of matrix attachment, apoptotic cell death presents another response to stress induced transformation [3]. In cancer the normal homeostatic balance between proliferation and cell death that acts to maintain normal tissue, is disrupted [40] [41].

The binding of ligands to cell surface receptors, mediates the primary signalling events that lead to the extrinsic pathway of apoptosis in response to external stimuli with the more relevant intrinsic pathway functioning in response to a variety of intracellular stresses compatible with apoptosis [3].

This process leads to a shift in balance, favouring pro apoptotic over anti apoptotic proteins, a destabilisation of the mitochondrial outer membrane permeabilization (MOMP) and the activation and release of molecules in the intermembrane space [42] [3].

The initiation of apoptosis from either pathway results in activation of caspases, cleavage proteins that induce cell death [41 43 44].

Cancer cells exhibit several mechanisms that enable them to bypass the apoptotic response. Mutations that involve the inactivation of p53 result in cancer cells become insensitive to many apoptotic stimuli, fortunately however p53 independent cell death pathways exist [3].

Epigenetic modifications often lead to the upregulation of anti-apoptotic or loss of pro apoptotic proteins in a variety of tumours, and cancer cells on the occasion, have been noted to inhibit caspase activity despite the occurrence of MOMP [45 3].

Although the net outcome of the above alterations is increased tumour survival, this does not necessarily imply that all tumour cells are insensitive to apoptotic signals [3].

On the contrary tumour cells are in fact more likely to be sensitive to apoptotic stimuli than normal cells and the process of apoptosis is a frequent cellular event. It is thought that apoptosis may serve an evolutionary purpose, by imposing a selective pressure and eliminating less fit lineages, thus enabling cancer progression [46].

Autophagy

Autophagy describes the process by which intracellular components are recycled. It functions at a low basal rate and physiologically provides a quality control mechanism where by pathologic long lived, damaged and misfolded proteins are removed [47].

It also has been implicated in the process of unconventional protein secretion. In addition to this, it serves as a protective response and is an upregulated reaction to a number of stresses including those that are pathogenic, metabolic and genotoxic in nature [48] [49]

Aspects of its tumour suppressor capability were established when it was observed that the loss of the beclin gene (encoding for an essential autophagy protein) in engineered mice resulted in the death of mice during embryogenesis, whereas those mice that were haploinsufficient developed improvised tumours with age [50] [51].

The autophagy gene has been found to be mono – allelically deleted in 40-75% of human sporadic human breast, ovarian and prostate cancer cases [52] [3].

While the exact mechanism by which autophagy elicits its tumour suppression role still remains unclear, it has been suggested that it may involve the selective removal of damaged mitochondria during periods of stress [47].

In so doing reducing the number of reactive species ROS [3], regulating metabolic homeostasis, degradation of overexpressed proteins, contribution to immune surveillance, as well as potential function in the defence against carcinogenic bacteria and viruses [3] [50] [53] [54].
Alternatively, autophagy has also been found to have a tumour promoting role and is implicated in tumour survival and progression, with upregulated autophagy and autophagy dependence, being characteristic to a number of malignancies [53].

In a variety of cancer settings, autophagy may enable cancer cells to proliferate and survive by facilitating growth under harsh conditions, such as metabolic stress and hypoxia [55].

Autophagy can also help cancer cells to evade immune surveillance, acquire metastatic and invasive properties and secrete tumour microenvironment reshaping proteins [49] [48] [56].
Incidentally, autophagy represents another cancer hallmark whose stress response needs to be viewed in a context dependant manner and whose role varies according to tumour setting and stage [53].

Senescence

Another way in which proliferating cells respond to stress is by initiating a permanent state of cell cycle arrest, termed cellular senescence [57]. Once the DNA replication potential has been exhausted, and telomere shortening has occurred, the induction of senescence follows[58].

This protective measure, ensures that successive divisions which would otherwise result in genomic instability and accumulation of transforming alterations, are halted [57] [59].

Both benign and pre malignant growths are in almost all cases characterised by telomere shortening [60]. In fully transformed cells however, this protective mechanism needs to be bypassed mainly by means of the enzyme telomerase [61].

Telomerase has been found to be upregulated in 85-90% of cancers where it has the role of reconstituting telomere length and maintaining sufficient length for DNA replication [62] [63].

It is also worth noting that around 10- 20% of tumours utilise alternate pathways in order to maintain telomere length, however this is a topic of ongoing research [63]. Senescence can be induced by a plethora of other stressors beyond telomeric DNA damage [64].

These stressors include, damage caused my reactive oxygen species and anti-cancer treatment, unbalanced mitogenic induction as well as the activation and upregulation of tumour suppressors consistent with the cellular protective role of senescence [57] [60].

In recent years the seemingly passive role of senescent cells has been scrutinised and challenged. It has been observed that senescence is not limited to the arrest of cell proliferation and likewise is not restricted to its tumour suppressive and protective role [65].

Senescent cells have in fact been found to remain metabolically active and undergo widespread alternations in protein secretion and expression [66].

This characterisation mainly occurs through the acquisition of a senescence-associated secretory phenotype (SASP) whereby soluble signalling factors, insoluble proteins, matrix components and proteases secreted by senescent cells acquire the ability to manipulate and alter the surrounding microenvironment [52] [67].

Conflicting roles, both beneficial including autocrine tumour suppression, tissue repair and clearance of senescent/ transformed cells in addition to a detrimental role, involving the promotion of inflammation, angiogenesis and metastasis have been attributed to SASP, thus painting a far from simplistic picture of the multidirectional tumour suppressive senescence response [65].

As a result, senescence remains poorly understood and remains a target that is yet to be exploited fully for therapeutic intervention [67] [68].

Invasion and metastasis

The ability to invade surrounding tissue, disseminate and metastases to distant sites to form secondary tumours is a central feature that defines the process of malignancy [69].

For cancer cancers to disseminate and metastasise, they must undergo a series of carcinogenic events commonly termed as the metastatic cascade. First, they must acquire the ability to invade through the extracellular matrix (ECM), which includes the basement membrane and stromal cells [70].

They then need to enter the newly formed vessels or existing ones, a process known as intravasation. It is essential that they also can survive transport in the circulation. Once they have reached a distant organ/site they then must escape into the surrounding tissue, via a process called extravasation [71].

Subsequent survival in and manipulation of the foreign microenvironment, is essential for the formation of micro metastases, which may go on to form clinically relevant macro metastases by means of a rate limiting step known as colonisation [3 72 73].

It's becoming increasingly evident, that the process of invasion occurs in a collective fashion resulting in the formation of polyclonal metastases [74].

Despite the fact that a majority of human carcinoma cells migrate in clusters, cells being investigated in in vivo and in vitro studies, have been observed to migrate individually, this could be attributed to the TME evolving in conjunction with the former group [3 75].

What is becoming apparent from a number of studies however, is that tumour microenvironment and in particular stromal organisation play major roles in determining the mode and dynamics of cancer cell invasion [75].

Furthermore, mouse and in vitro models have been shown to display several 'modes' of migration, from single isolated cells with round or elongated phenotypes to loosely-/non-adherent 'streams' of cells or collective migration of cell strands and sheets [75].

Epithelial cells are characterised as being immotile and tightly adherent to each other and to the surrounding matrix [3].

To overcome this, a process known as epithelial mesenchymal transition (EMT) is usually employed [76]. EMT is described as the reversible biochemical alteration that facilitates polarised epithelial cells to take on a mesenchymal phenotype, a phenomenon that usually occurs during embryogenesis, would healing and organ fibrosis, all part of adult physiological and pathological events [77].

It was originally thought that the process of EMT could be described in dual like states, either full epithelial or full mesenchymal, however this view has been developed more broadly to encompass a more fluid phenomenon that includes several intermediary phases, referred to as partial EMT, that can progress, revert or exist as an end stage [78].

Several factors contribute to the process of EMT and have been found to be context dependant and tissue specific. These factors include a variety of growth factors [12], signalling pathways [79], tissue hypoxia [80], metabolic as well as mechanical stress and matrix stiffness [81].

Signalling triggers commonly come together on the level of one of the principal EMT transcription factors, that act to inhibit epithelial genes and activate mesenchymal ones [73].
In addition to this, regulators of EMT also include epigenetic effectors thus highlighting how control of the process can be indirect, and adjustable [78]. Despite the body of evidence that points towards the role of the EMT in cancer invasion and migration [76] [82], more recent emerging evidence has begun to question this involvement [83] [84].

As it currently stands however, there is not enough evidence to include/exclude EMT in cancer progression, with further experimental work required in order to debate the role of EMT more extensively [85]. The degradation of the ECM, is fundamental to local invasion, of which the metal metalloproteases (MMPs) play a crucial role [86].

These endopeptidases are involved in a variety of processes not limited to invasion including, cell proliferation, survival, immune response and angiogenesis [87] [88].

MMPs are upregulated in most types of cancers, with expression of specific members of the protein family, being associated with poor prognosis [89].

The invasion of cells into the Lumina of vessels, known as intravasation can be both a passive or active process, depending on the tumour type, TME and vasculature [90].

So far, we have a limited understanding of the mechanistic underpinnings of intravasation owing to the challenges associated with modelling the process in vitro [91]. A recent microfluid model however, could potentially help provide some insight [92].

Once in the circulation, circulating cancer cells must be able to adapt to the selective conditions that they find themselves exposed to [73] [93].

Some of these adaptive mechanisms include, platelet coats that shield cells from shear force and from immune clearance as well as metabolic rewiring acting to reduce oxidative stress [72] [94].

Isolating circulating cancer cells can be exploited as a useful probe providing a means for cancer screening, prediction of the risk of metastatic relapse, identification of potential druggable targets, understanding tumour heterogeneity in more detail, and monitoring therapeutic response [93] [95].

Further investigation is required however, before circulating cells can be utilised in a clinical setting.

Circulating cancer cells drifting in the circulation, become trapped in small capillaries where they can induce vessel growth and subsequent micro vessel rupture or become involved in extravasation [72].

Organs such as the liver and bone marrow possess sinusoidal vessels which are highly permeable, perhaps explaining why a high rate of metastasis is observed in these sites [3].

Comparatively, and in most other organs endothelial cells are observed to form a tightly adjoining lining supported by a basement membrane and pericytes [96].

Owing to the lack of support from the TME, essential for the process of intravasation at secondary tumour sites, extravasation can clearly be considered as a separate process, distinct from intravasation and a certainly more challenging process when compared to intravasation [73].

Our current understanding of extravasation is quite evidently incomplete; however, what is known, is that a variety of factors are involved in extravasation, these include ligand receptor interactions, chemokines and circulating non tumour cells [91 93 94].

Passive arrest or what is also termed as the anatomical mechanical hypothesis partially describes the metastatic preferences of human tumours [97].

A process known as organotropism, first proposed by Stephan Paget in his seed and soil hypothesis [98], where cancer subsets (metastasized cells) were found to favour organ subsets and where an interplay between genes involved in mediating organ specific metastasis and adaptive mechanisms [99] in the corresponding tissue have been observed [73 96 100].
This hypothesis is still relevant and can be observed in prostate cancers which tend to be coupled with bone metastasis, colorectal cancers which are often paired with liver metastasis and breast cancer where bone, liver and lung metastasis are evident [101].

Both the seed and soil mechanism and the anatomical mechanical hypothesis can work collaboratively, in a context dependant manner to varying degrees, rather than being considered as being mutually exclusive [72 98].
The foreign microenvironment presents a challenge to cell survival [73]. Cells must develop adaptive mechanisms to overcome the harsh conditions. Secondary sites are prepared to receive cancer cells by means of a variety of systemic signals.
These signals may come into effect quite some time prior to dissemination creating what is called as a premetastatic niche [102 103].

Several tumour derived secreted factors as well as bone marrow derived cells contribute to niche development [103] [104]. Recent studies have also implicated the role of exosomes in the process as well [105] [106].

Dormancy of surviving cells is caused by a resultant delay in adaptation at the niche. Dormant cells have been found to remain in the bone marrow of cancer patients long after removal of the primary tumour and may be the reason behind late relapses [107]. Dormancy can be categorised into three non-mutually exclusive types [108]:

1) Cellular dormancy which describes cells that enter into a state of quiescence, a similar process to senescence, but reversible in this case.
2) Angiogenic dormancy, characterised by a balance between dividing cancer cells and those lacking surrounding vasculature (subsequently leading to cell death) is achieved.
3) Immune facilitated dormancy, where in which the tumour mass remains constant by means of the continuous release of cytotoxic reagents by immune cells.

The precise mechanism by which cells escape dormancy and go on to develop and manifest to form metastasis, is very poorly understood [107]but has been observed to occur in an organ specific manner [72], supported by the notion that cells that escape dormancy have an increased capacity for self-renewal [73].

Furthermore, it is thought that these cells are usually unique and rare, forming subpopulations of cells which have stem cell like characteristics, that equip them with the added advantage when it comes to outcompeting other cells and overcoming metastatic hurdles [109]. This current understanding however, requires further experimental validation.

Metabolic rewiring

Tumorigenesis is heavily reliant on the reprogramming of metabolic pathways which result from direct and non-direct oncogenic mutations. Metabolic rewiring, confers a selective advantage when it comes to inducing tumour growth and progression thus, enabling cancer cells to acquire nutrients from a nutrient deficient environment [110].

Alteration in cancer cell metabolism can be subdivided into several hallmarks as recently described by Pavlova and Thompson [111].

1. Deregulation of glucose and amino acid uptake
2. Acquired mechanisms of nutrient acquisition
3. The use of intermediaries of glycolysis and the TCA cycle
4. Enhanced nitrogen demand
5. Changes in metabolite-initiated gene regulation
6. Metabolite interactions with the microenvironment

The above metabolic alterations have been noted to occur both partially and fully and are most likely dependant on tumour stage and setting [3].

Nutrient uptake

Growing cells are dependent on two main nutrients, glucose and glutamine. Both nutrients facilitate the building of macromolecules. The also assist in the generation of ATP, via controlled oxidation of the carbon skeleton in addition to maintaining cellular redox capability [111].

Glutamine, owing to its nitrogen donation capacity has been attributed additional roles, such as being a nitrogen provider for biosynthesis [112] [113] , maintaining the amino acid pool as well as contributing to gene expression and cell signalling [113].

The Warburg effect, which states that cancer cells can over utilise glucose even in the presence of oxygen was described some time ago [114], its application experimentally has only begun to be studied decades later, with the advent and use of [18F] fluorodeoxyglucose positron emission tomography scanners [115].

Glucose transporter (GLUT) proteins have been observed to be elevated in many cancers and have been linked to poor prognosis in some specific cancer types [116] [117] [118].

Glucose uptake is regulated by various signalling pathways [111] [116] [119] and by a variety of mechanisms, for example HIF is implicated in the increased expressed of GLUT1 and hexokinase, which both act to trap the influx of glucose [120].

Similarly, dysfunction in the PI3K/AKT pathway results in the elevation in expression of GLUT1 and in the shifting of proteins towards the cellular membrane. Oncogenic KRAS and BRAF have also been observed to cause the same effect [121] [3].

In contrast very, few studies have been carried out on glutamine in the context of tumorigenesis and only recently, it's substantial role in transformed cells has been highlighted[113]. That said, the regulators of glutamine uptake remain relatively uncharacterised [112].

What has been indicated however, is that MYC augments the operation and expression of glutamine transporters with RB having been observed to negatively regulate glutamine synthesis [122].

Tumour cells can employ alternate pathways other than transport for the acquirement of glutamine and amino acids, these include micropinocytosis of extracellular proteins in situations where nutrients are scarce, the engulfing and digestion of living cells, or alternatively the phagocytosis of neighbouring products of apoptosis [111] [112].

Thus, dysfunctional nutrient uptake encompasses other mechanisms that go beyond glucose and glutamine uptake (although these are the most characterised when it comes to reprogramming of metabolic pathways) [123].

The contribution of other amino acids, lipids or fatty acids and their implication in tumour metabolism is currently a subject of ongoing research and investigation [111] [124] [125] [126].

Over time, our understanding of the Warburg effect, has evolved. Our preliminary rationalisation of the described phenomenon was defective oxidative phosphorylation [111]; however, it has been observed that in most cancer cells have normal functioning mitochondria capable of oxidative phosphorylation [127].

Furthermore, it has been shown that targeting mitochondrial DNA in vivo and in vitro [119] [127], results in a reduction in the tumorigenic potential of cells.

More recently, the alternate explanation being offered and put forward is that cancer cells have a preference towards glycolysis, as it facilitates the constant shifting of glucose into intermediary pathways, the steps of which, are commonly overexpressed in cancer.

This shunting of glucose into intermediary pathways, also assists in the production of precursors or reducing counterparts necessary for tumour cell survival [128] [111].

Oxidative phosphorylation as a result occurs alongside glycolysis enabling tumour cells to keep up with their high anabolic rate needs [119].

Thus, tumour cells are required to devise mechanisms whereby they can maintain some mitochondrial flow while facilitating and sustaining a high rate of alternative pathway shunting [111 127].

This is commonly achieved by means of tightly regulated enzymatic activity which helps to control influx into the TCA cycle [129 130].

Although this process is regulated, TCA cycle overload does occur, resulting in the production of reactive oxygen species (ROS) [128]. In the right amounts, ROS can contribute to tumour progression, promoting stress signalling and adding to the mutation burden, and is therefore useful in cancer [131]. However, high levels of ROS can be detrimental to cells and thus tight regulation and control is essential.

A suggested model that has recently emerged describes an increase in metabolic activity and ROS in the initial stages of tumour progression contributing to tumorigenesis [3 132].

As the tumour continues to progress and face harsh oxygen and nutrient deprived microenvironments, there is an increase in the production of antioxidants to avoid the accumulation of ROS and to maintain its production at non-lethal levels [127].

In addition to this, glutamine is utilised by the mitochondria and is converted into glutamate which is then used directly or undergoes further processing to form α-keto - glutarate (α-keto KG) which under unfavourable conditions can act as a glucose substitute, producing citrate and contributing to fatty acid synthesis[112].

Cancer cells are often described as having a significant elevation in lipid production, with the upregulation of all major constituents of the fatty acetyl chain being observed [124].

This may be favourable for proliferating cancer cells in the formation of lipid bilayers as well as for the optimisation of membrane composition, towards a higher percentage of oxidative damage resistant saturated fatty acids [111].

Metabolic reprograming, does not only result as a passive consequence of tumour progression, but can in fact can take on more of an active contributing role in tumorigenesis. In addition to metabolite induced effects on cellular behaviour and tumorigenesis, the availability of metabolites also dictates epigenetic regulation in the form of the addition or removal of acetyl and methyl signatures [111].

The most well-known example of this, is the production of the oncometabolite, otherwise known as 2-HG. 2 -HG, is a structurally similar and competitive inhibitor of α- KG and is produced as a result of a point mutation in the genes that code for isocitrate dehydrogenase (IDH) expression [133].

This mutation confers an alteration in enzymatic activity, facilitating enzymes to act on α- KG instead of isocitrate, thus producing 2-HG. This process consequently inhibits dioxygenases with hypermethylation silencing of a variety of genes implicated in tumorigenesis [134] [135] [136].

Accumulation of 2-HG may also be observed in conditions wherein which IDH mutations are absent, as recently described in triple negative breast cancers [137] [3].

During all stages of carcinogenesis, the constant communication between cancer cells and stromal cells, creates a diverse and dynamic microenvironment with many hallmarks of cancer having several stromal compartments [3] [138].

This integration, between the hallmarks of cancer and the TME can be better understood by means of citing cancer associated fibroblasts as an example which alone are involved in selective growth, proliferative advantage [139] [140], checkpoint inhibition [141] [142], stress response conferred alterations, resistance to cell death [143], angiogenesis, the invasion metastatic cascade [144] and metabolic reprograming in cancer [111].

The powerful role that the TME plays in carcinogenesis, became clear with observance of TME related transformation. This was demonstrated when normal hematopoietic progenitors were shown to lose their integrity and became altered with myelodysplasia related changes being observed, when seeded on osteolineage cells harbouring Dicer 1 deletion [145].

Furthermore, it has been shown that 5% of acute myeloid leukaemia allograft receivers present with complete chimerism relapse with original leukemic cells, thus making the case for TME as an essential component of leukemogenesis more convincing [146].

Owing to difficulties in modelling the tumour associated stroma which consists of many different cell subtypes (spatial heterogeneity), at various stages of differentiation (temporal heterogeneity), TME studies have been challenging to pursue [3].

To get a full picture, spatial mapping of the TME alongside molecular imaging could prove useful [147] [148].

Temporal heterogeneity however, is more complicated, with most studies having chosen to focus on mature stromal cells as opposed to pursuing the origin of stromal cells [149], the first settlers, which may arise from the mesoderm, and could potentially be the mesenchymal cells [150].

More recent studies have highlighted these original cells to be under the regulation of endocrine and signalling pathways as well as being subjected to metabolic rewiring [151] [152] [153] [154] [155].

This is further complicated by the fact that different cancer cell populations can act as the TME, supporting and encouraging one another a concept known as intra-tumoral heterogeneity [156].

Consequently, removal of such supporting cell populations by means of monoclonal transplantation results in the inability to represent and reproduce parental tumour behaviour [157]. This provides yet another challenge for xenograft assays that depend on single cell transplantation methods [3].

Therefore, considering the cancer therapeutic response as an organ response instead of a cellular response may be a more efficient way of looking at resistance in the context of cancer therapy [158].

Immune modulation

Early experimental data has shown that there is an immune rejection of transplanted tumours in mice, giving rise to the theory of cancer immune surveillance [159]. This is further emphasised by the observation that primary and acquired immunodeficiency in humans and mice also promote tumorigenesis [3].

The tumour immune micro environment consists of a multitude of complex interactions between tumour cells, antigen presenting cells (immune cells such as T cells, natural killer cells and B cells) and tumour stroma [160]. The host immune response against tumour, results from inhibitory and stimulatory signals that are in constant competition which each other [160].

Immune checkpoints function to maintain immune homeostasis and prevent autoimmunity. These checkpoints are made up of stimulatory and inhibitory pathways, essential for maintaining self-tolerance as well as controlling the type, extent and length of the immune response [160]. Under normal situations, immune checkpoints modulate the immune response against infection and malignancy, while simultaneously protecting tissues from any harm that may come about as a result of this process [161].

Despite the presence of this immune surveillance however, tumours can express some of these immune checkpoints proteins, which act to disrupt the anti-tumour immunity, and thus favour persistent growth, progression and development of cancer cells [160 161].

The inhibitory pathways consisting of cytotoxic T lymphocyte associated molecule 4 (CTLA -4), programmed cell death receptor 1 (PD-1) and programmed cell death ligand 1 (PD-L1) are the most broadly studied checkpoints. A number of biological agents that target these checkpoints are used in a variety of malignancies, albeit with modest results in the clinic [160].

The immune system can eliminate and define malignant disease in a process known as immunoediting which can be broken down into three stages: elimination, equilibrium and escape [162].

During the elimination phase both the innate and adaptive immune responses converge to destroy developing tumours. Dunn et al, put forward four phases of elimination [163]:

1. Recognition of cancer cells by innate immunity and their limited killing.
2. Maturation and migration of antigen presenting cells and cross priming of T lymphocytes.
3. The production of tumour antigen specific T lymphocytes as well as the activation of cytotoxic pathways.
4. Directing of tumour antigen specific T lymphocytes to the tumour site and the removal of tumour cells.

Once the elimination phase is complete, equilibrium ensues. The equilibrium phase of immune surveillance involves the constant shaping and moulding of tumour cells, such that cells that have reduced immunogenicity are selected, and the production of resistant variants is increased [161].

The equilibrium phase is the longest of the three phases with cancer cells having the ability to remain latent for long periods of time, extending to several years in cases [3].

During the equilibrium phase, new variants, expressing a variety of immune resistant mutations can appear [162].

Although cancer cells are constantly under immune selection pressure, some clones arise which can escape immune surveillance [164].

This ability to evade immune detection and elimination by means of genetic and epigenetic modifications resulting in the formation of a clinically detectable tumour, defines the final phase of cancer immunoediting [3].

The mechanisms by which cancer cells can escape immune surveillance can be categorised into three major groups [165]: Alterations in either tumour or effector cells, which result in a lack of tumour antigen recognition, resistance to cell death and the secretion of immunosuppressive factors which confer an immunological tolerance [166].

Cancer cells can also disable the cytotoxic constituents of the immune system by means of producing and secreting immunosuppressive factors or enlisting immunosuppressive inflammatory cells [167].

Furthermore, stromal cells can also produce immunosuppressive components, which can induce the upregulation of immunosuppressive factors from other molecules [168].

Exosomes that originate from tumours also express signals involved in immune suppression. Metabolic reprograming in addition to modification to the microbiome are of relevance as well [169] [170].

1.2 Angiogenesis a hallmark of Cancer?

Vascularisation

Tumours cannot exceed 2-3 mm^3 in growth nor can they metastasize without new vasculature [3]. The role of vessels in cancer has been a topic of much debate [171] and the process of angiogenesis has a longstanding role as one of the vital hallmarks of cancer [172].

Although angiogenesis is the most widely discussed mode of tumour vascularisation, other modes exist [173] and perhaps this redundancy in usage in part, reflects the issue of resistance that results as a consequence of targeting a single mode [174].

What isn't clear however, is why tumour growth undergoes one mechanism over the other. While a minority of tumours are noted to be completely non-angiogenic, in many tumours, it is common to have both angiogenic and non-angiogenic areas [171].

Tumour growth is heavily dependent on the availability of oxygen and nutrients supplied by the vascular network of blood vessels. The understanding that cancers contain blood vessels, dates back to the dawn of medicine [172].

The interaction of cancer cells with blood vessels is a topic that has generated much intrigue and has formed the basis of numerous studies.

Angiogenesis, or what is known as neovascularisation, is a process which involves the sprouting, cell division, migration and assembly of endothelial cells from pre - existing blood vessels and was first coined in 1787 [1].

Angiogenesis is employed in the expansion and remodelling of primitive vascular networks, a common feature in for example embryogenesis. It is also involved in postnatal events, such as female reproduction, wound healing and chronic inflammation. Where angiogenesis is switched off and in events where it may be prolonged, it is usually self – limiting [175].

The term angiogenesis was only used in association with tumours in the 1960's, and unlike normal cellular events as mentioned above, in malignancies, angiogenesis is continuously activated.

Folkman's theory of angiogenesis

In 1971, Folkman introduced his theory which was primarily based on animal "in vitro" studies [173], this theory stated that tumours cannot grow without angiogenesis and it was upon this premise that angiogenic targeted therapy came about.

The Angiogenic switch

At the core of Folkman's theory, is a concept known as the angiogenic switch. The angiogenic switch is defined by the transformation of cancer cells from an early phase of limited growth to the acquisition of angiogenic properties resulting in tumour progression [176].

The balance of pro angiogenic factors versus anti angiogenic factors regulates the status of the angiogenic switch. This process can only occur however when balance is triggered and tipped in favour of pro angiogenic factors facilitating vascular inactive tissues to become angiogenic, as in the case of malignancy [177].

One of the most important triggers of angiogenesis is hypoxia [178]. Endothelial cells employ a variety of oxygen sensing mechanisms that interact with the hypoxia inducible transcription

factor family, involved in controlling the expression of a multitude of genes associated not only with angiogenesis but are implicated in cell survival, metabolism and inflammation as well.

In response to hypoxia, stabilised HIF induces an adaptive transcriptional response that results in the upregulation of a number of factors involved in the activation of the angiogenic switch [67, 68]

The elevated levels of hypoxia and subsequently HIF that are characteristic of tumours have been observed to correlate with poor prognosis [179].

Other factors that are involved in the regulation of the angiogenic switch include metabolic rewiring of endothelial cells which contributes to an acidic tumour microenvironment, alterations to the genes that control the production of the regulators of angiogenesis, mechanical stress and inflammatory cell infiltrate [177 180].

As with the other hallmarks of cancer, the factors that are involved in triggering angiogenesis have also been found to be tumour and tissue specific and vary in expression depending on the stage of tumorigenesis [181].

VEGF and angiogenesis

One of the most potent pro angiogenic effectors of angiogenesis is the VEGF signalling pathway [182 183]. VEGF is upregulated and overexpressed in a multitude of malignancies, and is directly regulated by both HIF activity and also by growth signalling pathways [179].

Activated VEGF signalling results in endothelial proliferation, survival, migration and differentiation in addition to the facilitation of vascular permeability [3 182 184].

Multiple VEGF independent signalling pathways exist which can either work in a complimentary, independent or compensatory manner. Furthermore, anti-angiogenic factors that act to oppose angiogenesis and which present other susceptible targets, stand on the other end of the angiogenic balance [185].

Anti - angiogenic treatment

Treatment of cancer by means of interfering with tumour angiogenesis as proposed by Judah Folkman almost 45 years ago, forms the basis of cancer treatment routinely used by oncologists [186] [173]. Although much still remains to be found out on when and how to use this treatment precisely [151] [187].

It has been shown in a variety of pre-clinical models that blocking tumour angiogenesis could present an effective treatment option in the treatment of all solid tumours. Indeed, a number of anti-angiogenic agents whose use alone pre clinically have been shown to inhibit angiogenic factors, producing anti-tumour activities [188]. That said, use of these inhibitors in the clinic have produced rather disappointing results [187] [189] with very few benefits being seen in most patients in which angiogenic inhibitors have been used alone [190].

From a mechanistic point of view, it's very challenging to understand these differences seen between mouse model studies and human cancer patients. In addition to this, most of the anti-angiogenic agents available clinically, work primarily by targeting an anti VEGF component as tumours may stimulate the production of anti VEGF factors, resulting in the upregulation of angiogenesis [191].

Therefore while a small cohort of patients will respond to anti VEGF therapy, the majority of patients however, being intrinsically resistant to these anti VEGF agents, will not [192].

In a majority of pre-clinical tumour models, the anti-tumour effect of anti-angiogenic targets is determined by means of assessing the inhibition of tumour growth [188].

Tumour size however, is not an entirely accurate measure of survival, as large tumours may not necessarily corelate with shortened lifespan [193] rather metastasis itself, is most likely to be the most common cause of cancer related deaths [194].

Cancer invasion and metastasis occurs early on in tumorigenesis [195] depending on the type of neoplasia [69] . In rare cases, metastasis is usually the first sign of malignant disease with primary tumours remaining undetectable [196] [197]. In some tumours, dissemination of cancer cells from primary sites, early on in tumour development most likely occurs when the tumour is microscopic in size [192].

Studies in zebrafish have supported this understanding, with cancer cell intravasation being found to occur when the primary tumour only had a few hundred cells [195] [196].

Furthermore, it has been observed that small intravasation of cancer cells occurs through the vessel walls of neighbouring pre - existing vessels rather than angiogenic ones [192]. Therefore, with primary tumours lacking angiogenic phenotypes, treatment with anti-angiogenic drugs would have a limited effect on cancer cell intravasation.

The lack of pre - clinical models that truly mimic clinical situations in patients is something that needs to be addressed in order for studies to yield more reliable results that are applicable in the clinical setting [198] [199].

Small compound-based anti – angiogenic drugs

Anti-angiogenic drugs fall into two classifications, protein based and chemical based anti-angiogenic drugs [191]. Both types of drug target the VEGF signalling pathway but exhibit different responses. The antibody based drugs such as Bevacizumab, are the most commonly used and they act by binding specifically to epitopes of target molecules [200] [201].

Despite the fact these antibodies are specific in their binding to target antigens, neutralisation of a shared target potentially blocking functions of multiple angiogenic factors. For example, ramucirumab, binds specifically to VEGF 2 receptor, in so doing blocking its interactions with VEGF – A, VEGF -C, and VEGF -D. In contrast, bevacizumab acts only on VEGF – A without interfering with other signalling pathways [192].

Small chemical compounds on the other hand, are not as specific. Tyrosine kinase inhibitors (TKIs) are the most commonly used, and they work by blocking VEGFR mediated pathways and act on a broad spectrum of kinases [202]. Examples of these TKIs include, sunitunib, sorafenib and pazopanib [192] which all target VEGFR1, VEGFR2, VEGFR3 signalling pathways. In addition to this, these inhibitors also block a variety of other receptors related to angiogenic pathways but which are not necessarily part of the VEGFR family such as platelet derived growth factor and fibroblast growth factor receptor families [203].

Non angiogenic growth in tumours and the case for co-option

Contrary to the assumption that inducing angiogenesis is a hallmark of cancer, several non - angiogenetic modes of tumour vascularisation have been discovered, and although these modalities are given less attention, they play an important role in understanding tumour vascularity and similarly aid in rational drug design.

Co-option growth patterns in lung metastases

An increasing body of evidence from histopathological studies, clinical trials and animal models has uncovered an additional layer of complexity, that is that some malignant tumours grow in the absence of neo angiogenesis by means of co-opting pre-existing vasculature [204].

This observation was first detected clinically in non-small lung carcinomas. It was shown in this non angiogenic subtype that cancer cells only grew within the alveolar air spaces [205] [206] [207]. Facilitating the intact alveolar walls to be incorporated into the tumour and allowing to the tumour to co-opt the alveolar capillaries contained in the alveolar walls [205].

A similar pattern has been observed in cases of human lung metastasis [208] [209] . In addition to this, pre-clinical studies of tumour vascularisation in lung metastasis highlighted co-option of alveolar capillaries facilitated by tumour cells occupying the alveolar air spaces [210].

In the case of lung cancer metastases, histopathological studies carried out on 164 human lung metastases show three distinct mechanisms of vessel co-option [211]. Four histological growth patterns (HGP's) have been described: the alveolar HGP, the interstitial HGP, the perivascular cuffing HGP and the pushing HGP [211]

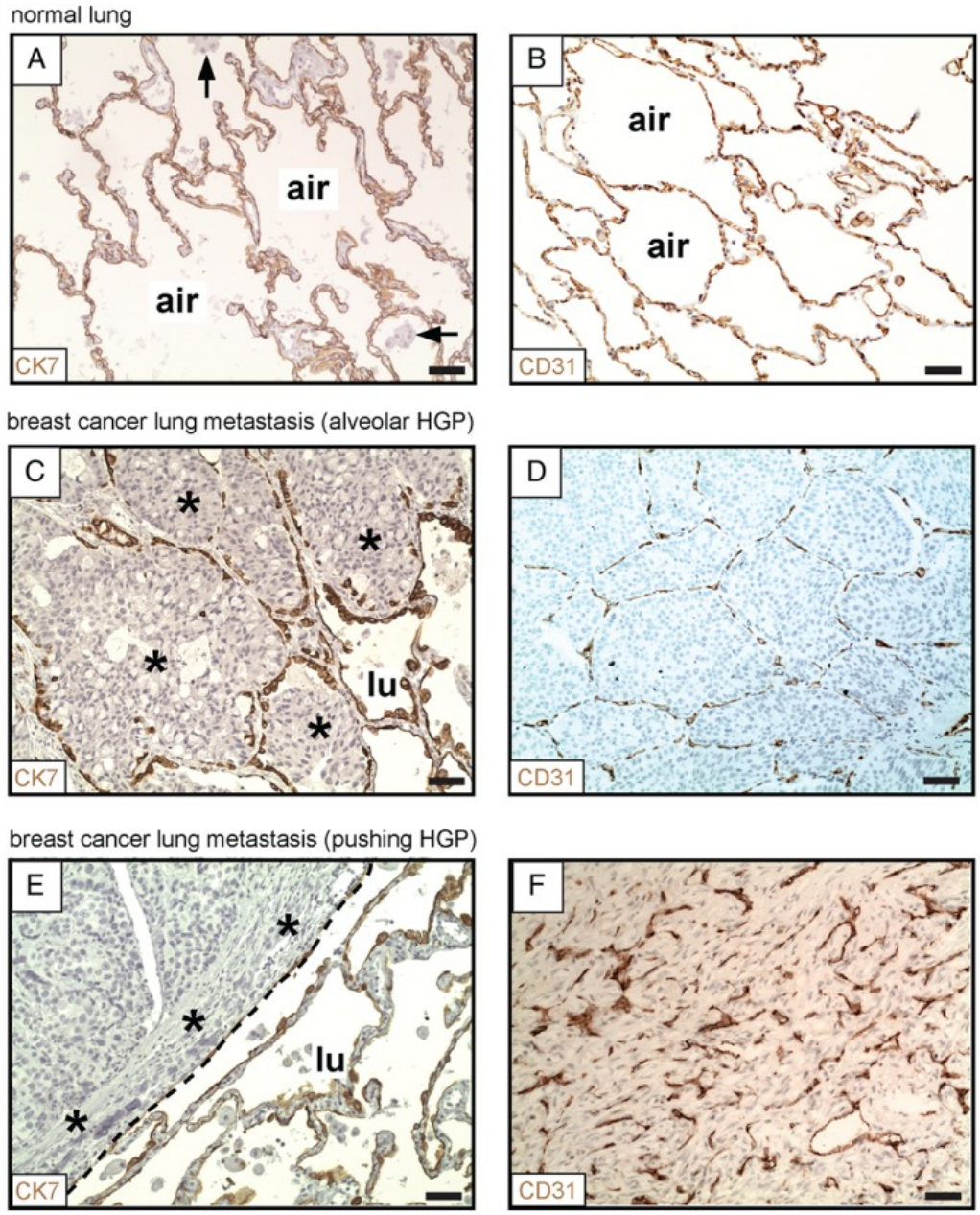


Figure 2: Alveolar and pushing growth patterns of human lung metastases: (A, B) Normal lung parenchyma stained for CK7 (A) or CD31(B). (C, D) Alveolar HGP of breast cancer lung metastasis. Staining for CK7 is shown in (C). Staining for CD31 (within tumour) is shown in (D). (E, F) pushing HGP of human breast cancer lung metastasis. Staining for CK7 at tumour interface is shown in (E). Staining for CD31 (within tumour) is shown in (F). Cancer cells: asterisks. Alveolar macrophages: arrows. Alveolar air space: air. Tumour lung interface: dashed line. Normal lung: lu. Scale bar: 50 μm

Figure and caption taken from: J Pathol.2017 Vessel Co-option is common in human lung metastasis and mediates resistance to anti angiogenic therapy in pre-clinical lung metastasis models.

The alveolar HGP is defined by the incorporation of intact alveolar walls into lung metastases, with tumour vessels being found to resemble vascular architecture of normal lung, thus suggesting these tumours co-opt pre-existing alveolar capillaries by growing within the alveolar air spaces [205] [211].

In contrast, the pushing HGP was found to contain abnormal, disorganised and chaotic vessels, typical of vessels generated by tumour angiogenesis [211] .

In the Interstitial HGP, cancer cells were seen to co-opt alveolar capillaries by means of growing within the alveolar walls of the lung [211]. However, with this particular HGP it was noted that angiogenic patterns were observed especially towards the centre of the metastasis [211].

Co-option can also exist in the form of a perivascular cuffing HGP. This mechanism involves cancer cells growing exclusively like a cuff around the larger vessels of the lung, as opposed to the smaller capillaries. As a result, cancer cells can therefore utilise the central co-opted vessel as their main supply in this growth pattern [211]

These studies confirm that tumours can exhibit a mix of both angiogenic and non-angiogenic phenotypes which are commonly seen, adding further to the complexity [205].

It is thought that both angiogenesis and co-option initiate microtumours in distinct ways, with the former being responsible for exponential growth and the latter being an essential and important alternate mechanism for the survival of cells [212].

Drug resistance in the context of anti-angiogenic therapy

It was originally believed that anti angiogenic agents would not infer drug resistance especially since the endogenous inhibitors such as angiostatin and endostatin for example, act on endothelial cells rather than tumour cells [213] [214]. Furthermore, endothelial cells were understood to have stable genomes and utilisation of drug resistant mechanisms was thought to be uncommon [192].

However, both experimental and clinical studies have shown that endothelial cells contain abnormal genomes, not found in healthy vasculatures [215].

What remains unclear is the mode of transmission of this aberrant genomic material, whether it is transferred from the tumour or is part of an intrinsic instability in endothelial cells [192].

Inhibiting tumour angiogenesis has the capacity to change both cellular and molecular aspects of the tumour microenvironment, resulting in drug resistance. An example of this has been demonstrated where in which anti angiogenic treatment resulted in in the creation of tissue hypoxia in the local microenvironment, as a consequence of vascular induced regression. This was found to increase the expression levels of a number of angiogenic factors unrelated to the drug targets [202] [216].

Furthermore, anti – VEGF agents disrupts the balance of various cellular components, including inflammatory cells and stromal fibroblasts, both of which are central sources of cytokines as well as non-angiogenic factors. Thus, contributing further to drug resistance [192] [217] [218].

Other mechanisms that contribute to drug resistance include, the selection and overgrowth of hypoxia resistance tumour cell variants which function independently of angiogenesis [219], tumour vessel re modelling[220] as well as the recruitment of bone marrow derived angiogenic cells [221].

Studies have also pointed to the potential role of molecular interactions involving integrins as well as receptor tyrosine kinases (RTKs) [222].

These modes of resistance all point towards the importance of combination therapy. In addition to understanding the cross talk and synergistic effects of different angiogenic signalling pathways, such that a number of angiogenic factors and pathways can be targeted in a dynamic fashion, at once.

Co-option and its role in drug resistance

It has been hypothesised that co-opting vessels elicit resistance in response to anti-angiogenetic therapy [181] [223] [224]. Vessel co-option has been reported as a mechanism of resistance to anti angiogenic drugs in glioblastoma [225] [224], hepatocellular carcinoma [226] , lymph node metastases [227], liver metastases[228] and brain metastases [229].

Moreover, it was shown that in animal models, inactivation of p53 was found to result in resistance to anti angiogenic therapy by enabling cells to survive despite the hypoxic environment [219].

A pilot study based on this observation was therefore carried on a small set of lung cancers where in which an increase in the level of p53 mutations in non- angiogenic tumours was observed[230] . Thus, implicating inactivated p53 as a possible mechanism by which neoplastic cells could grow without initiating neo angiogenesis.

The same lung metastasis study that characterised the three growth patterns of co-option in lung metastases also attempted to investigate drug resistance in lung metastasis. In the pre-clinical syngeneic renal cancer tumour model of lung metastases (RENCA), the pushing HGP (corresponding to an angiogenic phenotype) was predominant [211].

In sunitinib treated mice however, the alveolar/ interstitial growth pattern was found to be prevalent. The situation in this model of lung metastasis was therefore more complicated in that a mix of pushing HGP metastases and alveolar/ interstitial HGP metastases was found[211].

Interestingly when vessel density was compared between a vehicle group and sunitinib treated mice, vessel density was found to be lower in the pushing HGP RENCA lesions however, no significant difference was noted with the alveolar/ interstitial HGP RENCA lesions. It was proposed that this may provide a mechanistic reasoning for why sunitinib elicits only a modest effect on tumour burden in the RENCA lung metastasis model [211].

Other alternate modes of angiogenesis

Another alternative mode of vascularisation termed Intussusceptive microvascular growth (IMG) or splitting angiogenesis, has been reported in a variety of tumour types [231].

IMG is a process which facilitates the expansion of the capillary network within itself, by means of allowing existing vessels to split into daughter ones. The advantage of this mechanism is the capillaries formed are less leaky and the vessels are formed more rapidly [232].

Since IMG has been observed to form faster, more energy conserving and more physiological permeable vessels compared to the sprouting mechanism, it is thought that it potentially serves as either an adaptive response in restoring tumour vasculature hemodynamic homeostasis or another way in which tumours can escape the effects of anti - angiogenic therapy [231] [233].

Although IMG has been linked to sheer stress and blood flow, no molecule has yet been directly associated with this mechanism of vascular splitting, to date [231] [3].

In addition to angiogenic sprouting and IMG/ angiogenic splitting, vasculogenic mimicry (VM) presents yet another mechanism employed by almost all major types of malignancies [234] and which has been observed to correlate with poor prognosis [235].

VM confers a characteristic functional plasticity to tumour cells, such that cells are able to express a stem cell like phenotype, resulting in the production of new vascular networks [232] [234]. VM thus provides a functional advantage, facilitating the survival and maintenance of aggressive tumour phenotypes.

Biological experiments have highlighted the presence of physiological flow within VM networks as well as anticoagulant properties of the cancer cells lining VM channels, with these features being found to promote perfusion [236].

Hypoxia seems to be a critical driver of VM, however other molecules and pathways are currently being pursued [234].

Clinical pathology of angiogenesis

The newly acquired tumour vasculature differs from the normal one in many ways. Sprouting tumour vasculature is often described as being leaky, with endothelial cells forming irregular monolayers and loose associations with pericytes as well as a characteristically irregular basement membrane [237] [177].

The chaotic blood flow in these vessels induces areas of hypoxia and acidosis, resulting in a stress response, potentiating angiogenesis, increasing the likelihood of resistant clonal expansion, and lowering therapeutic efficiency [3].

From clinico – pathological studies it has been shown that stage 1 non angiogenic tumours have a worse overall and disease free survival, compared with their angiogenic counterparts [205] [238].

Interestingly, it was also found that micro vessel density had no prognostic value in this group of patients [239]. In addition to this, lung metastases were observed to grow in a non-angiogenic fashion[209] despite the primary tumour exhibiting an angiogenic phenotype (Breast Cancer Progression Working Party, 2000).

This observation questioned the grounds upon which angiogenesis is linked to progression of disease and highlighted that the angiogenic switch can be reversed during disease progression. Immunohistochemical studies which looked into the expression of LH39 (an epitope present in the basal membrane of mature vessels) and aVb3 (overexpressed in newly formed endothelium) confirmed the absence of newly formed vessels and the persistence of pre-existing lung vasculature demonstrating that vessels observed in the non-angiogenic tumours exhibited the same phenotype as that of the normal lung [240].

Furthermore, a three-dimensional reconstruction of normal tissue when compared to that of lung carcinomas confirmed that the vasculature infrastructure of the non-angiogenic tumour could not be distinguished from that of the normal tissue[230].

To this end, despite the immense research that has been carried out with anti-angiogenic drugs our understanding of vessel co-option and thus non angiogenic tumours, remains limited.

The molecular characterization of non-angiogenic growth

Although a lot of effort and work has gone into defining non angiogenic growth from a histological growth pattern perspective, it has been more challenging to identify the molecular mechanisms underpinning the signalling pathways that facilitate tumour vessel co-option.

Non angiogenic growth patterns have been observed in a number of tissues including intra alveolar growth in the lung, hepatocyte replacement in the liver and parenchyma infiltration in the brain.

Studies in mice and humans have highlighted the significant contribution of non-angiogenic tumour growth [241]. This alongside more recent studies support the notion that non angiogenic tumours are one of the causes of resistance to anti- angiogenic drugs. Thus, indicating how essential it is to target both angiogenic and non-angiogenic vessels when it comes to therapeutic intervention in the setting of cancer [242].

Different patterns of non-angiogenic growth suggest that different underlying biological mechanisms may be at play and that these mechanisms are likely to be tissue type dependant.

Thus, to characterise and investigate this phenomenon further, the basic characteristics of neoplastic growth by vascular co- option in primary non-small cell lung carcinoma was examined.

The findings of this characterisation were not striking, with only minor differences being found in necrosis; with angiogenic tumours having more necrosis while chronic inflammation and fibrosis predominantly characterised non angiogenic tumours. No differences were observed in micro-vessel density and apoptosis [230].

Immunohistochemical based studies failed to highlight any major difference in both expression markers of angiogenesis and hypoxia, with the only exception being stromal thrombospondin - 1 (TSP1), which was found to be close to absent in non -angiogenic tumours but present abundantly in the angiogenic sub type [230].

Furthermore, mRNA expression profiling by microarray studies confirmed that no differences in classic hypoxia or angiogenic pathways were found, with the exception of TSP1, once again. Thus, supporting the hypothesis that activation of classic hypoxia pathways is not enough to induce angiogenesis[230] .

In context of angiogenic versus non angiogenic tumour growth, the increase in expression of TSP1 was thought to serve an anti-angiogenic role, however elevated levels of TSP1 found in angiogenic neoplasms [230] contradicted this theory. As a result, the relevance of TSP1 may be dependent on its differential localisation within the tumour mass, as opposed to its level of expression in tumour cells [243].

What was interesting to note however, was the increased expression of a set of genes linked to oxidative phosphorylation in non - angiogenic tumours which gave rise to the premise that metabolic reprograming may be the underlying cause for this difference in non - angiogenic tumours [230].

Gene expression profiling

Gene expression profiling analysis has also helped to shed some light on the angiogenic versus non angiogenic conundrum. Human cancer biopsy samples and human brain tumour xenografts in nude rats [244] [245] highlighted and confirmed the link between the non-angiogenic phenotype and the PI3K – AKT and WNT pathways.

It was also found that activation of the hepatocyte growth factor receptor (MET) was elevated in response to a decrease in VEGF levels [246] [247].

Importantly, Inhibition of both VEGF AND MET signalling pathways reversed the non-angiogenic phenotype from invasive to non-invasive [246] [247].

It was also noted that total and phosphorylated MET in addition to markers of hypoxia, glucose transporter (GLUT1) and carbonic anhydrase 9 (CA9) were also elevated [248] [249].

In contrast, levels of T cadherin (cadherin 13) and E cadherin (cadherin 1) were abolished, resulting in the non-angiogenic cancer cells being less adherent with the increased likelihood to invade [246] [247] [171].

The role of the EMT, signalling pathways and dynamic changes in focal adhesion

The implication of the PI3K and WNT pathways in non-angiogenic tumours [250], namely glioblastomas, suggests roles in focal adhesion and subsequently involvement in dynamic changes in adhesion status. Likewise, the association with WNT pathway potentially links increased motility and migration of non-angiogenic tumour cells as well as the probable involvement of the EMT, resulting in the loss of adhesion, an association with an increase in N cadherin (cadherin 2) and vimentin conveying a more invasive phenotype [251].

These studies along with others, are forming the basis upon which emerging models of angiogenesis versus co-option are founded on.

The role of adhesion

In addition to this, a decrease in the level of a set of adhesion molecule genes in the same tumours were noted, suggesting that perhaps diminished cell to cell contact might be implicated in the inability to form a vascular infrastructure[245]

The role of vessel co – option in metastasis, motility and stromal remodelling

Vessel co - option has also been implicated in the preliminary stages of metastatic seeding. Kienast et al [252], demonstrated by means of multiphoton laser scanning that proliferation of brain metastases was heavily dependent on the ability to co - opt.

In a model described by Raymond et al [253] metastatic cancer cells were observed to extravasate from blood vessels by firstly attaching to endothelial cells, resulting in the breaking of their junctions, causing endothelial retraction and then embedding themselves in the endothelial monolayer between endothelial cells in a process known as intercalation.

The authors went on to further demonstrate using a lung metastatic lung mouse model, the critical role CDC42 plays in extravasation via inducing transcription of B1 integrin. B1 integrin was found to be required for adhesion of cancer cells to endothelial cells and its blockage was shown to impair adhesion of cancer cells to the basement membrane as well as preventing colonization and subsequently metastases [171].

Following on from the study on the U87 glioma cell line, which implicated IRE1 upregulation as an initiator of angiogenesis, Auf et al [254] compared the U87 wild type glioma cell line which promotes angiogenesis in the CAM assay with its non - angiogenic counterpart where IRE1 was silenced.

From this comparative study he was able to show that IRE1 is involved in the upregulation of VEGFA, thus highlighting that there are other pathways apart from hypoxia that determine whether a tumour will adopt angiogenesis or choose to employ vessel co – option [254].

Once VEGFA binds to VEGFR2, the PI3K – AKT pathway is upregulated in angiogenic cells [230 245]. The initiation of the PI3K – AKT pathway is maintained by elevated levels of integrin expression, which is further stimulated in the presence of VEGFR2 expression [255].

Independent analysis of the differentially regulated genes from the non-small cell lung cancer study [245] and the Auf et al study [254] have revealed the involvement of the PI3K pathway in angiogenesis and stromal remodelling.

This was found to be achieved, by activation of integrins promoting cell adhesion and inhibition of actin production, preventing motility [230 245].

In the non-angiogenic cells however, the PI3K -AKT pathway has been observed to have a role in conjunction with the canonical and non-canonical WNT pathways. These signalling pathways however, have been shown to be connected with alterations in cell motility and invasion as opposed to angiogenesis and stromal remodelling [254] [171].

Another striking difference between angiogenic and non-angiogenic growing tumours is that angiogenic tumours have been shown to eradicate existing components of the infiltrated organ, whereas non angiogenic co-opting tumours maintain these pre - existing networks [205].
Interactions between cancer cells and the associated stroma are important in determining a tumours ability to invade and metastasise. There is an increased body of evidence, which points to non-angiogenic cancer cells being increasingly motile and invasive.

Insights from primary brain tumours

Much of our understanding about vessel co – option is based on studies carried out on primary brain tumours which have shed some light on the molecular underpinnings that direct angiogenic versus not angiogenic tumour growth, the affinity of cancer cells to pre - existing vessels, and the mechanisms that facilitate attachment of cancer cells to co – opted vessels.

In both a mouse transplant model and a chick embryo chorioallantoic membrane (CAM) model of glioblastoma, inositol requiring enzyme (IRE1) which acts as essential regulator of the unfolded protein response and a proximal endoplasmic reticulum detector of stress signalling was found to be critical in directing the type of blood supply utilized by tumours [254].

Furthermore, it was observed in U87 wild type glioma cells tumours grew as a distinct angiogenic mass whereas in IRE1 silenced U87 cells tumours developed as non- angiogenic infiltrative tumours that were found to co -opt existing vessels. IRE1 levels were dictated by interleukin 6 (IL -6) whose activity was inhibited as a result of IRE1 silencing [254].

Transfection of IRE1 silenced U87 cells along with IL-6 reverted the blood flow back to an angiogenic phenotype, while preventing co - option from occurring [254].

IRE1 missense mutations have been observed in gastric adenocarcinomas. glioblastomas and lung adenocarcinomas to name a few however, there are no studies of human tumours that further validate IRE1 mutations and their association with angiogenic patterns [256].

Clinical trials for Anti-angiogenic drugs

The importance of tumour vascularisation in the development of tumours and likewise metastases, has been well established [173]. Interrupting the process of tumour vascularisation, specifically the VEGF pathway, therefore presented a promising therapeutic option initially, when focusing on metastatic disease [257].

The most widely studied strategy in anti - angiogenic treatment, involves the blocking of vascular endothelial growth factor (VEGF), namely VEGFR-A and its pro angiogenic mediated signals. Inhibitors of the VEGF pathway are the most clinically advanced at present, with a number of approved inhibitory agents in use, as well as those undergoing further evaluation [258].

The VEGFR-A targeted monoclonal antibody bevacizumab, is considered to be the pioneer amongst this group of inhibitors [259] [260].

Bevacizumab was FDA approved for use in breast cancer in 2008 (colorectal cancer in 2004) and was shown to almost double progression free survival when combined with chemotherapy, compared with chemotherapy alone [261].

However, much like other anti VEGF drugs, the effect of bevacizumab in other breast cancer trials, was found to be modest with no effect on overall survival, resulting in withdrawal of FDA approval for use in breast cancer. It is still approved for single and combination use, in the treatment of a variety of other advanced cancer types/stages such as nonsquamous non-small cell lung cancer, ovarian cancer, recurrent glioblastoma and metastatic renal carcinoma [261].

Other strategies that target the VEGF signalling pathway involve blocking growth factor receptors and signal transduction with the use of tyrosine kinase inhibitors (TKI). Inhibition can be multi targeted and includes targets such as the VEGF receptor, platelet derived growth factor (PDGF) receptor, tyrosine kinase (KIT) receptor and mesenchymal - epithelial transition factor (cMet) [262] [263] [264] [265]. Sunitinib and sorafenib, are examples of this type of inhibitor and have been approved for single therapies, which include treatment of pancreatic cancer, gastrointestinal stromal cancer, hepatocellular carcinoma and renal cell carcinoma respectively [266] [267].

Similarly, agents with similar targets but better toxicity profiles, have been developed and are known as second generation multi kinase inhibitors, as they can target several TKI's involved in tumour angiogenesis, oncogenesis and tumour microenvironment [261].

Examples of these include Regorafenib, which is approved for treatment of metastatic colorectal cancer, gastrointestinal stromal tumours and hepatocellular carcinomas [268].

In addition to the aforementioned types of anti-angiogenic inhibitors, anti VEGFR antibodies such as ramucirumab, a human monoclonal antibody that blocks ligand binding of the VEGF to the VEGFR2 receptor, have also undergone clinical investigation [269].

Inhibitors of the VEGF pathway, have also been investigated in both the adjuvant (post-surgical) and neoadjuvant (pre - surgical) settings. Adjuvant clinical and pre-clinical studies have highlighted the lack of efficacy of VEGF pathway inhibitors in the adjuvant setting, whereas the use of bevacizumab alongside chemotherapy in the neo adjuvant setting shows more promise [270] [271].

Despite the partial success of VEGF targeted therapies in cancer, patients can either develop intrinsic resistance to treatment, or undergo acquired resistance after observing transitionary benefits. This observed resistance to the use of anti-angiogenic agents can differ according to the inhibitor used, the type of cancer and the metastatic setting [261].

It is worth noting that in clinical trials, it has been reported that patients with non-angiogenic tumours, developed more metastases in comparison to those patients whose tumours were angiogenic. In addition to this, the non-angiogenic phenotype was found to corelate with poor prognosis [205].

Subsequently, investigations in preclinical tumours models have highlighted that disabling the VEGF pathway, can lead to a switch from angiogenic to non-angiogenic tumours wherein which the cancer cells were observed to be more motile and invasive [211 226 272 273 274246 247 275].

Thus, the partial effect of angiogenic therapies, alongside the wide-ranging mechanisms that can result in intrinsic and acquired resistance, has led to the development of innovative drug combination strategies [261].

For example, combining anti-angiogenic treatments with other compounds that target other major biological processes (e.g. apoptosis) as well as other treatment approaches such as, DNA repair inhibitors and immunotherapy has been reported to improve efficacy in many experimental and human settings, [276].

Of particular interest is the critical role VEGF plays in modulating immune suppression. It has been noted that tumour vasculature is a critical co- regulator of the immune system with different anti angiogenic pathways converging alongside anti-tumour immunity processes, through a variety of mechanisms [277]. In patients with colorectal cancer, bevacizumab increased the antigen presenting capacity of dendritic cells, highlighting an alternate function for bevacizumab in the context of check point inhibition [278].

In addition to this, a correlation was observed between high levels of VEGF and a decreased overall survival in advanced melanoma patients treated with ipilimumab, an anti CTLA4 antibody [279].

This points to the potential positive impact VEGF blockade may have on the immune processes that control the anti-tumour response, presenting the opportunity to exploit anti-

angiogenic inhibitors, along with molecules involved in regulating innate and adaptive immunity [261].

Furthermore, the lack of precise therapeutic anti angiogenic interventions also highlights the importance of establishing reliable markers that monitor anti angiogenic drug activity and predict responder and non-responder patients [280 281].

1.3 Transcriptional approaches to biomarker discovery

High throughput sequencing technologies have facilitated the detection of protein coding RNA's (mRNA being one example). mRNA's, are the first type of RNA biomarker that were well studied and differential expression of which was applied to disease states. RNA sequencing has emerged as a powerful tool in transcriptomics, gene expression profiling and biomarker discovery.

The field of transcriptomics has provided researchers invaluable insights into gene expression patterns which has facilitated the identification of novel drug targets and the measurement of expression of fundamental disease biomarkers allowing researchers to obtain expression snapshots of entire genomes.

1.4 Metabolomics analysis for biomarker discovery

The last few decades has seen a change in biomedical research, with whole genomic, transcriptomic, proteomic and metabolomic studies taking the forefront when it comes to biomarker discovery [282]. The comprehensive analysis of all metabolites in a system, known as metabolomics is a more recent advancement in the omics field [282]. Metabolites play an important role in biology and the understanding of the biochemical pathways disrupted in disease [283]. Compared to classical diagnostic approaches and more conventional clinical

biomarkers, metabolomics presents advantages in both sensitivity and strength and therefore shows great potential in clinical/health settings, as a biomarker discovery tool.

1.5 The role of proteomics in biomarker discovery

The use of mass spectrometry in molecular biology and human genetics has undergone rapid advancement. Mass spectrometry techniques, alongside bioinformatic analysis has provided a powerful tool to pursue biomarker research.

Omics technology which culminates mass spectrometric analysis and bioinformatics, the results of which are then compared to the human proteome library have improved our understanding of disease, contributing greatly to biomarker discovery.

In addition to this MS technology has provided a robust method to study post translational modifications, protein abundance, subcellular localisation in both a dynamic and unbiased manner and link these findings to disease states.

Label free quantification

Label free quantification involves no pre-sample prepping or manipulations prior to MS analysis. For this reason, it considered to be a simpler approach in comparison to label based methods. It has as a result reduced complexity and a greater dynamic range, providing increased protein coverage [284].

Recent developments in MS software analysis for quantification has meant label free quantification is becoming an increasingly preferred option when it comes to proteome studies owing to the more robust quantification it provides in comparison to what the method was able achieve previously [284].

Proteomic analysis of Laser Capture Micro dissected tissue (FFPE)

To study tissue specific protein expression profiles, an isolation of the source tissue is required. Laser capture microdissection (LCM) technology facilitates the isolation of cell of a specific morphology, identified by microscopic examination. It helps to reduce the problems associated with tissue heterogeneity observed in homogenates of entire tissues [285] [286].

Acquiring reliable tissue specific protein profiles from tissue samples represents a major advance in research. That said, the complexity of the process of isolating specific areas from formalin fixed samples by (LCM), collecting enough tissue material, and maintaining tissue and protein integrity remains relevant methodological challenges.

Application of proteomics in understanding vascular states in cancer

Applying proteomics to in – vitro and in vivo models of angiogenesis is a relatively unexplored application and despite the recent advances made in both field, proteomic methods are still poorly exploited in the study of angiogenesis [284].

Undoubtedly, this approach has a great potential to significantly expand and impact on the current knowledge of the complexities and dynamics of tumour vessel growth, as well as open new perspectives in the context of disease states such as cancer.

1.6 Project objectives

Consequently, and by means of a vessel co-option model developed in mice, by Andy Reynolds in the ICR, London; I hope to embark on this very challenging yet highly interesting investigation into understanding this phenomenon of co-option in the context of lung metastases in more depth.

In so doing, I hope to uncover the mechanisms driving this behaviour, which in turn will generate new therapeutic approaches to tackling these resistant tumours, ultimately closing the gap between bedside and bench top research.

In this project I use a multi omics approach in order to better understand the molecular mechanisms that differentiate between classic angiogenesis and vascular co-option, with the hope to shed more light on new potential molecular targets and biomarkers that have yet to be discovered.

By exploiting the mouse model of co-option established by A. Reynolds, I aim to expand on what is currently known about anti- angiogenic drug resistance in the context of co-option in lung metastasis by carrying out the following:

1. Characterisation of the in – vitro cell lines.
2. Performing proteomics, transcriptomics and metabolomics on the in vivo xenograft.
3. Revealing potential molecular signatures that are associated with the in vivo tumour behaviour, i.e. whether the tumour remains dormant or undergoes growth (angiogenic or non-angiogenic).

Chapter 2 Experimental Procedures

2.1 General reagents

General reagents met the criteria of the purity standard and were purchased from Sigma Aldrich and Thermo Fisher apart from TRIzol™ which was purchased from Invitrogen. Buffers and solutions were prepared with ultra-pure water obtained from the water purification system Purelab option DV25 and optionally sterile filtered through 0.2um membrane filters.

2.2 General cell culture techniques

786 and 6450 cell lines were cultured in RPMI medium (containing 5% L – Glut) supplemented with 10% FBS (heat inactivated fetal bovine serum) (Gibco) and 5% Pen Strep (Sigma) under humidified atmosphere of 5% CO_2 at 37^{o}C. In the case of the starvation experiments, cells were cultured in RPMI medium (without D – glucose) (Sigma) and RPMI medium (without L – Glutamine) (Sigma). Low pH medium (6.7) was made using supplemented RMPI medium with added HEPES (sigma). 1M HEPES was made and added to normal supplemented RPMI medium until pH 6.7 was achieved. Medium was then filtered using 0.2um membrane filter before use with cells.

For cell counting purposes the Scepter™ 2.0 Cell Counter from Merck Millipore was used. Cells were typically passaged when reaching 80-90% confluent or as required. Cells were passaged by removing growth medium, washing gently with Dulbecco's Phosphate Buffered Saline (Sigma) and then detached using 0.5% Trypsin/EDTA (Sigma) at 37 ^{o}C, 2-4 mins.

Trypsin was then inactivated by addition of fresh FBA containing growth medium. The cell suspension was transferred into a 15ml Falcon tube and cells were spun down at 500xg 5mins. Finally, the trypsin containing medium was aspirated, cells were re suspended in fresh growth medium and transferred into a new flask for general maintenance.

Cyro – conservation and thawing of cells

For cyro conservation, 2-4x 10^6 cells were grown to log phase, were re suspended in 1.2ml of growth medium containing 10% FBS and 10% DMSO, transferred to cryo- vials (Greiner bio-one) and slowly cooled down over 24-48 hours at -80 ^oC using a Mr Frosty^{TM} Freezing container (ThermoFisher). Afterwards, cryo-vials were transferred to the -170 ^oC liquid nitrogen tank for long term storage.

For recovering cells from frozen stocks, cryo – vials were quickly thawed in a water bath at 37^oC. After thawing, cells were instantly transferred into 10 ml of pre-warmed supplemented growth medium and then spun down (500xg 5 mins) for DMSO removal. Finally, cells were re suspended in supplemented medium into appropriate cell culture flasks.

Preparation of cell lysates

Cell lysates for western blot analysis were prepared as follows: After generating the cell pellet by trypsination and centrifugation (500xg for 5mins) cell pellets were washed once with PBS and then either stored at -80 ^oC until further processing or were directly lysed in RIPA lysis and extraction buffer (Pierce) containing cOmplete^{TM} protease inhibitor cocktail for 30 mins on ice. Cell debris were removed by centrifugation 10,000xg, 30 mins, 4 ^oC and the resulting supernatants were transferred to fresh eppendorf tubes.

Protein concentrations of the lysates were then determined using Pierce^{TM} BCA protein assay kit (ThermoFisher) according to the manufacturer's instructions. Following this assay, samples were either used for further analysis or stored at -20^oC.

2.3 mRNA preparation

Prior to RNA extraction, all surfaces and materials used were cleaned with 70% EtOH and RNaseZap RNase decontamination solution (Ambion) 1ml Tryzol was added to tissue samples on ice and under the hood. Tissue samples were homogenised in TRIzol™ using the thorax handheld tissue homogeniser (Omni TH) adjusting speed according. Samples were placed on ice intermittently in between homogenisation to prevent overheating. The Homogeniser was washed after use with 1% SDS (1x), Milli-Q water (2x) and 96% ethanol (1x) before homogenising the next sample. Tubes containing washing reagents were discarded and replaced after use on each sample. Once the tissue was homogenised the TRIzol™ Invitrogen reagent protocol was followed. Subsequent RNA clean-up was carried out using the Qiagen RNeasy® Mini kit. Care was taken while carrying out RNA work to ensure RNase free tips, tubes and water was used at all times and that samples were kept on ice when required. Samples were submitted to the single cell facility at the WIMM, Oxford University for sequencing. RNA extraction carried out on cells was done in the same way with cells pellets with resuspension rather than homogenisation.

2.4 Western blotting and immunodetection of proteins

Western blotting and immunodetection of proteins were carried out following the western blot analysis guidelines by Li-COR Biosciences. After protein separation by SDS -PAGE, proteins were transferred electrophoretically onto Immobilon – FL PVDF (Merek) membranes (activated with MeOH (p.a.), pore size 0.45 um) for 70 -80 mins 400 mA in WB transfer buffer containing 20mM Tris HCL (pH 8.3), 200 mM glycine, 20 % MeOH (wet western transfer). Transfer was routinely controlled with Ponceau S staining (Sigma) for 1-2 mins which then was subsequently removed by several dH_2O washes. After this membrane were blocked with 5% milk (BLOT -Quick blocker^{TM} Reagent (Calbiochem) in TBS -T (20mM Tris-HCL pH

7.6, 150mM NACl, o.1% Tween -20) for 1 hours at RT. For immunodetection, the membranes were first incubated with primary antibodies prepared in 2% milk/TBS-T or 2% BSA (sigma)/TBS-T O/N at 4^{o}C and then washed four times with TBS-T (5 min per wash) before incubation with secondary antibody for 45-60 mins bat RT, protected from light. Finally, membranes were washed six to eight times (10 mins washes) and protein detection was carried out using the Odyssey CLx imaging system (LI-COR) at the 700 and 800 channels. Precision Plus Protein^{TM} All Blue Prestained Protein Standards (BioRad) were used for sizing the sample proteins.

Antibodies

Target	Antibody ID (Company)	Description
Anti -PKM2	Ab38237 (abcam)	Rabbit polyclonal to PKM2 1/1000
Anti - COX IV	Ab16056 (abcam)	Rabbit polyclonal to COX IV 0.5ug/ ml
Anti - ADAMTS2	Ab125226 (abcam)	Rabbit polyclonal to ADAMTS2 1ug/ml
Anti-L1CAM antibody [2C2]	Ab 24345 (abcam)	Mouse monoclonal [2C2] to L1CAM 1/1000
Anti - Nhe-1 Antibody	PA5-20444 (Invitrogen)	Rabbit polyclonal to NHE1 1-2 µg/mL
Anti – SMAD4 antibody	AF2097 (R&D systems)	Goat polyclonal to SMAD 4 0.25ug

Anti-pan Cadherin antibody	Ab6529 (abcam)	Rabbit polyclonal to pan Cadherin 1/500
Anti-Thrombospondin-1 Antibody	AF3074 (R & D systems)	Goat polyclonal to Thrombospondin 1 1 µg/mL
Anti-Glutathione S Transferase pi antibody	Ab135535 (abcam)	Rabbit polyclonal to GST pi 1/50
Anti-Carbonic Anhydrase II antibody	Ab124687 (abcam)	Rabbit monoclonal [EPR5195] to Carbonic Anhydrase II
All secondary antibodies used were purchased from LI-COR with an IRDye (800nm)	LICOR	Secondary antibodies against the appropriate species (specified above)
Anti-Endomucin antibody	Ab106100 (abcam)	Rat monoclonal [V.7C7.1] to Endomucin
Anti-Rat secondary	P0450 Dako	Rabbit Polyclonal HRP 1/1000

2.5 Metabolomics

Chemicals and metabolic standards

Chloroform and tert-butyl methyl ether were purchased from Fisher Scientific. Methanol and methoxyamine hydrochloride were from Sigma-Aldrich. N-methyl-N-trimethylsilyltrifluoroacetamide (MSTFA) with 1% chlorotrimethylsilane (TMCS) was purchased from Thermo Scientific. Metabolic standards used in this study were purchased

from Sigma Aldrich with the exception of the following ones: cholesterol and pyridine (Alfa Aesar), creatinine (Acros Organics), myristic acid-14,14,14-d_3 used as an internal standard (Cambridge isotope Laboratories) and N-oleoyl glycine (Cayman Chemical) [287]

Metabolite extraction from tissue

Extraction of metabolites was carried out at room temperature if unspecified. The samples were vortexed for 5 min after adding 1 ml of tert-butyl methyl ether (MTBE). The suspensions were shaken for 5 min and centrifuged for 20 min at 13,000g at 4 °C. The organic phase (MTBE) was transferred to a glass vial and dried in a Speed Vac. Subsequently, 800 µl methanol was added into the aqueous remains, the suspension was vortexed for 5 min and centrifuged for 20 min at 13,000g at 4 °C. The supernatant (aqueous) was collected and added into the glass vial containing the organic phase to dry under vacuum. The dried samples were kept at −80 °C until use [287].

13 mg of Tissue was used for the extraction of metabolites. Tissue material was washed twice with ice cold PBS, resuspended in ice cold methanol and H_2O (1:1 v/v) (400 µl) and 5 µl myristic acid-14,14,14-d_3 (1mg/ml), and crude extracts were transferred into a bead beater tube containing washed glass beads (same as tissue piece). Samples were subsequently homogenized in a bead beater (Precellys 24, Bertin Technologies) for four cycles (6500 Hz, 45 s), followed by the addition of 1 ml of tert-butyl ether (MTBE) to extract metabolites [287].

After vortexing for 5 min and centrifugation for 20 min at 13,000g and 4 °C, the organic phase was transferred to a glass vial and dried by Speed Vac centrifugation. To the remaining aqueous phase, 800µl of methanol was added, samples homogenized for one cycle (6500 Hz, 45 s), kept at −80 °C for one hour and centrifuged for 20 min at 13,000g and 4 °C. 1 ml of aqueous phase was added to the glass bead vial containing the organic phase and the samples dried in vacuo (Speed Vac Centrifugation) [287].

Chemical derivatization

In brief, samples were resuspended in a solution of 20 µg/µl methoxyamine hydrochloride in pyridine (50µl/sample) and shaken (1200 rpm) for 90 min at 30 °C. 70 µl N-Methyl-N-trimethylsilyltrifluoroacetamide (MSTFA) with 1% chlorotrimethylsilane (TMCS) and 30 µl pyridine were added to the samples, followed by incubation for one hour at 60 °C at a shaking speed of 1200 rpm. The samples were cooled down to and injected directly for GC-MS analysis [287].

GCxGC-MS analysis

The samples were immediately analysed using a GCxGC-MS system comprising of a gas chromatograph coupled to a quadrupole mass spectrometer (Shimadzu GCMS QP2010 Ultra) and a Shimadzu AOC-20i/s auto sampler as described. The first-dimension separation was carried out on a SHM5MS capillary column (30 m×0.25 mm i.d.×0.25 µm film thickness, Shimadzu) while the second-dimension separation was on a BPX-50 capillary column (5 m×0.15 mm i.d.×0.15 µm film thickness, SGE). Helium gas was used as a carrier gas at a 73 psi constant inlet head pressure. The modulation period was set as 6 s. The samples were injected at 280 °C in different split ratios (between 1:1 to 1:200) [287].

The oven temperature was programmed from 60 °C to 320 °C at 10 °C/min unless stated otherwise and held at 320 °C for 8 min. The interface temperature to the mass spectrometer was set at 330 °C and ion source was heated at 230 °C. The MS was operated at scan speeds between 5000 and 20,000 amu covering a range of m/z 45–600. Electron Ionization spectra were recorded at 70 eV [287].

Data processing and analysis

Raw GCxGC MS data were processed using GCMSsolution software (v2.72/4.20 Shimadzu), and Chromsquare software (v2.1.6, Shimadzu) and GC Image (v2.3) in combination with the NIST 11/s, OA_TMS, FA_ME and YUTDI in-house libraries were used for data analysis. The annotation of metabolites was carried out by comparing them to external standards (IM spectra and retention times adjusted to the internal standard myristic acid-14,14,14-d_3) and by spectrum matching based searches with the above databases for those metabolites without external standards. The similarity score threshold was set to 80 (out of 100), and the confidence of identification further validated by manual inspection of matches between experimentally observed and reference EI spectra. In case those detected peaks (blobs) were assigned to more than one metabolite (all scores above 80), only the highest score assignment was reported. For peak picking and peak quantitation using the GCMS Solution software (v4.2), we used the following parameters: i) for 1D-GC-qMS data: Slope: 100/min, width: 2 s, min area 20,000, drift 0/min and T. DBL: 1000 min without any smoothing methods used; ii) for 2D-qMS data: Width: 0.2 s, min area 20,000, drift 0/min and T. DBL: 1000 min without any smoothing methods used. For the samples using different injection ratios, we adjusted the slope/min parameter as follows: injection ratio (slope/min) 0.5/200 (7200), 1/200 (22,000), 1/100 (22,000), 1/40 (22,000), 1/20 (22,000), 1/10 (68,000), 1/5 (230,000), 1/1 (440,000).(Limit of detection (L.O.D) values were calculated based on the following equation: L.O.D. (L_D)=3.3xσ/S, where σ is the standard deviation observed for the analyte at a quantifiable concentration and S is the slope of the calibration curve [287].

2.6 Label free proteomics

In Solution digestion

Samples were adjusted to a total of 10ug of total protein and reagent volumes were adjusted to a volume of 200ul. 5ul of DTT reducing agent (final concentration 5mM) (200 mM DTT in 0.1 M Tris buffer, pH 7.8) was added to the samples and incubated for 30 -60 min at room temperature. 20ul of iodoacetamide alkylating reagent (final concentration 20 mM) was added and samples were then vortexed. The mixture was then incubated for 30 – 60 mins at room temperature. Protein samples were then precipitated via methanol/Chloroform extraction for proteins (see below). The protein pellet was then resuspended in 50ul 6M urea buffer (6 M Urea in Tris buffer, pH 7.8) by vortexing or sonication. The urea concentration was then reduced to give a final concentration of < 1M by diluting the reaction mixture with 250ul MilliQ-H_2O and vortexing. Trypsin (25 µl of ice-cold Tris stock and 75 µl of ice-cold MilliQ-H20 water to 20 µg of sequencing-grade modified trypsin (Promega) were added and re-suspended carefully, giving a final concentration of 0.2 µg/µl – trypsin was kept on ice until use) was then added in a 1:50 ratio regarding the total protein content of the samples. Samples were then mixed carefully, and digestion was carried out overnight at 37^{o}C.

Methanol/ Chloroform Extraction

Sample sizes of 200ul per sample were used with MilliQ-H_2O being used to bring the volume up to 200ul in samples which had la volume of less than 200ul. Similarly, samples which had a larger volume than 200ul were split. 600ul of methanol was added following addition of 150ul chloroform. Samples were then vortexed and 450ul of MilliQ-H_2O was added. Samples were centrifuged (max speed) at room temperature for 1 min.

The upper aqueous phase was then pipetted off without disrupting the precipitate at the interface.

450ul of methanol was added to each sample containing the organic phase (with precipitate). Samples were then vortexed and centrifuged for 2 mins at room temperature. Supernatant was then removed.

SEP – PAK C18 purification

A syringe was added to the Sep – Pak column (both attached to a vacuum manifold) (Waters C18 Sep-Pack cartridges: Sep-Pak PlusTM, WAT020515 (up to 1mg) Light (up to ~100µg) Thermo Solar. Care was taken to avoid air bubbles in the column at all steps of the protocol. The column was then equilibrated by flushing the column with 5ml of solution B (65% CH3CN 35% MilliQ-H20 0.1% TFA (recommended) or FA Use HPLC-grade Acetonitrile and FA, and MilliQ-H20) or Acetonitrile. 10ml of solution A (98% MilliQ-H20 2% CH3CN 0.1% TFA (recommended) or FA was added followed by slow addition of the peptide digest sample into the 10ml of solution. The sample was then washed with 10ml solution A. The samples were then eluted with 2x 600ul of solution B (collected in a 2ml Eppendorf tube). The purified peptides were then dried down completely in a speed – vac and resuspended in solution A (up to 20ul).

Filter-aided sample preparation (FASP) for tryptic digestion of tissues

Tissue samples were cut into smaller segments (washed in PBS solution and kept on ice at all times) 20mg and were homogenised in 1ml optimised RIPA lysis buffer (150mM sodium chloride, 1.0% NP-40 or Triton X -100, 0.5% sodium deoxycholate, 1% SDS, 50mM Tris, pH 8.0).

Protease inhibitor (Roche) and Phospho protease inhibitor (Sigma) was added and samples were homogenised on a bead beater (zirconia beads 1.0mm diameter) (Precellys 24, Bertin Technologies) for 40 seconds at speed 6500 rpm x 3 repeats. Samples were then centrifuged at 10,000 g for 5 mins at 4ºC. The protein concentration was determined by a BCA assay (BSA standard using the same buffer for cell lysate was prepared).

50ug of total protein was then loaded on 30 KDa filters (Millipore), filter units were then centrifuged at 14 000g for 15 min to remove other detergents. 200ul of urea buffer (10 mM DTT 8M urea (Sigma) in 0.1 M Tris/HCl pH 8.5) was then added to the filter and left at room temperature for 1 hour to reduce proteins. The filters were centrifuged at 14000 g for 15 min to remove DTT. 200 ul of 50 mM IAA in urea buffer were added to the filters and left for 30 min in the dark. The filters were centrifuged as before to remove IAA. The samples were then buffer exchanged twice to remove detergents using 200 ul of urea buffer, and one more time using 200 ul of 50 mM NH4HCO3 in water. 40 ul of 50 ng/ul trypsin in 50 mM NH4HCO3 was added to the filters, filters were vortexed briefly and proteins were digested at 37 °C for overnight. After tryptic digestion, the filters were transferred to new collection tubes, and peptides were collected by placing the filter upside down and spinning.

The filters were washed with 200 ul of 500 mM NaCl and the washing solution was collected by placing the filter upside down spinning. The filter was then washed with 100 ul of water and spun @ 14 000 g for 15 min in the same collection tube. The samples were acidified with CF3COOH and desalted with C18 cartridge (Waters).

The pure peptides were then dried in the Speed vac (Millipore) and resuspended with 20 ul of 2% ACN, 0.1% FA. 5ul of samples were injected into Q Exactive mass spectrometer.

2.7 LCM Collection and Tissue Lysis

Areas of tissue were isolated from the prepared slides using a laser capture microscope equipped with laser pressure catapulting, which allows for contactless transfer of regions of interest into the cap of a 600 µL microcentrifuge tube. Areas of interest were collected in 40 µL of RIPA buffer (Pierce, 89900). Annotation of areas/cells for dissection was performed manually on the microscope. Cutting and catapulting were performed along annotations automatically using a 40x objective lens and the following settings: Cutting: Energy 43, Focus 55. Catapulting: Energy 20, Focus -15. After isolation, samples were immediately placed on dry ice and later stored at -80 °C.

Proteomic sample processing

After thawing, the tubes containing lysis buffer and tissue were centrifuged to collect the tissue in the body of the tube. Samples were then heated to 95 °C for 2 hours. After cooling to room temperature, 25 units of Benzonase (Sigma, E1014) were added to digest DNA for 30 minutes at RT. Proteins released were reduced with 5 mM DTT for 30 minutes at RT and then alkylated with 20 mM iodoacetamide for 30 minutes at RT.

Proteins were processed using a modified form of the SP3 protocol (Sielaff et al 2017). 4 µL of SP3 beads (prepared as in Hughes et al 2014) were added and samples shaken at 1000 rpm for 18 minutes to bind proteins. After a 2-minute incubation on a magnetic rack, the supernatant was transferred to a new tube containing 4 µL of SP3 beads and the protein binding step repeated to capture any unbound protein. Beads were washed on the magnet 2 times with 180 µL of 70 % (v/v) ethanol and 1 time with 180 µL 100 % acetonitrile. Beads were resuspended in 50 mM ammonium bicarbonate containing 25 ng of trypsin (Promega, V5111) and samples were incubated at 37 °C overnight. After digestion, the beads were resuspended by bath sonication and 180 µL of 100 % acetonitrile was added and samples

shaken at 1000 rpm for 18 minutes to bind peptides. After a 2-minute incubation on a magnetic rack, the acetonitrile was removed. The beads containing proteins from the same samples (i.e. proteins bound to beads in the first binding step and protein bound to beads in the second binding step) were pooled after resuspension in 2 % dimethylsulfoxide, which causes peptides to elute from the beads. After a 5-minute incubation on a magnetic rack, peptides were transferred to glass vials and acidified with trifluoroacetic acid to 0.1 % (v/v). Prior to analysis by LC-MS/MS, samples were stored at -20 °C.

LC-MS/MS

Peptides were analysed by nano-UPLC-MS/MS using a 75 µm x 50 cm C18 column (Thermo scientific, ES803) with a 30-minute gradient consisting of a linear ramp from 2 % acetonitrile in 0.1 % formic acid 5 % DMSO to 35 % acetonitrile in 0.1 % formic acid 5 % DMSO at a flow rate of 250 nL/min using a Dionex Ultimate 3000 UPLC coupled on-line to an Orbitrap Fusion Lumos. MS1 survey scans were acquired at a resolution of 120,000 between 400 – 1500 m/z with an AGC target of 4.0 $x10^5$ ions in the orbitrap. MS/MS fragment spectra were acquired in the linear ion trap after higher energy collisional dissociation (HCD) fragmentation at a collision energy of 28 % with an AGC target of 4.0 $x10^3$ ions, if this was not reached the fragmentation would occur after 80 ms. Masses selected for fragmentation were not selected again for at least 30 seconds. The maximum time allowed between two survey scans was 1 second.

Data Analysis

Raw data was processed with MaxQuant (version 1.6.2.3) and searched against the UniProt human and mouse proteomes (retrieved Feb 2017) along with a common contaminants database provided by MaxQuant.

Cysteine carbamidomethylation and methionine oxidation were allowed as variable modifications and a false discovery rate of 1 % was allowed for both peptides and proteins. Enzyme specificity was set to trypsin, allowing for a maximum of 2 missed cleavages. The allowed mass deviations were 4.5 ppm for peptide precursors and 0.5 Da for-fragment masses. Protein were quantified using MaxLFQ with a minimum ratio count of 1. Further downstream processing was performed using Perseus (Version 1.6.0.7) [288 289 290 291].

2.8 Cellular assays

Seahorse experiments

The extracellular rate (ECAR) and the oxygen consumption rate (OCR) of cells were monitored in real time with the seahorse XF96 bioanalyser (Agilent) using the seahorse XF glycolysis stress test kit (Agilent), according to the manufacturer's instructions. The day prior to the assays (or in the case of starvation experiments 42 and 72hrs prior to running the assay), 786 and 6450 cells were seeded at a density of 20,000 cells/ well in an XF96 cell culture microplate containing complete growth medium (in the case of the control wells) and an XF96 sensor cartridge was equilibrated in XF solution O/N at 37 C in a non-CO_2 incubator prior to the assay. Cells were incubated in unbuffered RPMI recipe based XF base medium (without phenol red, 0mM glucose) (Agilent) for 15mins in a non-CO2 incubator prior to the assay.

Cells were then placed into the pre-equilibrated XF96 analyser and ECAR and OCR were recorded under sequential injection of 10mM glucose, 2uM oligomycin and 50mM 2 – deoxy – glucose. All measurements were normalised to cell number determined after the assay by staining with 2uM Hoechst33342 reading the plate on an Envision 2103 multilabel reader (Perkin Elmer) using a pre-customised wavelength setup. Seahorse data was analysed using Wave desktop 2.3.0.

MitoXpress intracellular probe to detect oxygen consumption rates

Despite the Seahorse XF Analyzer (Agilent) system has a higher publication profile, the MitoXpress Luxcel probe systems are becoming increasingly used by researchers. The MitoXpress Luxcel has significant advantages over the Seahorse system including compatibility with many plate readers, multiplexing and when using the MitoXpress intra probe, experiments can be run over several days [292] .

Experiments were carried following the manufactures instructions. 786 and 6450 (early and late) cells were plated (50,000 per well) in 96 well plates (CellCarrier – 96 well black) and left to adhere overnight before the Luxcel MitoXpress Intra probe (Agilent) was added and cells incubated overnight (5% CO_2, 20% O_2). The assay incorporated control cells grown in normal supplemented medium (pH 7.4), glucose and glutamine starvation and low pH (6.7). The next day, cells were washed in PBS and media replaced: starvation and pH medium were used in addition to supplemented medium (described in cell culture section). All treatments were carried out in triplicate wells. A cocktail of Antimycin A (1μM) and rotenone (10 μM) were used to inhibit oxygen consumption. Using the plate reader's atmospheric control unit and with the plate lid off, the oxygen levels was reduced in a step wise manner. Ambient oxygen was set to 5%.

Oxygen scale calibration

The conversion of fluorescent values to lifetime fluorescence values reduces assay noise and allows the construction of an oxygen calibration curve with a particular lifetime value reflecting a specific oxygen concentration.

The intracellular probe is loaded into cells and then the mitochondrial respiration is inhibited with a cocktail of antimycin A and rotenone to eliminate any contribution of respiration from the lifetime values measured. Therefore, the measured lifetime values are reflective of the applied O2 and not influenced by any O2 consuming factors within the cell. Once a steady state is reached the O2 in the reader is reduced and this process is repeated until 1% O2. The reader can't be set to zero so to achieve zero, so glucose oxidase is added as a last step and this gives out maximum lifetime values (i.e. lowest O2 conc).

The lifetime values for each O2 conc are then plotted against their respective O2 values and a one phase exponential decay curve is fitted. The equation for this curve which should be noted is slightly different from the generic one Luxcel quote in their booklet is:

$\%\ O2 = 345\ \exp^{(-x/10.29)}$ where x is the lifetime values obtained from the assays.

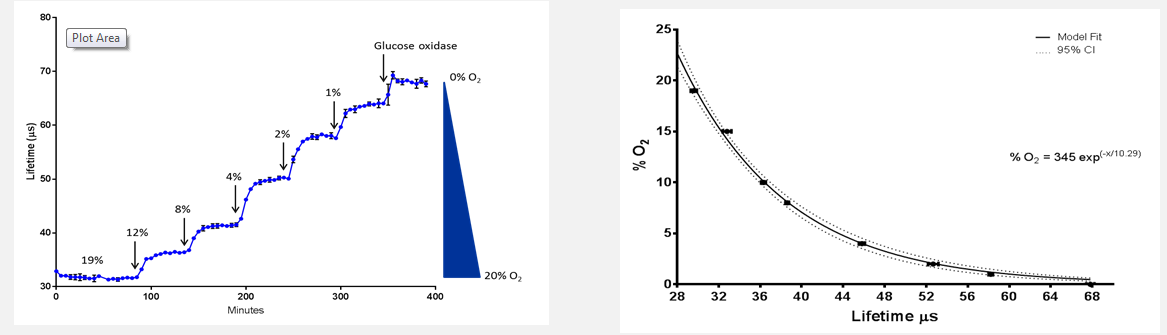


***Figure 3: Sample Calibration Data*:** MitoXpress - Intra Lifetime profiles measured at decreasing [O2] with parallel glucose oxidase treatment to achieve 0% O2 (left hand side) The relationship between probe lifetime (T) and applied [O2]. Applying a first order exponential fit generates a calibration function of O2 = O2 = 345 $\exp^{(-x/10.29)}$.

2.9 Migration and intercalation experiments

Isolation and culture of LMVECs

Primary LMVECs were isolated as previously described [293] (Lucotti S., et al. Aspirin prevents metastasis by blocking COX-1-Thromboxane A_2 pathway in platelets. JCI - under revision). Lungs from 3 female C57BL/6 mice were pooled, dissected and digested in a 0.5 mg/mL collagenase solution (Thermo Fisher Scientific) for 1 hour at 37°C and filtered through a 70 μm cell strainer (Thermo Fisher Scientific). The Cell suspension was then washed, blocked with 10 μg/mL murine IgG (I5381, Sigma-Aldrich) and stained with anti-Isolectin-B4-FITC (L2895, Sigma-Aldrich), anti-CD31-PE (102408, Biolegend) and anti-CD105-APC (120414, Biolegend) antibodies, diluted to 1 μg/mL in PBS with 2.5% FBS.

Isolectin-$B4^+CD31^+CD105^+$ cells were sorted using a Beckman Coulter Legacy MoFlo MLS High Speed Cell Sorter and cultured in flasks coated with 2% gelatin (Sigma-Aldrich) in an enriched DMEM medium [293].

Tumour cell intercalation assay in static conditions

$3x10^5$ LMVECs were seeded in each well of a 48-well plate, previously coated with gelatin 2%, and fresh growth medium was replaced after 24 and 48 hours. At 2 days after seeding, exponentially growing 786 and 6450 (early/late) cells were labelled with CMFDA and harvested. $2x10^4$ CMFDA 786/6450 (early vs late) cells were then loaded into the wells prior to acquisition. Intercalation was monitored in 2 fields of view per well for 18 hours through an epifluorescence microscope equipped with an incubator that maintained a 5% CO_2 humidified atmosphere at 37˚C. It was not possible for Tumour cell intercalation to be quantified visually from microscopic fields, as a result Fiji software (ImageJ) was used to quantify the cells manually using the threshold tool for counting.

Transwell migration and invasion assay

For the transwell migration and invasion assays, 786 and 6450 (early vs late) cells seeded at 50,000 cells per well and were resuspended in serum-free RMPI medium and seeded on a transwell insert (8 μm pore size, BD Biosciences) coated with growth factor reduced Matrigel^{TM} matrix (300μg/μL, BD Biosciences. The bottom chamber contained RPMI medium supplemented with 0% or 10% FBS as chemoattractant. After 20 hours, non-invading cells were removed by wiping the upper part of the insert membrane with a moistened cotton swab. Cells adhered to the bottom surface of the insert were labelled with CMFDA (Thermo Fisher) and Hoechst (thermos fisher) (1:1000 dilution in PBS), fixed with 4% PFA and imaged with a Celigo S Imaging Cytometer (Nexcelom Bioscience LLC). The number of migrated cells was measured through surface reconstruction of tumor cells with Imaris software (version 8.2 and 9, Bitplane) and the ratio between migrated cells at 10% versus 0% serum was calculated. Incorporation of the broad acting carbonic anhydrase drug Acetazolamide (Sigma) at 5mM concentration was used.

2.10 Immunostaining

Immunostaining was carried out as dictated in the protocol used by the Nuffield department of clinical neurosciences (Neuropathology). Sections were De-paraffinized for 3x 5 minutes in Histoclear/Xylene. Following which sections were Hydrated 10-15 dips in 3x 100% IMS, 90% IMS, 70% IMS and tap water. Endogenous peroxidase was blocked H_2O_2/PBS (25mL Hydrogen Peroxide + 225 mL PBS) on a plastic container, immerse the rack and put onto the shaking table – 30 minutes. Slides were then washed well in tap water. Slides were then moved to a black plastic rack and then into a black lidded box filled with Citrate Buffer pH6. Black

box was autoclaved on a metal silver tray for 1 hour and then washed in tap water. Slides were then mounted on cover plates and placed into Sequencers.

Slides were then washed twice with TBS/T pH 7.6 – 2 x 5 minutes. Primary Antibody (Endomucine dilution 1:100) was added with TBS/T pH 7.6 120µL/slide and left to incubate Overnight at 4ºC. Slides were then washed twice with TBS/T pH 7.6 2 x 5 minutes and the Secondary Antibody (Anti Rat HRP Dako) 120 µL/slide and incubated for 1 hour. Slides were then washed twice with TBS/T pH 7.6 2 x 5 minutes. DAB + Substrate Buffer (Dako Envision Kit's brown bottles) was made up according to the table on the lid of the kit and was then mixed well and pipetted from the control slide 120 µL/slide for 5 minutes. Slides were washed with TBS/T pH 7.6 to stop reaction for 5 minutes. Slides were then removed from Cover plates, put back into a metal rack and washed well in tap water. Counterstaining was carried out with Harris Haematoxylin for 1-minute following 'blue up' in running tap water for 5 minutes.

Sections were dehydrated 10-15 dips in 70% IMS, 90% IMS, 2x 100% IMS and 3x Histoclear/Xylene. Slides were mounted with DPX, avoiding any air bubbles between the slide and coverslip.

Preparation of LCM slides

FFPE blocks were sectioned at 5µm and mounted onto 1.0 polyethylene naphthalate (PEN) membrane slides. Prior to mounting PEN slides were incubated for 30 minutes under 254nm UV radiation to destroy contaminants and to decrease the hydrophobic nature of the membrane slides to allow for better tissue adhesion. Sections were briefly air-dried to increase adhesion to the membrane.

H&E Staining

Sections were placed on a Thermo Shandon Linistainer for automated Haematoxylin & Eosin staining. Briefly, sections were deparaffinated in Xylene and fixed in 70% IDA (industrial denatured alcohol), washed in water, stained with Harris' Haematoxlin, incubated in 0.4% acid alcohol and Scot's tap water, stained with Eosin, washed and dehydrated with increasing concentrations of IDA.

Chapter 3 Characterisation of cancer cells isolated from co – option vs angiogenesis mouse models in vitro

3.1 Introduction

3.1.1 "In vitro work" versus animal model

Implanted tumours, tumour cells and human xenograft mouse models are routinely used in the field of cancer research. Human xenograft mouse models can be divided into orthotopic and heterotopic transplant animal models. The advantage of using heterotopic mouse models over orthotopic, is that heterotopic modelling is usually rapid, of lower cost and is easily managed [294]. Moreover, heterotopic mouse models are best suited for expanding human tumour networks and present a means to convert tumour specimens into cell lines.

The anatomical site in which cancer cell lines are injected, has been demonstrated to impact on the vascular status of the tumour [294]. The use of subcutaneous tissue sites therefore, is useful in understanding the mechanisms behind what determines whether a cancer cell will undergo angiogenesis or a non-angiogenic alternate mechanism [295].

In some models, the subcutaneous tissue has been found to be characteristic of an angiogenic phenotype and the lung (in the same model) shows non angiogenic behaviour [171].
However, what is important to note is that this phenotype classification cannot by extension be applied to cell lines being investigated in vitro [171]

Over the past two decades a number of therapeutic strategies that target the growth of tumour vasculature have been employed. However, thus far, anti-angiogenic therapy has been found to be less effective in humans as predicted from "in vitro" pre-clinical tests in mice with the occurrence of intrinsic and induced resistance [296].

For improved understanding of tumour angiogenesis, there is a need for new models of angiogenesis that better summarise the multistep process of tumorigenesis from molecular neoplastic transformations seen in single cells, to tumour progression in tissue [297].

3.1.2 A model of vessel co – option

This project aims to describe and characterise the human renal cancer cell line 786 -0 (786) and the derived – sunitinib resistant cell line 786 – M or what is referred to as the 6450-cell line. The daughter 6450 cell line was isolated from the lung non angiogenic metastases growing in a vessel co – option mouse model, developed and provided by Andy Reynolds in the ICR, London.

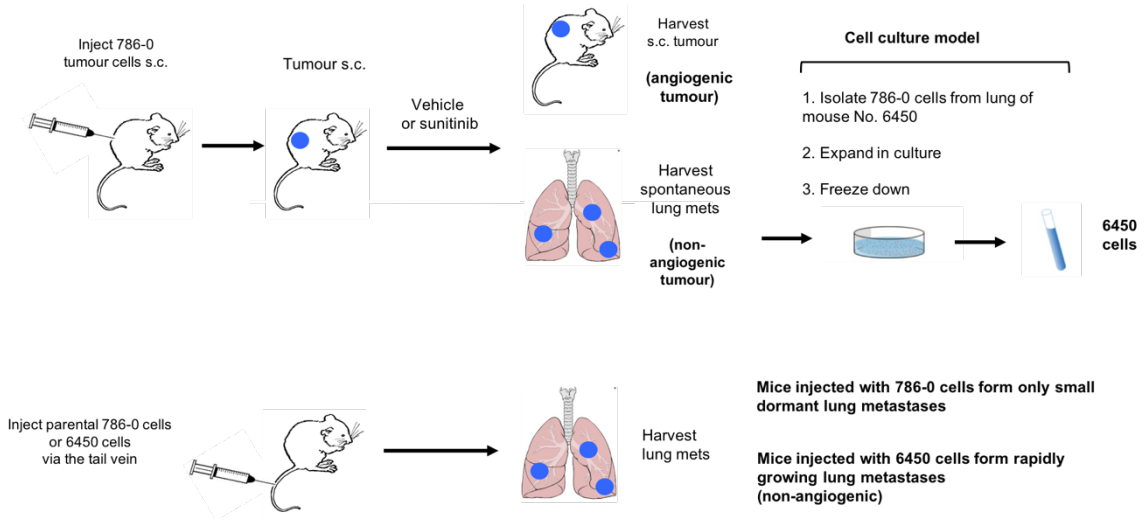


Figure 4: Mouse model of vessel co- option: a) Renal carcinoma cell line (786) injected subcutaneously in mice was found to metastasise in the lung after treatment with anti - angiogenic drug (sunitinib) b) In vein injection of both isolated metastatic cell line (6450) from the lung and the 786-cell line, yield either small dormant or rapid growing lung metastasis.

The 786 cells are the parental renal cancer cell line. As illustrated in Figure 4, when injected via the tail vein of the mice, these cells do not successfully from lung metastases and remain dormant. Mice injected via the tail vein with these cells appear to survive indefinitely.

In contrast when the 6450 cells are injected via the tail vein of the mice, these cells form large lung metastases in the mice. 6450 lung metastases appear to be non-angiogenic i.e. they utilise vessel co – option instead of angiogenesis.

Therefore, the 786-cell model can be considered to be a cell line that despite successfully being able to survive in the lung, remains dormant, a phenomenon that has been associated with the perpetuation of a "perivascular niche", which can either promote dormancy or initiate metastasis [298]. In contrast, the 6450 cells are a cell line that is very successful in colonising the lung.

It is important to note that both cell lines will form angiogenic tumours when injected subcutaneously.

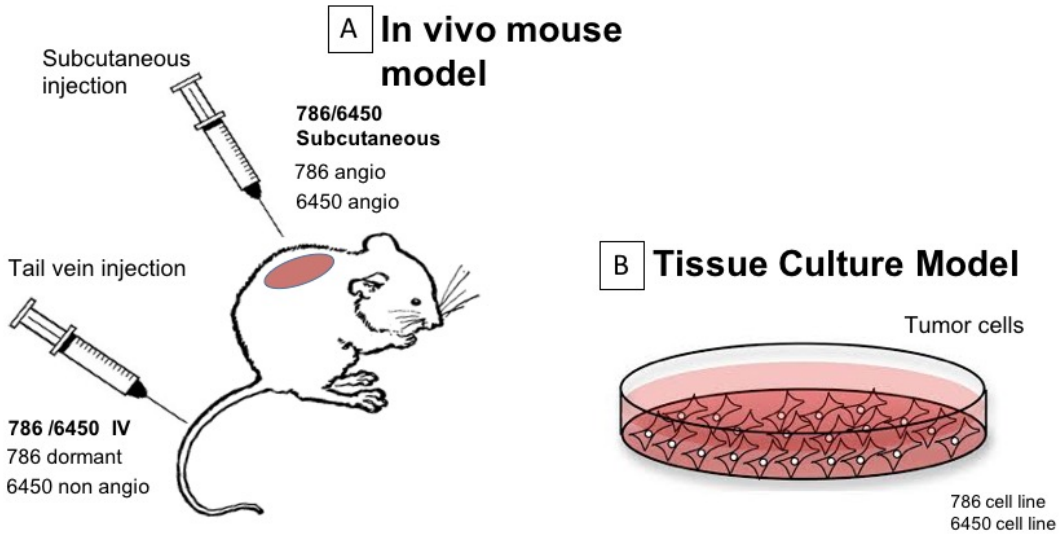


Figure 5: In vivo mouse model vs tissue culture model: A) represents the in vivo mouse model discussed in the subsequent chapter B) represents the in vitro tissue culture model made up of the 786 and 6450 cell line (derived from 786 drug resistant clones). Studies carried out on the tissue culture model are discussed in this chapter.

The model shows distinct histological and phenotypical differences in vascular status depending on the injection site of the cancer cells in the mouse. The cells injected subcutaneously show angiogenic behaviour and the cells that undergo in-vein injection result in co – optive behaviour.

However, it cannot be implied by extension, that the 786-cell line is representative of an angiogenic phenotype and likewise it cannot be said that the 6450-cell line represents a co-optive phenotype.

In this chapter, a series of "in vitro" experiments involving these two cell lines, will be presented. The aim being to characterise some of their biological characteristics, in addition to investigating how much their behaviour is subject to change in an "in vitro" setting.

This work involves interrogating the protein and mRNA expression signatures, studying the metabolic status, analysing the migration and invasion patterns, as well as determining the intercalation capability of the cells.

In the subsequent in vivo chapter, xenografts growing in this murine model will be investigated, after injection of these cell lines either subcutaneously or in - vein.

3.2 Results

3.2.1 Assessing the identity of the mother and daughter cell lines

Prior to going ahead with experiments, a cell authentication test was carried out to check the true identity of the cells and to ensure there was no cross - contamination.

From the results of the test, it was clear that the 6450-cell line was clearly derived from the 786-cell line in that there were no differences in genetic makeup, apart from the loss of a Y chromosome and the gain of an X chromosome instead (see Authentication Report in the supplementary material).

3.2.2 Investigating "In Vitro" growth patterns

Very early on in the project it became quite apparent that the cells (786 vs 6450) grew quite differently and appeared morphologically different depending on the passage number in culture. In as little as 3-4 passages from the time a 6450-cell line vile was thawed and cells seeded and expanded, it was noted that there were changes to both morphology (Figure 6) and growth rate.

Beyond 3-4 passages in culture, it was observed that the 6450 - cell line became less distinct and in fact more similar to that of the 786-cell line, as far as morphology and growth rate were concerned.

For every new batch of 6450 cells that was thawed, morphology and growth rate were used as strict monitoring parameters, in the absence of any sort of quantitative biological marker.

In order to maintain a sufficient number of early passage batches, cells were frozen down after 1 passage in culture (when confluency has been reached) and once the 6450 cells had exceeded 3-4 passages, a new early batch would be grown and expanded accordingly.

The 6450 cells exceeding 4-5 passages were kept in culture as late 6450 passages and were frozen down accordingly (see methods).

The 6450-cell line would on average take around 3-4 weeks before a confluent T-175 flask could be harvested, and experiments could commence. In addition to this, earlier batches of the 6450-cell line were thawed and grown simultaneously to prevent too much of a delay when it came to carrying out experiments and biological repeats.

These factors limited the number of experiments that could be carried out in any one go, making experimental investigations and the generation of biological replicates very challenging.

For the purpose of generating growth curves, cells were seeded in 96 well plates (see methods) and growth was recorded, with morphology being documented by means of the incucyte live cell analysis system. The cell lines were seeded at the same number (3,000-4,000 cells) and 3 biological replicates with 3 technical replicates of cell growth were carried out.

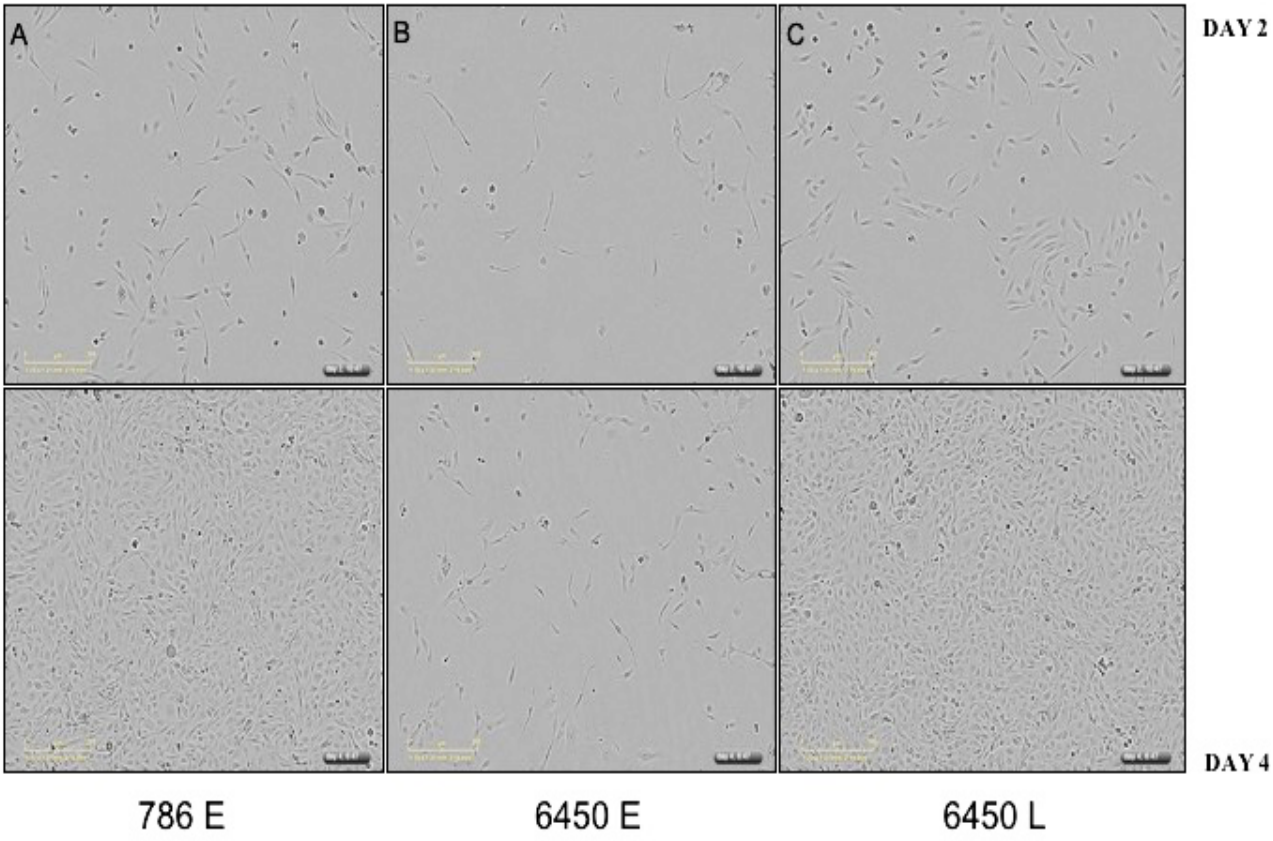


Figure 6: Representative images of cell morphology and confluency show differences in growth rate: Panels (A-C) shows characteristic morphology and confluency of the cell lines, 786 early, 6450 early and 6450 late respectively. The top row of images represent day 2 of cell growth and subsequently day 4 is represented in the bottom row of images. E and L denote the corresponding early and late cell passages. 6450 early passage cells grow very slowly and have an elongated morphology compared to the 786 early and late passages which grow much faster with a more rounded cell morphology. These images represent 1 out of 4 fields of view).

3.2.3 Characterisation of the 786 and 6450 cell lines in "Early" and "Late"

One of the first objectives was to document the difference in cell growth rate over time with simple, yet illustrative growth curves (see figure 7). In addition to this, capturing images of the cells mid growth was important in order to clearly illustrate the differences in morphology and cell confluency visually, over time (see figure 6).

As a result of the observed disparity between the cell lines, it was proposed that perhaps the noted difference in growth rate was due to the influence of the tissue culture microenvironment. In particular, the abnormally high concentrations of nutrients in the tissue culture growth medium (namely glucose and glutamine).

It is a well-known fact that the heterogeneous genetic landscape of tumours facilitates tumour growth and progression, with its implication in drug resistance becoming increasingly well-defined [299]. However, what dictates genetic expression, in this heterogeneous landscape, is the intratumor microenvironment and its influence on drug resistance and tumour progression. Microenvironmental cues, such as hypoxia, nutrient levels and infiltrating immune cell and stromal cell signalling, have been shown to conjoin together to determine the invasive potential and therapeutic response of a tumour [299].

Thus, investigations were carried out on the two cell lines, in early and late conditions, in addition to observing how they responded to changes in the cell culture medium.

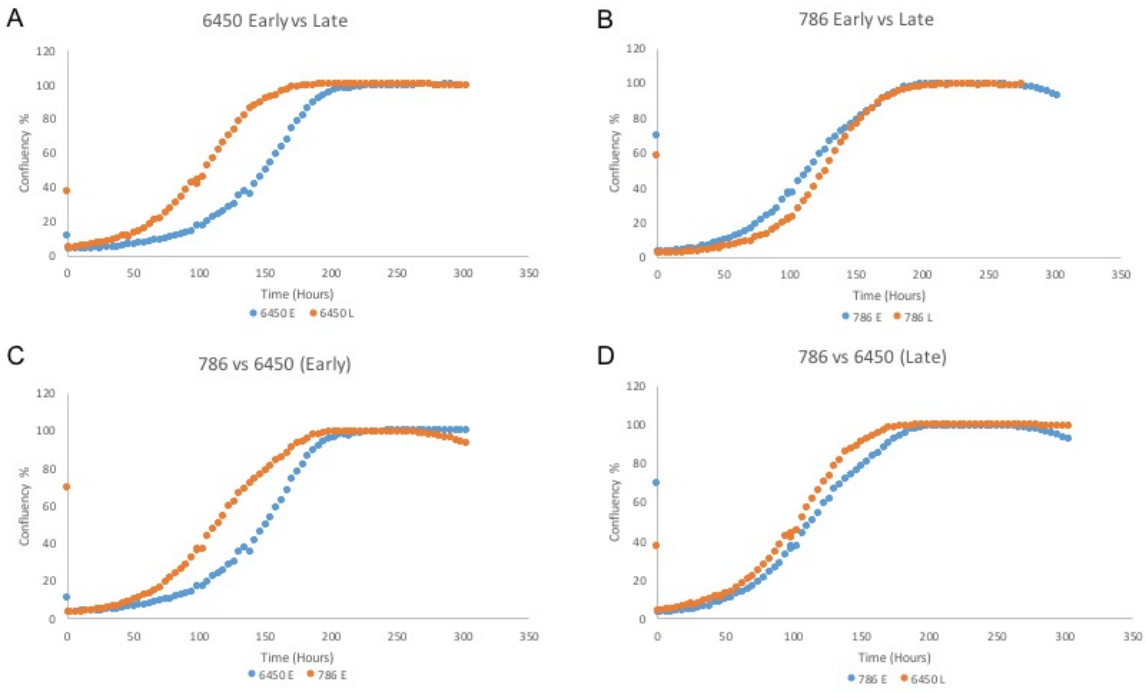


Figure 7: Comparing growth curves in 786 vs 6450 cell lines (early vs late) reveals differences in growth rate: **A**) graphical representation of the growth rate between 6450 early vs late passages **B)** growth curves 786 early vs late **C)** growth curves comparing 786 vs 6450 early passage **D)** growth curves comparing 786 vs 6450 late passage. 2 biological replicates were carried out with 3 technical replicates.

3.2.4 Influence of acute nutrient starvation and low pH on cell growth

Starvation of glucose, glucose and glutamine and low pH (6.7) and the effects on growth of early and late passages of the 786 and 6450 cell lines, was investigated. Cells were seeded in supplemented medium (see methods), the next day the supplemented medium was removed, cells were then washed gently, and the starvation/ low pH medium was added. Growth was monitored until confluency was reached.

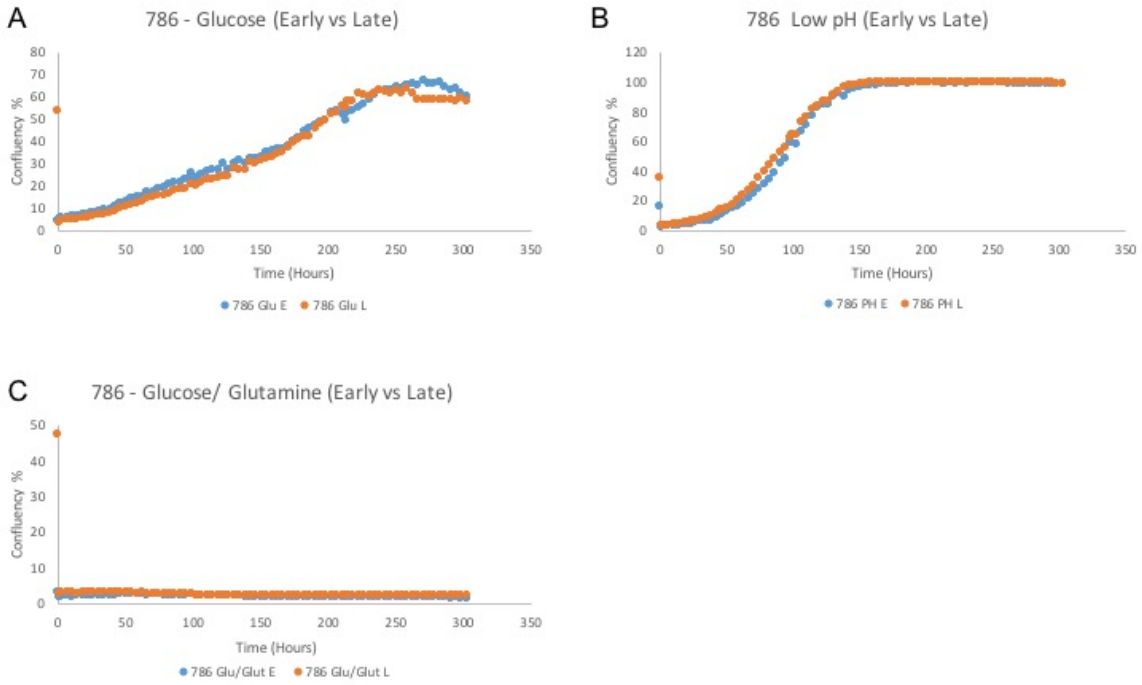


Figure 8: Growth rates under starvation conditions show no differences in growth between 786 early vs late passages: **(A)** Glucose starvation growth curve comparing growth rate of the 786-cell line early passage (blue) vs late passage (orange) **(B)** Low pH growth curve comparing growth rate of the 786-cell line, early (blue) vs late (orange) passage **(C)** Glucose and Glutamine starvation growth curve comparing growth rate in early 786 passage (blue) with a late 786 passage (orange). 2 biological replicates with 3 technical replicates were carried out.

Looking at the growth rate patterns under starvation conditions, it is clear that there seems to be no significant difference in response to starvation and change in pH between early and late passages of the 786-cell line. This confirms the initial observation that, the 786-cell line is stable regardless of passage and time in culture.

A change in growth pattern can be observed when cells are starved of glucose with the exponential growth being somewhat hindered. Growth rate seems to be less affected by low pH however, with a lagged response in growth being observed during exposure to a low pH environment.

It was thus concluded, that the 786-cell line adapts quite well when exposed to different conditions albeit with changes to the normal growth pattern (see figure 8 vs figure 9). Growth rates in general however, do not seem to be affected dramatically.

Following on from this, the early and late passages of the 6450-cell line in the above described conditions, were investigated.

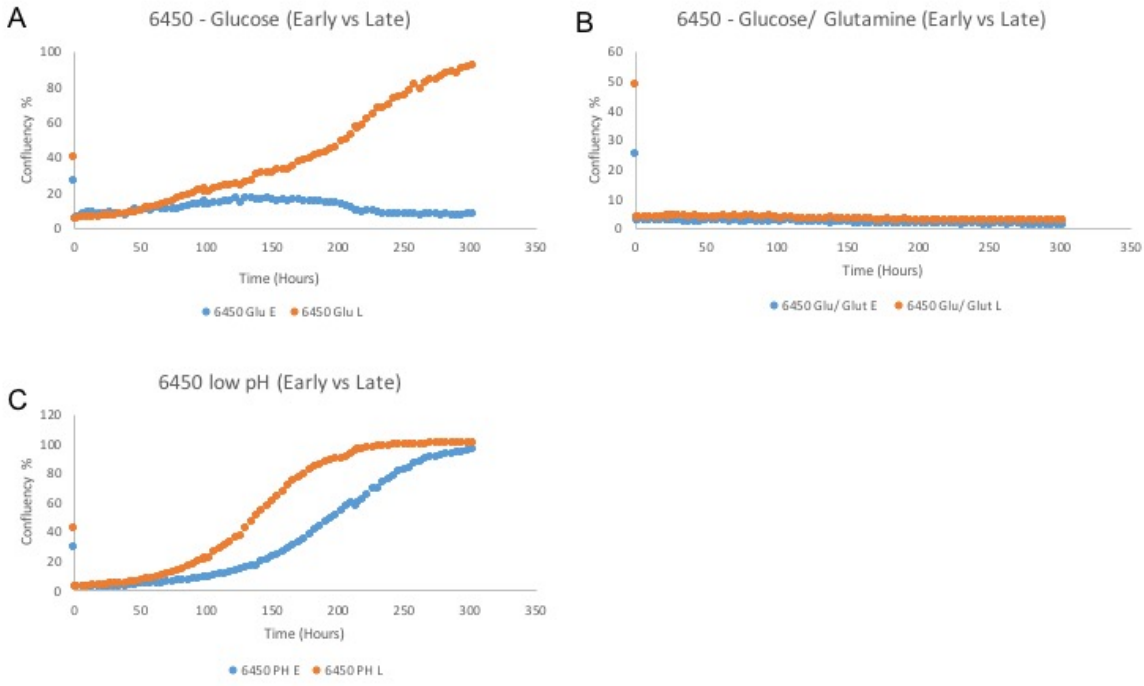


Figure 9: Growth rates under starvation conditions in 6450 cells reveal differences in growth between early vs late passages: **(A)** Glucose starvation growth curve comparing proliferative rate of the 6450 - cell line early passage (blue) vs late passage (orange) **(B)** Glucose and Glutamine starvation growth curve comparing an early 786 passage (blue) with a late 786 passage (orange) **(C)** Low pH growth curve comparing proliferative rate of the 6450-cell line, early (blue) vs late. (orange) passage. 2 biological replicates with 3 technical replicates were carried out.

The early passage of the 6450-cell line, is observed to adapt less efficiently than its later counterpart, in the context of both glucose starvation and low pH, highlighting the instability observed with this cell line. It is thought that it is this instability that leads to alterations enabling the 6450 late passages to adapt more efficiently to changes in medium conditions.

Similar to the 786-cell line, absence of both nutrients, glucose and glutamine, effects cell growth rate dramatically, regardless of passage number, with cell growth being stunted. This confirms how essential both these nutrients are for cancer cell survival, emphasizing what has already been cited in publications [300].

Likewise, both cell lines grown under low pH conditions are observed to adapt and grow, albeit with a reduction in growth rate. No significant change in growth exponential is noted in either cell line, however growth of the 6450-cell line is observed to take longer to plateau under low pH exposure, consistent with the fact the early passage of the 6450-cell line grows slower than the 786-cell line in normal culture conditions.

3.2.5 Pilot proteomic study shows differential regulation of proteins in 786 vs 6450 cell lines

As an initial approach, it was proposed that mass spectrometry analysis would be used, to facilitate the pull down of an entire database of potential proteins found in both cell lines (786 and 6450). This would aid in finding significant differences in the biology of these cell lines.

After having established the growth rate patterns between the cell lines (early and late passages) both in normal and starvation conditions, it was concluded that for the purpose of the initial pilot proteomic study, it would be wise to use only the early passage of the 6450-cell line. Using only the early 6450 passage, would probably be more representative of the metastatic phenotype in the mouse model. The early passage would have also undergone less influence and alteration, as a consequence of the tissue culture microenvironment.

The cells were grown in supplemented RMPI medium (see methods). Three biological replicates were taken from each cell line and run on the mass spectrometer.

An initial basic fractionation was carried out, so that we could isolate both the nuclear and subsequently the cytoplasmic compartments of both cell lines in order to further identify potential protein hits, however owing to the fractionation method not yielding substantial results, it was decided that this approach would be discarded.
The fractionation method was very crude and hence did not provide sufficient enrichment of cytoplasmic and nuclear fractions however, this would need to be optimised in future investigations. As a result, it was decided that proteins would be extracted from whole cells.

To ensure accuracy and reliability, cell numbers were measured, and it was ensured that numbers were equal between the two cell lines, by means of protein concentration quantification.

As detailed in the materials and methods section, the samples were then run on the Q – Exactive which has a high-resolution precursor ion selection.

Label free preparation of the samples was carried out which also facilitated a whole proteasome analysis while comparing multiple biological states in a single experiment, (workflow shown in methods section).

All the proteins with an ANOVA p-value lower than 0.05 and a fold change higher than 2 were selected for further investigation. Comparing both the enriched (ANOVA p-value lower than 0.05 and a fold change higher than 2) and unenriched lists of the protein pull downs obtained from the mass spectrometry analysis) it was observed that proteins involved in metabolism make up a significant proportion of the overall proteins identified (see figure 14), therefore confirming the potential role metabolic factors may play in metastasis.

In total (prior to applying any filters), 3,023 proteins were identified. Normalisation was achieved using all of the proteins identified (housekeeping proteins).

Samples were injected over a one-hour gradient and subsequently analysed using progenesis software and principal component analysis (PCA) was subsequently carried out.

PCA acts to simplify complex data while retaining trends and patterns [301]. PCA is unsupervised and therefore is not subject to biases when it comes to treatment groups or phenotypical differences. It works by transforming data into fewer dimensions and produces a summary of features.

High dimensional data is very common in biology and occurs when a number of features such as gene expression are quantified for each sample. As a result such high dimensional and complex data presents researchers with challenges such as increased error rate and computational expense, which PCA helps to mitigate [301]

3.2.6 Correlation analysis shows independent clustering of protein groups in 786 versus 6450

Proteins or peptides are sorted together based on their expression patterns by means of hierarchical clustering and correlation analysis.

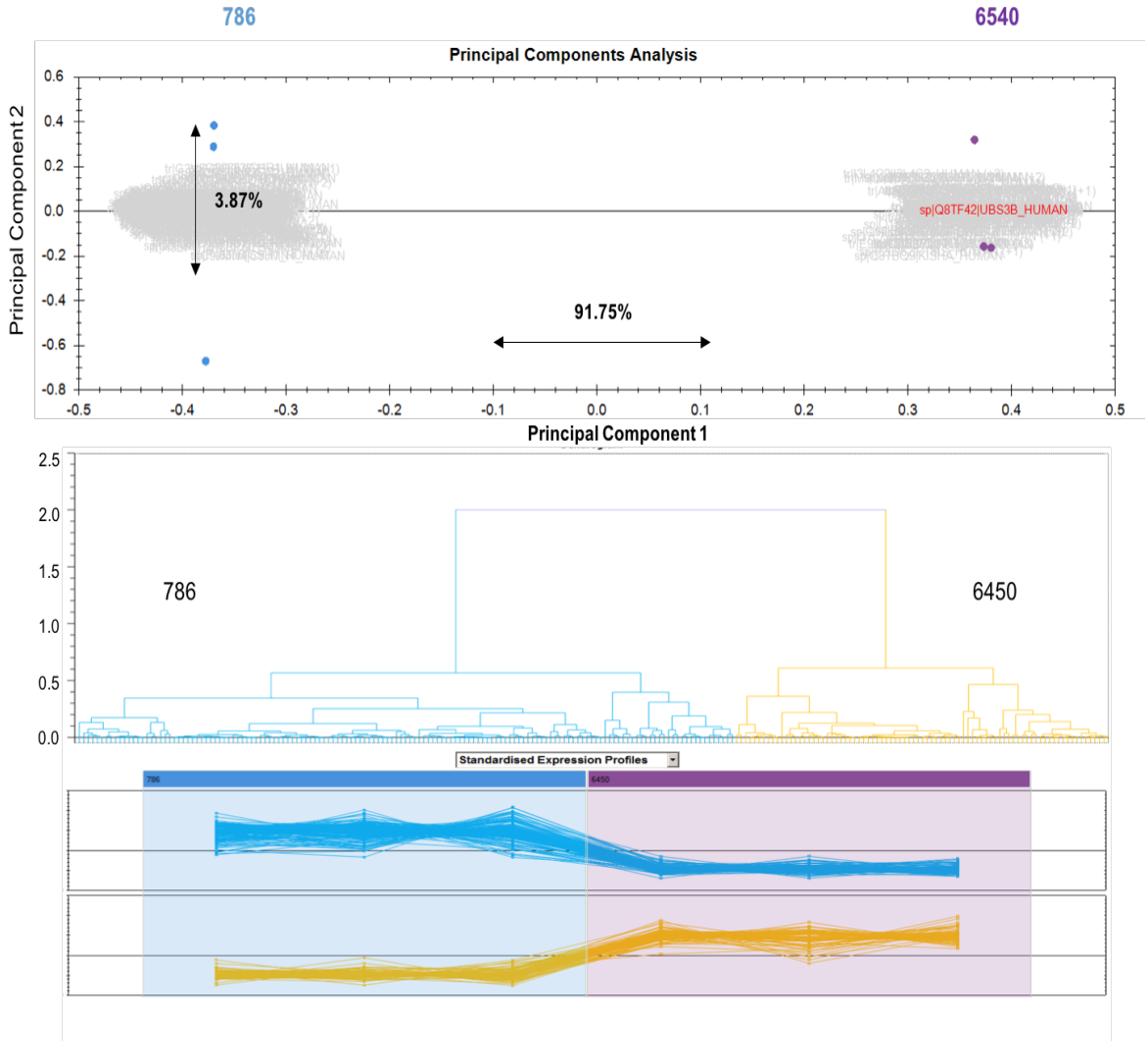


Figure 10: Differential proteome analysis*:* Description from top to bottom: top principal component analysis (PCA) graph shows the protein expression of 3 biological replicates both within the same cell line (PCA 2) and between the two different cell lines (PCA 1). The middle schematic shows the grouping of proteins that follow the same trend between the two cell lines, yellow (786) – blue (6450) and the bottom schematic shows the expression profiles of the upregulated and down regulated proteins in each cell line – blue (786) and purple (6450).

This unbiased multivariate analysis offers an accurate snapshot of protein activity within an experiment, as well as help identify features that contribute to disease states.

Data output can be in the form of an interactive dendrogram tree, where in which similar expression profiles cluster together. Data can then be studied at a group level on the dendrogram or by means of the related expression profiles.

From the PCA analysis it is clear that the 786-cell line and the 6450-cell line (early passage only) show good separation (only one outlier in the 786-cell line), forming two clustered networks, with what is observed to be distinct protein signatures.

In progenesis, peptides can be tagged, and a statistically significant filter can also be applied. A filter where in which peptides that were found to have a minimum two- fold change and a p value of less than 0.05 formed the selection window for our analysis. Thus, enabling the identification of unique peptides and providing more reliable quantification.

From the list of protein filtered for significance and looking into the individual protein hits (p value/ fold change applied), Thrombospondin - 1, Carbonic anhydrase 2 and Glutathione S transferase were interesting hits and thus were chosen for further validation (Fig3).

The longstanding role of Thrombospondin-1 (TSP -1) in angiogenesis has been cited in a number of research publications with TSP -1 has being linked to VEGF processing, namely in the uptake and clearance of VEGF from the extracellular space [302] .

As a consequence, TSP -1 expression was looked into, in order to validate its expression profile between the two cell lines, seeing that it is a protein marker that has already has been highlighted as a possible variant in the regulation of angiogenesis, cancer cell metastasis and cell adhesion to vessel walls [243] . Despite TSP-1 not showing differential expression in vitro however, it could still play a role and hence validation of its expression was pursued.



Figure 11: Differential protein expression between cell lines: Screen shot from progenesis: 786 cell line represented in blue and the 6450 - cell line in purple. Arrow points represent biological replicates, with distribution in points corresponding with variation in detection within individual samples.

Looking at the differential regulation of these three proteins (Thrombospondin 1, Carbonic anhydrase and Glutathione S Transferase) we can observe that Thrombospondin -1 levels are observed to not change in 6450 cell line when compared to the 786-cell line. Glutathione S Transferase is also higher in the 6450-cell line and Carbonic anhydrase 2 is downregulated in the 6450-cell line and upregulated in the 786-cell line.

3.2.7 Pathway analysis shows enrichment of well-known cancer pathways

Pathway analysis was carried out by Dr. Giovanni Stracquadanio (Computational Intelligence Lab for Biology and Medicine, School of Computer Science and Electronic Engineering, University of Essex, UK) and implemented the use of the human interactome retrieved from Menche et al [303]. Two most central nodes were identified between the 786 and 6450 cell lines, EEF1A and VIM which are well known cancer drivers. An anova p value of ≤1E-4 was applied in order to determine protein significance.

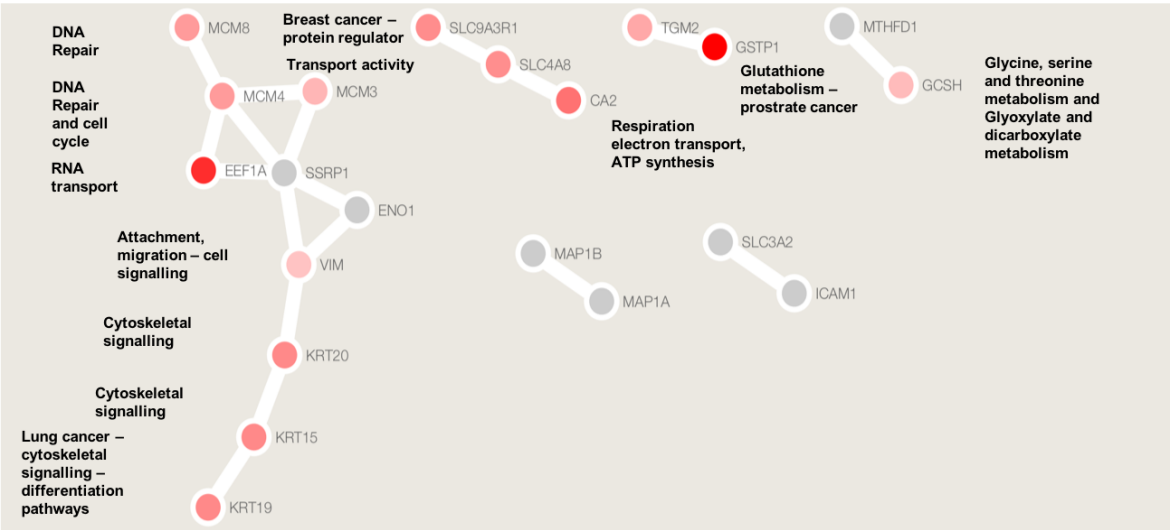


Figure 12: Pathway analysis highlights significant upregulated protein interactions: reported networks contain at least 2 proteins. Proteins are coloured with red gradients based on their fold change between 786 vs 6450 cell lines. Proteins with fold– change ≤ 2 are reported in grey.

3.2.8 Western blot validation shows differential expression of targets highlighted in proteomic pull down

In order to confirm and validate that these findings were truly representative, and that proteomic protein quantification and detection was carried out accurately, a series of western blots using the same biological triplicate samples that were injected into the mass spectrometer was carried out.

Thrombospondin 1, Glutathione S Tranferase and Carbonic Anhydrase 2 were bloted for, based on the proteomic flitering and pathway analysis results. In the case of Thrombospondin – 1, although no differiential expression between the two cell lines in either proteomics or pathway analysis was seen, its important role in angiogenesis, as highlighted by numerous studies [243] encourged the pusuit of its validation.

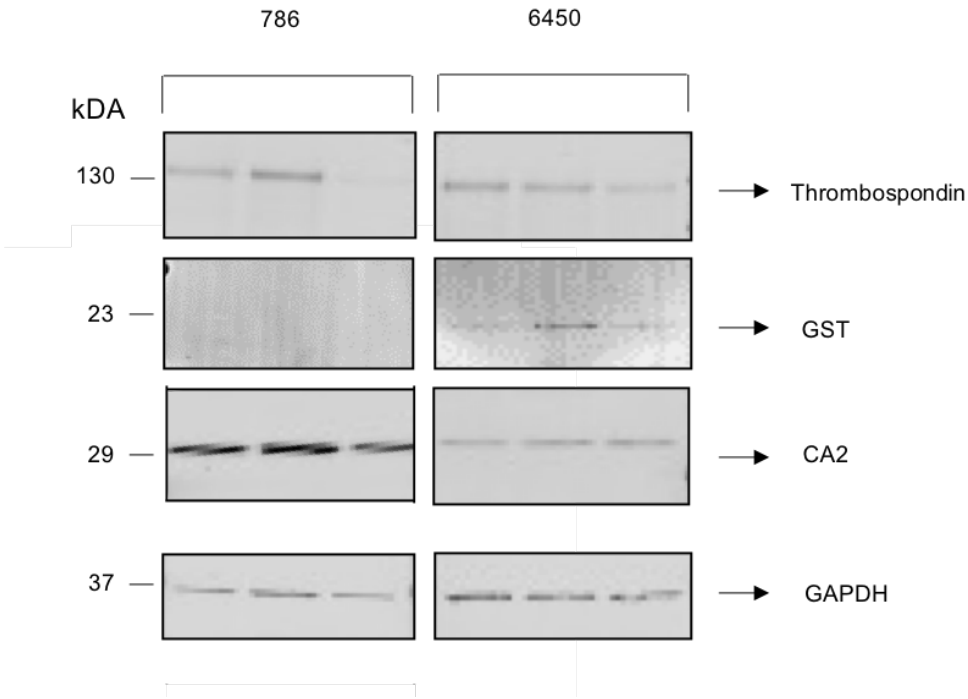


***Figure 13: Validation of differential protein expression by western blot*:** the same biological triplicates injected into the mass spectrometer were validated via western blot. Only the 786-cell line vs the 6450-cell line early passage were compared in this experiment. GAPDH was used as a control for protein loading.

From the western blot analysis, Thrombospondin – 1 does not show any differential regulation between the 786 and 6450 cell lines. Glutathione S transferase was observed to be upregulated in the 6450-cell line and absent in the 786-cell line. Carbonic anhydrase 2 shows upregulation in the 786-cell line and downregulation in the 6450-cell line.

Further differential proteomic analysis also highlighted the upregulation of proteins associated with metabolism (see figure 11). As a result, investigative metabolic studies were carried out, in order to understand the defining metabolic features of these two cell lines.

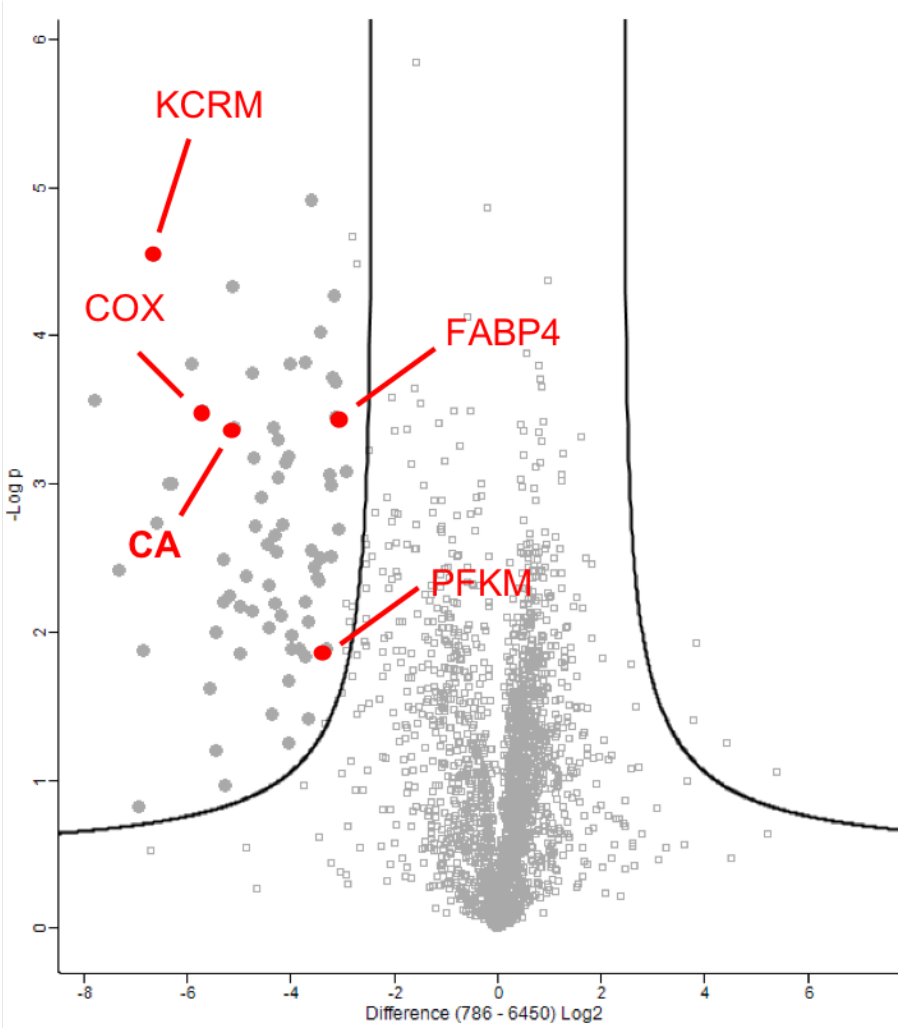


Figure 14: Volcano plot showing upregulation of metabolic proteins in the 6450-cell line (early) vs 786 cell line: Volcano plot to show the upregulated metabolic proteins (KCRM, COX, FABP4 AND PFKM) in the 6450-cell line (gene names highlighted in red).

3.2.9 Metabolic profiling of 786 and 6450 cell lines

Earlier unpublished studies from Karl Morten's group (the Nuffield Centre for Women's and reproductive health, Oxford University), reported that the 786-cell line is more glycolytic in its metabolic profile with the 6450-cell line undergoing more oxidative phosphorylation. This metabolic characterisation was made using the Luxcel metabolic MitoXpress extracellular assay system (very similar to the seahorse assay).

Owing to these noted differences in metabolic signatures suggested by these previous unpublished studies, as well as the upregulation in metabolic proteins seen in the mass spectrometry results (see figure 14), attempts were made to verify this established difference and confirm it could still be observed. Thee metabolic profiles of both cell lines were analysed, using the seahorse bioscience XF analyser (see methods).

In order to dynamically characterise the metabolic profiles of both cell lines, a series of optimisation experiments were initially carried out on the seahorse machine. These experiments involved varying the medium conditions and adapting the basic seahorse glycolytic assay to meet our experimental requirements.

These initial studies carried out on the seahorse system, involved varying the amount of pyruvate and glucose while keeping the amount of glutamine in the medium constant. As a result, five medium conditions were established, and each cellular condition was then injected with both oligomycin (inhibitor of oxidative phosphorylation) and 2-Deoxy – glucose (a glucose analogue that inhibits glycolysis) to observe how the cells would respond when glycolysis was shut down and likewise how they would respond when the process of oxidative phosphorylation was inhibited.

Five different medium sets were set up (see supplementary) which included adding glucose (10mM) as a drug injection in port A rather than include it in the medium for ease of preparation of the other medium constituents. In port B, oligomycin (2μM) was injected and in port C, 2-Deoxy – glucose (50mM) was injected. Cells were stained with Hoechst to quantify cell number after the assay, and measurements were normalised to cell number.

This assay setup proved to be very challenging and owing to a high degree of variability, and the difficulties ensuring experimental reproducibility, meant that this kind of assay was not entirely suitable.

Furthermore, interpretation of the results was difficult with the incorporation of multiple conditions, it was decided to simplify this assay and just focus on comparing base line metabolic rates (results of this initial assay can be found in the supplementary material).

For the subsequent metabolic assays that are shown here, the same port injections (A, B and C) were used, but the medium conditions were replaced with either control supplemented medium and/or glucose starvation medium. Thus, reducing the four medium conditions previously used down to two.

In the initial instance, investigation of the basal metabolic profiles was carried out and although incorporation of the drug injections was included, it was decided that data would not be interpreted, prior to fully understanding and establishing the basal metabolic rates first.

For this reason, focus was placed on measuring and interpreting the basal metabolic rate of the cells under normal (supplemented medium) conditions and also under glucose starvation. As a result, interpretation was much easier.

Metabolic assays were carried out in three biological replicates and eight technical replicates to accommodate for the high variability often observed with the seahorse assay. All measurements were normalised to cell number.

Pilot studies were also carried out to determine the optimum time points for glucose starvation and metabolic readouts. 48hrs and 72hrs were chosen as a result, and because the seahorse assay is a real time assay, these timepoints helped to ensure the cells were sufficiently starved prior to starting the experiment. Cell number was determined by Hoechst staining after completion of the assay.

3.2.10 Base line metabolic profiling shows differences in OCR and ECAR between cell lines

Focusing on just the baseline metabolic rate of the cell lines, it was observed that the oxygen consumption rate (measure of oxidative phosphorylation - OCR) of the 786-cell line was consistently lower in comparison to the OCR of the 6450-cell line therefore confirming that the 786-cell line undergoes less oxidative phosphorylation (OCR) and more glycolysis (ECAR). This was also in alignment with the results Karl Morten obtained in his lab.

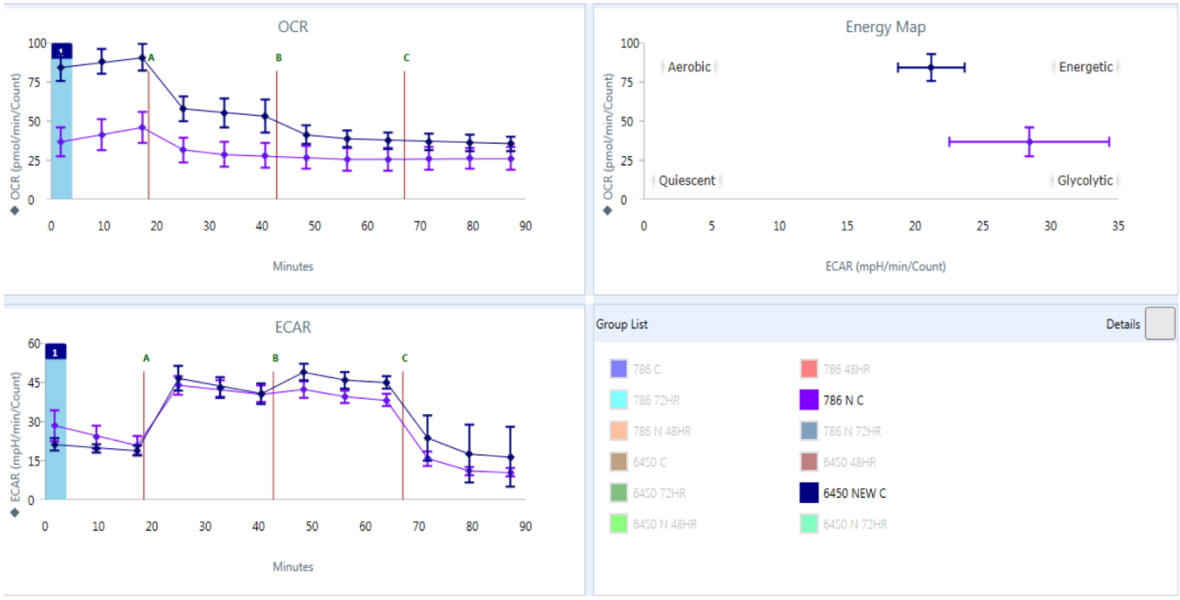


Figure 15: Metabolic profiling data output: Screenshot from Seahorse bioscience XF analyser showing differences in metabolic profiles of cell lines. Only the groups highlighted in the group list box are represented. Highlighted in purple is the 786-cell line and highlighted in blue is the early passage of the 6450-cell line. The panel on the top left shows the output for Oxygen consumption rate (OCR) the measure of oxidative phosphorylation between the two cell lines 786 (purple) and 6450 (dark blue). The panel on the bottom left represents the output for Extracellular acidification rate (ECAR) the measure of glycolysis between the 786 (purple) and 6450 (dark blue) cell lines. The energy map shown on the top right panel shows the metabolic profiles of the cells lines expressed as a ratio between the cell lines. A, B and C represent the drug injections (Glucose in A, Oligomycin in B and 2- deoxy -glucose in C).

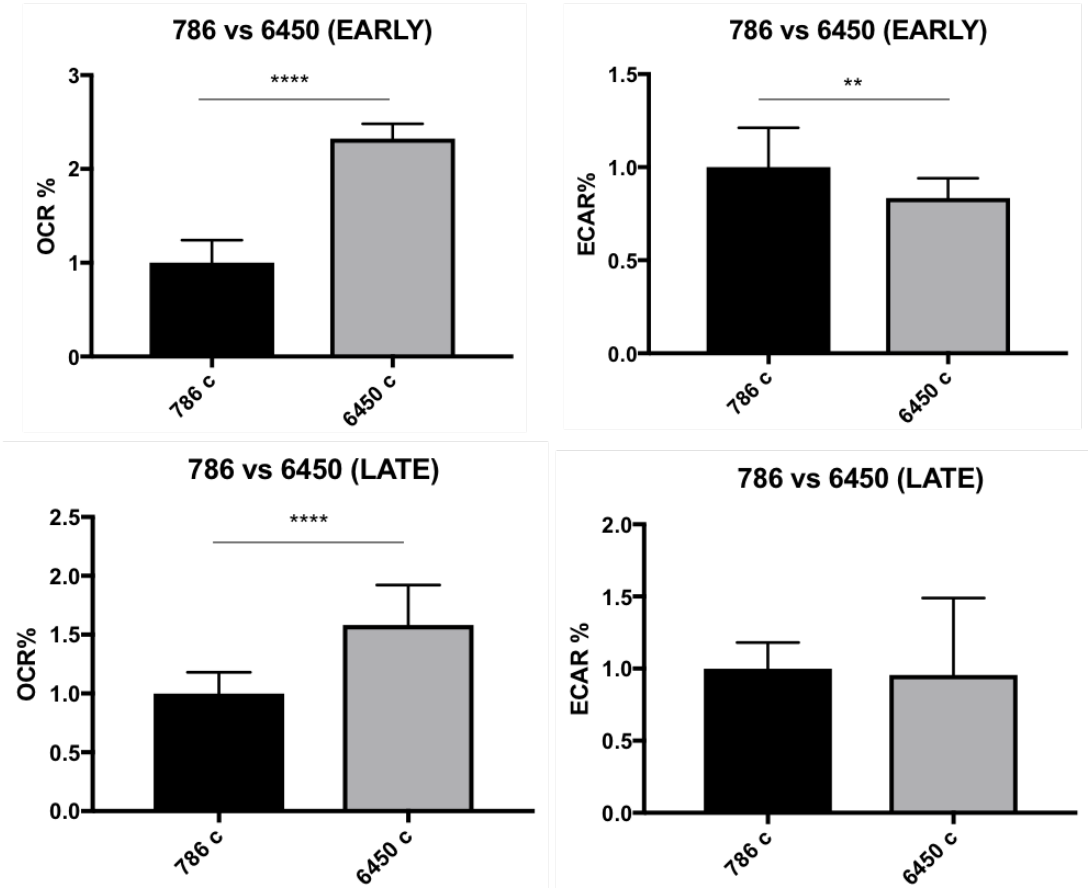


Figure 16: Metabolic profiling of early vs late passages show metabolic difference between cell lines: visual representation in the form of bar charts that reflect the differences in percentage OCR and ECAR between cells lines and passages. The left-hand side panel shows the percentage OCR between the 786 vs 6450 cell lines (early passage) adjusted p value <0.0001. Subsequently below this is the percentage OCR compared between the 786 vs 6450 cell lines (late passage) adjusted p value <0.0001. The right-hand side panels (tom and bottom) show the percentage ECAR comparing the 786-cell line with early 6450 (top) and late 6450 (bottom) adjusted p value 0.0013. Note: readings normalised to cell number. 3 biological replicates and 8 technical replicates.

Confirmation that the metabolic profiles between early vs late passages of the 6450 - cell line differ (as would be expected given the instability of the cell line) was made. What can also be observed is that the percentage OCR decreases in the 6450 late passage when compared to the early passage. Similarly, there is no significant difference in the percentage ECAR which is shown to decrease to match that of the 786-cell line.

Thus, it can be concluded from the seahorse results, that the 6450 early passages retain an oxidative phosphorylation metabolic phenotype even in later passages albeit at reduced levels.

3.2.11 The effect of glucose starvation on metabolic status – 786 versus 6450 (early passage)

In addition, the metabolic phenotypes of these cells under glucose starvation were investigated (figure 17). The experimental conditions were minimised, and focus was placed on just the early passage of the 6450-cell line for this particular experimental setup.

The result from this set of experiments show that in the 786-cell line, the percentage ECAR decreases as you starve with glucose over time. Whereas with the 6450-cell line a slight decrease in percentage OCR is seen but the reduction is not as significant as with the 786-cell line.

In contrast, when looking at the ECAR, the results show that in the 786-cell line the percentage OCR increases significantly after 48hr glucose starvation but then subsequently returns back to the basal OCR rate after 72hrs. The 6450-cell line however, shows an incremental decrease in percentage OCR over the starvation period, with a very significant decrease in OCR percentage after 72hr glucose starvation.

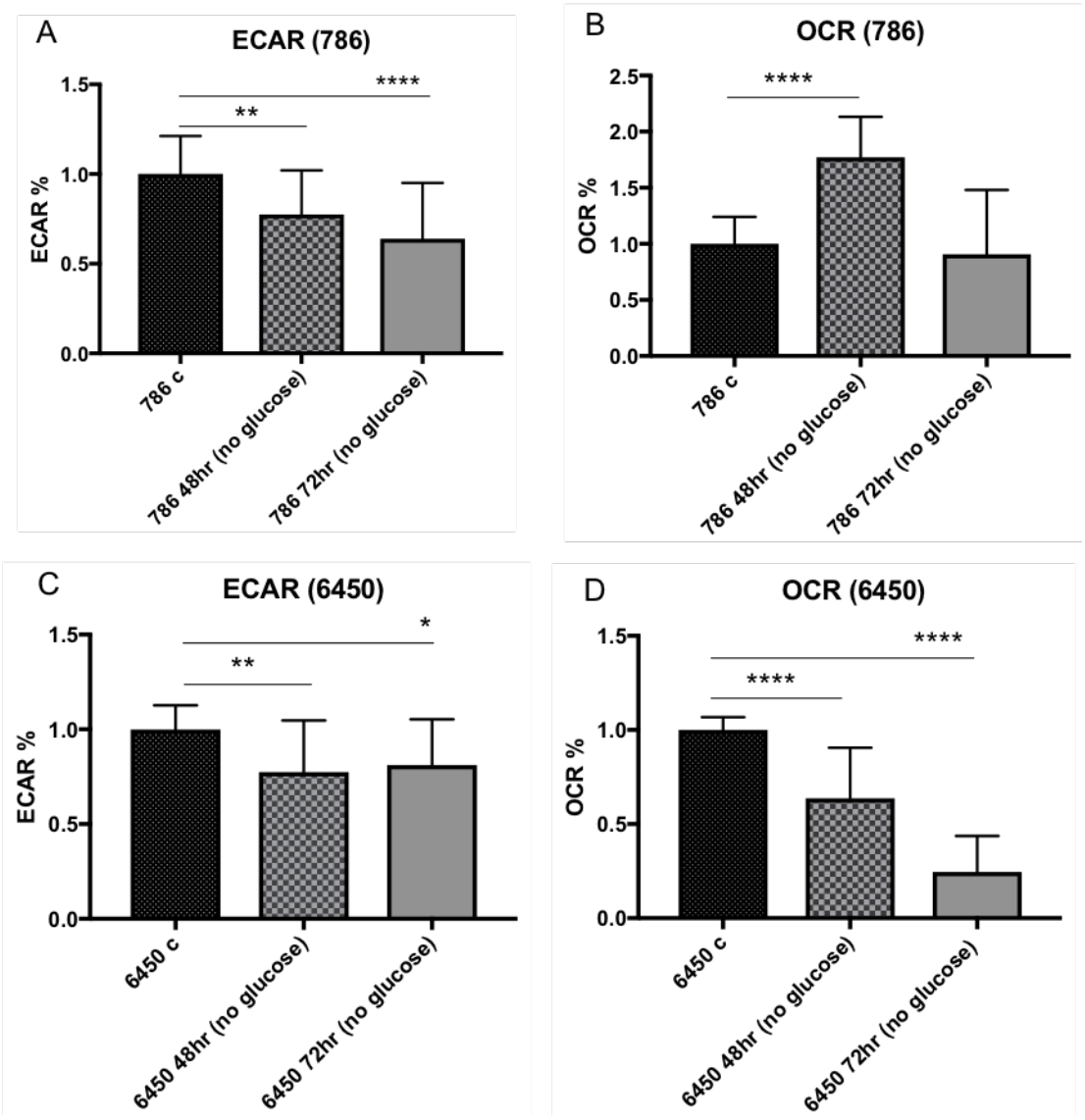


Figure 17: Metabolic profiling of the 786-cell line versus early 6450 passage under glucose starvation shows metabolic differences: visual representation in the form of bar charts that reflect the differences in percentage OCR and ECAR measured between the 786-cell line and the 6450 early passage under glucose starvation (48hr and 72hrs) when compared to control cell lines (supplemented medium conditions). A) shows percentage ECAR measured between 786 control and 786 starved of glucose (48hr and 72hr) adjusted p values 0.0070 and <0.0001 accordingly. B) shows percentage OCAR measured between 786 control and 786 starved of glucose (48hr and 72hr) adjusted p value <0.0001 C) shows percentage ECAR measured between 6450 control and 6450 starved of glucose (48hr and 72hr) adjusted p values 0.0015 and 0.0104 accordingly D) shows percentage OCAR measured between 6450 control and 6450 starved of glucose (48hr and 72hr) adjusted p values <0.0001.

3.2.12 Fixing ambient oxygen to 5% influences the metabolic profiles of the cells

Emerging research is increasing the appreciation for the fact that the cell culture environment does not accurately reflect the in vivo condition. This has led to a number of researchers, carrying out experiments under more physiological conditions, in particular when it comes to nutrient availability, and oxygen concentrations.

The importance of oxygen concentrations in in vivo modelling has been indicated from observations that oxygen concentration is involved in a number of cellular mechanisms. These mechanisms include metabolic status, cellular differentiation and senescence. Furthermore, the development of localised hypoxic regions has been associated and linked with disease states, such as cancer.

Impeded oxygen supply, can push oxygen concentration below normal physiological levels, inducing a cascade of complex adaptive responses that are regulated by a variety of mediators such as hypoxia inducible factor (HIF) [304].

This process is of particular relevance in solid tumours, where oncogene led proliferation causes nutrient and oxygen deprivation, impacting on vascular angiogenesis status as well as the initiating oxygen sensitive survival pathways [305].

It is important to note that the assumption that cellular oxygenation status can be extrapolated from ambient oxygen measurements, is somewhat invalid [292]. As a result, it is important to measure and monitor intracellular oxygen to maintain the physiological relevance of experimental observations.

Consequently, further metabolic profiling was carried out using the Luxcel metabolic apparatus (figure 18), a system which unlike the seahorse, can be used to fix the ambient oxygen and thus measure intracellular oxygen. This system measures cellular oxygenation by means of a nanoparticulate intracellular probe (see methods).

Using the intracellular oxygen sensing probe an immediate readout of intracellular oxygen levels can be generated, with glycolytic cell lines reflecting the oxygen concentration of the environment (5% in my experiments), and cells with an oxidative phenotype having significantly lower levels of intracellular oxygen. Inhibition of oxygen consumption in lines with high oxygen consumption increases intracellular oxygen levels towards environmental levels [306] .

In order to investigate the cellular metabolic response to hypoxic conditions the ambient oxygen level was set to 5%. It was proposed that this would be more representative of the oxygenated environment in the lung and thus the premise upon which a lower more "hypoxic" concentration was not used instead [307].

Characterisation of the cells under a variety of starvation conditions (in a 5% ambient oxygen environment), was carried out. This included glucose starvation, low pH (6.7) and glutamine starvation (figures 19 and 20). In addition to this, the cell lines were treated with Antimycin (1μM) and Rotenone (10μM), inhibitors of the electron transport chain (figure 21).

Experiments were run for a total of approx. 2 days and were carried out on 2 biological replicates and 3 technical replicates. For the glucose starvation conditions, cells were starved of glucose 24hrs prior to the assay to ensure efficient depletion of glucose from the medium, therefore replicating the 42hr/72hr glucose starvation timepoints carried out on the seahorse assay. Cell were stained with propidium iodide (PI) after the assay to calculate live/dead cells (see supplementary).

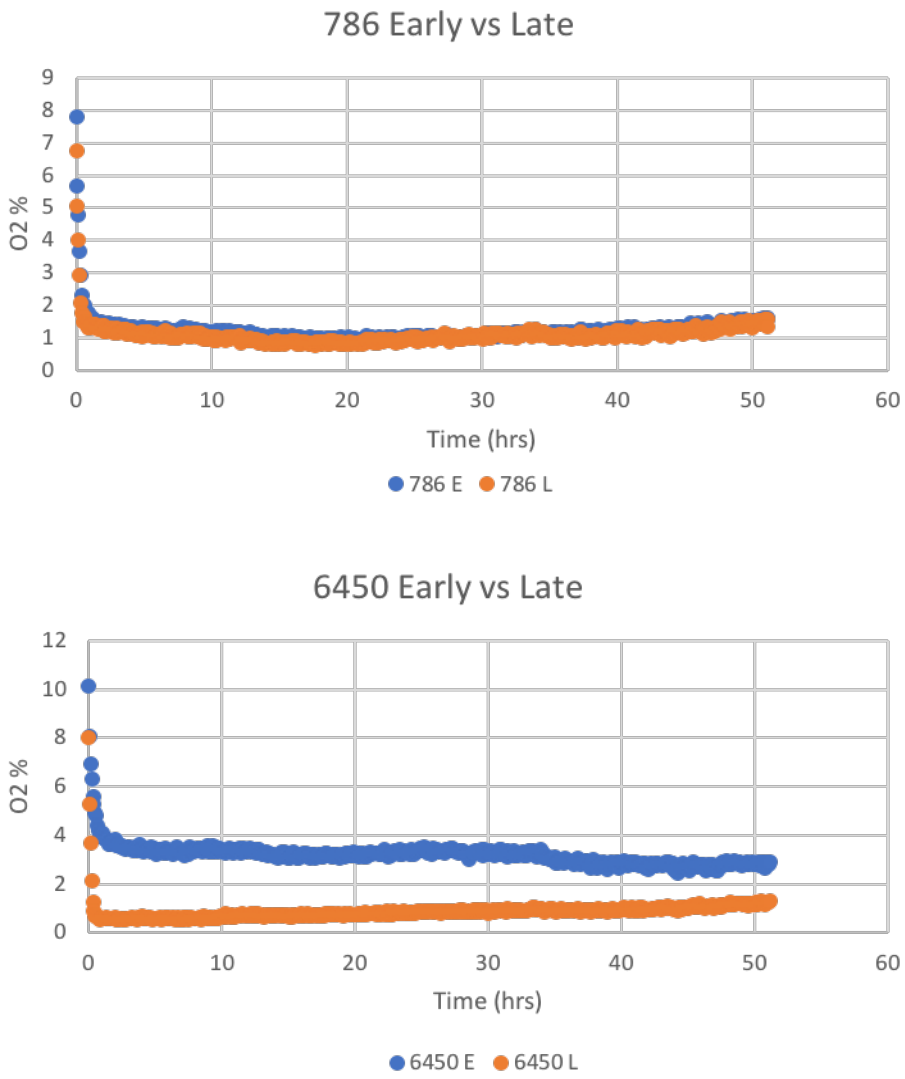


Figure 18: Metabolic profiles of 786 vs 6450 (early and late passages) in 5% oxygen environment show different metabolic signatures: *Graphical representation to show intracellular oxygen levels in cells 786 early vs late (top) and 6450 early vs late (bottom) under 5% environmental oxygen. Experiment was carried out on 2 biological replicates and 3 technical replicates.*

A number of observations were deduced from this particular assay, highlighting the potential significance of incorporating a fixed ambient oxygen level when analysing metabolic profiles.

As mentioned above, low intracellular oxygen levels correspond with oxygen consumption processes whereas higher intracellular oxygen levels indicate less oxygen consumption processes are taking place.

With the 786-cell line, it was clear to see that there is no difference between passages. However, looking at the 6450-cell line, early passage vs late passage a stark difference in metabolic status can be noted. The 6450 early passage, has a much higher intracellular level of oxygen closer to the fixed 5% oxygen in the environment, inferring less oxygen consuming processes are taking place.

Whereas, the 6450 late passage has a similar metabolic profile to that of the 786-cell line, showing a reduced intracellular oxygen reading, thus suggesting that more oxygen consuming processes are taking place.

3.2.13 The influence of glucose starvation and low pH on intracellular oxygen capacity

It was observed that the 6450 early passage starved of glucose did not fluctuate much when compared to the 6450 control (grown in normal glucose supplemented medium), whereas the 6450 late passage starved of glucose remains at a low intracellular oxygen level relative to the control and to the 6450 early passage.

The 786-cell line control and starved showed a similar intracellular oxygen profile to what was observed with the 6450 late passage under glucose starvation, in that it remains at a low intracellular oxygen level in the presence of no glucose.

When the 6450 cells are grown in low pH conditions in addition to a low oxygen environment, the 6450 early passage low pH showed a reduced intracellular oxygen level when compared to the control 6450 (grown in normal pH medium 7.4). The 6450 late passage low pH showed the exact opposite, with the intracellular oxygen level shown to increase substantially.

The 786-cell line follows a similar pattern to that of the 6450 when subjected to a low pH environment, with an increased intracellular oxygen level relative to that of the 786 control.

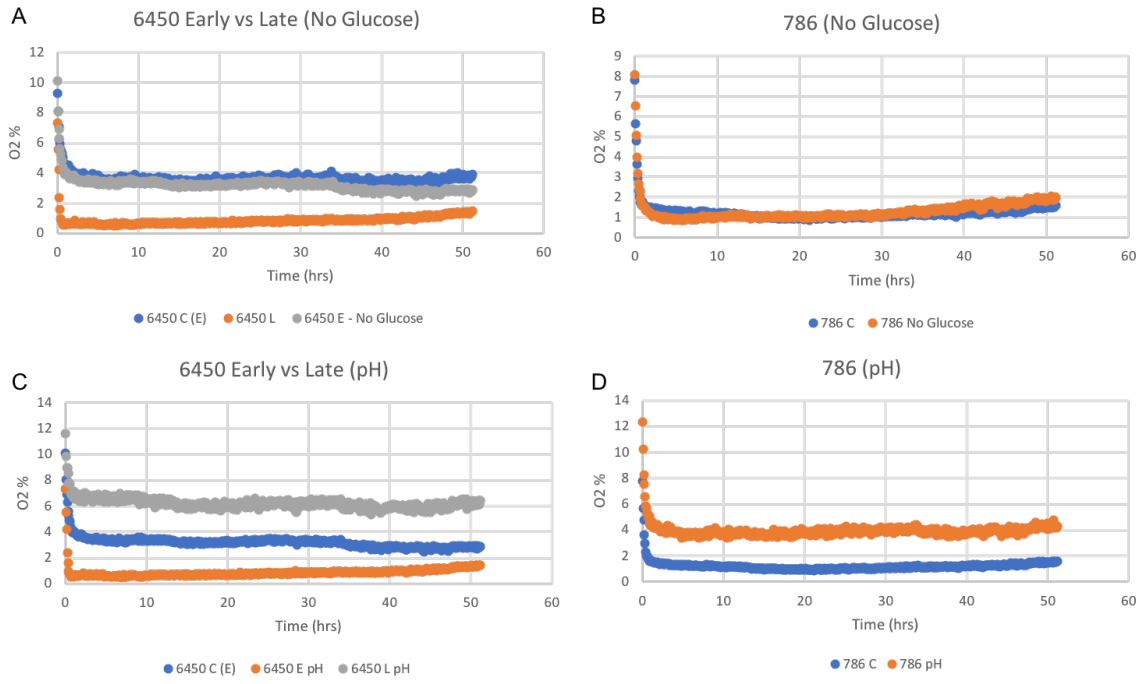


Figure 19: Metabolic profiles of 786 vs 6450 (early and late passages) in 5% oxygen environment show different metabolic signatures: **A)** shows the intracellular oxygen levels comparing 6450 early vs late passages when starved of glucose **B)** shows the 786 intracellular oxygen profile when starved of glucose C) shows the intracellular oxygen profile of the 6450 early vs late passages under low pH (6.7) D) shows the intracellular oxygen levels of the 786-cell line under low pH (6.7). Control cell lines represent cells grown in supplemented medium/ normal pH condition 7.4). Experiments carried out on 2 biological replicates and 3 technical replicates.

3.2.14 The influence of glutamine starvation on intracellular oxygen capacity

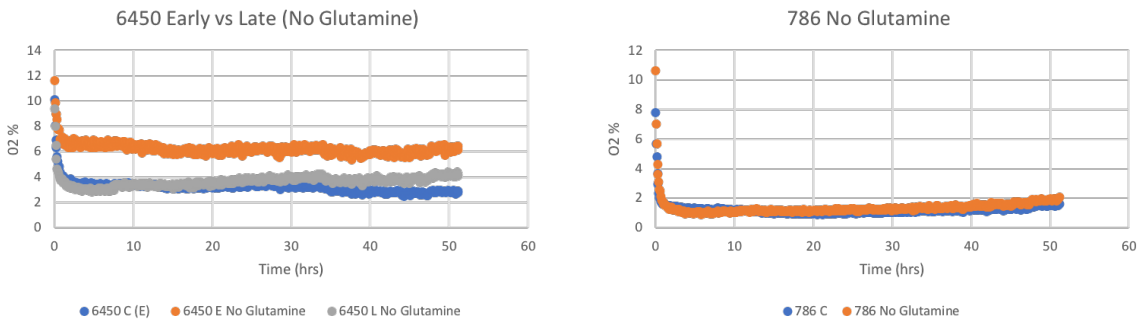


Figure 20: Influence of glutamine starvation on intracellular oxygen capacity: Graphical representation of the intracellular oxygen profiles comparing 6450 early vs late passages under glutamine starvation (left) and the intracellular oxygen profile of the 786-cell line under glutamine starvation (right). Control cells represent cells grown in supplemented medium. Experiments carried out on 2 biological replicates and 3 technical replicates.

When the 6450 early passage is starved of glutamine, a two-fold increase in the intracellular oxygen level was observed relative to the control 6450 (grown in glutamine supplemented medium). Interestingly, the 6450-glutamine starved late passage was observed to show an intracellular oxygen level very similar to that of the 6450 control.

In contrast the 786-cell line was observed to show no difference in intracellular oxygen under glutamine starvation and when compared to the 786 control (grown in glutamine supplemented medium).

3.2.15 The effect of electron transport chain inhibitors on intracellular oxygen levels

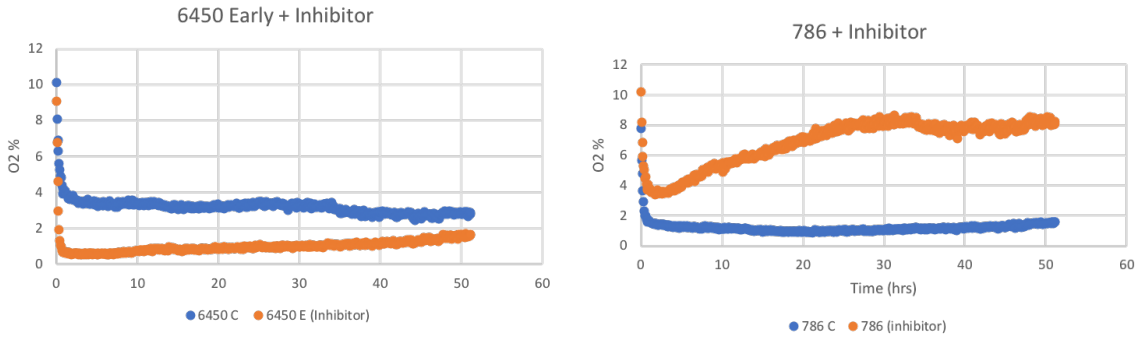


Figure 21: Treatment with electron chain inhibitors highlights differences in intracellular oxygen levels: Graphical representation of the 6450 early vs late passage +/- inhibitor Antimycin (1 μM + rotenone 10 μM) (left) 786 +/- inhibitor (right). Experiment carried out on 2 biological replicates and 3 technical replicates.

Upon treatment with a mix of Antimycin and rotenone, inhibitors of the electron transport chain, a reduction in the intracellular oxygen was observed in the 6450-cell line with added inhibitor when compared with the 6450 control (no inhibitor). Furthermore, and rather surprisingly the 786-cell line (with inhibitor) showed a dramatic increase in intracellular oxygen level even with treatment with potent inhibitors of electron transport chain.

3.2.16 mRNA profiling shows differential regulation of proteins in the 6450-cell line (early vs late passages)

In order to further characterise the cell lines and following on from my proteomic study outlined at the start of this chapter, an mRNA profiling of the cell lines was carried out. The 786 early and late passages were compared with 6450 early and late passages. It was decided that both 6450 early and late passages were worth comparing and hence both passages were investigated, unlike in the proteomics study where the study was focussed on just the early 6450 passage. mRNA profiling was carried out by Dr. Giovanni Stracquadanio (Computational Intelligence Lab for Biology and Medicine, School of Computer Science and Electronic Engineering, University of Essex, UK).

When 786 late vs early passages were compared, only two differentially regulated genes were observed (see figure 22) whereas 1176 genes were found to be differentially regulated in the 6450 late vs early passages. This confirms the instability of the 6450-cell line from the perspective of mRNA gene expression.

Genes with low read count (# reads < 10) were removed and differential expression analysis was carried out using DESeq2. DESeq2 takes in input raw counts and uses a negative binomial model to find genes with significant change in expression. Experiments were carried out on 3 biological replicates.

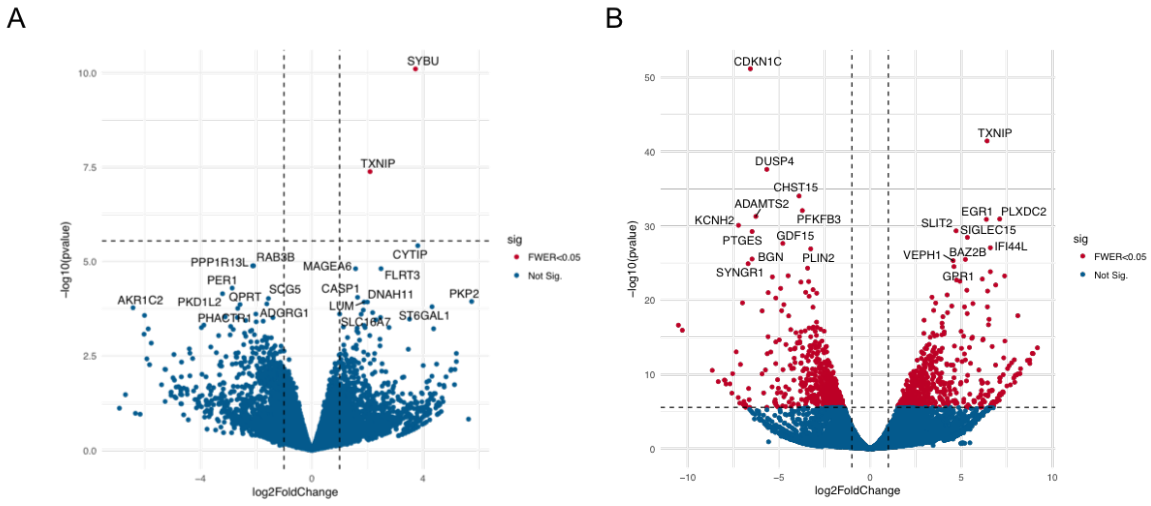


Figure 22: Volcano plots showing differential regulation of genes between cell lines late vs early: A) shows the differential regulation of genes between late and early passages of the 786-cell line B) shows differential regulation of genes between late and early passages of the 6450-cell line. Red dots signify statistically significant (p value less than 0.05) upregulated proteins. Experiments carried out on 3 biological replicates.

3.2.17 Downstream global analysis of the 6450 cell line highlights top variable pathways

Owing to substantial differential gene expression between the early and late passages of the 6450 cell lines, it was decided that focus should be placed on this cell line with the aim to further characterise these genes by means of both enrichment and pathway analysis. As a result, a global analysis was carried out in the initial instance to broad overlook of the potential pathways enriched and thuds the top variable pathways across early and late passages. Future investigations will include a differential analysis comparing 6450 early and late passages.

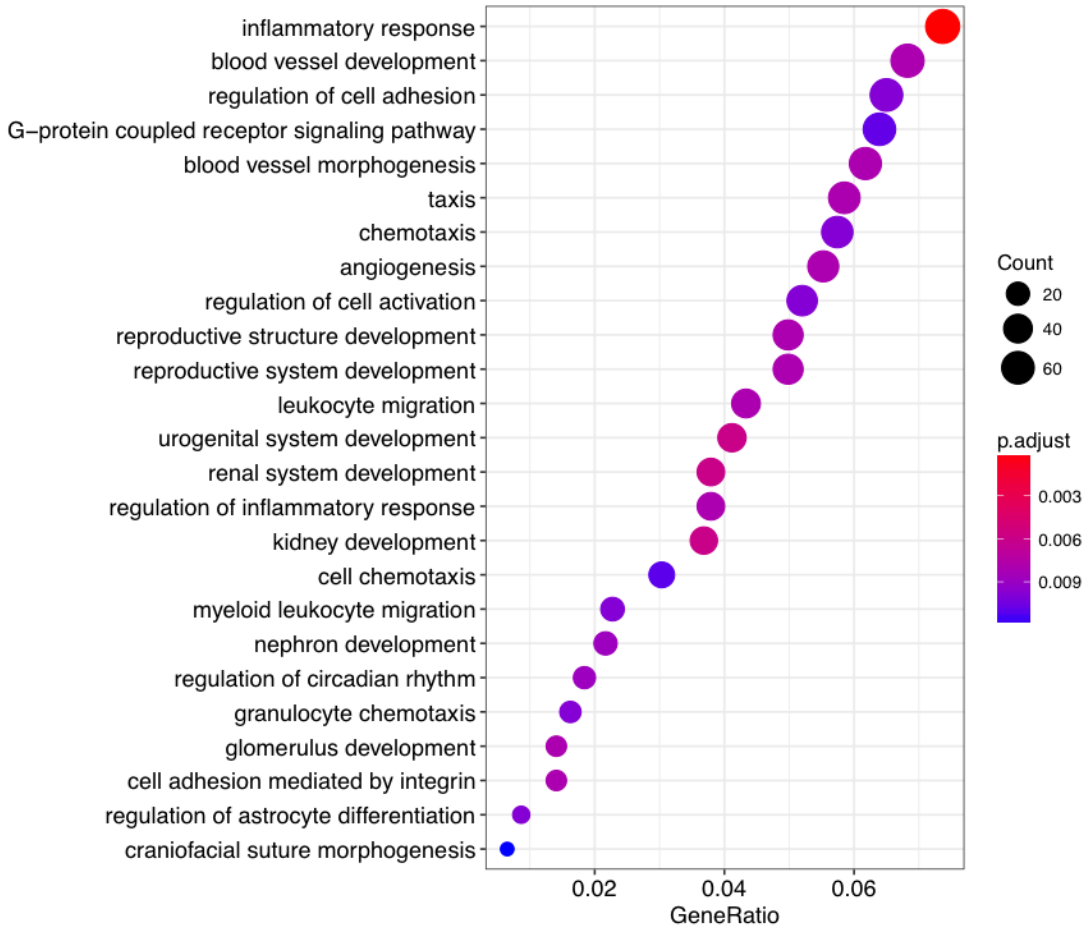


Figure 23: Pathway analysis of mRNA protein profiles reveals upregulated molecular pathways in the 6450 cell lines: shows the upregulated and significant pathways upregulated in the 6450 cell lines. The bigger the circle the higher the count for proteins involved in a particular pathway. The red gradient colour coding denotes significance, red implies high significance and purple /blue implying lower significance.

Gene ontology analysis was used to determine which molecular and biological functions were contributing to gene expression in the 6450-cell line (global analysis – top variable hallmarks) with inflammatory response, blood vessel development, regulation of cell adhesion, angiogenesis and hypoxia related pathways being found to be the most significant.

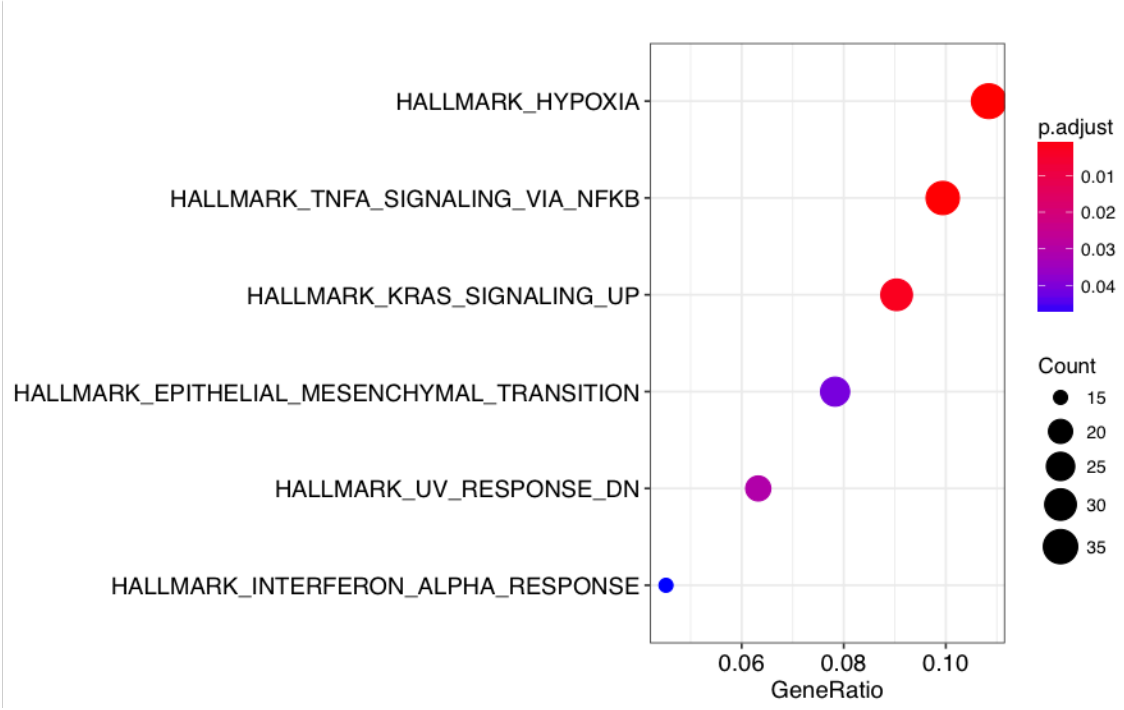


Figure 24: Canonical pathway analysis reveals upregulated hallmark signalling pathways in the 6450-cell line: Schematic to Show the upregulated hallmark signalling pathways in the 6450-cell line. The bigger the circle represented the high the protein count in a specific pathway. The red gradient colour coding denotes significance, red implies high significance and purple/ blue implying lower significance.

Global mRNA investigations highlighted the top variable pathways from both the hallmark data set and canonical pathway databases. These pathways included hypoxia associated pathways as well inflammatory and immune response related pathways. However, only two predominant and enriched pathways were observed with the canonical database comparison, those being HIF and lysosome associated pathways.

3.2.18 Characterisation of migration and invasion profiles between cell lines

Both the proteomics and gene expression studies highlighted a number of potential variable regulatory proteins and global pathways associated with the mouse model derived cell lines. Sorting through the lists of statistically significant genes and proteins as well as investigating specific disease state pathway involvement, it became apparent that the adhesion, migration and invasion profiles of the cell lines, would be worth probing further.

These studies would not only aid in characterising the cell lines, expanding on what we already know, but could also shed some light on the metastatic and invasion potential, independent of observed proliferation rates.

Cell migration is a crucial aspect, forming the basis of many studies in cancer research. Both the transwell and wound healing cell migration and invasion assays can be used to provide extensive information pertaining to cell migratory behaviours as well as enabling researchers to investigate in more detail the molecular mechanisms of cell migration [308].

Owing to the static nature of the wound healing assay, namely the absence of a migratory barrier (such as the basement membrane found in physiological settings) the transwell matrigel assay was opted for instead.

This assay not only incorporated a matrigel plug but also involved the use of 10% FBS as a chemoattract (see methods for full description). Optimisation experiments were carried out to determine matrigel concentration and optimum cell number. 300 ug/ml matrigel and 50,000 cells per well insert was found to produce representative results.

Cells were counted prior to the assay, to ensure the same number of cells were used and measurements were normalised to percentage migration of cells in the presence of 0% chemoattract. Cells were also starved in 0% FBS one day prior to the assay to properly assess affinity and migratory potential towards the 10% FBS (chemoattract).

Owing to the fact that the carbonic anhydrase family (more recently Ca2 in particular) has been implicated in inhibition of epithelial mesenchymal transition and metastasis [309], a broad acting inhibitor of Carbonic anhydrases, (Ca2 potentially valid protein target from my previous mentioned studies) Acetazolamide (5mM) was also added to the assay to see if this would influence migration /invasion. A negative control containing no matrigel was also employed.

It was hypothesised that this assay would help better characterise and study the aggressiveness of tumour cells, since it is known that the that a variety of cancer cells must degrade the tissue basement membrane (represented by the matrigel plug in this assay) in order to invade and disseminate [310].

Furthermore, it has been highlighted that dormant cells maintained their quiescent status in studies involving a representative basement membrane. Whereas when grown in tissue culture plastic alone, they were found to proliferate well [311].

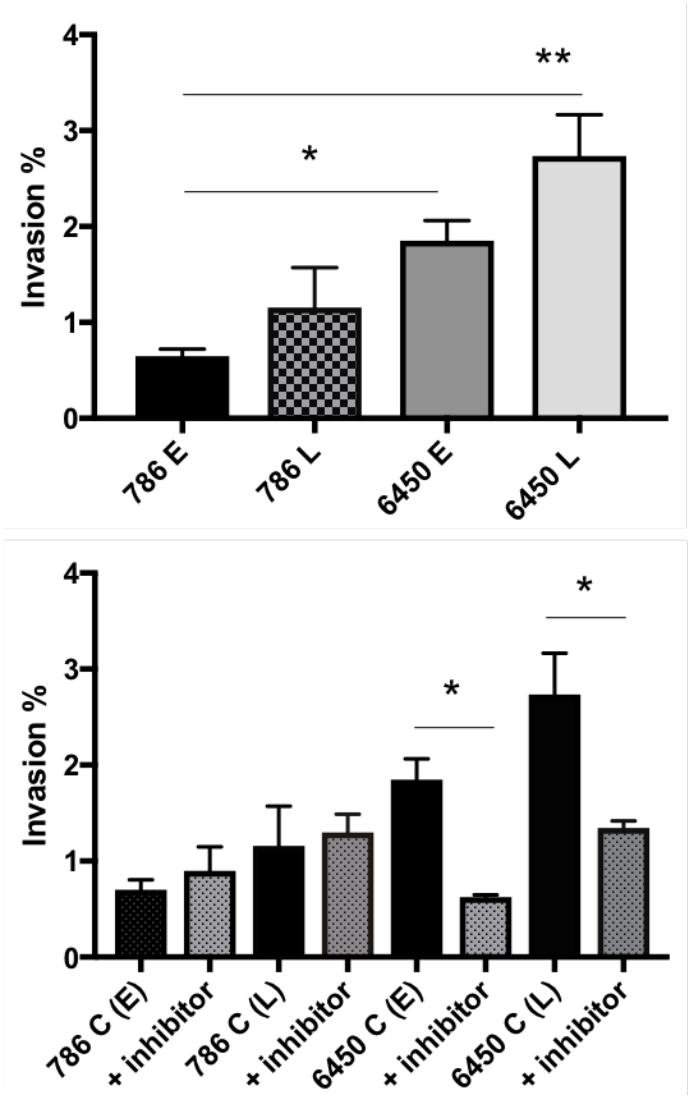


Figure 25: Characterisation of migration and invasion profiles between cell lines (early vs late) shows differences in invasion profiles: Graphical representation showing the percentage invasion comparing the 786-cell line (early vs late) with the 6450-cell line (early vs late) (top) and the percentage invasion +/- CA2 inhibitor acetazolamide (bottom). Measurements were normalised to cell number and the experiment was carried out on 3 biological replicates and 2 technical replicates. Adjusted p values for invasion without inhibitor (top) 0.0442 and 0.0065 respectively. Adjusted p values for invasion with inhibitor (bottom) 0.015 and 0.045 respectively.

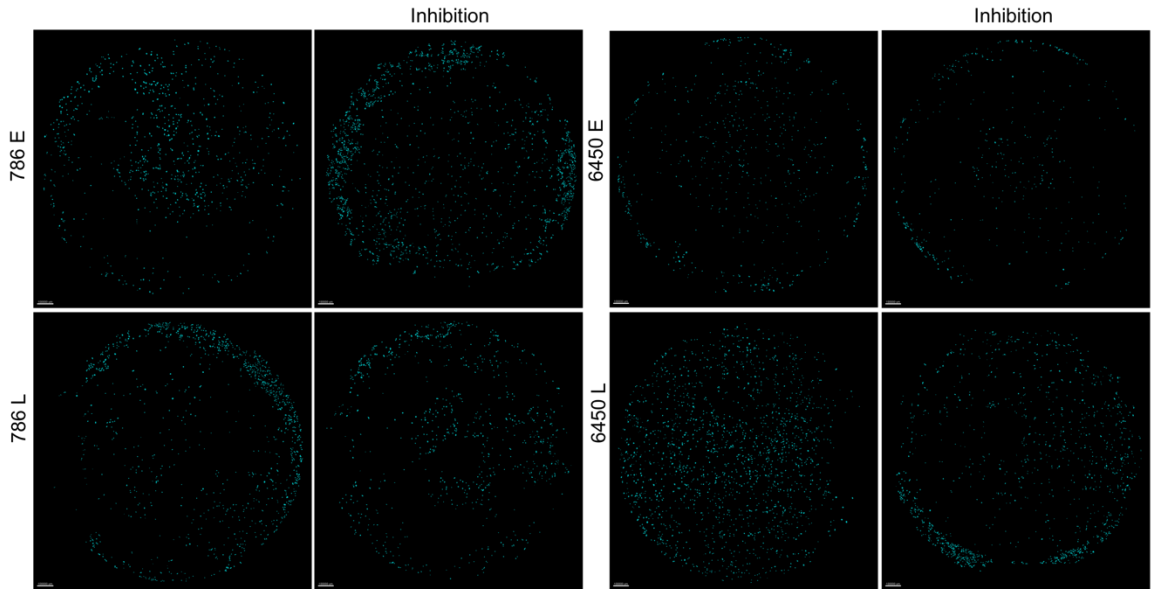


Figure 26: Visual differences in cell invasion between cell lines and before and after treatment with inhibitor: Fluorescent images showing giving a visual representation of the migration/ invasion profiles of the cell lines 786 and 6450 (early vs late) +/- the inhibitor. The fluorescently stained cells (CMFDA) represent the cells that have migrated /invaded through the Matrigel.

From the invasion assay, no significant difference was observed in percentage invasion between 786 early vs late passages. However, the 6450 early passage showed a significantly higher percentage of invasion when compared to the 786-cell line. The 6450 late passage was observed to be the most invasive cells when compared to the 786-cell line.

3.2.19 Preliminary assessment of the Intercalation capability of the cell lines

In order to assess the intercalation ability of the cells, and further investigate the differences in intravasation capacity between cell lines, an intercalation assay was carried out. The Intercalation assay differs from the standard adhesion assay in that it is not a static assay (as it can be argued that the cells will adhere to any surface they come in contact with including plastic). Thus, it is an assay that is more closely representative of what happens in vivo.

Furthermore, in order to keep our investigations as close as possible to physiological conditions found in the vivo mouse model, isolated mouse lung endothelial cells were used, instead of standard Human umbilical vein endothelial cells (HUVEC's), that are routinely used in these types of assays.

Cells were grown in either normal supplemented medium or in glucose and glutamine deficient medium (48hr prior to the assay). Cell lines were counted and plated on isolated lung endothelial cells (see methods) at a density of 6000 cells per 50 uL in each well.

The assay was run overnight for approximately 18hrs in total. 2 fields of view were taken per well and 3 biological replicates were carried out with 5 technical replicates of each condition.

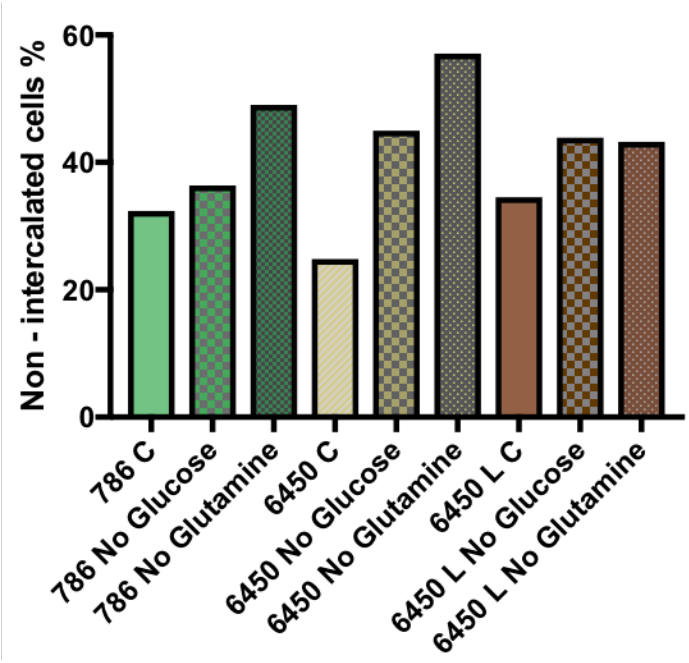


Figure 27: Measuring intercalation in the cell lines 786 vs 6450 (early vs late) highlights differences in intercalation capability: Graphical representation of the intercalation capability of the cell lines, control 786 (normal supplemented medium), no glucose and no glutamine and control 6450 early and late (normal supplemented medium), no glucose and no glutamine. Intercalation was assessed at two timepoints (t0 and t8hrs). Round cells were counted as non-intercalated – elongated cells were counted as intercalated cells. Measurements are represented as the average of two fields of view per technical replicate, owing to variability with the assay. Experiment was carried out on 3 biological replicates and 5 technical replicates. Measurements were normalised to cell number.

From the assay we can conclude that the 786-cell line shows a higher percentage of non-intercalated cells, thus indicating that it is compromised in its ability to intercalate with the lung endothelial cells. The 6450 early passage shows a lower percentage of non-intercalated cells, and therefore is shown to intercalate more than the 786-cell line. The 6450 late passage resembles that of the 786-cell line in terms of its ability to intercalate.

Glucose starvation is observed to hinder intercalation in all cell lines with cell lines showing an overall increase in the percentage of non-intercalated cells. However, starvation with glutamine is shown to have more of a detrimental effect on intercalation, especially in the 6450 early passage and 786 cell line, with the 6450 late passage showing no noticeable difference in percentage of non - intercalated cells when compared to its intercalation profile when starved of glucose.

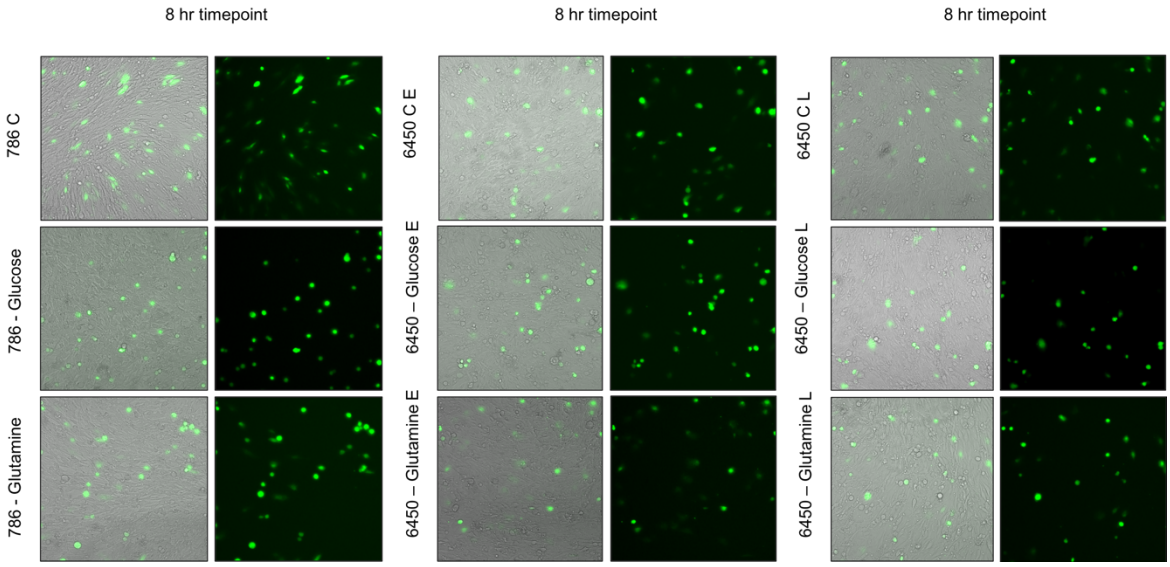


Figure 28: Visual representation of differences in intercalation between the cell lines 786 vs 6450 (early vs late) under starvation conditions: Corresponding bright field and fluorescent microscopy images showing the effect of glucose and glutamine starvation on intercalation relative to the control (cells grown in normal supplemented medium) at the 8hr timepoint. Round cells are considered non-intercalated whereas more elongated cells are considered to be intercalating/ intercalated. Left hand panel shows the intercalation differences between 786 control cells, 786 no glucose and glutamine. Middle panel shows the intercalation differences between 6450 control cells (early), 6450 no glucose (early) and 6450 no glutamine (early). Right hand panel shows the differences in intercalation between 6450 control (late), 6450 no glucose (late) and 6450 no glutamine (late). Only one field of view is shown at the 8hr timepoint.

3.9.20 Discussion and limitations

This chapter summarises all the in vivo work that was done in order to characterise the cell lines in relation to how they can be utilised to interrogate and better understand the molecular underpinnings that define the in vitro mouse model.

Of particular interest was understanding why the 786-cell line when injected subcutaneously (in the mouse), is unable to colonise the lung and remains dormant, whereas the 6450-cell line is successful at colonising the lung and becomes metastatic as a result.

From the experiments carried out it becomes very apparent how challenging this aspect of the project has been. Not only was the 6450 cell lines observed to be unstable when introduced into the tissue culture environment, but when experiments were carried out, it was important to ensure that the early 6450 cell line had not switched phenotype and reverted back, resembling that of its 786-cell line counterpart. The cell authentication report supports this instability.

Without any type of biomarker to distinguish between early and late passages, it became very cumbersome to monitor both growth and morphology at all times prior to experiments, making experimental reproducibility extremely difficult (maintaining 6450 early passages from the same batch for example).

In addition to this, and as noted from the proliferation growth curves, a lot of time was spent waiting for the 6450-cell line grow so that it could be expanded for use in experiments while maintaining the phenotype characteristic to the early passage.

Despite these challenges, phenotypical differences between the cell lines were demonstrated successfully, particularly the 6450 early vs late passages from multiples perspectives.

Documenting the growth capability of the cell lines highlighted that the seemingly metastatic cell line in vitro (6450 early passage) was very slow in growth whereas the 786-cell line was found to have a fast-growth rate. It has also been documented in a number of scientific studies that slow growth rate may be a feature of highly invasive and metastatic cancer cell lines, with cancer progression being found to be inversely related to tumour growth in a variety of cancer types[312] .

There are a number of possible explanations for this, as mentioned earlier this could be due to the cells being grown in tissue culture plasticware as well as exposure to the tissue culture environment, which influences both metabolic profiles and cell growth patterns (as shown in our studies). Further analysis, where data comparing the cell line in vitro model and the in vivo, could potentially help understand this switch better.

In addition to cell growth rates, an observed difference in morphology with the 6450-cell line being more spindle like and the 786-cell line more rounded in its cell morphology, was noted. The association of morphology and metastatic potential remains somewhat unresolved, however it has been noted that spindle like cells have been linked with more aggressive and metastatic cancer traits [313].

These characterisations are difficult to ascertain from the in vivo work alone but are necessary in order to understand and interpret these findings accurately.

It thus becomes clear, going forward with this project, that comparing the 786-cell line with both the 6450 early and late passages is essential.

Proteomics has proven to be a very useful tool in addressing this challenging in vitro characterisation task. Unfortunately, due to time restraints and limitations with the cell culture model as mentioned above, a proteomic study comparing the 786-cell line with 6450 early passage was only carried out, and therefore combining the transcriptomics results (carried out on early versus late cells) with the proteomics data, was not possible.

From the protein pull down, proteins that were found to be differentially regulated between the two cell lines could be compared. From the analysis studies, it was found that a significant number of proteins that were being expressed in both cell lines, were proteins that are implicated in metabolic activity, which has been cited previously.

Furthermore, several proteins of interest were found to show a significant difference between the two cell lines, including Glutathione S transferase and Carbonic anhydrase as well as a number of proteins involved in metabolic pathways such as oxidative phosphorylation and glycolysis.

The potential link with the Na+ - H+ exchanger carbonic anhydrase 2 (NHE1), is of particular interest, seeing that the carbonic anhydrase family has been implicated in both the creation and maintenance of pH differential in tumour cells as well as playing a critical role in tumour cell metabolism, migration and invasion [314].

In particular carbonic anhydrase has been associated not only with migration and cell proliferation but has also been found to serve as a point of attachment for the actin cytoskeleton with the plasma membrane [315].

Furthermore, carbonic anhydrase is heavily involved in the acidification of the developing tumour environment contributing to genetic instability and enhancing tumour invasion and metastasis [315].

Although the role of carbonic anhydrase in cancer remains somewhat obscure, a recent study has implicated carbonic anhydrase in facilitating hepatocellular carcinoma (HCC) metastasis [309]. Furthermore, it was shown that carbonic anhydrase acts as a tumour suppressor of HCC metastasis and EMT, correlating with favourable overall survival in HCC patients [309].

This potentially may coincide with the noted observation that under low pH conditions (6.7) metabolic profiling was observed to change the most between cell lines (intracellular oxygen assay). However, further investigations into tumour acidosis and the role of carbonic anhydrase would need to be carried out before any conclusions can be made.

Glutathione S transferase is also an interesting candidate that we identified from our proteomic pull down. The super family of glutathione transferases (GSTs) have multiple biological roles which include protection of DNA against oxidative stress (including DNA promoting mutations in cancer) and cytotoxic molecules [316].

GST's are also able to conjugate to toxic molecules such as therapeutic drugs and products of oxidative metabolism inferring a detoxification function which acts to make these molecules less toxic, facilitating the discharge of the these molecules from the cell [316].

In addition to this, GST's are also involved in signal transduction where they control the activity of the mitogen activated protein kinase (MAPK) family and protect tumour cells from apoptosis[316].

Although TSP1 was not differentially expressed in our proteomic pull down, it has been associated with the regulation of adhesion, migration, and angiogenic modulation, its exact effects on tumour progression are multifaceted and expression of TSP1 is often dependant on molecular and cellular composition of the microenvironment as well as localisation rather than expression level [317].

Findings from the metabolic experiments that were carried out suggest that fixing ambient oxygen to 5% rather than keeping it at 20% (percentage ambient oxygen is kept at most assays are carried out in) highlight the potential importance of lowering the ambient oxygen in order to attain representative physiological environments.

Results from the seahorse experiment, which was carried out in normal ambient oxygen levels (~18-20%) suggest the 786-cell line undergoes glycolysis (Warburg effect) and the 6450 early passage undergoes oxidative phosphorylation (reverse of the Warburg effect).

However, upon fixing the ambient oxygen level to 5% and measuring the intracellular oxygen, the 786-cell line is shown to undergo more oxygen consuming processes with the 6450 early passage being observed to have an intracellular oxygen level close to 5%, suggesting that it is undergoing less oxygen consumption.

The results from the metabolic studies are difficult to understand and thus interpret. The differences in seahorse versus intracellular oxygen assay adds to the complexity of the metabolic profiling.

For example, the observation that was observed with the 786 - cell line responding with an increase in intracellular oxygen after treatment with electron transport chain inhibitors could be explained in a number of ways. It could be due to an interaction between the intracellular probe and the drugs or alternatively this observation could also be due to the accumulation and production of reactive oxygen species and oxidative stress. Thus, highlighting the challenge of interpreting such dynamic data.

In addition to this, it's worth noting that an attempt was made, to replicate the Seahorse assay setup (namely keeping the ambient oxygen between 18-20% oxygen) with the Luxcell intracellular assay, however technical issues were encountered. This would need to be pursued again in the future.

Looking into the literature surrounding cancer and metabolism brings up a multitude of explanations for the observance of different metabolic profiles in cancer cells. However, microenvironment seems to be the most obvious explanation.

Cancer cells, unlike normal cells show a preference for incomplete metabolism of glucose in order to maintain their high proliferative rate [318].

Malignant cells have been found to have significantly increased rates of glucose metabolism in comparison to normal cells. It has been suggested that glucose provides reducing equivalents required for H_2O_2 detoxification via the production of pyruvate which has been shown to scavenge hydrogen peroxide directly [319] [320] in addition to the regeneration of the reduced nicotinamide adenine dinucleotide phosphate (NADPH) as the source of electrons for glutathione and thioredoxin dependant enzymes[321] [322].

Studies have shown that glucose deprivation selectively enhances oxidative stress and cell death in a variety of cancer cell lines [323] [324] [325]. Furthermore, electron transport chain blockers have been shown to increase the production of H_2O_2 and O_2 as well as contribute to increased cytotoxicity with glucose deprivation [324].

It also has been noted that cancer cells that conduct high levels of glycolysis produce large amounts of lactate which is funnelled through into the extracellular environment.

This lactate is converted lactate dehydrogenase which results in the production of NAD+ in the cytosol which facilitates continued high rate glycolysis, essentially a means by which the cancer cells can re fuel themselves, a requirement for oncogenesis [318].

Furthermore, it has been shown that the relationship between glycolysis and oxidative phosphorylation is cooperative and competitive. In hypoxic environments glycolysis is enhanced to compensate for reduced oxidative phosphorylation and in the same way highly oxygenated environments will dictate a more oxidative energy profile.

This goes against what was originally thought when it came to cancer cell metabolism, namely that an increased glycolytic profile as suggested by the Warburg effect is a result of mitochondrial dysfunction resulting in an impaired ability to carry out oxidative phosphorylation.

In fact, emerging research cites adaptation to different cellular environments as opposed to dysfunctional mitochondria, with some studies suggesting that enhanced glycolysis can result in suppression of oxidative phosphorylation [326].

Moreover, this inherent plasticity found in the tumour and its constituent cells display a multitude of molecular and metabolic phenotypes, with cancer cells changing their metabolic phenotype in order to give cells a selective advantage.

An increasing number of studies hypothesise a phenomenon termed the reverse Warburg effect which supports the function of oxidative phosphorylation in cancer cells [326]. In the reverse Warburg effect epithelial cancer cells promote aerobic glycolysis in carcinoma associated fibroblasts which results in the production of lactate, ketones and pyruvate fuelling oxidative phosphorylation in cancer cell by means of entry into the TCA cycle [327].

Further studies have shown that lactate produced by glycolysis in hypoxic tumour cells and or stromal cells, can also be used as fuel for oxygenated tumour cells [327].

Interestingly studies have shown a link between oxidative stress and senescence with hydrogen peroxide being widely used to achieve oxidative stress induced senescence [328].

The role of the tumour microenvironment plays a fundamental role in tumour growth and progression. The effects of the environment are activated by specific metabolites such as oxygen and glucose in addition to growth factors that initiate tumour cell dissemination in early stages of the disease [329].

The growth of a tumour revolves around circulating cycles of hypoxia and normoxia. As the tumour progresses it results in the depletion of available resources (glucose and oxygen for example) and the hypoxia environment resulting in the induction of angiogenesis [329].

With new blood vessel formation, more resources become available and allow for fast tumour growth which again results in hypoxia and further angiogenesis. Thus, cell dissemination therefore should be altered and adjusted in accordance with nutrient availability [329].

Based on the assumption that proliferative and invasive clones are genetically distinct [330]and are difficult to switch, the compromise may be to facilitate the co-existence of both clones in the tumour thereby allowing dissemination to occur under different nutrient environments [330].

This phenomenon has been referred to as the "bet hedging" mechanism an alternative method independent from collective decision making which involves the maintenance of a percentage cells in each type of state by means of intracellular signalling and phenotype switching [330].

Based on the above literature studies, perhaps it could be concluded that the differences observed are simply the result of changes in nutrient availability.

In addition to this the process itself may in fact arise as a consequence of this so called "bet hedging" mechanism which allows for different subpopulations to exist, thus facilitating dissemination of tumour cells in varying microenvironment conditions.

Furthermore, results from the migration and invasion studies suggest that although the 786 may have a faster growth rate when compared to the 6450 early passage which tends to grow much slower, the 786 cells seem to not be able to migrate, invade and intercalate as well as the 6450-cell line. This could be attributed to the internal competition between invasion and growth/proliferation which under stressful conditions such as starvation, may result in there being too much energy invested in growth/proliferation such that there is no available energy for tasks such a migration, invasion and intercalation[329] .

This brings us back to the limitations of this particular model, and the fact that every batch of the 6450 early passage may contain different amounts of adapted sub populations (more cells with the late phenotype vs the early phenotype and vice versa) which could result in experimental inconsistencies.

In addition to this quantification challenges were encountered, with both the migration/ invasion and intercalation assay. For example, with the intercalation assay, most of the quantification had to be carried out manually due to the fact the cells tended to clump together (very sticky) and thus made quantification very difficult.

Similarly, with the migration assay, cells that hadn't migrated through the matrigel were difficult to remove from the top part of the matrigel insert and thus produced a rim of cells obstructing the field of view, making quantitation extremely challenging.

Furthermore, and specifically with the intercalation assay, due to time restraints I was unable to quantify each and every timepoint (overnight imaging) and as a consequence timepoint 0 and 8hrs were only analysed, which doesn't not give a complete intercalation profile.

This therefore could result in missing out a substantial finding within this 8-hr window, such that 786 cell line was noted to intercalate slower in addition to its inability to intercalate very well when compared to the 6450-cell line. As a result of these difficulties with quantification, average readings were plotted owing to variability in automated quantification. With further investigation this should be rectified.

Despite the challenges and limitations inherent to the project, the approach taken to unravel the underlying characteristics that define metastatic potential, using a combination of methods is proving to be highly informative, and remains a highly warranted field of research with immense biological and clinical implications.

Chapter 4 in – vivo characterisation

4 .1 Introduction

4.1.1 The in vivo model

This chapter will summarise the in vivo work carried out on the mouse model of vessel co-option. With the aid of global proteomics, metabolomics and proteomics carried out on laser captured micro dissected tumours and vessels, it is hoped that a better understanding of the molecular signatures that differentiate angiogenic tumours from co optive tumours will be gained. Furthermore, the aim of this chapter is to shed more light on the molecular pathways that dictate the "switch" from angiogenesis to vessel co-option in tumour metastasis, as reflected in the mouse model.

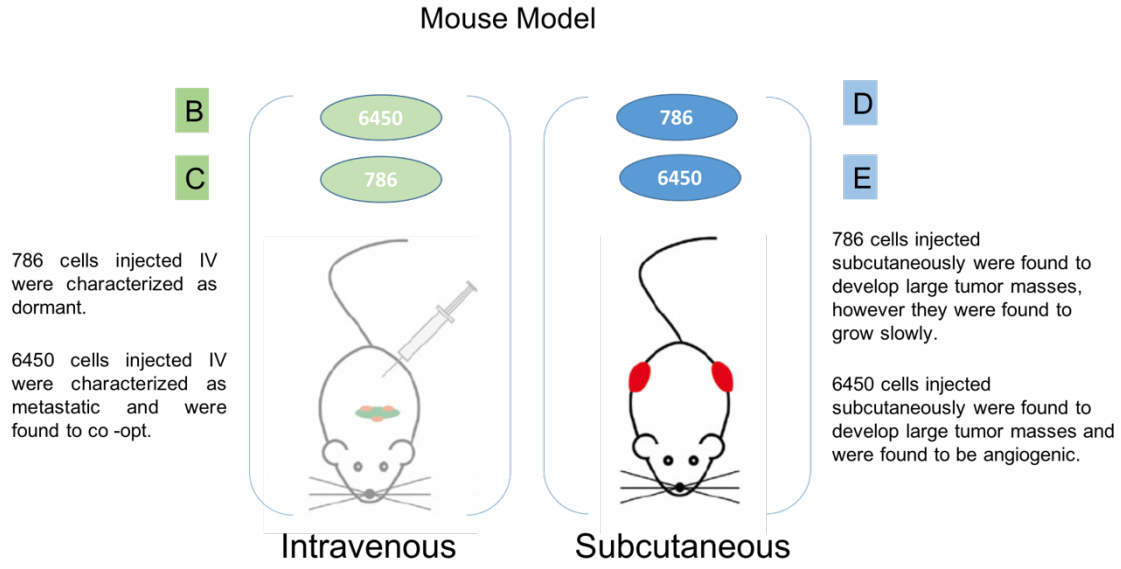
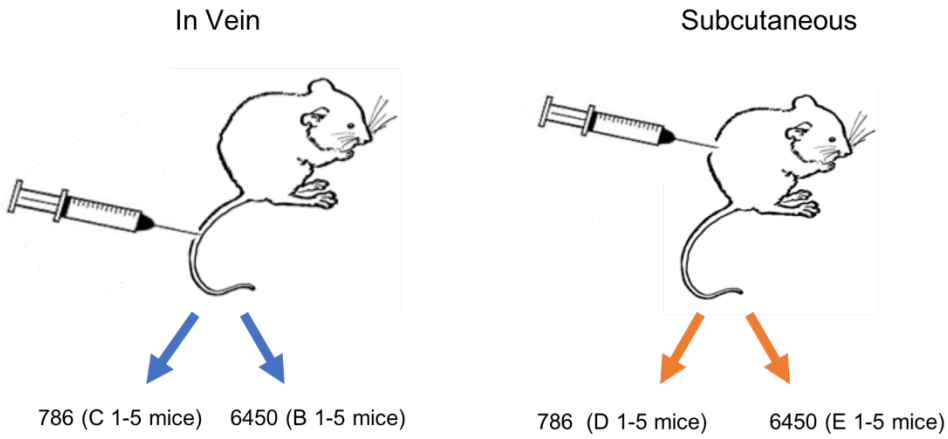


Figure 29: Characterisation of the mouse in vivo model: Schematic detailing the animal model setup. 786 cells injected in vein were found to be dormant whereas 6450 cells injected in vein were characterised as metastatic as well as being found to exhibit a co-option phenotype. Sample B represents tissue from the 6450 cells injected in vein and sample C represents tissue from the 6450 cells injected in vein. 786 cells injected subcutaneously were found to develop large tumour masses however were found to grow slowly. 6450 cells injected subcutaneously were found to develop large tumour masses and were also found to be angiogenic. Sample D represents tissue from the subcutaneous 786 cell mouse injection and sample E represents tissue from the subcutaneous 6450 cell mouse injection. Tissue excised was either directly stored in the -80 or kept in formalin for immunohistochemistry work.



Study	786	6450
Global Proteomic Analysis	1x	1x
Global Metabolomic Analysis	1x	1x
Western blot validation	3x	3x
Transcriptomics - pending analysis	1x	1x

Study	786	6450
Global Proteomic Analysis	1x	1x
Global Metabolomic Analysis	1x	1x
Western blot validation	3x	3x
Transcriptomics - pending analysis	1x	1x

Figure 30: Summary of in vivo studies carried out: Schematic summarising the studies carried out in this chapter, detailing the number of mice per condition (1-5) that I was provided with and how many replicates were used per condition/cell line (786 and 6450 in vein injection on the left and 786 and 6450 subcutaneous injection on the right).

4.1.2 Characterising vessel co-option in vivo

The process of angiogenesis is considered to be crucial prerequisite for tumour growth and progression. However, numerous studies have indicated that many human tumours rely on non-sprouting vessels for their microcirculation, in addition to the fact that several tumours can in fact grow and metastasise without angiogenesis [223].

Vessel co – option presents one alternative pathway whereby tumours use pre-existing vessels for their blood supply. Vessel co-option has been reported in many types of malignancies, however co-option tends to be observed more commonly in highly vascularised tissues such as the brain, lung and liver [223].

Furthermore, vessel co-option can provide a possible explanation for anti-angiogenic drug resistance, however not much is understood about the relation between co-option and drug resistance, a phenomenon that is still being explored [223]

4.1.3 Histopathology of vessel co-option

Studies on non-small cell lung cancer (NSCLC) have highlighted that some NSCLC's employ vessel co-option in favour of angiogenesis [223].

In this non angiogenic subtype, cancer cells were found to grow within the alveolar spaces alone, in so doing, facilitating the incorporation of the alveolar walls and thus allowing the tumour cells to co-opt the alveolar capillaries [211].

Several pre-clinical models of lung metastasis show co-option of alveolar capillaries and the occupying of the alveolar space by tumour cells. Three out of four Histopathological Growth Pattern's (HGP's) have been identified in different types of lung metastatic cancers and characterise different modes of vessel co-option [211] .

These include the alveolar HGP which enables the tumour cells to co-opt the alveolar capillaries, the interstitial HGP where in which cancer cells can infiltrate the alveolar wall and co-opt the alveolar capillaries (distinct from alveolar HGP) and the perivascular cuffing HGP where cancer cells grow as a cuff around large pre-existing vessels [211].

The fourth HGP known as the pushing HGP lung metastases has been found to utilize angiogenesis and shows characteristic chaotic and disorganised vasculature typical of tumour angiogenesis [211].

However, what is worth noting is that both angiogenesis and vessel option can co-exist within the same lesion, with lung metastases presenting with a combination of growth patterns albeit in different areas [211].

Moreover, it has been noted that in both alveolar HGP and interstitial HGP, new vessels have the ability to sprout from co-opted vessels located at the centre of the metastasis making understanding and investigating vessel co – option induced resistance even more challenging.

In this part of the project and in the context of the in – vivo model, an attempt to investigate to important aspects, are made: why the 6450 cells (after treatment with sunitinib) escape dormancy, whilst the 786 cells do not? In addition to this, understanding why the 6450-cell line when injected in vein (IV) shows evidence of undergoing co-option, whereas when injected subcutaneously is clearly angiogenic, is equally as important.

4.1.4 Results

Prior knowledge of the histopathology of angiogenesis and vessel co - option was crucial before embarking on this particular aspect of the project. This was to ensure and confirm that the tissue samples still held characteristic tumour phenotype profiles characteristic of the mouse model (angiogenesis vs co-option) as indicated previously by Andy Reynolds, at the ICR in London (see figure 31 A).

Tissue sections were received from the ICR in London already fixed in formalin. Once received, tissue sections were dehydrated and embedded on paraffin wax blocks and stored. Tissue sections were cut using a microtome (5-micron slices), rehydrated and immuno-stained with either hematoxylin and eosin (H&E) stain or endomucine accordingly (see methods).

H and E staining enabled the characterisation of the large tumour masses attributed to the 6450 IV injection of cells and also confirmed the small tumour growths characteristic of the dormant phenotype, developed when the 786 cells were injected in the tail vein.

Furthermore, seeing that the mouse had been injected with a human renal carcinoma cell line (786 cell line), it therefore was expected that the tumours would be human in origin and the vessels would as a result originate from the mouse. Staining the vessels with a mouse endothelial cell marker, endomucine helped to confirm this.

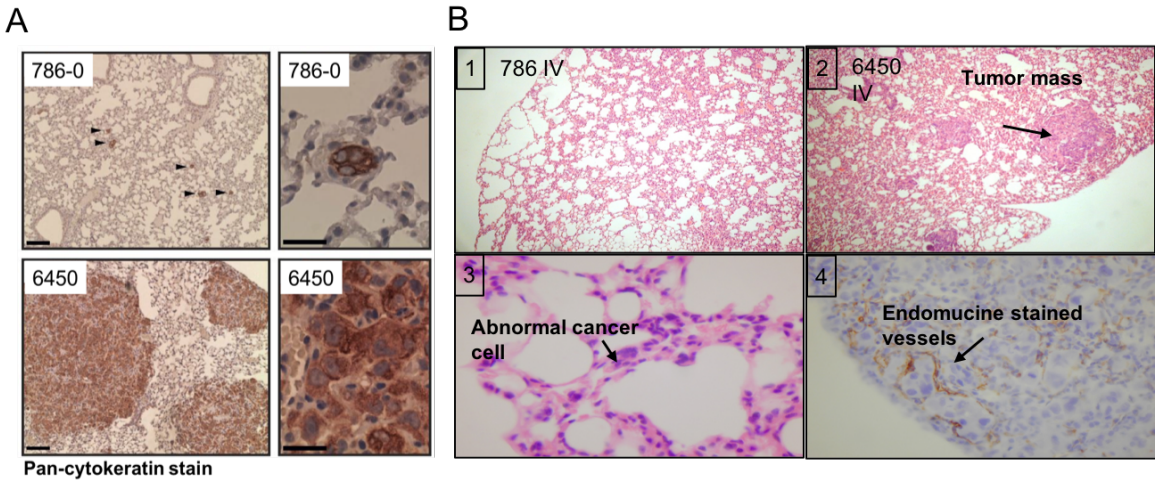


***Figure 31: Immunostaining validation of metastatic capability*:** A) shows immunostaining validation carried out at the ICR in London using pan – cytokeratin. B) shows immunostaining validation I carried out with H & E and endomucine respectively. Figure B 1 shows the small (invisible to the naked eye) tumours formed when the 786 cell is injected IV, B 2 shows the large tumour masses that are characteristic to the IV injection of the 6450-cell line. B3 shows the small tumours generated by the 786 IV injection at a higher magnification in order to showcase potential abnormal cancer cells (verifies the presence of tumour cells). B4 shows endomucine staining of the blood vessels.

Similarly, characterisation of the IV injections and the subcutaneous injections by means of H and E staining was carried out, with the subcutaneous sections showing the features characterised by a typical angiogenic tumour phenotype, such as irregular and disorganised blood vessels surrounded by tumour metastases.

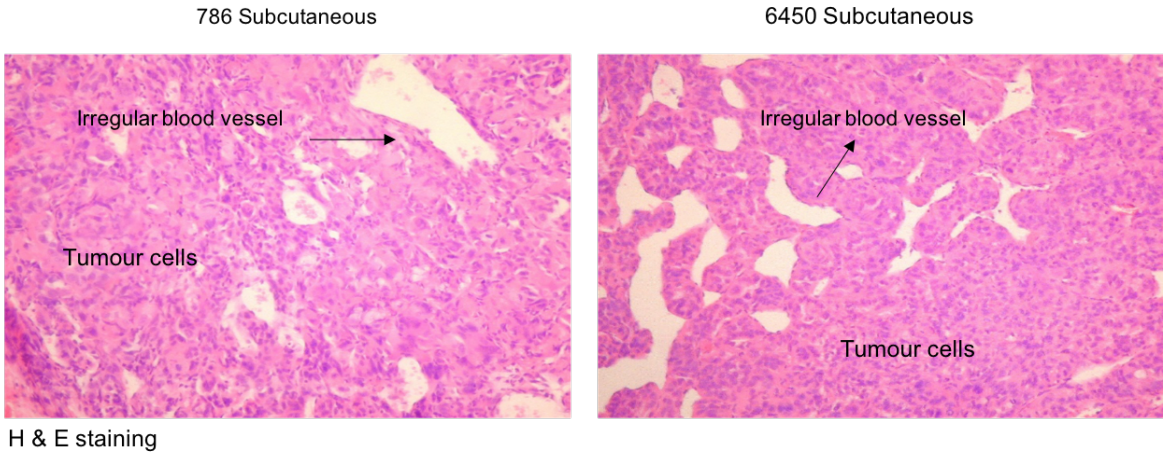


Figure 32: H & E staining of tissue representing subcutaneous injections highlights angiogenic features: H&E stained images (left and right) of 786 and 6450 subcutaneous injections showing characteristic irregular blood vessels surrounded by tumour metastasis, typically found in angiogenic phenotypes.

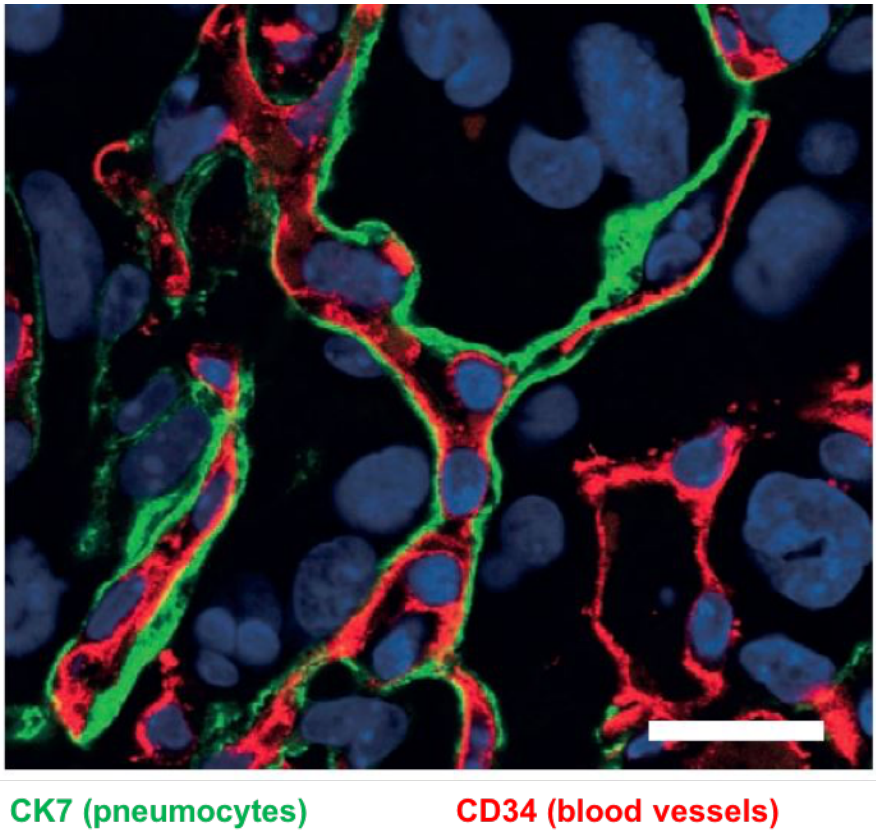


Figure 33: Vessel co-option in growing lung metastasis: Fluorescent image provided by Andy Reynold, ICR London, representing vessel co-option produced by the 6450-cell IV injection. Tumour cells are seen to occupy the alveolar spaces in the lung, showing incorporation with the alveolar cells (pneumocytes) lining the lung blood vessels, a classic feature of co-option. Structurally vessels are shown to be intact unlike vessels found in angiogenic phenotypes which are leaky, disorganised and have an irregular structure.

4.1.5 Global tissue proteomic analysis (preliminary)

In the initial instance, and while 786-cell line developed tumours subcutaneously in the mouse (slow growing), it was decided to carry out a pilot proteomic study with the tissue samples that had already been collected and received. In order to avoid excess use of the mouse lung tissue, 786 IV with 6450 IV tissues were compared in order to determine how much tissue was needed for proteomic processing. This also facilitated the optimisation of the filter aided sample preparation (FASP) protocol, for isolating proteins (see methods).

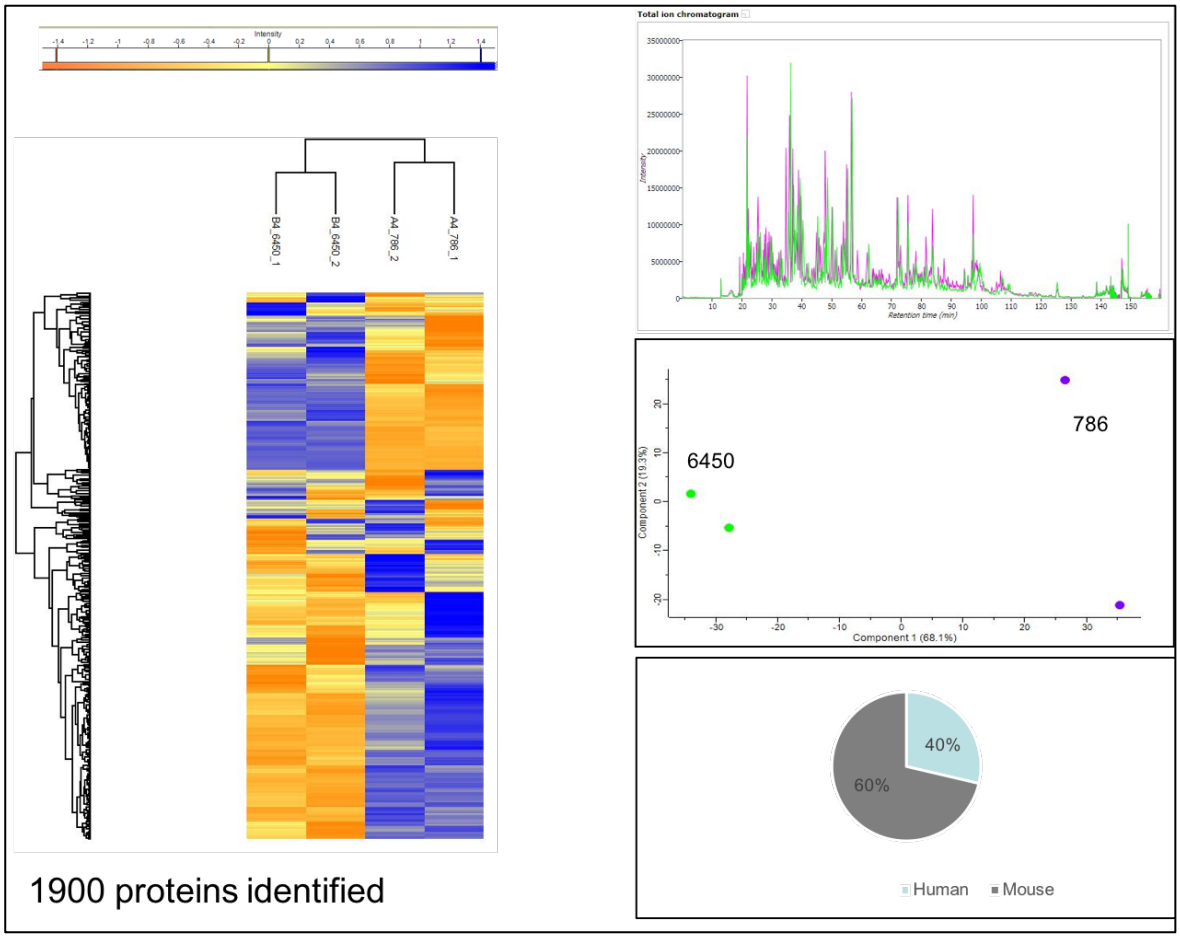


Figure 34: Pilot proteomic experiment shows differential protein expression between 786 and 6450 cells injected IV: Schematic showing a global protein expression heat map (left hand side image) that highlights potential differential protein expression between tissue injected with 786 cells IV and tissue injected with 6450 cells IV. Right hand side panel (top – bottom) shows an ion chromatogram which shows slight skewing of peaks due to presence of highly abundant haemoglobin. Principle component analysis shows good separation of the groups being investigated (786 IV vs 6450 IV). Pie chart shows the percentage of human to mouse proteins. From this pilot proteomic study 1900 proteins were identified (both human and mouse).

Prior to tissue processing, tissue samples were weighed, and homogenised with a bead beater. BCA protein quantification was carried out in order to normalise tissue samples to protein amount.

From a pilot study, 1900 proteins were identified, and sorted proteins based on species, filtering out for human proteins only.

Correlation patterns with replicates clustering together were detected however, there was a lot of blood still contained in the samples owing to the fact the tissues had not been perfused prior to being frozen down. This resulted in a high intensity haemoglobin peak, which contributed to the irregular chromatogram observed, indicating that tissue should be washed beforehand to get rid of any excess blood.

Following on from the pilot study, and when the 786 subcutaneous tumours had been grown and collected, the first global proteomic study was carried out. Again, simply to ensure enough tissue remained for future work and validation, it was decided that a global proteomic study using only one replicate per condition would be attempted.

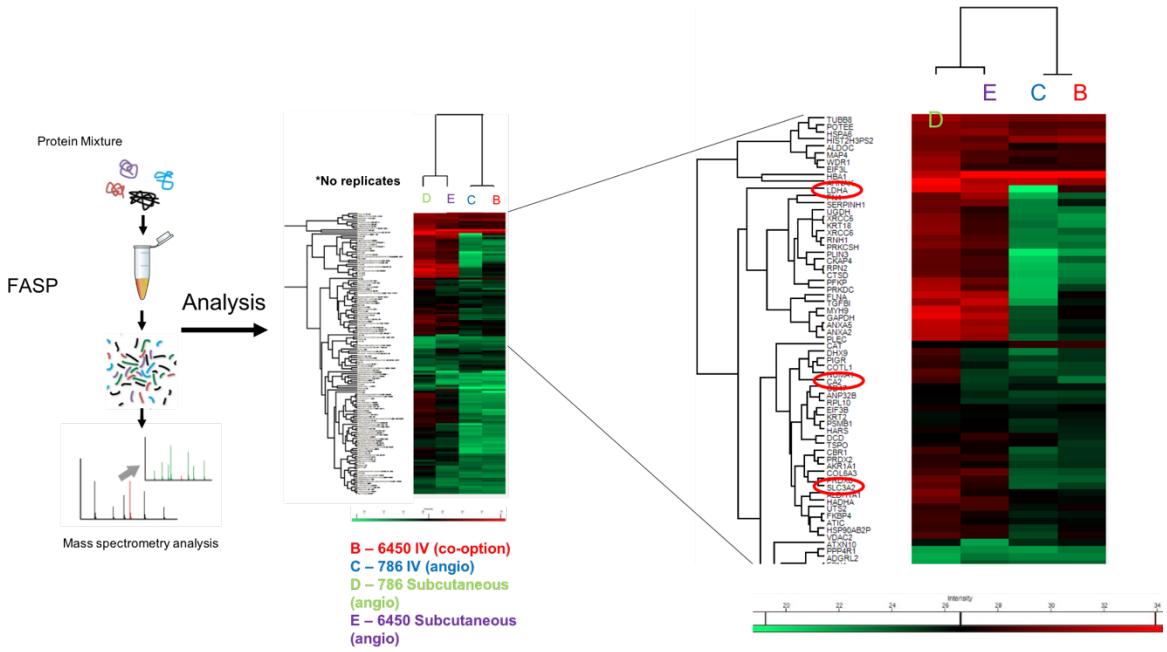


Figure 35: Preliminary label free proteomics reveals differential expression of proteins involved in metabolism & cell receptor signalling: Schematic (left to right) shows the workflow involving filter aided sample preparation protocol for extraction of proteins from tissue. Once proteins have been isolated and samples injected on the mass spectrometer, differences in protein expression can be visualised in the form of a heat map which when zoomed in reveals the protein ID's / gene names that are variable across samples B (6450 IV co-option), C (786 IV angio), D (786 subcutaneous angio) and E (6450 subcutaneous angio).

From the pilot proteomic pull down comparing all four conditions (786 and 6450 IV and 786/ 6450 subcutaneous injections) a total of 3,902 proteins were identified (list in supplementary). After subsequent filtering for human proteins only, this number came down to 1,693 human proteins in total.

Owing to the lack of replicates, differential protein analysis was not possible, however in order to characterise our preliminary findings, identifying the most variable proteins across the samples was focussed on instead. In order to do this, the standard deviation of each sample was calculated and plotted against the standard deviation rank with the top part of the curve representing the top variable proteins.

Results from the proteomic pull down revealed a number of structural proteins that were found to be highly variable across our samples, namely vimentin.

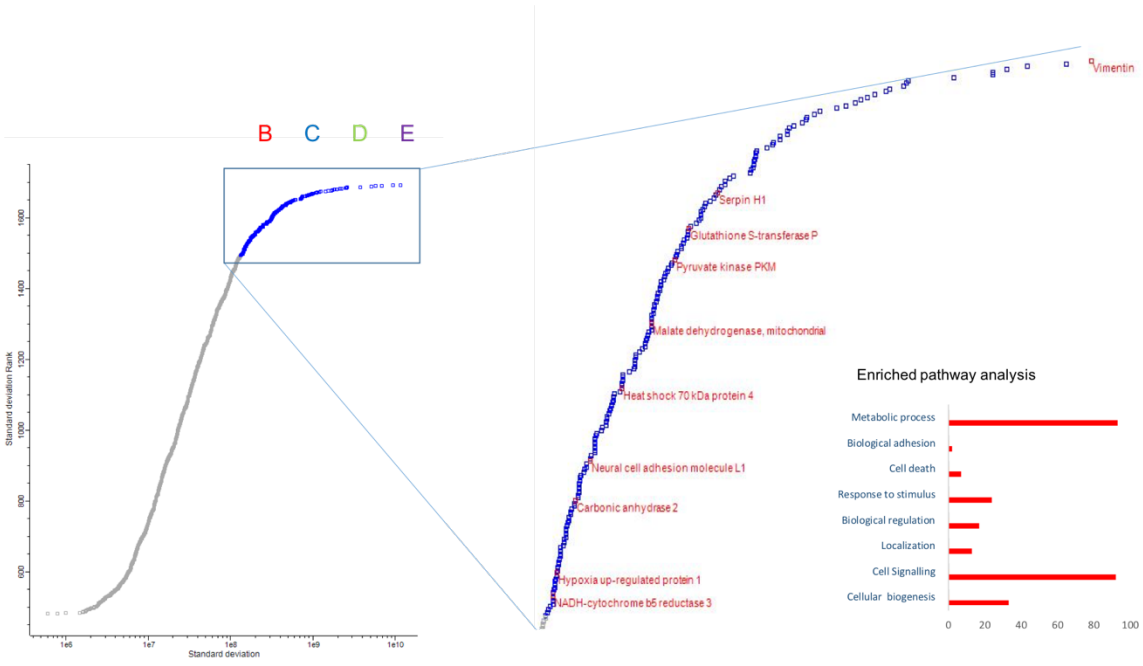


Figure 36: Top variable proteins across all tissue samples highlight key roles in metabolism and cell receptor signalling: Graphical representation of the calculated standard deviation plotted against standard deviation rank highlighting the top variable proteins found across the samples (BCDE) and enriched pathway analysis which shows involvement of metabolic pathways and cell receptor signalling pathways.

In addition to this, the detection of previous targets that were identified in the tissue culture model were re confirmed, such as carbonic anhydrase 2, Glutathione S Transferase and Hypoxia up regulation protein 1 (from the RNA sequencing data).

Enriched pathway analysis also revealed and enlisted proteins implicated in metabolism in addition to cell signalling pathways.

Alongside identifying the potential protein candidates and molecular markers across samples B, C, D and E, of interest (as outlined by the research objectives) was understanding the differences in protein signatures between the angiogenic vs the vessel co - option tissue phenotype. As a result, focus was placed on the differentially expressed regions as highlighted in the heat map (figure 37) on just tissue samples B and E which reflect the co optive vs angiogenic phenotypes respectively. Owing to the fact that the analysis was carried out on one replicate, this "differential analysis" cannot however be taken as entirely representative.

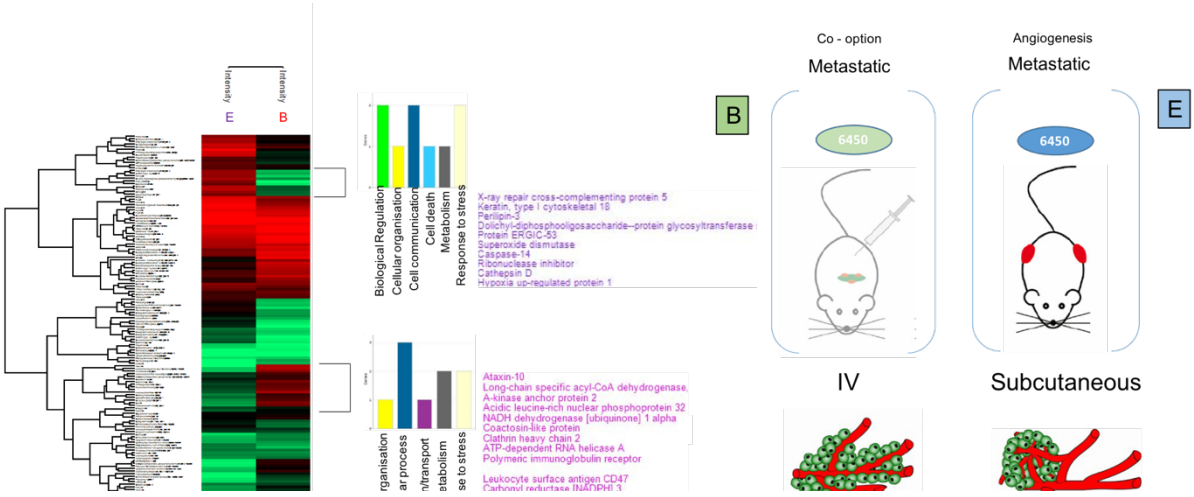


Figure 37: Comparison of 6450 co-option versus angiogenic phenotype reveals involvement of proteins associated with cell communication, metabolism and response to stress: Schematic showing the corresponding heat map (left hand side) which highlights the expression of proteins between samples B (6450 IV injection co-option) and E (6450 IV injection angio) alongside the respective pathway analysis enrichment corresponding to the variable protein expression region on the heat map. Mouse model schematic (right hand side) highlights the vessel phenotype produced by injection of 6450 cell IV and 6450 cells injected subcutaneously representing vessel co-option (B) and angiogenesis (E) respectively.

4.1.6 Western Blot validation highlights potential differentially expressed proteins

Western blot validation was carried out on three biological replicates (tissue from 3 mice) to overcome the fact that the proteomic analysis was characterised based on one replicate. Normal lung tissue obtained from a healthy mouse in addition to cell lysates from U20S and MCF-7 human cancer cell lines were used as controls to normalise for protein expression from mouse and human respectively, since tissue samples contained both mouse and human counterparts and owing to cross reactivity issues with the antibodies used. Coomassie staining served as a loading control (in the absence of a house keeping protein that wasn't variable) and proteins were quantified and normalised for protein amount.

In order to interpret the western blot validation accurately, a Uniprot search for established modifications for each target protein was carried out. Protein size was then calculated from the suggested protein length (amino acids) given in Uniprot using the following calculation: Predicted size of protein = number of amino acids x 0.11kDa.

4.1.7 COXIV and PKM2: energy metabolism

A number of metabolic proteins were shown to be highly variable from both pathway analysis and the proteomic study of top variable proteins across all samples. For this reason, validation of two metabolic proteins that were detected in the proteomic pull down and were indicated as being highly variable, Cytochrome C oxidase (COX IV) and Pyruvate Kinase M2 (PKM2), was carried out.

Results from the western blot show an upregulation of PKM2 in samples B1 and B2 with expression of PKM2 remaining relatively equal across samples B3 -E3.

A potential double band can be detected in samples C3, D1, D2 which could be a post translational modification or simply the human form of the PKM2 enzymes as it corresponds with the expression level of PKM2 observed in the human cancer cell lines. COX IV expression is observed to be upregulated in samples E1, E2 and E3 with some upregulation observed in B1 as well.

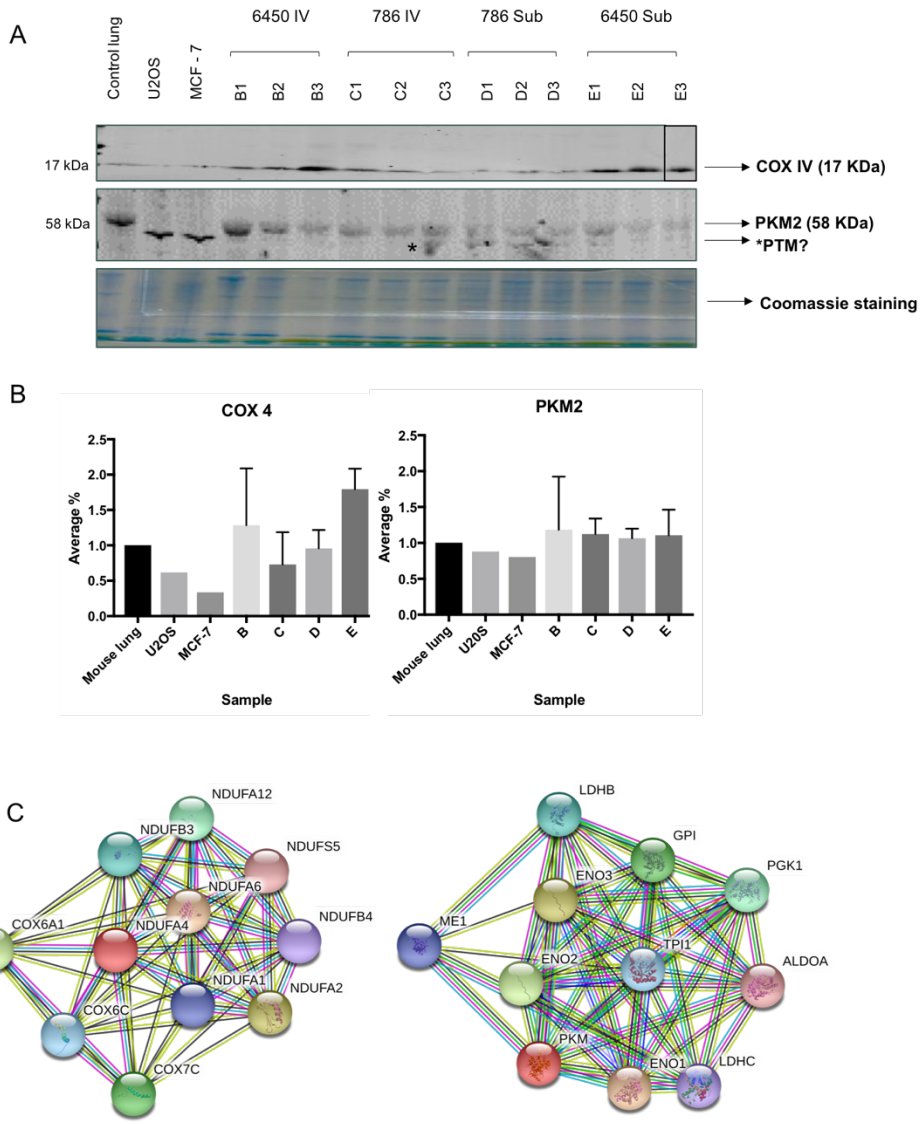


Figure 38: Western blot validation highlights the potential role of metabolism in defining tumour phenotype: A) Western blot validation showing expression of enzymes PKM2 and COX IV across triplicate samples B 1-3, C1-3, D1-3 and E1-3. Healthy mouse control lung, U2OS and MCF -7 were used to control for mouse and human protein expression profiles respectively. Coomassie staining was used as a loading control. B) String analysis showing the interconnecting protein nodes associated with central nodes PKM2 (PKM) and COX IV (NDUFB4).

4.1.8 L1CAM and Pan cadherin: adhesion receptor landscape

Similarly, due to the noted high variability seen with L1CAM in the global tissue proteomics in addition to the observation that adhesion receptor regulation seems to be enriched from the pathway analysis studies, it was decided to validate L1CAM in addition to Pan cadherin (also suggested to be variable) in order to investigate the adhesion receptor landscape.

Western blot validation shows a clear upregulation in L1CAM in tissue samples D1-D3 (786 subcutaneous injection – angio slow growing). Pan cadherin is observed to show differential expression across tissue samples, namely between tissue sets B - C (1-3) and D- E (1-3) with a possible post translation modification (potential degradation) with a noticeable double band observed on samples B-C and its removal on tissue samples D-E (1-3).

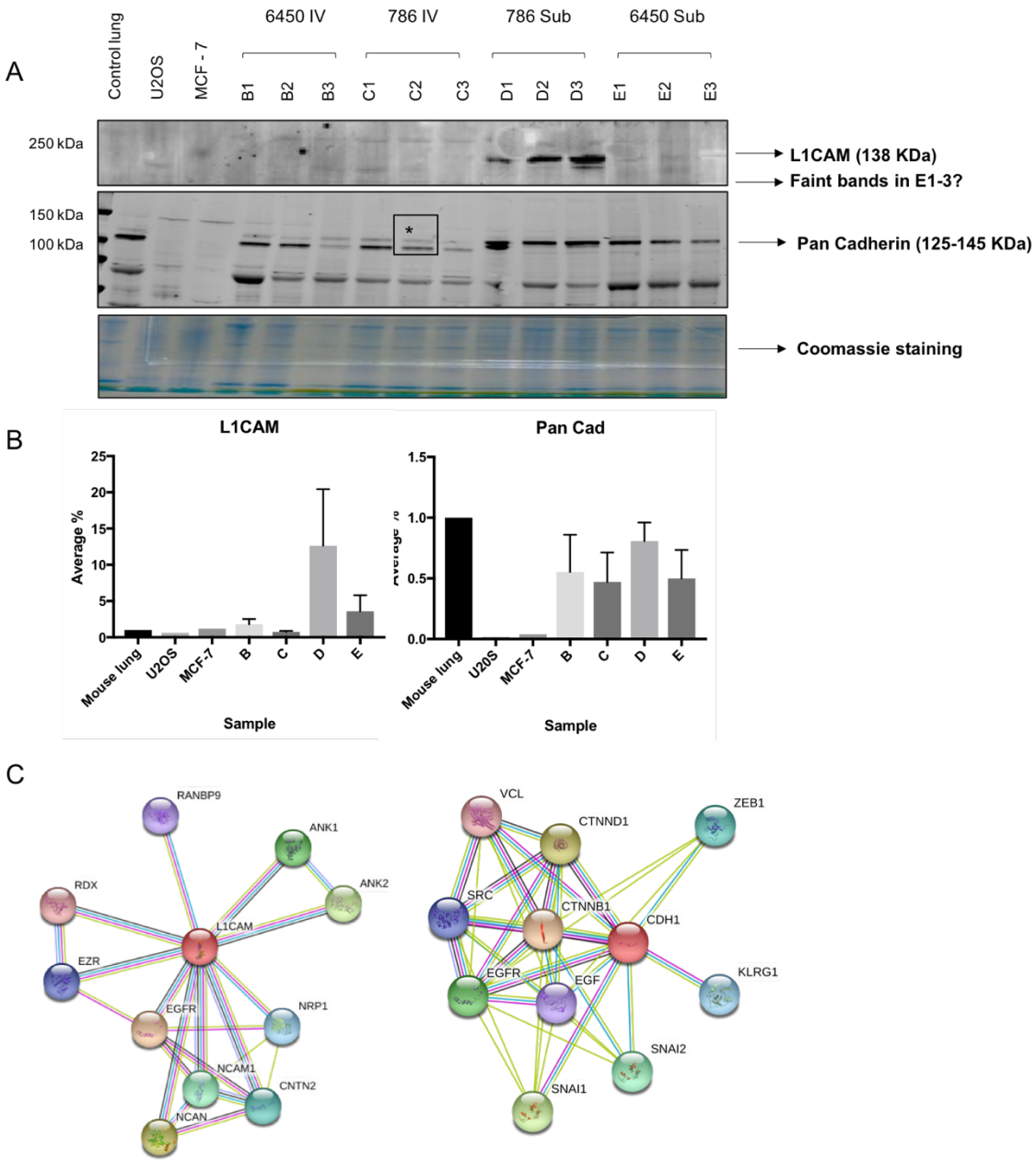


Figure 39: Western blot validation highlights the potential role of adhesion in defining tumour phenotype: A) Western blot validation showing expression of L1CAM and Pan cadherin across triplicate samples B 1-3, C1-3, D1-3 and E1-3. Healthy mouse control lung, U2OS and MCF -7 were used to control for mouse and human protein expression profiles respectively. Coomassie staining was used as a loading control. The * denotes a possible PTM. B) String analysis showing the interconnecting protein nodes associated with central nodes L1CAM and the cadherins (CDH1).

4.1.9 SMAD 4: TGF-β pathway

Another protein that was detected from the proteomic pull down was Smad 4. Smad 4 has been shown to act as a central regulator of transforming growth factor beta (TGF-β). TGF-β signalling pathway plays an important role in cancer progression, in that it drives progression of immune suppression, angiogenesis, and mesenchymal transition, all of which contribute to cancer metastasis [331] [332].

Activation of TGF-β is implicated in a number of cellular processes with signal transduction being achieved by phosphorylation of the Smad proteins [333]. In particular TGF-β/Smad4 signalling has been found to induce a tumour suppressive effect [334].

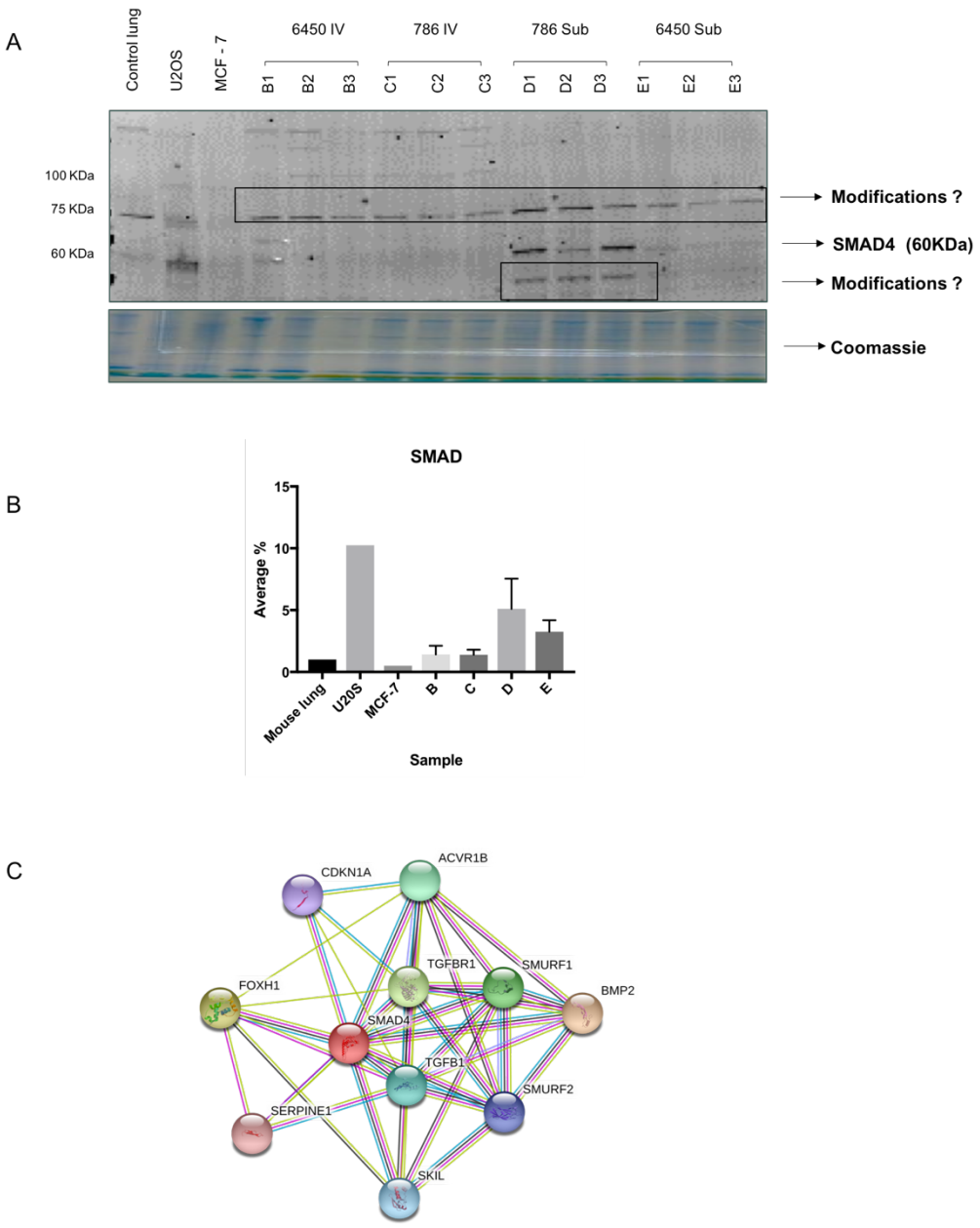


Figure 40: Western blot validation highlights the potential role of Smad 4: A) Western blot validation showing expression of Smad 4 across triplicate samples B 1-3, C1-3, D1-3 and E1-3. Healthy mouse control lung, U2OS and MCF -7 were used to control for mouse and human protein expression profiles respectively. Coomassie staining was used as a loading control. B) String analysis showing the interconnecting protein nodes associated with central node Smad 4.

Results from the Smad 4 western blot validation show what seems to be upregulation of Smad 4 in tissue samples D1-3 (786 cell line injected subcutaneously –angio/metatastic). In addition to this, potential faint bands were observed in samples E1-3, but this would need to be verified.

4.1.10 TSP1 and ADAMTS2: angiogenesis and remodeling

Despite not observing any variable expression in Thrombospondin -1 (TSP1), I wanted to validate its expression across the tissue samples. In addition to this and owing to the detection of ADAM metallopeptidase with thrombospondin type 1 motif 2 (ADAMTS2) in the mRNA profiling carried out on the cell lines, it was thought to validate its expression in relation to TSP1 expression.

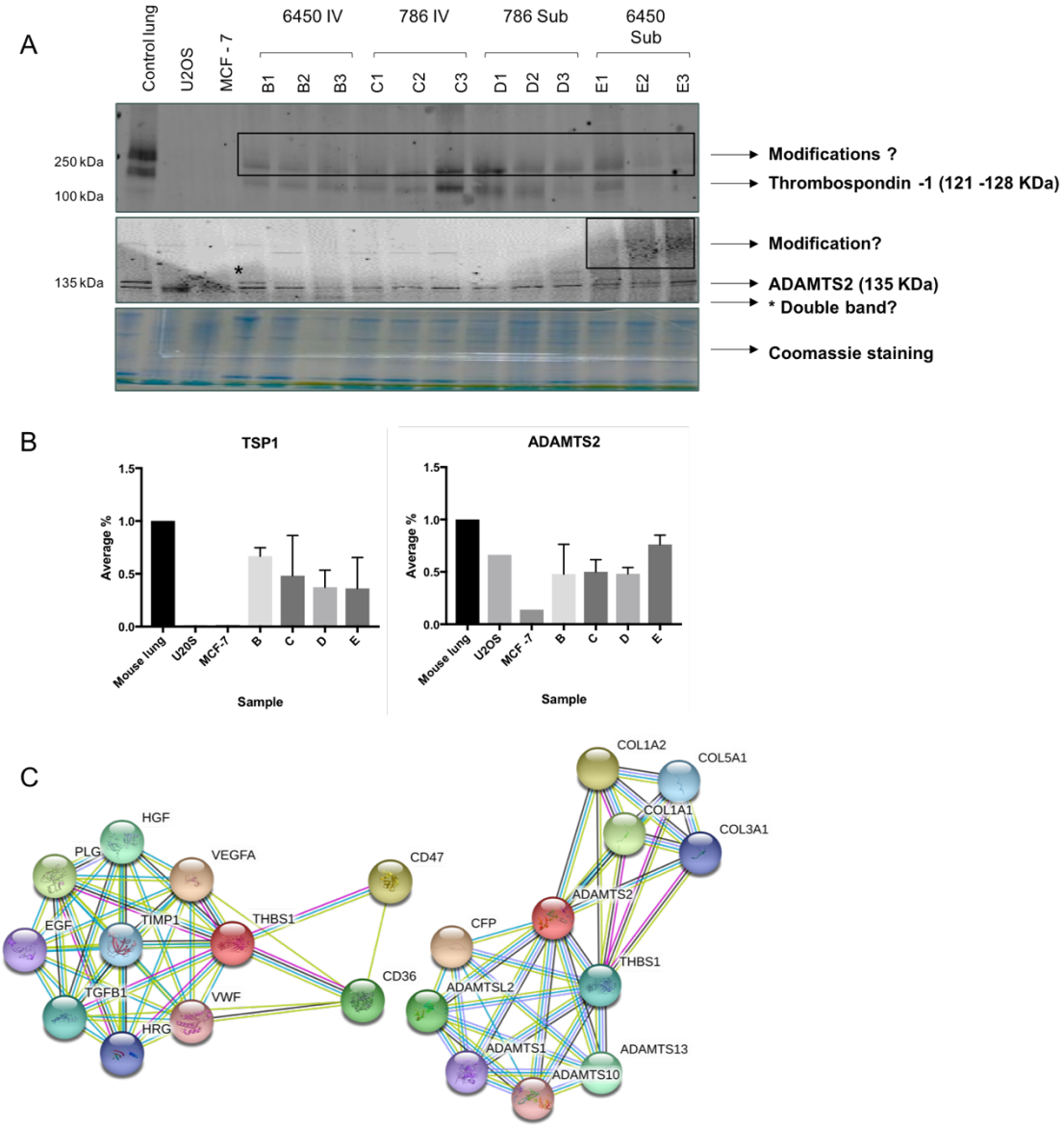


Figure 41: Western blot validation highlights the potential role of Thrombospondin -1(TSP1) and ADAMTS2: A) Western blot validation showing expression of TSP1 and ADAMTS2 across triplicate samples B 1-3, C1-3, D1-3 and E1-3. Healthy mouse control lung, U2OS and MCF -7 were used to control for mouse and human protein expression profiles respectively. Coomassie staining was used as a loading control. B) String analysis showing the interconnecting protein nodes associated with central nodes TSP1 and ADAMTS2.

ADAMTS2 has been implicated in angiogenesis, with studies showing its inhibition of vascular endothelial growth factor stimulated endothelial cell proliferation [335].

Results from the western blot validation of TSP1 are unclear, TSP1 seems to be expressed at equal levels across the tissue samples with some upregulation seen in C3, D1 and D2 and E1. ADAMTS2 validation shows equal expression levels across the tissue samples, however smearing (samples E1-3) and the presence of what may seem to be double bands in samples B1 and E1-3) is also observed.

4.1.11 Ca2 and SLC9A1: pH regulation

Following on from the detection of Carbonic anhydrase 2 as being another variable protein (proteomic tissue pull down) across the tissue samples, validation was carried out.

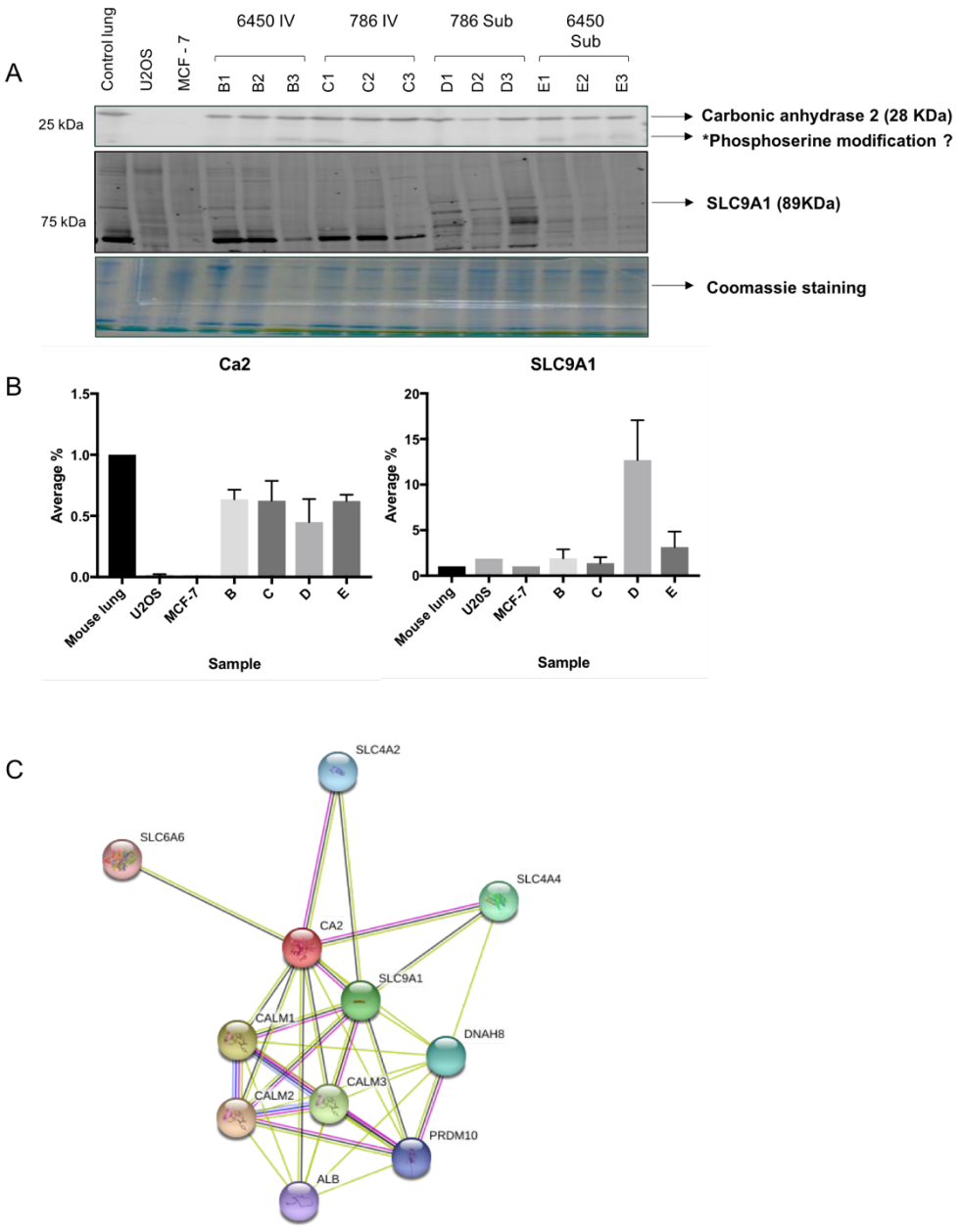


***Figure 42: Western blot validation highlights the potential role of Carbonic anhydrase and SLC9A1 (Na/H exchanger) in defining tumour phenotype*:** A) Western blot validation showing expression of Carbonic anhydrase 2 across triplicate samples B 1-3, C1-3, D1-3 and E1-3. Healthy mouse control lung, U2OS and MCF -7 were used to control for mouse and human protein expression profiles respectively. Coomassie staining was used as a loading control. B) String analysis showing the interconnecting protein nodes associated with central node Carbonic anhydrase 2 (CA2) and connected node SLC9A1.

Results from Carbonic anhydrase 2 validation, a target that consistently has been seen in previous investigations, shows what seems to be equal expression across samples. However, what could be possible phosphoserine modification (18 KDa) is also observed.

4.1.12 GSTP1: xenobiotic metabolism

Another protein that was consistently detected as being highly variable across tissue samples was Glutathione S Transferase Pi (GSTP1) and for this reason, it was validated.

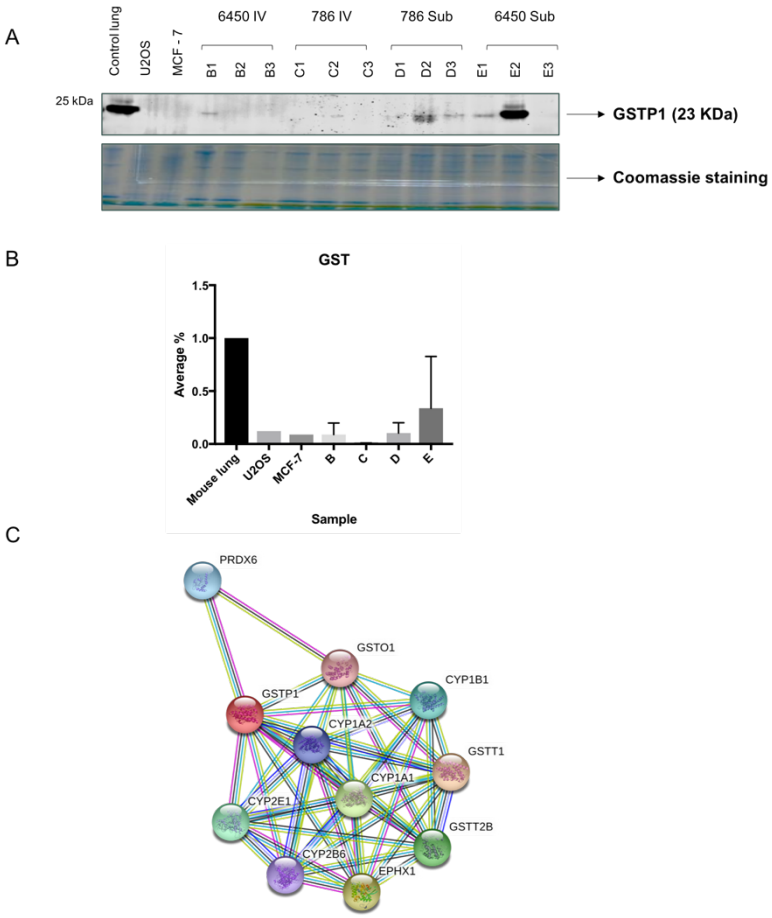


Figure 43: Western blot validation highlights the potential role of Glutathione S transferase pi in defining tumour phenotype: A) Western blot validation showing expression of GSTP1 2 across triplicate samples B 1-3, C1-3, D1-3 and E1-3. Healthy mouse control lung, U2OS and MCF -7 were used to control for mouse and human protein expression profiles respectively. Coomassie staining was used as a loading control. B) String analysis showing the interconnecting protein nodes associated with central node GSTP1.

Results from the GSTP1 validation show variation in expression in what seems to be upregulation of GSTP1 in tissues samples D2, D3, E1 and E2.

4.1.13 Metabolomic analysis

Owing to the significant contribution of metabolic proteins observed in both in vitro work and preliminary proteomic global tissue analysis, it was decided to carry out a metabolomic analysis of the tissue samples in order to characterise potential differential metabolite expression across the samples. Of particular interest was the differential profiling of metabolites between the angiogenic tumour phenotype and the co optive tumour phenotype.

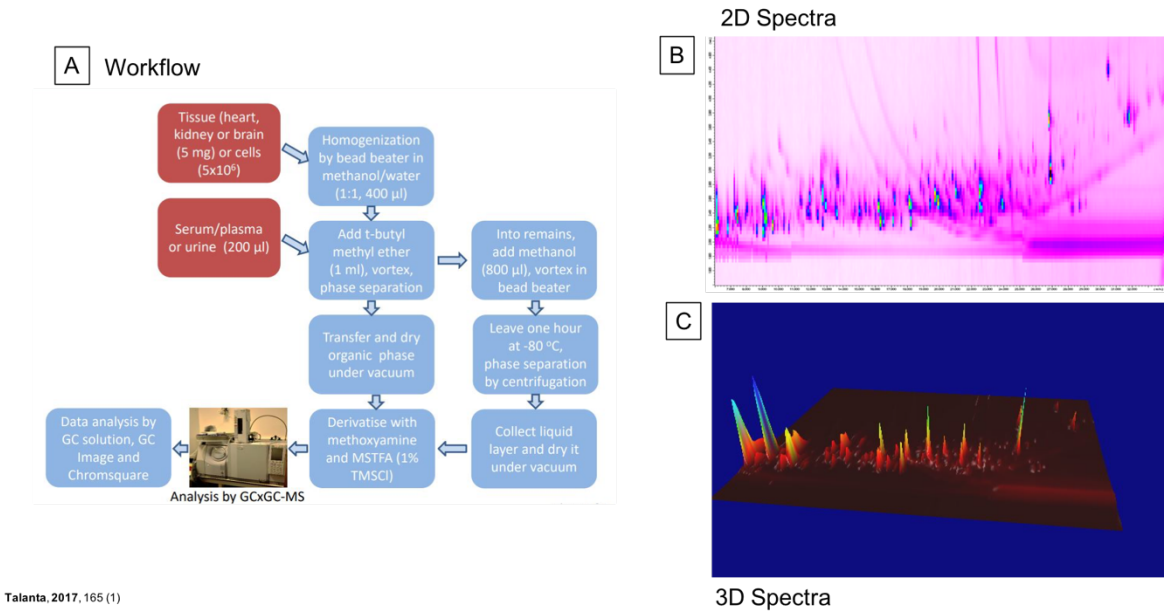


Figure 44: Comprehensive GCxGC-MS profiling of cancer cell extract: A) GCxGC MS workflow B) 2D-GC map showing separation and detection of molecular features in cell extracts, from which metabolites were identified either by database matching and/or by corresponding standards. C) 3-dimensional representation of GCxGC-MS analysis of a cellular extract, where GC (1st dimension) is on the X-axis, GC (2nd dimension) on the Y-axis and ion intensity is on the Z-axis.

By employing an optimised method for metabolite extraction from cell/tissue biopsy developed in the Kessler lab [287] two dimensional gas chromatography mass spectrometry (GCxGC-MS) was used to interrogate the metabolite features across our tissue samples and compare them accordingly.

Samples were injected in technical replicates to enable us to compare expression levels of the individual metabolites detected in each sample. In total 43 metabolites were identified. Owing to the fact that sample C consistently showed the highest metabolite intensity across the samples, all samples were normalised and compared relative to the metabolite intensity of sample C. This applies to both the heat map generated (fig 45) and the individual metabolite assessment (fig 48).

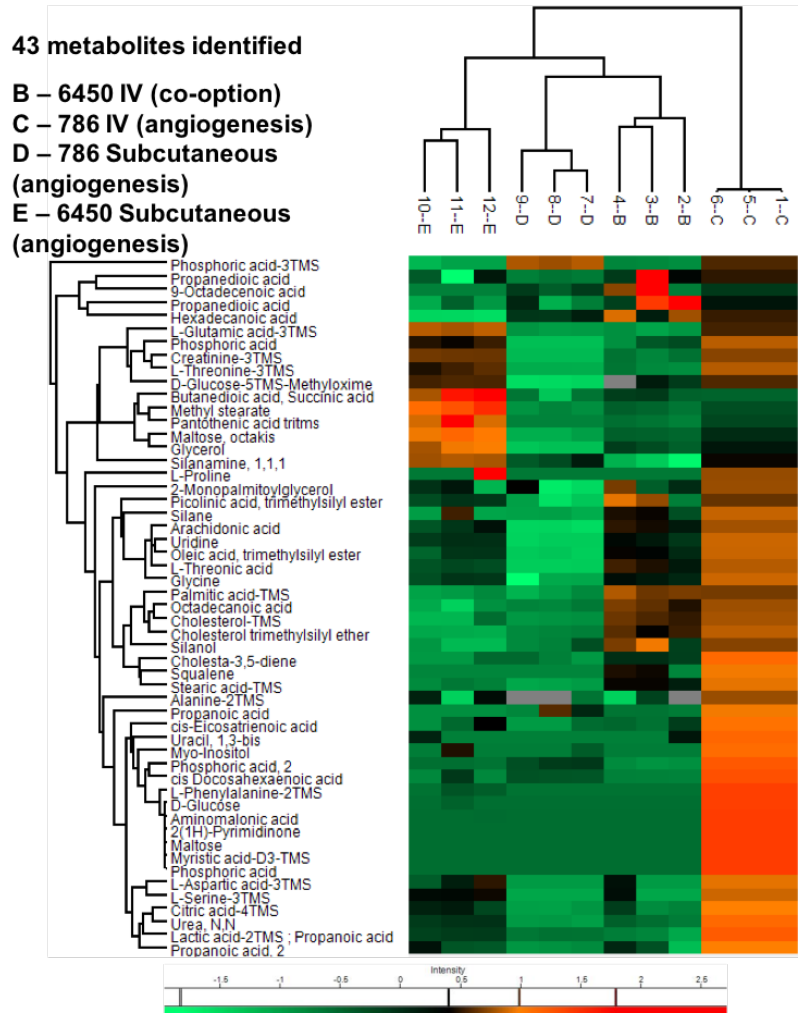


Figure 45: Global metabolomic analysis highlights variable metabolite profile across tissue samples: Heat map to show the variation in metabolite profiles (43 metabolites identified) across samples B (6450 IV co-option), C (786 IV angio), D (786 subcutaneous angio) and E (6450 subcutaneous angio). Intensity bar (bottom) shows gradient of colour that corresponds with protein intensity (red = high) (green =low).

4.1.14 Pathway analysis of proteomic pull-down highlights role of metabolism

In order to better understand which metabolic pathways were being enriched, pathway analysis was conducted on the proteomic pull down in order to ascertain which metabolic enzymes (detected by proteomics) were most variable across which metabolic pathways. Pathway analysis was carried out using path view which uses KEGG pathway analysis.

Values were logged, and the variability of any given metabolite detected across the tissue samples was displayed in the form of colour coded intensity bar (green to red) where red denotes high variability and green denotes low variability.

Results from the pathway analysis revealed that the majority of enzymes detected by proteomics were involved in glycolysis and gluconeogenesis as well as oxidative phosphorylation, albeit to a lesser extent.

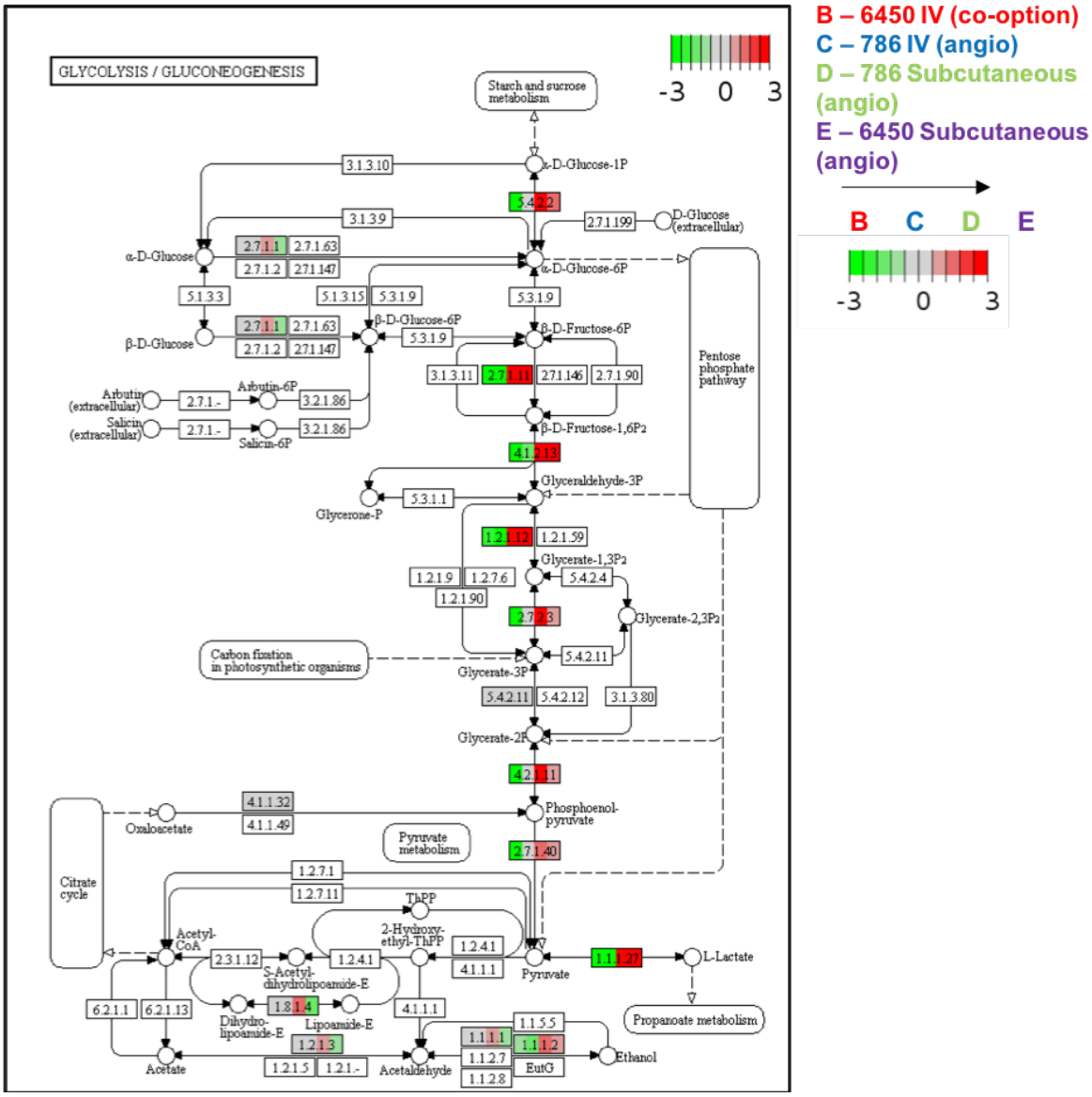


Figure 46: Pathway analysis reveals changes in enzymes involved in glycolysis and gluconeogenesis: Pathway analysis carried out in path view shows that the proteomic pull down of metabolic proteins detected are involved in glycolysis and gluconeogenesis (majority). Intensity bar is used to highlight variability level (red high and green low) across all tissue samples in the direction of B, C, D, and E. The 4 different coloured compartments of each enzyme relate to the intensity of that particular enzyme in each sample (B- C- D- E).

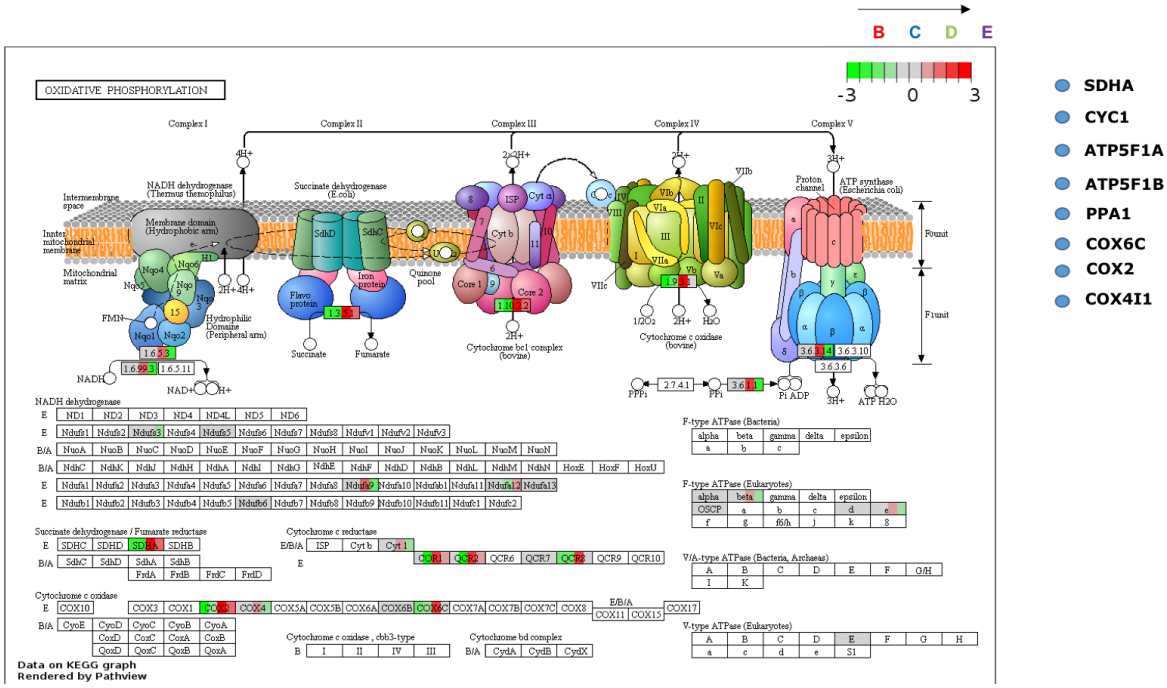


Figure 47: Pathway analysis reveals changes in enzymes involved in oxidative phosphorylation: Pathway analysis carried out in path view shows that the proteomic pull down of metabolic proteins detected are involved in oxidative phosphorylation. Intensity bar is used to highlight variability level (red high and green low) across all tissue samples in the direction of B, C, D, and E. The 4 different coloured compartments of each enzyme relate to the intensity of that particular enzyme in each sample (B- C- D- E). Legend on the right highlights the gene names of the metabolic enzymes detected.

4.1.15 Metabolomic analysis reveals differences in metabolites involved in cellular metabolic processes

Based on the findings from the pathway analysis carried out the metabolomic data was revisited and 8 metabolites of potential interest from the 43 detected, were selected for. As an initial preliminary study, metabolites implicated in the TCA cycle, glycolysis, fatty acid synthesis, and protein metabolism were investigated.

Investigating the variation in expression of these 8 metabolites in more detail across samples B-E highlights differences between the samples. Notably Glucose seems to be highly variable between samples B and C compared to samples D and E. Similarly, Glutamine appears to be highly variable as well with samples C and D showing high intensities.

Lactic acid and citric acid show similar profiles with both acids being shown to be highly variable with sample C showing the highest intensity. Succinic acid appears to be highly variable mostly in sample E, however with the remaining metabolites the results are not so clear, thus warranting further investigation.

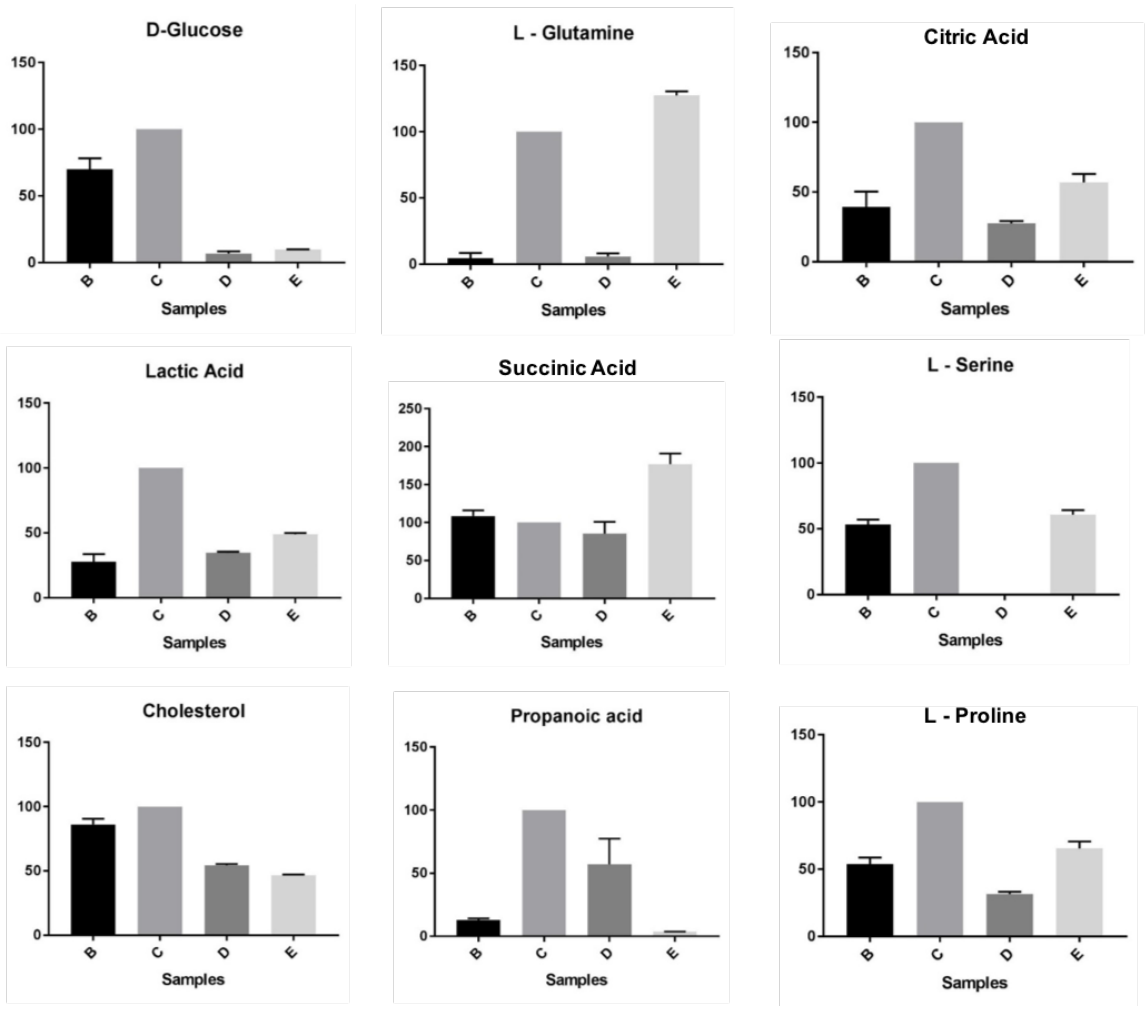


Figure 48: GC-MS analysis across samples B-E show differences in metabolites involved in cellular metabolism: Bar graphs shows the 8 metabolites (from the 43 detected by GC-MS) selected for further investigation. Values were relative to sample C which was observed to have the highest intensity of metabolites.

4.1.16 Laser capture microdissection

The samples obtained from the in vivo mouse model were heterozygous in that they contained a mix of human mouse protein, making the isolation of particular populations (human or mouse protein only) very challenging. Although a filter for human proteins only was applied in the proteomic analysis, this potentially resulted in a loss in protein detection owing to human/mouse sequence overlap.

As a consequence, it was thought to employ laser capture microdissection (LCM) in order to overcome this limitation. LCM was carried out on formalin fixed paraffin embedded tissues samples as opposed to fresh tissue, owing to the limited amounts of tissue material available.

Due to time restraints and owing to the difficulty identifying the small tumour nodules characteristic to the 786 IV injection, it was decided to focus on just the 6450 IV injection (co – option) and 6450 subcutaneous injection (angio) respectively.

Immunohistochemistry was carried out in order to highlight the areas of tumour mass (H&E) and the subsequent vessels (endomucine). Owing to the potential issues surrounding the use of antibodies and protein analysis /detection on the mass spectrometer, staining was minimised as much as possible. LCM was conducted on 3 replicates per condition (6450 IV and 6450 Subcutaneous).

Pilot studies were carried out to determine the amount of protein required for proteomic analysis and the routine proteomic protocol was optimised (see methods) to include heating of the samples for an extended period, in order to break down the cross linkages created by the immunostaining.

From the pilot experiments it was decided that a collection area of 192,400 cm^2 for each sample would be sufficient (equates to around 9,000 – 10,000 cells).

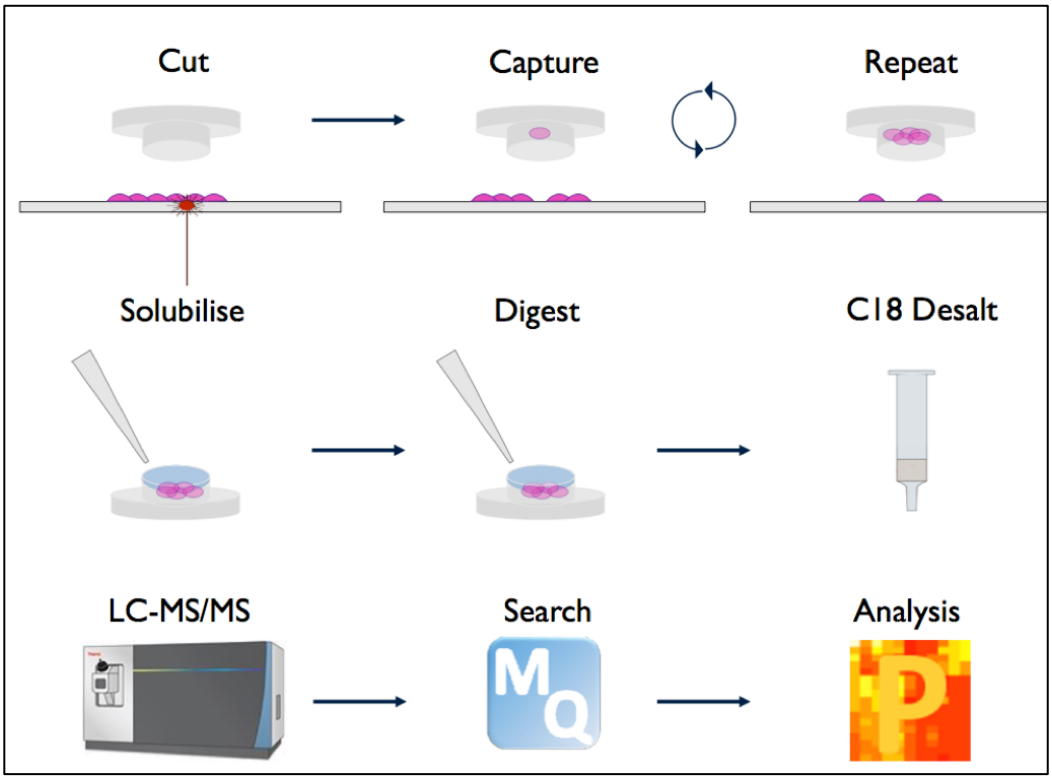


Figure 49: LCM workflow: Areas of tissue are isolated from the prepared slides using a laser capture microscope equipped with laser pressure catapulting, which allows for contactless transfer of regions of interest into the cap of a 600 µL microcentrifuge tube. Areas of interest are collected in RIPA buffer. Samples are digested in trypsin and following digestion are de salted using a C18 column to remove salts and buffers and to enable the capture of hydrophobic peptides. Samples are then injected on to the LC- MS/MS and the raw data then undergoes a maxquant search, followed by subsequent protein identification. and quantification.

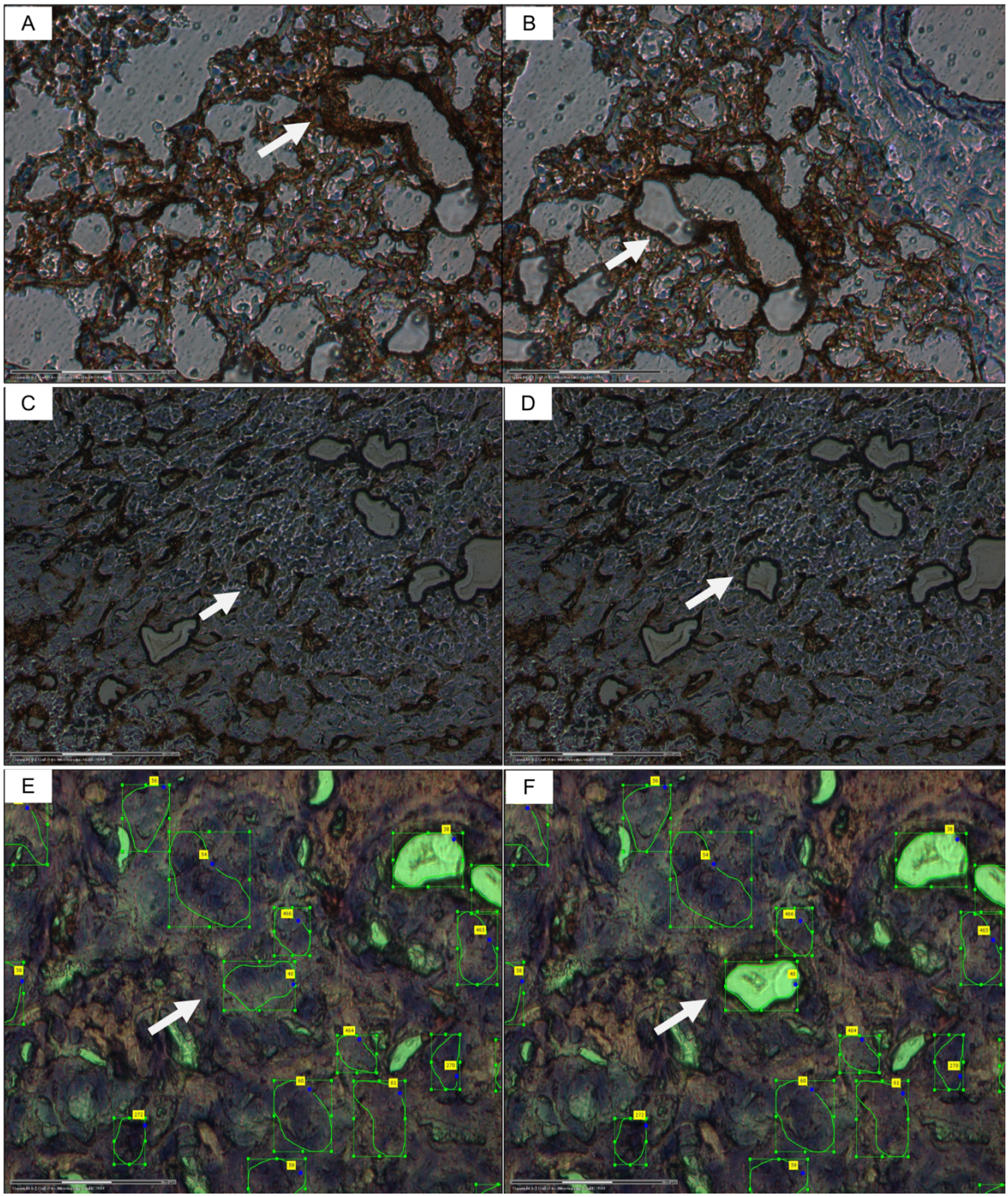


Figure 50: LCM collection of tumour and vessel material: Images showing the before and after cutting using LCM. Slides are visualised on the microscope and magnification is adjusted accordingly. A) shows an endomucine stained vessel slide before cut (20x magnification) B) shows an endomucine stained vessel slide after cut (magnification 20x) C) shows an endomucine stained slide before cut (10x magnification) D) shows an endomucine stained slide after cut (10x magnification) E) shows a H & E tumour stained slide before cut (20x magnification) F) shows a H & E tumour stained slide after cut (20x magnification). Arrows point to the area of the laser cut (before and after cutting).

Once the samples had been processed, identified and quantified using MaxQuant an mass spectrometry data analysis software, principle component analysis was applied in order to determine the separation achieved between the injections (IV and subcutaneous) and the tissues (tumour and vessels). The PCA plot was generated from Clustvis (https://biit.cs.ut.ee/clustvis/) a free web programme.

Data used was log2 transformed MaxQuant label free (LFQ) data and only proteins quantified in all samples were included (209 proteins).

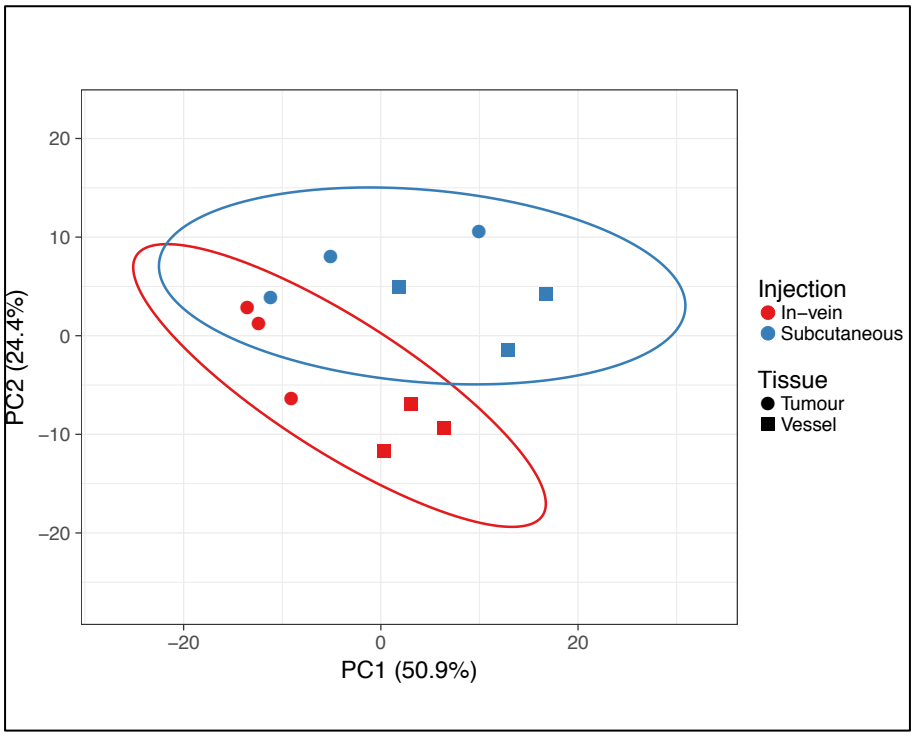


Figure 51: Principal component analysis shows independent clustering of in vein injection versus subcutaneous injection and tumour versus vessels: Principal component analysis (PCA) showing the protein expression profiles between the tissue and vessels from the same injection site (IV or Subcutaneous) (PCA 2) and between the injection groups (IV and subcutaneous) PC2. Coloured ellipses correlate with injection site (IV=red and Subcutaneous= blue) Tissue type is indicated by either a square (vessels) or a circle (tumour). Ellipses were added and represent a 0.95 confidence level that a new observation will fall within the same ellipse. Unit variance scaling is applied to rows; singular value decomposition with imputation is used to calculate principal components. X and Y axis show principal component 1 and principal component 2 that explain 50.9% and 24.4% of the total variance, respectively. N = 12 data points.

In addition to PCA, Venn diagrams were generated in order to identify the total number of proteins detected (triplicates combined) without applying any filters and to determine how much overlap of these proteins was shared between the two groups (Tumours from sample B and tumours from sample E and Vessels from sample B and Vessels from sample E).

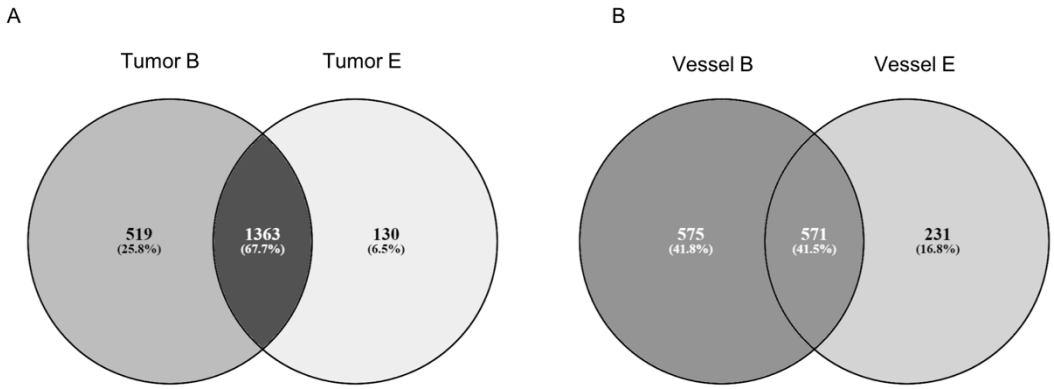


Figure 52: Venn diagrams showing total number of proteins detected with percentage overlap between groups: A) Shows the total number of proteins detected in the three tumour replicates (Sample B and E) and the subsequent overlap between the two groups. B) Shows the total number of proteins detected in the three vessel replicates (Sample B and E) and the subsequent overlap between the two groups.

Protein groups were then visualised on a volcano plot whereby different groups could be compared, and differential expression of proteins could be assessed. Following this, protein groups were subjected to statistically significant testing (Pearson co efficient) in order to generate an ANOVA p value where only proteins with a p value of less than 0.05 were selected for (table included in supplementary).

Owing to time restraints, only the differential expression of proteins in Vessels B compared to Vessels E (6450 IV vs 6450 subcutaneous) were assessed.

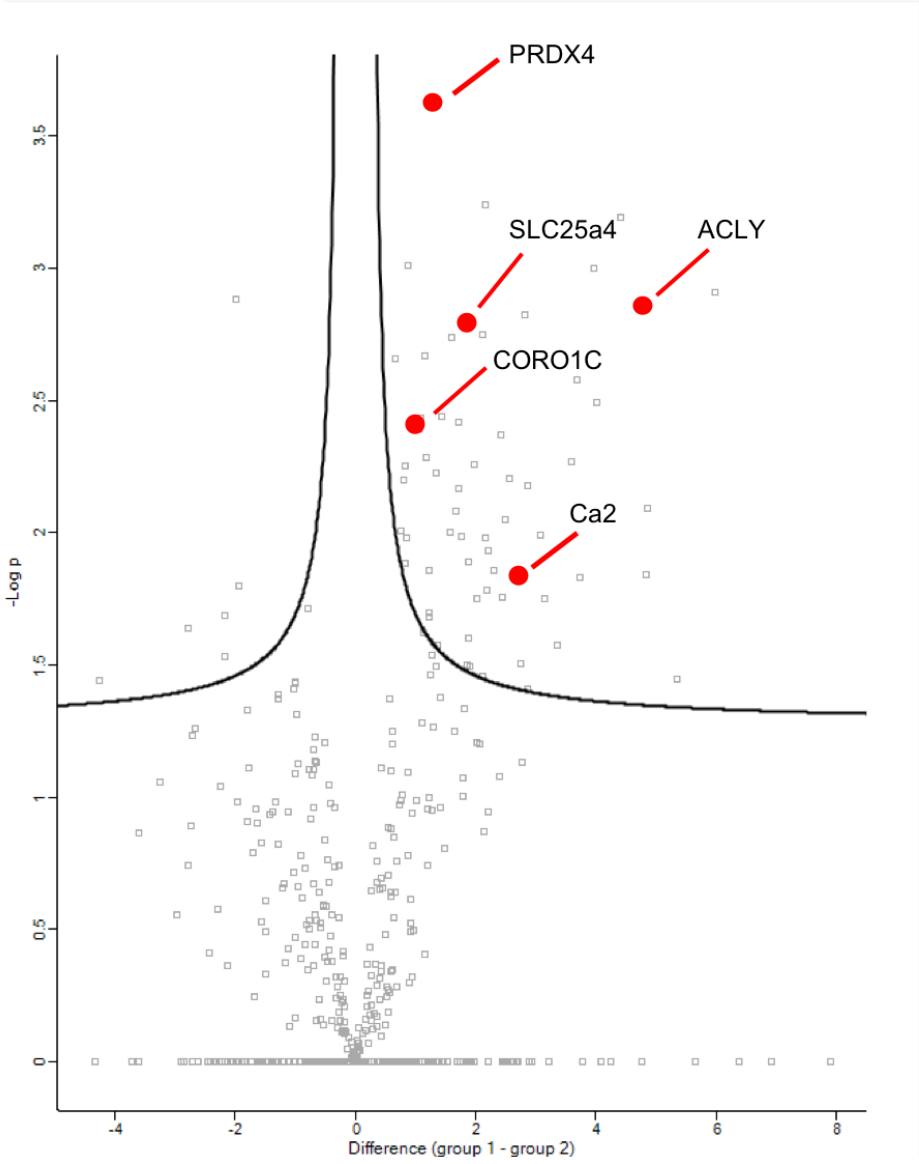


Figure 53: Volcano plot highlighting the upregulated proteins in Vessels B verses Vessels E: Volcano plot comparing differential expression of proteins found in sample B (group 1) versus Sample E (group 2) Highlighted in red are some proteins of interest that are showed to be upregulated in B vessels versus E vessels.

4.1.17 Discussion and limitations

Using proteomics as a first line approach, the aim of this part of the project was to carry out a protein profiling of the in vivo mouse co-option model with the view to identify and characterise the defining protein signatures unique to the two cell lines when injected intravenously versus when injected subcutaneously.

Global proteomic and metabolomic studies on frozen tissue was successful as well as proteomics analysis of laser capture micro dissected formalin fixed paraffin embedded tissue. A reasonable amount of separation of human and murine proteins from the proteomic analysis was also achieved. Although the analysis was carried out on one biological replicate and thus only presents a preliminary differential analysis, confirmation of a number of molecular profiles that have already been highlighted in previous studies, such as the involvement of energy metabolism, adhesion receptor landscape and cell apoptotic pathways, was made [223]. Previous studies investigating angiogenesis vs co-option have focused on mRNA profiling, as a result proteomic molecular characterisation in the context of understanding tumour vascular status (using proteomics as a first line approach) is one of the first of its kind [223].

That said, there were a number of challenges inherent to this in – vivo aspect of the project. One of the very first challenges with the in vivo work that was encountered was the heterogeneity of the tissue samples. This was overcome to some extent with the application of a human only protein filter (proteomic analysis). However, this led to the loss of potential protein hits owing to sequence overlap between human and mouse proteins, thus limiting the ability to obtain a true representative picture of the molecular signatures and compare these profiles accurately across samples.

Furthermore, this heterogeneity impacted on the validation of potential protein targets suggested from the proteomic analysis. An attempt to control for this was made by loading both control mouse tissue and control human cancer cell lysate, nevertheless antibody cross reactivity could not be avoided. As a result, interpretation remained difficult and for this reason no solid conclusions can be made without further investigative studies.

It however could be argued that western blot validation can still be considered relevant in the case where cross reactivity was significant (high expression seen in the healthy mouse lung western blot lane) and significant loss in target protein expression was observed. For example, in the case of PKM2, Pan Cadherin, GSTP1and ADAMTS2.

Furthermore, according to the literature L1CAM has been found to be overexpressed in the co optive tumour phenotype[336] whereas these studies show it as being overexpressed in the angiogenic tumour phenotype. This potentially points to the pleiotropic role L1CAM may play which could be dependent on cancer type and stage [337].

From the preliminary western blot analysis however, the pattern that seems to be emerging is that differences in expression profiles can perhaps be grouped into comparative IV injection vs subcutaneous injection and this may be where the most differences in protein expression and where differential regulation of molecular pathways can be found.

As mentioned, results from the protein validation were not very clear and in fact highlight the molecular complexity of the research question and aims. However, what seems clear is the potential role metabolism plays in defining tumour/vessel status.

One major challenge with the metabolomic study was the inability to separate out murine metabolites from human metabolites. This is something to bear in mind when analysing this data and presents a significant limitation.

Comparing both the metabolomic and proteomic profiles highlights the fact that although not much differential change may be occurring on the protein level when we compare differential protein expression between tissue samples B (6450 IV co-option) and E (6450 subcutaneous – angio) a lot more seems to be happening metabolically.

Moreover, the pattern that seems to emerge is that when comparing the IV injection group (786/6450 cells injected IV) and the Subcutaneous group (786/6450 cells injected subcutaneously) is that the IV injection group seems to have a fatty acid component to its metabolism whereas the subcutaneous injection group seems to undergo more glycolysis.

The potential implication of COXIV which was shown to have a variable expression from proteomic studies, is interesting. Studies have indicated that COXIV an important regulatory subunit of COX could inhibit COX activity at high ATP/ADP ratios by binding to ATP[338].

It also has been suggested that HIF-1α controls COXIV expression by stimulating the transcription of genes that code for COXIV-2 and LON a mitochondrial protease which has been implicated in COXIV degradation [339].

Furthermore, it has been reported that mammalian cells have the ability to optimise respiration capability by means of altering COX subunit arrangement in order to adapt to hypoxic conditions [340]

Similarly, the Cadherins show variable expression in western blot validation as well as in the proteomic pull-down. Of particular interest is the pan cadherin validation blot which shows potential proteolytic cleavage of the cadherins when comparing the IV tissue sample group (786 and 6450 injected in vein) and the subcutaneous tissue sample group (786 and 6450 injected subcutaneously).

The cadherins have a longstanding role in cell growth, invasion and migration. More recently they have also been shown to be potent inducers of angiogenesis in ovarian cancer[341].

Although E cadherin is typically a transmembrane protein, it has also been showed that ovarian cancer cells can release a soluble form E – cadherin involving ectodomain shedding, and requiring cleavage from exosomes[341].

Moreover, soluble E cadherin has been shown to heterodimerise with vascular endothelial cadherin on endothelial cells inducing NFκB signalling[341].

The fact evidence of proteolytic cleavage from the western blot validation is observed, may imply the involvement of a soluble form of cadherin involving exosomes however, further validation would be needed to assess this further.

The use of laser capture microdissection has helped reduce the amount of heterogeneity within the tissue samples and although it was quite challenging to accurately dissect out vessels and tumours respectively, the results from the PCA plot show a good degree of separation between the two injection groups (IV and subcutaneous) and between the tumour and vessels groups.

Comparing vessels from sample B (metastatic – co optive phenotype) with vessels from sample E (metastatic – angio) a number of proteins can be observed to undergo upregulation.

Owing to time restraints, a comprehensive investigation of these expression profiles has not been possible however, from the preliminary analysis carried out, proteins of interest include peroxiredoxin 4, Coronin 1C, ATP citrate lyase (ACLY), Solute carrier family 25 member 4 and Carbonic anhydrase 2.

Peroxiredoxin 4 (PRDX4) is a member of the antioxidant enzyme family and is involved in metabolising intracellular H_2O_2 [342]. Peroxiredoxin 4 has also been implicated in the regulation of HIF-1α activity. Studies have shown that prolonged periods of hypoxia results in the decay of HIF-1α [343]. Furthermore, it has been observed that under prolonged exposure to hypoxia PRDX4 knockdown increases the expression of select HIF target genes [342]. It was thus concluded that PRDX4 is involved in the inhibition of HIF-1α transactivation (select HIF target genes) [342]. In addition to this it was proposed that PRDX4 may be a negative regulator of glucose reprogramming in cancer cells exposed to prolonged hypoxia, owing to the observation that mRNA levels of (SLC2A3, GPI, and PDK3) were selectively decreased by PRDX4 [342].

Coronin 1C is a multi-domain protein, that has been implicated in actin binding. In addition to this Coronin 1C has been found to bind to both RAC1 and RCC2. In its active state, RAC1 binds to a number of effector proteins and regulates a variety of cellular responses [344] which include epithelial cell polarization, neuron adhesion, migration and differentiation [345]. Furthermore, Rac1 p21/rho GDI heterodimer forms the active component of the cytosolic factor sigma 1, and has been implicated in the stimulation of NADPH oxidase activity [346].

As mentioned, Coronin 1 C can also bind RCC2 which has been found to be a component of fibronectin-associated adhesion complexes [347] and an inhibitor of RAC1. By associating with the actin cytoskeleton or adhesion complexes [347], RCC2 and coronins have been associated with regulation of GTPases [348], which in turn, are involved in cell motility, mesenchymal cell migration, and may have a role in cancer cell metastasis [349].

ATP citrate lyase (ACLY) is involved in catalysing the conversion of cytosolic citrate to acetyl – CoA and oxaloacetate [350]. ACLY is considered an important enzyme associated with lipid biogenesis and has been linked with glucose metabolism. Studies have also shown a role for ACLY in tumorigenesis, where increased levels of the enzyme have been observed to result in increased metabolism by via Akt signalling [351]. Furthermore, increased levels of ACLY expression have been noted in many cancer types such as glioblastoma, colorectal cancer, breast cancer and non-small cell lung cancer [351] with inhibition of ACLY resulting in changes in cancer metabolism that induces tumour growth and proliferation [351].

Solute carrier family 25 member 4 is involved in catalysing the exchange of ADP and ATP across the mitochondrial inner membrane. It is also involved in the regulation of the mitochondrial permeability transition pore [352]. Overexpression of SLC25a4 has been implicated in apoptosis and tumour growth suppression in vivo [352 353].

Carbonic Anhydrase 2 plays a vital role in pH balance and regulation of ion transport and is a target that has consistently appeared in our studies. Interestingly, it also was found to be significantly differentially regulated in vessels (B vs C) and although its role in cancer remains obscure, its overexpression has also been shown to be involved in the inhibition of epithelial mesenchymal transition by limiting cell migration and invasion in hepatocellular carcinoma [309].

Thus, once again it can be observed that metabolism, namely glucose related metabolism and lipid metabolism play a potential role in angiogenic vs co optive tumour phenotypes in addition to the differences in regulation of the adhesion receptor landscape including cell motility and cell migration modulation.

However, what still remains to be determined is whether or not these angiogenic vs co optive phenotypes result solely as a consequence of off target/acquired responses (post treatment with an anti - angiogenic drug) leading to selective differential regulation of metastasis, which seems to be heavily dependent on injection site (IV vs Subcutaneous injections).

Chapter 5 Conclusions and future perspectives

In the introductory chapter, the hallmarks of cancer are discussed in detail, owing to the longstanding presence they have had in the field of cancer research, acting as blueprints to understanding core cancer traits and providing the rationale for drug discovery and design. However, allusion to the fact that many of these "hallmarks" are in fact shared by both benign and malignant growth (including non-cancerous conditions) is made, and therefore the premise upon which the term "hallmarks" i.e. distinguishable factors are used is questioned [354].

Furthermore, taking angiogenesis as an example, or what should be more accurately be termed vascular status (the topic of this thesis), an attempt to showcase how reductionist the original defined hallmarks can be is made, and despite the effort to provide an organisational framework, they fail to present a holistic view of cancer in its complexity.

Similarly, the translational clinical benefit of using drugs that are specifically linked to targeted hallmarks is touched upon and their ineffectiveness is highlighted [355] further emphasising the importance of the concept of shifting hallmark dependence during therapies [1].

As the molecular knowledge of the hallmarks increases, summarising the dynamics of cancer as static/isolated molecular principles has become somewhat obsolete with a more evolutionary view of the hallmarks of cancer being adopted instead [356].

As a consequence, the hallmarks are presented with a more specific emphasis on angiogenesis and vascularisation in light of this evolutionary perspective.

Furthermore, choosing to interrogate the mouse model of co-option with a multi omics approach, has served to investigate the complex array of relationships ranging over several entities in a "systems biology" manner. Thus, ensuring a comprehensive assessment of the hallmarks and their roles in relation to vascular status in cancer.

Experimental findings in both the in vitro and in vivo models highlight what is challenged in the introduction, that being that the hallmarks work in a complementary, co-dependent and evolutionary fashion. Furthermore, attenuation to the pleiotropic nature of molecular profiles is made, the expression of which may vary depending on injection site, stage of metastasis, selective advantage and most importantly niche microenvironments. Thus, emphasising the need for combination therapies with respect to drug design and delivery.

5.1 Future Directions

Future directions for this work would need to include proteomic analysis of the cell lines (6450 early vs late) which then could be combined with the mRNA sequencing of the same sample set. This would facilitate a more comprehensive study of both the mRNA levels of expression in relation to differential protein expression profiles. Furthermore, metabolomics on the cells lines (6450 early vs late) could also be carried out, which would enable a multi omics comparison to be done on the in vitro cell line model, helping to confirm potential targets, and shed light on the upstream/ downstream regulatory pathways involved.

In addition to this, more in-depth proteomics studies could be carried out in order to highlight potential post translational modifications as well as sub fractionation protein analysis.

This would enable further investigations to be carried out in order to better understand the molecular underpinnings and involvement of targets highlighted in adhesion/migration and tumour acidosis processes.

Laser capture micro dissected tumours still remain to be analysed in addition to including micro dissected stromal compartments for further investigation. Furthermore, and worth noting is the application of these studies, as well as this particular the mouse model to the phenomenon of dormancy, which still remains a relatively elusive field. Laser capture microdissection could also be used to investigate the molecular signatures (by means of proteomics and RNA sequencing) where 786 dormant cells could be compared with their metastatic counterpart (786 injected subcutaneously). This undoubtedly would help expand our knowledge with regards to cancer and dormancy.

Further investigations would need to be carried out in order to match the in vitro 6450 cell line (early passage) with the in vivo model to enable accurate characterisation between the two models (in vitro and in vivo), thus facilitating better planning of experimental procedures, allowing for more efficient translation of results.

Further validation is required and thus immunohistochemical validation of potential targets would be needed to confirm and eliminate candidates of interest, before knockdowns and gene silencing can be carried out in order to further interrogate proteins involved in metabolism, adhesion, migration, pH regulation and tumour acidosis.

Repeating the metabolic experiments, namely the intracellular assay where cells would need to be monitored under normal ambient oxygen levels (18-20%) and metabolic profiles compared (5% ambient oxygen and 18-20% ambient oxygen). This would enable a full comprehensive assessment of metabolic profiles and the influence of varying levels of intracellular oxygen.

Techniques whereby single cell metabolic analysis on tissue can be carried out are now becoming more established and would perhaps warrant further investigation in order to further dissect the metabolic landscapes of the in vivo and vitro models.

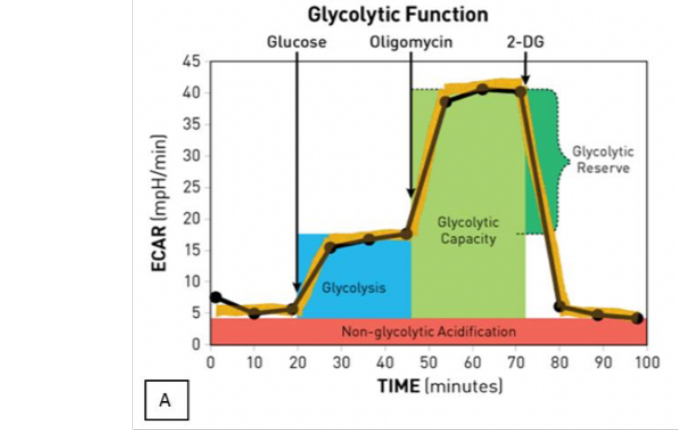
Global tissue mRNA, proteomics and metabolomics would need repeating on three biological replicates and or technical replicates and results incorporated to show multi-level differential regulation. In addition to this, all data sets including the laser capture microdissection results, need to be fully interrogated in more detail by means of bioinformatics, to facilitate future experimental setup and investigation.

Owing to the fact that studies have highlighted differences in the degree of metastasis and tumour aggressiveness, based on the type of immunosuppressed strain of mouse used for injection of human tumour cells in vivo [357]. It thus would be of interest to inject the 786-parental cell line into a different immune compromised strain of mouse, in addition to the one used in the in vivo model (nude mouse) presented in this study. This would help provide more insight, as well as determine whether it is an in fact an immune response component that is dictating the difference in metastatic capacity between the two cell lines.

Chapter 6

6.1 Appendix

Supplementary material chapter 3



Medium Condition	Glucose	Pyruvate	Glutamine
1	10mM	-	2mM
2	10mM	5mM	2mM
3	-	5mM	2mM
4	10mM	-	-
5	25mM	-	2mM

Port		Concentration	
A	Glucose	10mM	25mM
B	Oligomycin	1µM	-
C	2 DG	50mM	-

B

C

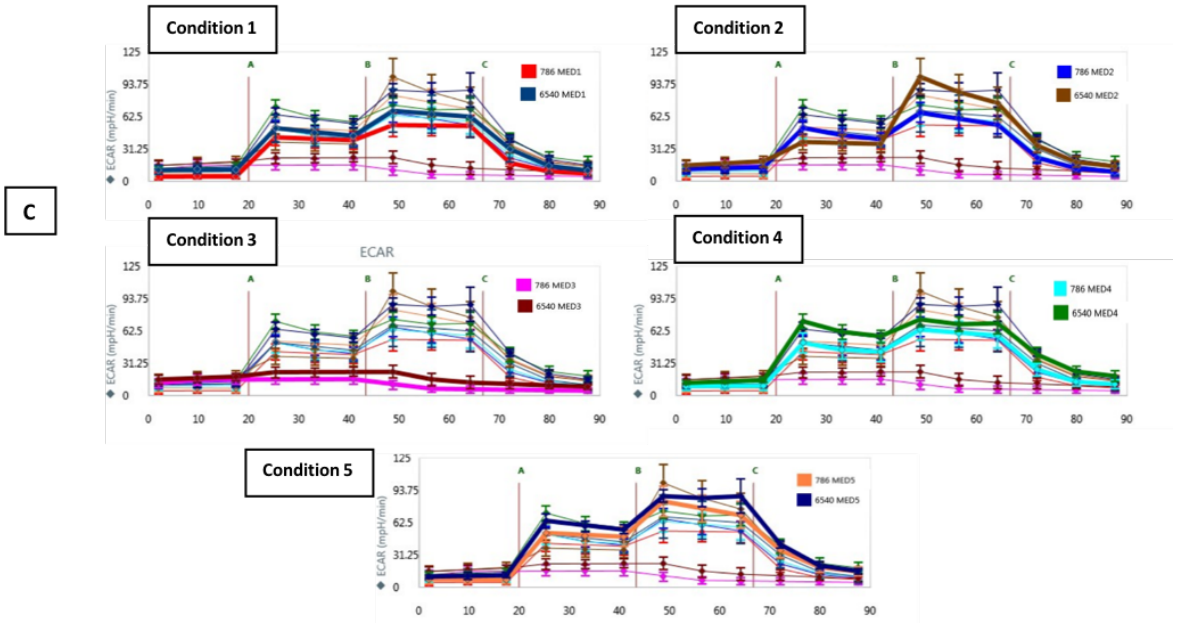
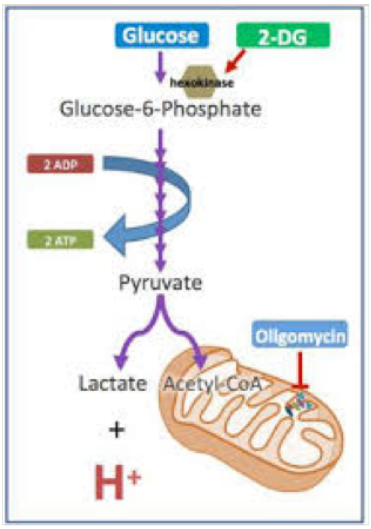


Figure S.3: Preliminary seahorse experiments using 5 medium conditions and drug injections shows differences in glycolytic profiles **A)** Schematic taken from the seahorse website showing an overview of the glycolytic assay including the injections and measurement parameters. B) table showing the different medium conditions. C) conditions 1-5 show the different metabolic profiles of the cell lines when exposed to different medium conditions. Condition 1 786 are shown in **red,** 6450 cells shown in **blue.** Condition 2 786 cells shown in **blue** and 6450 in **brown.** Condition 3 786 cells shown in **pink** and 6450 cells in **brown**. Condition 4 786 cells shown in **light blue** and 6450 cells shown in **green**. Condition 5 786 cells shown in **orange** and 6450 cells in **dark blue. Note:** only early passages of 6450 cells were used and condition medium was applied acutely immediately prior to the assay being carried out – i.e. cells were not fully starved. 2 biological replicates and 8 technical replicates were carried out.



Medium Condition	Glucose	Pyruvate	Glutamine
1	10mM	-	2mM
2	10mM	5mM	2mM
3	-	5mM	2mM
4	10mM	-	-
5	25mM	-	2mM

Port		Concentration	
A	Glucose	10mM	25mM
B	Oligomycin	1µM	-
C	2 DG	50mM	-

C

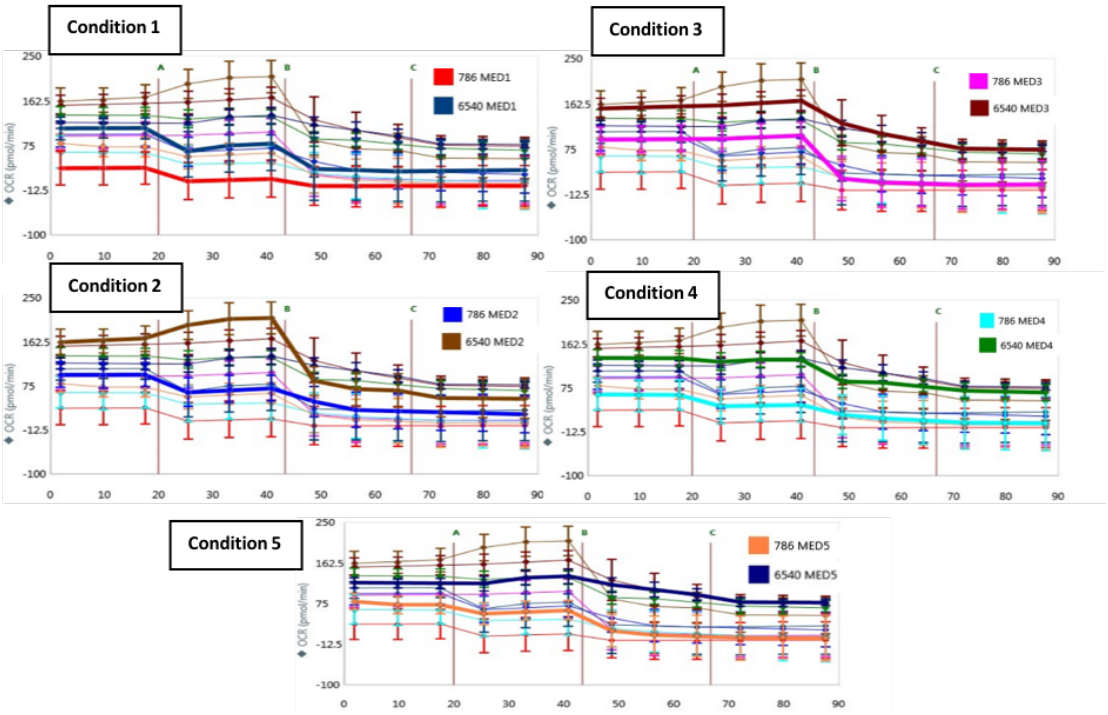


Figure S3.1: Preliminary seahorse experiments using 5 medium conditions and drug injections shows differences in oxygen consumption profiles **A)** Schematic taken from the seahorse website showing an overview of the oxygen consumption assay including the injections and measurement parameters. B) table showing the different medium conditions. C) conditions 1-5 show the different metabolic profiles of the cell lines when exposed to different medium conditions. Condition 1 786 are shown in **red,** 6450 cells shown in **blue.** Condition 2 786 cells shown in **blue** and 6450 in **brown.** Condition 3 786 cells shown in **pink** and 6450 cells in **brown**. Condition 4 786 cells shown in **light blue** and 6450 cells shown in **green**. Condition 5 786 cells shown in **orange** and 6450 cells in **dark blue. Note:** only early passages of 6450 cells were used and condition medium was applied acutely immediately prior to the assay being carried out – i.e. cells were not fully starved. 2 biological replicates and 8 technical replicates were carried out.

Certificate of Authentication (Cell lines)

eurofins | Forensik

DAkkS Deutsche Akkreditierungsstelle D-PL-18779-01-00

University of Oxford
Alia Komsany
Old Road Campus – Headington
Oxford, OX3 7FZ
UK

09.11.2017

Certificate

Order
By order of Alia Komsany (University of Oxford) we were requested to perform a cell line authentication test. Following samples were examined:

Our sample number	Client sample name
CL171103_105	6450 - old batch
CL171103_106	6450 - new batch
CL171103_107	786 - old batch

Method:
DNA was isolated separately from the samples.
Genetic characteristics were determined by PCR-single-locus-technology. 21 independent PCR-systems Amelogenin, D3S1358, D1S1656, D6S1043, D13S317, Penta E, D16S539, D18S51, D2S1338, CSF1PO, Penta D, TH01, vWA, D21S11, D7S820, D5S818, TPOX, D8S1179, D12S391, D19S433 and FGA were investigated (Promega, PowerPlex 21 PCR Kit).
In parallel, positive and negative controls were carried out yielding correct results.

eurofins | Forensik

DAkkS Deutsche Akkreditierungsstelle D-PL-18779-01-00

Results:

DNA-System	DNA-criteria 6450 - old batch CL171103_105	DNA-criteria 6450 - new batch CL171103_106	DNA-criteria 786 - old batch CL171103_107
AM	X, X	X, X	X, Y
D3S1358	16, 16	16, 16	16, 16
D1S1656	11, 12	11, 12	11, 12
D6S1043	11, 11	11, 11	11, 11
D13S317	8, 8	8, 8	8, 8
Penta E	7, 16	7, 16	7, 16
D16S539	12, 12	12, 12	12, 12
D18S51	13, 14	13, 14	13, 14
D2S1338	17, 18	17, 18	17, 18
CSF1PO	10, 10	10, 10	10, 10
Penta D	9, 12	9, 12	9, 12
TH01	6, 9.3	6, 9.3	6, 9.3
vWA	15, 17	15, 17	15, 17
D21S11	29, 30	29, 30	29, 30
D7S820	11, 12	11, 12	11, 12
D5S818	9, 9	9, 9	9, 9
TPOX	8, 11	8, 11	8, 11
D8S1179	13, 13	13, 13	13, 13
D12S391	17, 18	17, 18	17, 18
D19S433	14, 15	14, 15	14, 15
FGA	24, 24	24, 24	24, 24

Summary:
The following cell lines could be detected in the online database of the DSMZ (http://www.dsmz.de/de/service/services-human-and-animal-cell-lines/online-str-analysis.html):

Our sample number	Client sample name	DSMZ name
CL171103_105	6450 - old batch	786-O [786-0] (Y is missing)
CL171103_106	6450 - new batch	786-O [786-0] (Y is missing)
CL171103_107	786 - old batch	786-O [786-0]

Dr. Burkhard Rolf
Director Forensic Services

Dr. Michaela Bosch
Project Manager DNA-Forensics

Eurofins Medigenomix Forensik GmbH carries out all analyses with greatest care and on the basis of state of the art scientific knowledge. All results solely refer to the analysed samples. Our expert's reports must not be duplicated in extracts without consent of Eurofins Medigenomix Forensik GmbH.
Cell_line-certificate_eng_V05_21032017

Vorlage_Verwandtschaftsanalyse_EUROFINS_v02_121127

Supervised protein Lists from proteomic experiments on cell lines (786 vs 6450 early)

	A	B	C	D	E	F
3	Description	Anova p-value <= 0.05	Anova p-value <= 0.05 norm	up 786	up 6450	Max fold change >= 2
4	Ubiquitin-associated and SH3 domain-containing protein B OS=Homo sapiens GN=UBASH3B PE=1 SV=2	x	x		x	x
5	Glutathione S-transferase P OS=Homo sapiens GN=GSTP1 PE=1 SV=2	x	x		x	x
6	Superoxide dismutase [Mn], mitochondrial OS=Homo sapiens GN=SOD2 PE=1 SV=2	x	x	x		x
7	Neutral amino acid transporter B(0) OS=Homo sapiens GN=SLC1A5 PE=1 SV=2	x	x		x	x
8	Oligoribonuclease, mitochondrial (Fragment) OS=Homo sapiens GN=REXO2 PE=1 SV=1	x	x		x	x
9	DNA replication licensing factor MCM4 OS=Homo sapiens GN=MCM4 PE=1 SV=5	x	x	x		x
10	Glycine cleavage system H protein, mitochondrial OS=Homo sapiens GN=GCSH PE=1 SV=2	x	x	x		x
11	Acyl-CoA synthetase family member 2, mitochondrial OS=Homo sapiens GN=ACSF2 PE=4 SV=1	x	x	x		
12	Cytoskeleton-associated protein 4 OS=Homo sapiens GN=CKAP4 PE=1 SV=2	x	x		x	
13	Saccharopine dehydrogenase-like oxidoreductase OS=Homo sapiens GN=SCCPDH PE=1 SV=1	x	x	x		x
14	Isoform 2 of Collagen alpha-3(VI) chain OS=Homo sapiens GN=COL6A3	x	x		x	x
15	CD44 antigen OS=Homo sapiens GN=CD44 PE=1 SV=2	x	x		x	x
16	Intercellular adhesion molecule 1 OS=Homo sapiens GN=ICAM1 PE=1 SV=2	x	x	x		
17	Elongation factor 1-alpha 2 OS=Homo sapiens GN=EEF1A2 PE=1 SV=1	x	x	x		x
18	Rho-related GTP-binding protein RhoG OS=Homo sapiens GN=RHOG PE=1 SV=1	x	x		x	x
19	Isoform 2 of Proteasome subunit alpha type-3 OS=Homo sapiens GN=PSMA3	x	x	x		
20	Protein-glutamine gamma-glutamyltransferase 2 OS=Homo sapiens GN=TGM2 PE=1 SV=2	x	x	x		x
21	Melanoma-associated antigen D2 OS=Homo sapiens GN=MAGED2 PE=1 SV=2	x	x		x	x
22	CD151 antigen OS=Homo sapiens GN=CD151 PE=1 SV=1	x	x		x	x
23	Nuclear transport factor 2 OS=Homo sapiens GN=NUTF2 PE=1 SV=1	x	x	x		x
24	Tryptophan--tRNA ligase, cytoplasmic OS=Homo sapiens GN=WARS PE=1 SV=2	x	x	x		x
25	Galectin-3 OS=Homo sapiens GN=LGALS3 PE=1 SV=5	x	x	x		x
26	Isoform 2 of Coatomer subunit beta' OS=Homo sapiens GN=COPB2	x	x		x	
27	Pyruvate carboxylase, mitochondrial OS=Homo sapiens GN=PC PE=1 SV=2	x	x	x		x
28	Isoform 4 of Dehydrogenase/reductase SDR family member 4 OS=Homo sapiens GN=DHRS4	x	x	x		x
29	Sodium- and chloride-dependent taurine transporter OS=Homo sapiens GN=SLC6A6 PE=1 SV=2	x	x		x	x
30	Aldose reductase OS=Homo sapiens GN=AKR1B1 PE=1 SV=3	x	x	x		x
31	Microtubule-associated protein 1B OS=Homo sapiens GN=MAP1B PE=1 SV=2	x	x		x	
32	Delta(3,5)-Delta(2,4)-dienoyl-CoA isomerase, mitochondrial OS=Homo sapiens GN=ECH1 PE=1 SV=2	x	x	x		x
33	Keratin, type I cytoskeletal 19 OS=Homo sapiens GN=KRT19 PE=1 SV=4	x	x	x		x
34	Nicotinate-nucleotide pyrophosphorylase [carboxylating] OS=Homo sapiens GN=QPRT PE=1 SV=3	x	x		x	x
35	Cathepsin Z OS=Homo sapiens GN=CTSZ PE=1 SV=1	x	x		x	x
36	Vimentin OS=Homo sapiens GN=VIM PE=1 SV=4	x	x	x		x
37	DNA replication licensing factor MCM3 OS=Homo sapiens GN=MCM3 PE=1 SV=3	x	x	x		x
38	LIM and cysteine-rich domains protein 1 OS=Homo sapiens GN=LMCD1 PE=4 SV=1	x	x	x		x
39	C-type mannose receptor 2 OS=Homo sapiens GN=MRC2 PE=1 SV=2	x	x		x	x
40	Carbonic anhydrase 2 OS=Homo sapiens GN=CA2 PE=1 SV=2	x	x	x		x
41	C-1-tetrahydrofolate synthase, cytoplasmic OS=Homo sapiens GN=MTHFD1 PE=1 SV=3	x	x	x		
42	Ribonuclease T2 OS=Homo sapiens GN=RNASET2 PE=1 SV=1	x	x		x	x
43	Serpin H1 OS=Homo sapiens GN=SERPINH1 PE=1 SV=2	x	x		x	
44	WD repeat-containing protein 1 OS=Homo sapiens GN=WDR1 PE=1 SV=4	x	x	x		
45	Isoform 2 of Inactive hydroxysteroid dehydrogenase-like protein 1 OS=Homo sapiens GN=HSDL1	x	x	x		x
46	Adenylate kinase 4, mitochondrial OS=Homo sapiens GN=AK4 PE=1 SV=1	x	x	x		
47	Alpha-enolase OS=Homo sapiens GN=ENO1 PE=1 SV=2	x	x	x		
48	Isoform 2 of Follistatin-related protein 1 OS=Homo sapiens GN=FSTL1	x	x		x	
49	PITH domain-containing protein 1 OS=Homo sapiens GN=PITHD1 PE=1 SV=1	x	x	x		
53	DNA replication licensing factor MCM5 OS=Homo sapiens GN=MCM5 PE=1 SV=1	x	x	x		
54	Annexin A8-like protein 1 OS=Homo sapiens GN=ANXA8L1 PE=4 SV=1	x	x		x	x
55	Isoform B of Phosphate carrier protein, mitochondrial OS=Homo sapiens GN=SLC25A3	x	x	x		x
56	Syndecan binding protein (Syntenin), isoform CRA_a OS=Homo sapiens GN=SDCBP PE=1 SV=1	x	x	x		x
57	Isoform 3 of E3 ubiquitin-protein ligase HUWE1 OS=Homo sapiens GN=HUWE1	x	x		x	
58	Normal mucosa of esophagus-specific gene 1 protein OS=Homo sapiens GN=NMES1 PE=2 SV=1	x	x	x		x
59	Isoform 12 of Sodium bicarbonate cotransporter 3 OS=Homo sapiens GN=SLC4A7	x	x		x	x
60	Surfeit 4 OS=Homo sapiens GN=SURF4 PE=1 SV=1	x	x		x	
61	FACT complex subunit SSRP1 OS=Homo sapiens GN=SSRP1 PE=1 SV=1	x	x	x		
62	Isoform 2 of Protein FAM98B OS=Homo sapiens GN=FAM98B	x	x	x		
63	Ribose-phosphate pyrophosphokinase 1 OS=Homo sapiens GN=PRPS1 PE=1 SV=2	x	x		x	
64	Heat shock protein beta-1 OS=Homo sapiens GN=HSPB1 PE=1 SV=2	x	x	x		x
65	Annexin A4 OS=Homo sapiens GN=ANXA4 PE=1 SV=4	x	x	x		x
66	Glutathione peroxidase (Fragment) OS=Homo sapiens GN=GPX4 PE=1 SV=1	x	x	x		x
67	Isoform B of Manganese-transporting ATPase 13A1 OS=Homo sapiens GN=ATP13A1	x	x	x		x
68	Dipeptidyl peptidase 3 OS=Homo sapiens GN=DPP3 PE=1 SV=1	x	x	x		
69	HCG2043421, isoform CRA_c OS=Homo sapiens GN=RBPMS PE=1 SV=1	x	x		x	
70	Isoform 2 of Peripheral plasma membrane protein CASK OS=Homo sapiens GN=CASK	x	x	x		
71	Aminopeptidase N OS=Homo sapiens GN=ANPEP PE=1 SV=4	x	x	x		x
72	Ectonucleotide pyrophosphatase/phosphodiesterase family member 1 OS=Homo sapiens GN=ENPP1 PE=1 SV=2	x	x	x		x
73	Alpha-parvin OS=Homo sapiens GN=PARVA PE=1 SV=1	x	x		x	
74	Hypoxia up-regulated protein 1 OS=Homo sapiens GN=HYOU1 PE=1 SV=1	x	x		x	
75	Ubiquitin carboxyl-terminal hydrolase isozyme L1 OS=Homo sapiens GN=UCHL1 PE=1 SV=2	x	x		x	
76	Isoform 2 of Epimerase family protein SDR39U1 OS=Homo sapiens GN=SDR39U1	x	x	x		x
77	Acyl-coenzyme A thioesterase 1 OS=Homo sapiens GN=ACOT1 PE=1 SV=1	x	x	x		x
78	4F2 cell-surface antigen heavy chain OS=Homo sapiens GN=SLC3A2 PE=1 SV=1	x	x	x		
79	Isoform 2 of [Pyruvate dehydrogenase [acetyl-transferring]]-phosphatase 1, mitochondrial OS=Homo sapiens GN=PD	x	x	x		
80	O-acetyl-ADP-ribose deacetylase MACROD1 OS=Homo sapiens GN=MACROD1 PE=1 SV=2	x	x	x		x
81	Cytosolic non-specific dipeptidase OS=Homo sapiens GN=CNDP2 PE=1 SV=2	x	x	x		
82	SH3 domain-containing kinase-binding protein 1 (Fragment) OS=Homo sapiens GN=SH3KBP1 PE=1 SV=1	x	x		x	
83	2'-5'-oligoadenylate synthase 3 OS=Homo sapiens GN=OAS3 PE=1 SV=3	x	x		x	x
84	Isoform 2 of Ribonucleoside-diphosphate reductase subunit M2 OS=Homo sapiens GN=RRM2	x	x	x		x
85	Na(+)/H(+) exchange regulatory cofactor NHE-RF1 OS=Homo sapiens GN=SLC9A3R1 PE=1 SV=4	x	x		x	x
86	Developmentally-regulated GTP-binding protein 2 OS=Homo sapiens GN=DRG2 PE=1 SV=1	x	x		x	
87	Methylcrotonoyl-CoA carboxylase subunit alpha, mitochondrial OS=Homo sapiens GN=MCCC1 PE=1 SV=1	x	x	x		
88	Isoform 2 of HD domain-containing protein 2 OS=Homo sapiens GN=HDDC2	x	x	x		
89	Ubiquitin-like protein ISG15 OS=Homo sapiens GN=ISG15 PE=1 SV=5	x	x		x	x
90	Cold-inducible RNA-binding protein OS=Homo sapiens GN=CIRBP PE=1 SV=1	x	x	x		x
91	PRA1 family protein 3 OS=Homo sapiens GN=ARL6IP5 PE=1 SV=1	x	x	x		

	A	B	C	D	E	F
90	Cold-inducible RNA-binding protein OS=Homo sapiens GN=CIRBP PE=1 SV=1	x	x	x		x
91	PRA1 family protein 3 OS=Homo sapiens GN=ARL6IP5 PE=1 SV=1	x	x	x		
92	Isoform 2 of Signal recognition particle receptor subunit alpha OS=Homo sapiens GN=SRPR	x	x		x	x
93	Isoform 2 of Glycogen phosphorylase, liver form OS=Homo sapiens GN=PYGL	x	x	x		x
94	Alanine--tRNA ligase, cytoplasmic OS=Homo sapiens GN=AARS PE=1 SV=2	x	x	x		x
95	Sulfhydryl oxidase 2 OS=Homo sapiens GN=QSOX2 PE=1 SV=3	x	x		x	
96	FH1/FH2 domain-containing protein 1 OS=Homo sapiens GN=FHOD1 PE=1 SV=3	x	x	x		
97	Valacyclovir hydrolase OS=Homo sapiens GN=BPHL PE=1 SV=1	x	x	x		x
98	Probable glutamate--tRNA ligase, mitochondrial OS=Homo sapiens GN=EARS2 PE=1 SV=2	x	x	x		
99	Isoform 4 of Inactive tyrosine-protein kinase 7 OS=Homo sapiens GN=PTK7	x	x		x	x
100	Isoform 2 of Keratin, type II cytoskeletal 8 OS=Homo sapiens GN=KRT8	x	x	x		
101	Aldo-keto reductase family 1 member C3 OS=Homo sapiens GN=AKR1C3 PE=1 SV=4	x	x	x		x
102	Cofilin-1 OS=Homo sapiens GN=CFL1 PE=1 SV=1	x	x	x		
103	DNA polymerase-transactivated protein 6, isoform CRA_b OS=Homo sapiens GN=SPATS2L PE=1 SV=1	x	x		x	
104	Bystin OS=Homo sapiens GN=BYSL PE=1 SV=3	x	x		x	
105	Uveal autoantigen with coiled-coil domains and ankyrin repeats OS=Homo sapiens GN=UACA PE=1 SV=1	x	x	x		x
106	Isoform 2 of 2-hydroxyacyl-CoA lyase 1 OS=Homo sapiens GN=HACL1	x	x		x	
107	Glutathione peroxidase 1 OS=Homo sapiens GN=GPX1 PE=1 SV=4	x	x	x		
108	Isocitrate dehydrogenase [NADP], mitochondrial OS=Homo sapiens GN=IDH2 PE=1 SV=2	x	x	x		
109	Adenine phosphoribosyltransferase OS=Homo sapiens GN=APRT PE=1 SV=2	x	x	x		
110	Isoform 2 of Disks large homolog 1 OS=Homo sapiens GN=DLG1	x	x	x		
111	Casein kinase II subunit alpha' OS=Homo sapiens GN=CSNK2A2 PE=1 SV=1	x	x	x		x
112	Isoform 2 of Septin-9 OS=Homo sapiens GN=SEPT9	x	x		x	
113	Isoform 2 of Matrix-remodeling-associated protein 7 OS=Homo sapiens GN=MXRA7	x	x		x	x
114	N(G),N(G)-dimethylarginine dimethylaminohydrolase 1 OS=Homo sapiens GN=DDAH1 PE=1 SV=3	x	x	x		x
115	RWD domain-containing protein 1 (Fragment) OS=Homo sapiens GN=RWDD1 PE=1 SV=1	x	x		x	
116	Proteasome subunit beta type-3 OS=Homo sapiens GN=PSMB3 PE=1 SV=2	x	x	x		
117	Dipeptidyl peptidase 1 OS=Homo sapiens GN=CTSC PE=1 SV=2	x	x		x	x
118	Annexin A3 OS=Homo sapiens GN=ANXA3 PE=1 SV=3	x	x	x		
119	Isoform 2 of DNA topoisomerase 2-alpha OS=Homo sapiens GN=TOP2A	x	x	x		
120	Isoform 3 of Branched-chain-amino-acid aminotransferase, cytosolic OS=Homo sapiens GN=BCAT1	x	x		x	
121	ERO1-like protein alpha OS=Homo sapiens GN=ERO1L PE=1 SV=2	x	x	x		
122	Single-stranded DNA-binding protein, mitochondrial OS=Homo sapiens GN=SSBP1 PE=1 SV=1	x	x	x		
123	Carbonyl reductase [NADPH] 1 OS=Homo sapiens GN=CBR1 PE=1 SV=3	x	x		x	
124	Ras-related protein R-Ras OS=Homo sapiens GN=RRAS PE=1 SV=1	x	x		x	x
125	Tumor necrosis factor alpha-induced protein 2 OS=Homo sapiens GN=TNFAIP2 PE=1 SV=2	x	x	x		x
126	Protein NipSnap homolog 1 OS=Homo sapiens GN=NIPSNAP1 PE=1 SV=1	x	x	x		
127	Vacuolar protein sorting-associated protein 26A OS=Homo sapiens GN=VPS26A PE=1 SV=2	x	x	x		
128	Mitochondrial 10-formyltetrahydrofolate dehydrogenase OS=Homo sapiens GN=ALDH1L2 PE=1 SV=2	x	x		x	x

	A	B	C	D	E	F
128	Mitochondrial 10-formyltetrahydrofolate dehydrogenase OS=Homo sapiens GN=ALDH1L2 PE=1 SV=2	x	x		x	x
129	Isoform 2 of RNA-binding protein 47 OS=Homo sapiens GN=RBM47	x	x	x		x
130	Vacuolar protein sorting-associated protein 29 OS=Homo sapiens GN=VPS29 PE=1 SV=1	x	x	x		
131	FACT complex subunit SPT16 OS=Homo sapiens GN=SUPT16H PE=1 SV=1	x	x	x		
132	Isoform 2 of Protein enabled homolog OS=Homo sapiens GN=ENAH	x	x	x		
133	Isoform 2 of Stomatin-like protein 2, mitochondrial OS=Homo sapiens GN=STOML2	x	x		x	
134	Isoform 2 of HEAT repeat-containing protein 3 OS=Homo sapiens GN=HEATR3	x	x	x		x
135	Actin-related protein 2/3 complex subunit 5-like protein OS=Homo sapiens GN=ARPC5L PE=1 SV=1	x	x		x	
136	Isoform 2 of RNA-binding protein 8A OS=Homo sapiens GN=RBM8A	x	x	x		
137	Isoform 2 of NAD(P)H-hydrate epimerase OS=Homo sapiens GN=APOA1BP	x	x	x		
138	Isoform 2 of 39S ribosomal protein L50, mitochondrial OS=Homo sapiens GN=MRPL50	x	x		x	
139	Dehydrogenase/reductase SDR family member 7B (Fragment) OS=Homo sapiens GN=DHRS7B PE=1 SV=1	x	x	x		x
140	Isoform 2 of Niban-like protein 1 OS=Homo sapiens GN=FAM129B	x	x		x	
141	Atlastin-3 OS=Homo sapiens GN=ATL3 PE=1 SV=1	x	x		x	x
142	RuvB-like 1 OS=Homo sapiens GN=RUVBL1 PE=1 SV=1	x	x	x		
143	Heat shock 70 kDa protein 1A/1B OS=Homo sapiens GN=HSPA1A PE=1 SV=5	x	x	x		x
144	DNA replication licensing factor MCM2 (Fragment) OS=Homo sapiens GN=MCM2 PE=1 SV=1	x	x	x		x
145	Transitional endoplasmic reticulum ATPase OS=Homo sapiens GN=VCP PE=1 SV=4	x	x		x	
146	Dihydrolipoyllysine-residue succinyltransferase component of 2-oxoglutarate dehydrogenase complex, mitochondrial	x	x	x		
147	Unconventional myosin-Ib OS=Homo sapiens GN=MYO1B PE=1 SV=1	x	x	x		
148	DNA-(apurinic or apyrimidinic site) lyase OS=Homo sapiens GN=APEX1 PE=1 SV=2	x	x	x		x
149	Glutathione synthetase OS=Homo sapiens GN=GSS PE=1 SV=1	x	x	x		
150	Cell adhesion molecule 1 (Fragment) OS=Homo sapiens GN=CADM1 PE=1 SV=1	x	x		x	x
151	Transmembrane protein 263 OS=Homo sapiens GN=TMEM263 PE=1 SV=1	x	x		x	
152	Williams-Beuren syndrome chromosomal region 22 protein (Fragment) OS=Homo sapiens GN=WBSCR22 PE=1 SV=1	x	x	x		x
153	Absent in melanoma 1 protein OS=Homo sapiens GN=AIM1 PE=1 SV=3	x	x		x	
154	Eukaryotic translation initiation factor 5 OS=Homo sapiens GN=EIF5 PE=1 SV=2	x	x	x		
155	Catenin delta-1 OS=Homo sapiens GN=CTNND1 PE=1 SV=2	x	x		x	
156	Retinal dehydrogenase 1 OS=Homo sapiens GN=ALDH1A1 PE=1 SV=2	x	x	x		
157	Methionine aminopeptidase 2 OS=Homo sapiens GN=METAP2 PE=1 SV=1	x	x	x		x
158	Ran-binding protein 6 OS=Homo sapiens GN=RANBP6 PE=1 SV=2	x	x		x	
159	Serine/threonine-protein kinase Nek9 OS=Homo sapiens GN=NEK9 PE=1 SV=2	x	x	x		x
160	Deoxyuridine 5'-triphosphate nucleotidohydrolase, mitochondrial (Fragment) OS=Homo sapiens GN=DUT PE=1 SV=1	x	x	x		
161	Cytochrome c oxidase subunit NDUFA4 OS=Homo sapiens GN=NDUFA4 PE=1 SV=1	x	x		x	
162	Transaldolase OS=Homo sapiens GN=TALDO1 PE=1 SV=2	x	x		x	
163	Acetyltransferase component of pyruvate dehydrogenase complex OS=Homo sapiens GN=DLAT PE=1 SV=1	x	x		x	
164	Protein VAC14 homolog OS=Homo sapiens GN=VAC14 PE=1 SV=1	x	x	x		x
165	Isoform Non-brain of Clathrin light chain A OS=Homo sapiens GN=CLTA	x	x		x	
166	Purine nucleoside phosphorylase OS=Homo sapiens GN=PNP PE=1 SV=2	x	x	x		x

	A	B	C	D	E	F
166	Purine nucleoside phosphorylase OS=Homo sapiens GN=PNP PE=1 SV=2	x	x	x		x
167	GDH/6PGL endoplasmic bifunctional protein OS=Homo sapiens GN=H6PD PE=4 SV=1	x	x	x		
168	Beta-lactamase-like protein 2 OS=Homo sapiens GN=LACTB2 PE=1 SV=2	x	x	x		
169	PDZ and LIM domain protein 7 OS=Homo sapiens GN=PDLIM7 PE=1 SV=1	x	x	x		x
170	Isoleucine--tRNA ligase, mitochondrial OS=Homo sapiens GN=IARS2 PE=1 SV=1	x	x	x		
171	G-rich sequence factor 1 (Fragment) OS=Homo sapiens GN=GRSF1 PE=1 SV=1	x	x	x		
172	Lysosomal Pro-X carboxypeptidase OS=Homo sapiens GN=PRCP PE=1 SV=1	x	x		x	x
173	UPF0160 protein MYG1, mitochondrial OS=Homo sapiens GN=C12orf10 PE=1 SV=1	x	x		x	
174	Methylmalonate-semialdehyde dehydrogenase [acylating], mitochondrial OS=Homo sapiens GN=ALDH6A1 PE=1 SV=	x	x	x		x
175	Enhancer of mRNA-decapping protein 4 OS=Homo sapiens GN=EDC4 PE=1 SV=1	x	x	x		
176	Serine--tRNA ligase, cytoplasmic OS=Homo sapiens GN=SARS PE=1 SV=1	x	x	x		
177	Isoform Cytoplasmic of Fumarate hydratase, mitochondrial OS=Homo sapiens GN=FH	x	x	x		
178	Cofilin-2 OS=Homo sapiens GN=CFL2 PE=1 SV=1	x	x	x		
179	Isoform 2 of Transcription factor BTF3 homolog 4 OS=Homo sapiens GN=BTF3L4	x	x	x		
180	Four and a half LIM domains protein 2 OS=Homo sapiens GN=FHL2 PE=1 SV=1	x	x		x	
181	Matrix-remodeling-associated protein 7 OS=Homo sapiens GN=MXRA7 PE=1 SV=1	x	x		x	
182	Pannexin-1 OS=Homo sapiens GN=PANX1 PE=1 SV=4	x	x		x	x
183	Isoform 3 of Deoxynucleoside triphosphate triphosphohydrolase SAMHD1 OS=Homo sapiens GN=SAMHD1	x	x		x	x
184	Lysophospholipid acyltransferase 7 OS=Homo sapiens GN=MBOAT7 PE=1 SV=2	x	x		x	
185	Proteasome subunit beta type-4 OS=Homo sapiens GN=PSMB4 PE=1 SV=4	x	x	x		
186	Fatty acid-binding protein, epidermal OS=Homo sapiens GN=FABP5 PE=1 SV=3	x	x	x		x
187	Isoform 2 of Leucine-rich repeat flightless-interacting protein 2 OS=Homo sapiens GN=LRRFIP2	x	x		x	
188	Neuroblast differentiation-associated protein AHNAK OS=Homo sapiens GN=AHNAK PE=1 SV=2	x	x		x	x
189	Aspartate--tRNA ligase, cytoplasmic OS=Homo sapiens GN=DARS PE=1 SV=2	x	x	x		
190	Importin-7 OS=Homo sapiens GN=IPO7 PE=1 SV=1	x	x		x	
191	Isoform 2 of C-Maf-inducing protein OS=Homo sapiens GN=CMIP	x	x	x		
192	Cation-independent mannose-6-phosphate receptor OS=Homo sapiens GN=IGF2R PE=1 SV=3	x	x		x	
193	Protein NAMPTL (Fragment) OS=Homo sapiens GN=NAMPTL PE=4 SV=1	x	x	x		
194	Nicotinamide phosphoribosyltransferase OS=Homo sapiens GN=NAMPT PE=1 SV=1	x	x	x		
195	Galactosylceramide sulfotransferase (Fragment) OS=Homo sapiens GN=GAL3ST1 PE=4 SV=1	x	x	x		x
196	Ras-related protein Rab-23 OS=Homo sapiens GN=RAB23 PE=1 SV=1	x	x		x	
197	Transmembrane protein 126A OS=Homo sapiens GN=TMEM126A PE=1 SV=1	x	x		x	x
198	Synaptobrevin homolog YKT6 OS=Homo sapiens GN=YKT6 PE=1 SV=1	x	x		x	
199	Isoform 2 of Glutamine-dependent NAD(+) synthetase OS=Homo sapiens GN=NADSYN1	x	x	x		x
200	Isoform LCRMP-4 of Dihydropyrimidinase-related protein 3 OS=Homo sapiens GN=DPYSL3	x	x		x	
201	Isoform Mitochondrial of Lysine--tRNA ligase OS=Homo sapiens GN=KARS	x	x	x		
202	Isoform 2 of Sec1 family domain-containing protein 1 OS=Homo sapiens GN=SCFD1	x	x	x		
203	Isoform 2 of Filamin-B OS=Homo sapiens GN=FLNB	x	x	x		
204	Isoform 10 of Fibronectin OS=Homo sapiens GN=FN1	x	x		x	x

	A	B	C	D	E	F
204	Isoform 10 of Fibronectin OS=Homo sapiens GN=FN1	x	x		x	x
205	Glutamate dehydrogenase 1, mitochondrial OS=Homo sapiens GN=GLUD1 PE=1 SV=2	x	x		x	
206	Protein Niban OS=Homo sapiens GN=FAM129A PE=1 SV=1	x	x		x	
207	Prefoldin subunit 4 OS=Homo sapiens GN=PFDN4 PE=1 SV=1	x	x		x	
208	Early endosome antigen 1 OS=Homo sapiens GN=EEA1 PE=1 SV=2	x	x	x		
209	Isoform 2 of EGF-like repeat and discoidin I-like domain-containing protein 3 OS=Homo sapiens GN=EDIL3	x	x	x		x
210	Protein FAM49B OS=Homo sapiens GN=FAM49B PE=1 SV=1	x	x	x		
211	Basal cell adhesion molecule OS=Homo sapiens GN=BCAM PE=1 SV=2	x	x	x		x
212	Isoform 2 of BRO1 domain-containing protein BROX OS=Homo sapiens GN=BROX	x	x	x		x
213	Succinate-semialdehyde dehydrogenase, mitochondrial OS=Homo sapiens GN=ALDH5A1 PE=1 SV=1	x	x	x		x
214	Protein HGH1 homolog OS=Homo sapiens GN=HGH1 PE=1 SV=1	x	x	x		x
215	Methylsterol monooxygenase 1 OS=Homo sapiens GN=MSMO1 PE=4 SV=1	x	x		x	
216	Isoform 2 of Thioredoxin-dependent peroxide reductase, mitochondrial OS=Homo sapiens GN=PRDX3	x	x	x		
217	Succinyl-CoA:3-ketoacid coenzyme A transferase 1, mitochondrial OS=Homo sapiens GN=OXCT1 PE=1 SV=1	x	x	x		
218	Isoform 2 of Insulin-like growth factor 2 mRNA-binding protein 2 OS=Homo sapiens GN=IGF2BP2	x	x		x	
219	Protein spinster homolog 1 OS=Homo sapiens GN=SPNS1 PE=1 SV=1	x	x	x		
220	Leukotriene A-4 hydrolase OS=Homo sapiens GN=LTA4H PE=1 SV=2	x	x	x		
221	Galectin-1 OS=Homo sapiens GN=LGALS1 PE=1 SV=2	x	x		x	
222	Protein NDRG1 OS=Homo sapiens GN=NDRG1 PE=1 SV=1	x	x	x		
223	Isoform 2 of Heterogeneous nuclear ribonucleoprotein H3 OS=Homo sapiens GN=HNRNPH3	x	x		x	
224	RELA protein OS=Homo sapiens GN=RELA PE=1 SV=1	x	x	x		
225	Isoform 2 of Vesicle-associated membrane protein-associated protein A OS=Homo sapiens GN=VAPA	x	x	x		
226	Isoform 2 of Charged multivesicular body protein 4a OS=Homo sapiens GN=CHMP4A	x	x	x		x
227	Signal transducing adapter molecule 2 OS=Homo sapiens GN=STAM2 PE=1 SV=1	x	x		x	
228	14-3-3 protein epsilon OS=Homo sapiens GN=YWHAE PE=1 SV=1	x	x		x	
229	Heat shock protein HSP 90-alpha OS=Homo sapiens GN=HSP90AA1 PE=1 SV=5	x	x	x		
230	Putative transferase CAF17, mitochondrial OS=Homo sapiens GN=IBA57 PE=1 SV=1	x	x	x		
231	Isoform 2 of Leucine-rich repeat-containing protein 16A OS=Homo sapiens GN=LRRC16A	x	x	x		x
232	Radixin OS=Homo sapiens GN=RDX PE=1 SV=1	x	x		x	x
233	Prostaglandin reductase 2 OS=Homo sapiens GN=PTGR2 PE=1 SV=1	x	x	x		x
234	Dipeptidyl peptidase 4 OS=Homo sapiens GN=DPP4 PE=1 SV=2	x	x	x		x
235	Isoform 2 of Heme oxygenase 2 OS=Homo sapiens GN=HMOX2	x	x		x	x
236	Isoform 2 of Protein tweety homolog 3 OS=Homo sapiens GN=TTYH3	x	x	x		x
237	Maleylacetoacetate isomerase OS=Homo sapiens GN=GSTZ1 PE=1 SV=3	x	x	x		x
238	Leukocyte elastase inhibitor OS=Homo sapiens GN=SERPINB1 PE=1 SV=1	x	x	x		
239	Striatin-3 OS=Homo sapiens GN=STRN3 PE=1 SV=1	x	x	x		
240	Isoform 2 of Na(+)/H(+) exchange regulatory cofactor NHE-RF3 OS=Homo sapiens GN=PDZK1	x	x	x		x
241	Glypican-6 OS=Homo sapiens GN=GPC6 PE=1 SV=1	x	x	x		x
242	Ras and Rab interactor 1 OS=Homo sapiens GN=RIN1 PE=1 SV=1	x	x	x		

	A	B	C	D	E	F
242	Ras and Rab interactor 1 OS=Homo sapiens GN=RIN1 PE=1 SV=1	x	x	x		
243	Monocarboxylate transporter 4 OS=Homo sapiens GN=SLC16A3 PE=1 SV=1	x	x		x	
244	Isoform 4 of Tyrosine-protein phosphatase non-receptor type substrate 1 OS=Homo sapiens GN=SIRPA	x	x		x	x
245	Nucleosome assembly protein 1-like 1 OS=Homo sapiens GN=NAP1L1 PE=1 SV=1	x	x	x		
246	Tripartite motif-containing protein 16 OS=Homo sapiens GN=TRIM16 PE=2 SV=1	x	x		x	
247	Coronin-1B OS=Homo sapiens GN=CORO1B PE=1 SV=1	x	x	x		
248	Rho GDP-dissociation inhibitor 1 OS=Homo sapiens GN=ARHGDIA PE=1 SV=3	x	x		x	
249	Caveolin-1 OS=Homo sapiens GN=CAV1 PE=1 SV=4	x	x	x		
250	Lamina-associated polypeptide 2, isoforms beta/gamma OS=Homo sapiens GN=TMPO PE=1 SV=2	x	x	x		
251	Ribosome-binding protein 1 OS=Homo sapiens GN=RRBP1 PE=1 SV=4	x	x		x	
252	Carbonyl reductase [NADPH] 3 OS=Homo sapiens GN=CBR3 PE=1 SV=3	x	x		x	x
253	Isoform Gamma-1 of Serine/threonine-protein phosphatase 2A 56 kDa regulatory subunit gamma isoform OS=Hom	x	x	x		
254	Isoform 2 of Acidic leucine-rich nuclear phosphoprotein 32 family member B OS=Homo sapiens GN=ANP32B	x	x	x		
255	Isoform 2 of Interferon-induced protein with tetratricopeptide repeats 1 OS=Homo sapiens GN=IFIT1	x	x		x	
256	Isoform 2 of Coiled-coil and C2 domain-containing protein 1B OS=Homo sapiens GN=CC2D1B	x	x	x		
257	Thioredoxin-related transmembrane protein 1 OS=Homo sapiens GN=TMX1 PE=1 SV=1	x	x	x		
258	Proteasome activator complex subunit 1 OS=Homo sapiens GN=PSME1 PE=1 SV=1	x	x	x		
259	Barrier-to-autointegration factor OS=Homo sapiens GN=BANF1 PE=1 SV=1	x	x	x		x
260	Partitioning defective 6 homolog alpha OS=Homo sapiens GN=PARD6A PE=1 SV=1	x	x	x		
261	Isoform 2 of CD97 antigen OS=Homo sapiens GN=CD97	x	x		x	
262	Lipopolysaccharide-induced tumor necrosis factor-alpha factor OS=Homo sapiens GN=LITAF PE=4 SV=1	x	x		x	x
263	Pirin OS=Homo sapiens GN=PIR PE=1 SV=1	x	x		x	
264	Isoform 2 of Optineurin OS=Homo sapiens GN=OPTN	x	x		x	
265	Isoform 4 of Cytosolic acyl coenzyme A thioester hydrolase OS=Homo sapiens GN=ACOT7	x	x		x	
266	Probable leucine--tRNA ligase, mitochondrial OS=Homo sapiens GN=LARS2 PE=1 SV=2	x	x	x		x
267	Centrosomal protein of 170 kDa (Fragment) OS=Homo sapiens GN=CEP170 PE=1 SV=1	x	x		x	
268	Isoform 3 of Pyrroline-5-carboxylate reductase 1, mitochondrial OS=Homo sapiens GN=PYCR1	x	x		x	
269	Isoform 2 of Methylcrotonoyl-CoA carboxylase beta chain, mitochondrial OS=Homo sapiens GN=MCCC2	x	x	x		
270	Transmembrane protein 41B OS=Homo sapiens GN=TMEM41B PE=1 SV=1	x	x		x	
271	MARCKS-related protein OS=Homo sapiens GN=MARCKSL1 PE=1 SV=2	x	x	x		x
272	Protein transport protein Sec23B OS=Homo sapiens GN=SEC23B PE=1 SV=2	x	x		x	x
273	Alpha/beta hydrolase domain-containing protein 14A OS=Homo sapiens GN=ABHD14A PE=1 SV=1	x	x	x		
274	Peroxiredoxin-4 OS=Homo sapiens GN=PRDX4 PE=1 SV=1	x	x	x		
275	Isoform Del-701 of Signal transducer and activator of transcription 3 OS=Homo sapiens GN=STAT3	x	x		x	
276	Vesicle-trafficking protein SEC22b OS=Homo sapiens GN=SEC22B PE=1 SV=4	x	x		x	
277	Annexin A5 OS=Homo sapiens GN=ANXA5 PE=1 SV=2	x	x	x		
278	Myeloid-associated differentiation marker (Fragment) OS=Homo sapiens GN=MYADM PE=1 SV=1	x	x		x	
279	High affinity copper uptake protein 1 OS=Homo sapiens GN=SLC31A1 PE=1 SV=1	x	x		x	x
280	Isoform 2 of Mannosyl-oligosaccharide glucosidase OS=Homo sapiens GN=MOGS	x	x		x	

	A	B	C	D	E	F	G
280	Isoform 2 of Mannosyl-oligosaccharide glucosidase OS=Homo sapiens GN=MOGS	x	x		x		
281	Transmembrane emp24 domain-containing protein 5 OS=Homo sapiens GN=TMED5 PE=1 SV=1	x	x	x			
282	Isoform 2 of Programmed cell death protein 4 OS=Homo sapiens GN=PDCD4	x	x		x		
283	Acyl-CoA synthetase family member 3, mitochondrial OS=Homo sapiens GN=ACSF3 PE=1 SV=3	x	x	x		x	
284	Isoform 2 of Coronin-1C OS=Homo sapiens GN=CORO1C	x	x		x		
285	Laminin subunit beta-2 OS=Homo sapiens GN=LAMB2 PE=1 SV=2	x	x		x		
286	F-actin-capping protein subunit alpha-1 OS=Homo sapiens GN=CAPZA1 PE=1 SV=3	x	x	x			
287	COMM domain-containing protein 2 OS=Homo sapiens GN=COMMD2 PE=4 SV=1	x	x	x			
288	Isoform B of Plasma membrane calcium-transporting ATPase 1 OS=Homo sapiens GN=ATP2B1	x	x	x		x	
289	Hydroxymethylglutaryl-CoA lyase, mitochondrial OS=Homo sapiens GN=HMGCL PE=1 SV=2	x	x	x			
290	Isoform 2 of Disabled homolog 2 OS=Homo sapiens GN=DAB2	x	x		x		
291	Isoform 2 of Echinoderm microtubule-associated protein-like 4 OS=Homo sapiens GN=EML4	x	x	x			
292	Nucleobindin-1 OS=Homo sapiens GN=NUCB1 PE=1 SV=4	x	x	x			
293	Trans-Golgi network integral membrane protein 2 OS=Homo sapiens GN=TGOLN2 PE=1 SV=1	x	x		x		
294	Glia maturation factor beta (Fragment) OS=Homo sapiens GN=GMFB PE=1 SV=1	x	x	x			
295	Glucosamine 6-phosphate N-acetyltransferase (Fragment) OS=Homo sapiens GN=GNPNAT1 PE=1 SV=1	x	x	x			
296	Plectin (Fragment) OS=Homo sapiens GN=PLEC PE=1 SV=2	x	x	x		x	
297	Annexin A8-like protein 2 OS=Homo sapiens GN=ANXA8L2 PE=2 SV=1	x	x		x	x	
298	Isoform A2 of Tight junction protein ZO-2 OS=Homo sapiens GN=TJP2	x	x		x		
299	L-lactate dehydrogenase B chain OS=Homo sapiens GN=LDHB PE=1 SV=2	x	x		x		
300	Protein sel-1 homolog 1 OS=Homo sapiens GN=SEL1L PE=1 SV=3	x	x	x			
301	NADH dehydrogenase [ubiquinone] 1 alpha subcomplex subunit 10, mitochondrial OS=Homo sapiens GN=NDUFA10 I	x	x		x		
302	Isoform Soluble of Catechol O-methyltransferase OS=Homo sapiens GN=COMT	x	x	x			
303	Transmembrane protein 65 OS=Homo sapiens GN=TMEM65 PE=1 SV=2	x	x	x		x	
304	Isoform 2 of Procollagen-lysine,2-oxoglutarate 5-dioxygenase 2 OS=Homo sapiens GN=PLOD2	x	x		x		
305	Isoform 8 of Filamin-B OS=Homo sapiens GN=FLNB	x	x	x			
306	Desmoglein-2 OS=Homo sapiens GN=DSG2 PE=1 SV=2	x	x	x		x	
307	Zinc finger protein 8 OS=Homo sapiens GN=ZNF8 PE=1 SV=1	x	x		x		
308	Isoform 3 of Protein phosphatase 1A OS=Homo sapiens GN=PPM1A	x	x	x		x	
309	OCIA domain-containing protein 1 (Fragment) OS=Homo sapiens GN=OCIAD1 PE=1 SV=1	x	x	x			
310	Isoform 2 of Kynurenine 3-monooxygenase OS=Homo sapiens GN=KMO	x	x	x		x	
311	Band 4.1-like protein 2 OS=Homo sapiens GN=EPB41L2 PE=1 SV=1	x	x		x		
312	Peptidyl-prolyl cis-trans isomerase FKBP2 OS=Homo sapiens GN=FKBP2 PE=1 SV=2	x	x	x			
313	Isoform AGX1 of UDP-N-acetylhexosamine pyrophosphorylase OS=Homo sapiens GN=UAP1	x	x		x		
314	Lamin-B receptor OS=Homo sapiens GN=LBR PE=1 SV=2	x	x		x		
315	Hypoxanthine-guanine phosphoribosyltransferase OS=Homo sapiens GN=HPRT1 PE=1 SV=2	x	x	x			
316	Golgi transport 1 homolog B (S. cerevisiae), isoform CRA_c OS=Homo sapiens GN=GOLT1B PE=4 SV=1	x	x		x	x	
317	Isoform 2 of Eukaryotic initiation factor 4A-II OS=Homo sapiens GN=EIF4A2	x	x	x			
318	Coatomer subunit gamma-1 OS=Homo sapiens GN=COPG1 PE=1 SV=1	x	x		x		

318	Coatomer subunit gamma-1 OS=Homo sapiens GN=COPG1 PE=1 SV=1	x	x		x	
319	Isoform 2 of MTSS1-like protein OS=Homo sapiens GN=MTSS1L	x	x	x		x
320	Transmembrane emp24 domain-containing protein 10 OS=Homo sapiens GN=TMED10 PE=1 SV=2	x	x	x		
321	Lysosome-associated membrane glycoprotein 1 OS=Homo sapiens GN=LAMP1 PE=1 SV=3	x	x	x		
322	COMM domain-containing protein 3 OS=Homo sapiens GN=COMMD3 PE=1 SV=1	x	x	x		
323	Isoform 4 of Ubiquitin carboxyl-terminal hydrolase 47 OS=Homo sapiens GN=USP47	x	x		x	
324	Ubiquitin-conjugating enzyme E2 H (Fragment) OS=Homo sapiens GN=UBE2H PE=1 SV=1	x	x	x		x
325	Cullin-5 OS=Homo sapiens GN=CUL5 PE=1 SV=4	x	x		x	x
326	Isoform Short of Very low-density lipoprotein receptor OS=Homo sapiens GN=VLDLR	x	x		x	
327	Nicotinamide N-methyltransferase OS=Homo sapiens GN=NNMT PE=1 SV=1	x	x		x	
328	Neural cell adhesion molecule 1 OS=Homo sapiens GN=NCAM1 PE=4 SV=1	x	x		x	x
329	Pleckstrin homology-like domain family B member 2 OS=Homo sapiens GN=PHLDB2 PE=1 SV=1	x	x	x		x
330	Selenocysteine lyase (Fragment) OS=Homo sapiens GN=SCLY PE=1 SV=1	x	x	x		
331	Protein kinase C alpha type OS=Homo sapiens GN=PRKCA PE=1 SV=4	x	x		x	
332	Isoform 2 of Importin-4 OS=Homo sapiens GN=IPO4	x	x	x		x
333	Isoform 3 of Nuclear autoantigenic sperm protein OS=Homo sapiens GN=NASP	x	x	x		
334	Isoform 2 of Glutamine--fructose-6-phosphate aminotransferase [isomerizing] 1 OS=Homo sapiens GN=GFPT1	x	x		x	
335	Isoform 2 of Integrin beta-8 OS=Homo sapiens GN=ITGB8	x	x		x	x
336	GTP-binding protein RAD OS=Homo sapiens GN=RRAD PE=1 SV=2	x	x	x		
337	Isoform 2 of Cysteine and histidine-rich domain-containing protein 1 OS=Homo sapiens GN=CHORDC1	x	x		x	x
338	Dihydroorotate dehydrogenase (quinone), mitochondrial OS=Homo sapiens GN=DHODH PE=1 SV=1	x	x	x		x
339	Dihydropteridine reductase OS=Homo sapiens GN=QDPR PE=1 SV=2	x	x	x		
340	Secretory carrier-associated membrane protein 3 OS=Homo sapiens GN=SCAMP3 PE=1 SV=3	x	x		x	
341	Isoform 2 of Proteasome assembly chaperone 1 OS=Homo sapiens GN=PSMG1	x	x		x	
342	Apolipoprotein L2 OS=Homo sapiens GN=APOL2 PE=1 SV=1	x	x		x	
343	Epoxide hydrolase 1 OS=Homo sapiens GN=EPHX1 PE=1 SV=1	x	x	x		x
344	Heat shock protein HSP 90-beta OS=Homo sapiens GN=HSP90AB1 PE=1 SV=4	x	x		x	
345	Nucleolin OS=Homo sapiens GN=NCL PE=1 SV=3	x	x	x		
346	Isoform 2 of Sodium/potassium-transporting ATPase subunit beta-1 OS=Homo sapiens GN=ATP1B1	x	x	x		
347	Beta-2-glycoprotein 1 (Fragment) OS=Homo sapiens GN=APOH PE=1 SV=1	x	x		x	
348	Isoform 2 of Cytoplasmic dynein 1 light intermediate chain 2 OS=Homo sapiens GN=DYNC1LI2	x	x	x		
349	Dynein light chain Tctex-type 1 OS=Homo sapiens GN=DYNLT1 PE=1 SV=1	x	x	x		
350	Vasodilator-stimulated phosphoprotein OS=Homo sapiens GN=VASP PE=1 SV=3	x	x		x	
351	Gamma-tubulin complex component 2 OS=Homo sapiens GN=TUBGCP2 PE=1 SV=1	x	x	x		
352	Isoamyl acetate-hydrolyzing esterase 1 homolog OS=Homo sapiens GN=IAH1 PE=1 SV=1	x	x	x		
353	Superkiller viralicidic activity 2-like 2 OS=Homo sapiens GN=SKIV2L2 PE=1 SV=3	x	x		x	
354	Isoform 2 of E3 ubiquitin-protein ligase RNF213 OS=Homo sapiens GN=RNF213	x	x		x	x
355	Isoform 2 of Serine/threonine-protein phosphatase 4 regulatory subunit 1 OS=Homo sapiens GN=PPP4R1	x	x	x		
356	L-2-hydroxyglutarate dehydrogenase, mitochondrial OS=Homo sapiens GN=L2HGDH PE=1 SV=3	x	x	x		x

	A	B	C	D	E	F
356	L-2-hydroxyglutarate dehydrogenase, mitochondrial OS=Homo sapiens GN=L2HGDH PE=1 SV=3	x	x	x		x
357	Deoxynucleotidyltransferase terminal-interacting protein 1 (Fragment) OS=Homo sapiens GN=DNTTIP1 PE=1 SV=1	x	x	x		x
358	Splicing factor 3B subunit 3 OS=Homo sapiens GN=SF3B3 PE=1 SV=4	x	x	x		
359	Isoform 2 of Phosphoribosyl pyrophosphate synthase-associated protein 2 OS=Homo sapiens GN=PRPSAP2	x	x	x		
360	Isoform 3 of Protein AHNAK2 OS=Homo sapiens GN=AHNAK2	x	x		x	
361	Tubulin gamma-1 chain OS=Homo sapiens GN=TUBG1 PE=1 SV=2	x	x	x		
362	Ras-related protein Rab-12 OS=Homo sapiens GN=RAB12 PE=1 SV=3	x	x	x		
363	Cyclin-dependent kinases regulatory subunit OS=Homo sapiens GN=CKS1B PE=1 SV=1	x	x	x		
364	Putative RNA-binding protein 3 OS=Homo sapiens GN=RBM3 PE=1 SV=1	x	x	x		x
365	Cathepsin D OS=Homo sapiens GN=CTSD PE=1 SV=1	x	x	x		
366	Calcium-binding protein 39 OS=Homo sapiens GN=CAB39 PE=1 SV=1	x	x	x		
367	Uncharacterized protein C9orf142 OS=Homo sapiens GN=C9orf142 PE=1 SV=2	x	x	x		
368	Interferon-induced transmembrane protein 3 OS=Homo sapiens GN=IFITM3 PE=4 SV=1	x	x		x	x
369	Catalase OS=Homo sapiens GN=CAT PE=1 SV=3	x	x		x	
370	Peptidyl-prolyl cis-trans isomerase FKBP3 OS=Homo sapiens GN=FKBP3 PE=1 SV=1	x	x	x		
371	Isoform 2 of Cyclin-dependent kinase 4 OS=Homo sapiens GN=CDK4	x	x	x		
372	DNA replication licensing factor MCM6 OS=Homo sapiens GN=MCM6 PE=1 SV=1	x	x	x		
373	Unconventional myosin-Ic OS=Homo sapiens GN=MYO1C PE=1 SV=1	x	x		x	
374	Acyl-Coenzyme A dehydrogenase, C-4 to C-12 straight chain, isoform CRA_a OS=Homo sapiens GN=ACADM PE=1 SV=	x	x	x		
375	Endophilin-B2 OS=Homo sapiens GN=SH3GLB2 PE=1 SV=1	x	x		x	
376	Isoform 3 of Inositol monophosphatase 1 OS=Homo sapiens GN=IMPA1	x	x	x		
377	Kinectin (Fragment) OS=Homo sapiens GN=KTN1 PE=1 SV=1	x	x	x		x
378	Coactosin-like protein OS=Homo sapiens GN=COTL1 PE=1 SV=3	x	x	x		
379	Glycosyltransferase 8 domain-containing protein 1 (Fragment) OS=Homo sapiens GN=GLT8D1 PE=4 SV=1	x	x		x	x
380	Formin-binding protein 1-like OS=Homo sapiens GN=FNBP1L PE=1 SV=1	x	x	x		
381	Isoform Cytoplasmic+peroxisomal of Peroxiredoxin-5, mitochondrial OS=Homo sapiens GN=PRDX5	x	x	x		
382	Isoform 2 of 6-phosphogluconate dehydrogenase, decarboxylating OS=Homo sapiens GN=PGD	x	x	x		
383	Isoform 3 of UDP-glucuronosyltransferase 1-6 OS=Homo sapiens GN=UGT1A6	x	x		x	
384	Kinesin light chain 1 OS=Homo sapiens GN=KLC1 PE=4 SV=1	x	x	x		
385	Thyroid hormone receptor-associated protein 3 OS=Homo sapiens GN=THRAP3 PE=1 SV=2	x	x	x		
386	Amyloid beta A4 precursor protein-binding family B member 1-interacting protein OS=Homo sapiens GN=APBB1IP P	x	x		x	
387	Cathepsin B OS=Homo sapiens GN=CTSB PE=1 SV=3	x	x		x	x
388	Formin-like protein 1 OS=Homo sapiens GN=FMNL1 PE=1 SV=1	x	x		x	
389	cAMP-dependent protein kinase type I-alpha regulatory subunit OS=Homo sapiens GN=PRKAR1A PE=1 SV=1	x	x	x		
390	Isoform 2 of Replication factor C subunit 1 OS=Homo sapiens GN=RFC1	x	x	x		
391	Aspartate aminotransferase, mitochondrial OS=Homo sapiens GN=GOT2 PE=1 SV=3	x	x	x		
392	Aflatoxin B1 aldehyde reductase member 2 (Fragment) OS=Homo sapiens GN=AKR7A2 PE=1 SV=1	x	x	x		
393	ATP-binding cassette sub-family F member 3 OS=Homo sapiens GN=ABCF3 PE=1 SV=2	x	x	x		
394	Monofunctional C1-tetrahydrofolate synthase, mitochondrial OS=Homo sapiens GN=MTHFD1L PE=1 SV=1	x	x	x		

	A	B	C	D	E	F
394	Monofunctional C1-tetrahydrofolate synthase, mitochondrial OS=Homo sapiens GN=MTHFD1L PE=1 SV=1	x	x	x		
395	Cytoplasmic aconitate hydratase OS=Homo sapiens GN=ACO1 PE=1 SV=3	x	x		x	
396	Heat shock 70 kDa protein 12A OS=Homo sapiens GN=HSPA12A PE=1 SV=2	x	x		x	x
397	tRNA-dihydrouridine(20) synthase [NAD(P)+]-like (Fragment) OS=Homo sapiens GN=DUS2 PE=4 SV=1	x	x	x		x
398	Isoform 3 of C2 domain-containing protein 2 OS=Homo sapiens GN=C2CD2	x	x		x	x
399	Transferrin receptor protein 1 OS=Homo sapiens GN=TFRC PE=1 SV=2	x	x	x		
400	Isoform 2 of Drebrin-like protein OS=Homo sapiens GN=DBNL	x	x		x	
401	Peptidyl-prolyl cis-trans isomerase-like 1 OS=Homo sapiens GN=PPIL1 PE=1 SV=1	x	x	x		
402	Isoform p22 of 7,8-dihydro-8-oxoguanine triphosphatase OS=Homo sapiens GN=NUDT1	x	x		x	
403	Synaptophysin-like protein 1 OS=Homo sapiens GN=SYPL1 PE=1 SV=1	x	x	x		
404	Hippocalcin-like protein 1 OS=Homo sapiens GN=HPCAL1 PE=1 SV=3	x	x		x	
405	Isoform 2 of Neuropathy target esterase OS=Homo sapiens GN=PNPLA6	x	x		x	
406	Eukaryotic translation initiation factor 2 subunit 1 OS=Homo sapiens GN=EIF2S1 PE=1 SV=3	x	x	x		
407	Proteasome subunit beta type OS=Homo sapiens GN=PSMB9 PE=1 SV=1	x	x		x	
408	Antigen peptide transporter 1 OS=Homo sapiens GN=TAP1 PE=1 SV=2	x	x		x	
409	Nascent polypeptide-associated complex subunit alpha, muscle-specific form (Fragment) OS=Homo sapiens GN=NA	x	x	x		
410	Isoform 2 of Retinol dehydrogenase 11 OS=Homo sapiens GN=RDH11	x	x	x		
411	Ubiquitin-conjugating enzyme E2 Z OS=Homo sapiens GN=UBE2Z PE=1 SV=2	x	x	x		
412	Ribonuclease inhibitor OS=Homo sapiens GN=RNH1 PE=1 SV=2	x	x		x	
413	Ubiquitin-associated protein 2 OS=Homo sapiens GN=UBAP2 PE=1 SV=1	x	x		x	x
414	Platelet-activating factor acetylhydrolase IB subunit beta OS=Homo sapiens GN=PAFAH1B2 PE=1 SV=1	x	x		x	
415	Biliverdin reductase A OS=Homo sapiens GN=BLVRA PE=1 SV=2	x	x		x	
416	Dolichyl-diphosphooligosaccharide--protein glycosyltransferase subunit STT3A OS=Homo sapiens GN=STT3A PE=1 SV	x	x		x	
417	DnaJ homolog subfamily B member 4 OS=Homo sapiens GN=DNAJB4 PE=1 SV=1	x	x		x	x
418	14-3-3 protein zeta/delta OS=Homo sapiens GN=YWHAZ PE=1 SV=1	x	x	x		
419	Sorting nexin-9 OS=Homo sapiens GN=SNX9 PE=1 SV=1	x	x		x	
420	DNA ligase OS=Homo sapiens GN=LIG1 PE=1 SV=1	x	x	x		
421	ATP-dependent RNA helicase DDX19A OS=Homo sapiens GN=DDX19A PE=1 SV=1	x	x	x		
422	Isoform 3 of Alpha-actinin-1 OS=Homo sapiens GN=ACTN1	x	x	x		
423	Peptidyl-prolyl cis-trans isomerase C OS=Homo sapiens GN=PPIC PE=1 SV=1	x	x	x		
424	Tropomyosin alpha-4 chain OS=Homo sapiens GN=TPM4 PE=1 SV=3	x	x		x	
425	Large neutral amino acids transporter small subunit 1 OS=Homo sapiens GN=SLC7A5 PE=1 SV=2	x	x	x		
426	DNA-dependent protein kinase catalytic subunit OS=Homo sapiens GN=PRKDC PE=1 SV=3	x	x	x		
427	ATP-dependent DNA helicase Q1 OS=Homo sapiens GN=RECQL PE=1 SV=3	x	x		x	
428	Isoform 3 of Delta-1-pyrroline-5-carboxylate dehydrogenase, mitochondrial OS=Homo sapiens GN=ALDH4A1	x	x	x		
429	Prostaglandin reductase 1 OS=Homo sapiens GN=PTGR1 PE=1 SV=2	x	x	x		x
430	T-complex protein 1 subunit zeta OS=Homo sapiens GN=CCT6A PE=1 SV=3	x	x	x		
431	60S ribosomal protein L36a OS=Homo sapiens GN=RPL36A PE=3 SV=1	x	x		x	
432	Isoform 3 of Golgin subfamily A member 3 OS=Homo sapiens GN=GOLGA3	x	x		x	

	A	B	C	D	E	F
432	Isoform 3 of Golgin subfamily A member 3 OS=Homo sapiens GN=GOLGA3	x	x		x	
433	PRKAR2A protein OS=Homo sapiens GN=PRKAR2A PE=1 SV=1	x	x	x		
434	Hsc70-interacting protein OS=Homo sapiens GN=ST13 PE=1 SV=2	x	x	x		
435	Isoform 2 of Integral membrane protein 2B OS=Homo sapiens GN=ITM2B	x	x		x	
436	Isoform 2 of Supervillin OS=Homo sapiens GN=SVIL	x	x	x		x
437	Uncharacterized protein OS=Homo sapiens PE=1 SV=1	x	x	x		x
438	Isoform 2 of Interferon-induced 35 kDa protein OS=Homo sapiens GN=IFI35	x	x		x	
439	Isoform 2 of Melanoma-associated antigen D1 OS=Homo sapiens GN=MAGED1	x	x		x	x
440	Insulin receptor substrate 2 OS=Homo sapiens GN=IRS2 PE=1 SV=2	x	x	x		
441	Isoform B of Transforming growth factor beta-2 OS=Homo sapiens GN=TGFB2	x	x	x		x
442	Heat shock protein beta-8 OS=Homo sapiens GN=HSPB8 PE=1 SV=1	x	x		x	
443	Glutamyl aminopeptidase OS=Homo sapiens GN=ENPEP PE=1 SV=3	x	x	x		x
444	Formin-like protein 3 OS=Homo sapiens GN=FMNL3 PE=1 SV=3	x	x		x	x
445	Cysteine and glycine-rich protein 2 OS=Homo sapiens GN=CSRP2 PE=1 SV=3	x	x	x		
446	Glutathione S-transferase theta-1 OS=Homo sapiens GN=GSTT1 PE=1 SV=4	x	x	x		
447	Magnesium transporter protein 1 OS=Homo sapiens GN=MAGT1 PE=1 SV=1	x	x		x	
448	Vigilin OS=Homo sapiens GN=HDLBP PE=1 SV=2	x	x		x	
449	Leucine zipper transcription factor-like protein 1 (Fragment) OS=Homo sapiens GN=LZTFL1 PE=1 SV=1	x	x	x		
450	Alpha-1,3-mannosyl-glycoprotein 2-beta-N-acetylglucosaminyltransferase OS=Homo sapiens GN=MGAT1 PE=2 SV=2	x	x		x	
451	Neurobeachin OS=Homo sapiens GN=NBEA PE=1 SV=1	x	x	x		
452	Isoform 2 of Stress-induced-phosphoprotein 1 OS=Homo sapiens GN=STIP1	x	x	x		
453	Glutamate--cysteine ligase regulatory subunit OS=Homo sapiens GN=GCLM PE=1 SV=1	x	x	x		
454	Isoform 2 of Dynamin-1 OS=Homo sapiens GN=DNM1	x	x		x	
455	Enoyl-CoA hydratase, mitochondrial OS=Homo sapiens GN=ECHS1 PE=1 SV=4	x	x	x		
456	N-acetylglucosamine-6-sulfatase OS=Homo sapiens GN=GNS PE=1 SV=1	x	x		x	
457	3-hydroxyacyl-CoA dehydrogenase type-2 OS=Homo sapiens GN=HSD17B10 PE=1 SV=3	x	x	x		
458	Calponin-3 OS=Homo sapiens GN=CNN3 PE=1 SV=1	x	x		x	
459	Aminopeptidase B OS=Homo sapiens GN=RNPEP PE=1 SV=2	x	x	x		
460	Choline-phosphate cytidylyltransferase A OS=Homo sapiens GN=PCYT1A PE=1 SV=1	x	x	x		
461	ATP-dependent 6-phosphofructokinase, platelet type OS=Homo sapiens GN=PFKP PE=1 SV=2	x	x		x	
462	Dual-specificity mitogen-activated protein kinase kinase 3 (Fragment) OS=Homo sapiens GN=MAP2K3 PE=1 SV=1	x	x		x	
463	Isoform 3 of Cystathionine gamma-lyase OS=Homo sapiens GN=CTH	x	x	x		
464	Isoform 2 of Ribose-phosphate pyrophosphokinase 2 OS=Homo sapiens GN=PRPS2	x	x		x	
465	Microtubule-associated protein OS=Homo sapiens GN=MAP4 PE=1 SV=1	x	x		x	
466	Transducin beta-like protein 2 OS=Homo sapiens GN=TBL2 PE=1 SV=1	x	x	x		
467	2-oxoisovalerate dehydrogenase subunit alpha, mitochondrial OS=Homo sapiens GN=BCKDHA PE=1 SV=1	x	x	x		
468	Heterochromatin protein 1-binding protein 3 OS=Homo sapiens GN=HP1BP3 PE=1 SV=1	x	x	x		x
469	Ubiquitin thioesterase OTUB1 OS=Homo sapiens GN=OTUB1 PE=1 SV=1	x	x	x		
470	Peptidyl-prolyl cis-trans isomerase (Fragment) OS=Homo sapiens GN=PPIH PE=1 SV=1	x	x		x	

	A	B	C	D	E	F
508	Isoform 2 of Fermitin family homolog 2 OS=Homo sapiens GN=FERMT2	x	x	x		
509	Isoform A of GDP-fucose protein O-fucosyltransferase 2 OS=Homo sapiens GN=POFUT2	x	x		x	
510	Isoform 3 of 60 kDa SS-A/Ro ribonucleoprotein OS=Homo sapiens GN=TROVE2	x	x	x		
511	Isoform 2 of Synaptopodin OS=Homo sapiens GN=SYNPO	x	x	x		
512	Isoform 2 of 2,4-dienoyl-CoA reductase, mitochondrial OS=Homo sapiens GN=DECR1	x	x	x		
513	AP-1 complex subunit mu-1 OS=Homo sapiens GN=AP1M1 PE=1 SV=1	x	x	x		
514	Elongation factor 1-beta OS=Homo sapiens GN=EEF1B2 PE=1 SV=3	x	x		x	
515	Serine/threonine-protein kinase WNK1 OS=Homo sapiens GN=WNK1 PE=1 SV=1	x	x		x	x
516	AH receptor-interacting protein OS=Homo sapiens GN=AIP PE=1 SV=2	x	x	x		
517	Isoform 2 of Zinc finger CCCH-type antiviral protein 1 OS=Homo sapiens GN=ZC3HAV1	x	x		x	
518	Cell growth-regulating nucleolar protein OS=Homo sapiens GN=LYAR PE=1 SV=2	x	x	x		
519	Epidermal growth factor receptor kinase substrate 8-like protein 2 OS=Homo sapiens GN=EPS8L2 PE=1 SV=2	x	x		x	
520	Annexin A1 OS=Homo sapiens GN=ANXA1 PE=1 SV=2	x	x	x		
521	Isocitrate dehydrogenase [NADP] cytoplasmic OS=Homo sapiens GN=IDH1 PE=1 SV=2	x	x	x		
522	Isoform 2 of Elongation factor 1-gamma OS=Homo sapiens GN=EEF1G	x	x		x	
523	Calcium/calmodulin-dependent protein kinase (CaM kinase) II delta, isoform CRA_e OS=Homo sapiens GN=CAMK2D	x	x		x	
524	Isoform 2 of Golgi apparatus protein 1 OS=Homo sapiens GN=GLG1	x	x	x		
525	Isoform Short of Ubiquitin carboxyl-terminal hydrolase 5 OS=Homo sapiens GN=USP5	x	x		x	
526	Isoform 2 of Cytosolic purine 5'-nucleotidase OS=Homo sapiens GN=NT5C2	x	x	x		
527	Isoform 2 of Calcium-binding mitochondrial carrier protein Aralar2 OS=Homo sapiens GN=SLC25A13	x	x	x		
528	Protein disulfide-isomerase TMX3 OS=Homo sapiens GN=TMX3 PE=1 SV=2	x	x		x	
529	Isoform 2 of Cadherin-2 OS=Homo sapiens GN=CDH2	x	x		x	
530	Isoform 2 of Ribosome biogenesis protein BOP1 OS=Homo sapiens GN=BOP1	x	x	x		
531	tRNA (guanine(26)-N(2))-dimethyltransferase OS=Homo sapiens GN=TRMT1 PE=1 SV=1	x	x		x	
532	Nucleolar and spindle-associated protein 1 OS=Homo sapiens GN=NUSAP1 PE=1 SV=1	x	x	x		x
533	Isoform 2 of WD repeat-containing protein 92 OS=Homo sapiens GN=WDR92	x	x		x	
534	Isoform 2 of Bifunctional UDP-N-acetylglucosamine 2-epimerase/N-acetylmannosamine kinase OS=Homo sapiens G	x	x		x	
535	7-dehydrocholesterol reductase OS=Homo sapiens GN=DHCR7 PE=1 SV=1	x	x	x		
536	Histone H1x OS=Homo sapiens GN=H1FX PE=1 SV=1	x	x		x	
537	Protein LSM14 homolog A OS=Homo sapiens GN=LSM14A PE=1 SV=1	x	x		x	
538	Isoform 4 of ER membrane protein complex subunit 1 OS=Homo sapiens GN=EMC1	x	x	x		
539	Methylosome protein 50 (Fragment) OS=Homo sapiens GN=WDR77 PE=1 SV=1	x	x	x		
540	ATP-dependent RNA helicase DHX29 OS=Homo sapiens GN=DHX29 PE=1 SV=2	x	x		x	
541	Phospholysine phosphohistidine inorganic pyrophosphate phosphatase OS=Homo sapiens GN=LHPP PE=1 SV=2	x	x	x		x
542	tRNA (guanine(37)-N1)-methyltransferase OS=Homo sapiens GN=TRMT5 PE=1 SV=2	x	x	x		x
543	Glucosamine-6-phosphate isomerase 1 OS=Homo sapiens GN=GNPDA1 PE=1 SV=1	x	x	x		
544	Heterogeneous nuclear ribonucleoprotein A/B OS=Homo sapiens GN=HNRNPAB PE=1 SV=1	x	x		x	
545	Isoform 6 of Dynamin-1-like protein OS=Homo sapiens GN=DNM1L	x	x		x	
546	Eukaryotic translation initiation factor 2 subunit 2 OS=Homo sapiens GN=EIF2S2 PE=1 SV=2	x	x	x		

	A	B	C	D	E	F
546	Eukaryotic translation initiation factor 2 subunit 2 OS=Homo sapiens GN=EIF2S2 PE=1 SV=2	x	x	x		
547	Isoform 2 of Dynamin-2 OS=Homo sapiens GN=DNM2	x	x	x		
548	Inter-alpha-trypsin inhibitor heavy chain H2 OS=Homo sapiens GN=ITIH2 PE=1 SV=1	x	x		x	
549	Neutral amino acid transporter A OS=Homo sapiens GN=SLC1A4 PE=1 SV=1	x	x		x	
550	[3-methyl-2-oxobutanoate dehydrogenase [lipoamide]] kinase, mitochondrial (Fragment) OS=Homo sapiens GN=BCI	x	x	x		
551	Uncharacterized protein OS=Homo sapiens GN=DCTN1 PE=1 SV=1	x	x		x	
552	Carnitine O-palmitoyltransferase 2, mitochondrial OS=Homo sapiens GN=CPT2 PE=1 SV=2	x	x	x		
553	Isoform B of Bifunctional 3'-phosphoadenosine 5'-phosphosulfate synthase 2 OS=Homo sapiens GN=PAPSS2	x	x		x	
554	Lysosomal-associated transmembrane protein 4A OS=Homo sapiens GN=LAPTM4A PE=1 SV=1	x	x		x	x
555	Replication protein A 70 kDa DNA-binding subunit OS=Homo sapiens GN=RPA1 PE=1 SV=2	x	x		x	
556	Glycine--tRNA ligase OS=Homo sapiens GN=GARS PE=1 SV=3	x	x		x	
557	Isoform 2 of Ubiquitin carboxyl-terminal hydrolase 10 OS=Homo sapiens GN=USP10	x	x	x		
558	Isoform 4 of IST1 homolog OS=Homo sapiens GN=IST1	x	x	x		
559	Isoform 2 of Clathrin heavy chain 1 OS=Homo sapiens GN=CLTC	x	x		x	
560	Coatomer subunit beta OS=Homo sapiens GN=COPB1 PE=1 SV=3	x	x		x	
561	Rho GTPase-activating protein 1 OS=Homo sapiens GN=ARHGAP1 PE=1 SV=1	x	x		x	
562	Flotillin-2 OS=Homo sapiens GN=FLOT2 PE=1 SV=1	x	x	x		
563	Phosphoenolpyruvate carboxykinase [GTP], mitochondrial OS=Homo sapiens GN=PCK2 PE=1 SV=3	x	x	x		
564	Isoform 2 of Ataxin-2-like protein OS=Homo sapiens GN=ATXN2L	x	x		x	
565	Isoform 4 of Alpha/beta hydrolase domain-containing protein 11 OS=Homo sapiens GN=ABHD11	x	x	x		x
566	Thioredoxin domain containing 14, isoform CRA_a OS=Homo sapiens GN=TMX2 PE=4 SV=1	x	x	x		
567	Family with sequence similarity 91, member A1, isoform CRA_c OS=Homo sapiens GN=FAM91A1 PE=1 SV=1	x	x	x		
568	Lon protease homolog, mitochondrial OS=Homo sapiens GN=LONP1 PE=1 SV=1	x	x	x		
569	Regulator of microtubule dynamics protein 1 OS=Homo sapiens GN=RMDN1 PE=1 SV=1	x	x	x		
570	Deoxyhypusine synthase OS=Homo sapiens GN=DHPS PE=1 SV=1	x	x		x	
571	DENN domain-containing protein 4C OS=Homo sapiens GN=DENND4C PE=1 SV=1	x	x		x	
572	Small ubiquitin-related modifier 1 OS=Homo sapiens GN=SUMO1 PE=1 SV=1	x	x		x	
573	Isoform 2 of Collagen alpha-1(VII) chain OS=Homo sapiens GN=COL7A1	x	x	x		
574	Moesin OS=Homo sapiens GN=MSN PE=1 SV=3	x	x		x	
575	Cytochrome c oxidase subunit 4 isoform 1, mitochondrial OS=Homo sapiens GN=COX4I1 PE=1 SV=1	x	x	x		
576	CD81 antigen (Fragment) OS=Homo sapiens GN=CD81 PE=1 SV=1	x	x		x	
577	Signal recognition particle receptor subunit beta OS=Homo sapiens GN=SRPRB PE=1 SV=3	x	x		x	
578	Isoform 2 of Pyruvate dehydrogenase E1 component subunit beta, mitochondrial OS=Homo sapiens GN=PDHB	x	x	x		
579	Isoform 2 of Septin-7 OS=Homo sapiens GN=SEPT7	x	x		x	
580	Inosine-5'-monophosphate dehydrogenase 2 (Fragment) OS=Homo sapiens GN=IMPDH2 PE=1 SV=1	x	x	x		
581	Tubulin beta-3 chain OS=Homo sapiens GN=TUBB3 PE=1 SV=2	x	x	x		
582	Mitochondrial ribonuclease P protein 1 OS=Homo sapiens GN=TRMT10C PE=1 SV=2	x	x	x		
583	Adenylosuccinate lyase OS=Homo sapiens GN=ADSL PE=1 SV=2	x	x	x		
584	Stress-70 protein, mitochondrial OS=Homo sapiens GN=HSPA9 PE=1 SV=2	x	x	x		

	A	B	C	D	E	F
584	Stress-70 protein, mitochondrial OS=Homo sapiens GN=HSPA9 PE=1 SV=2	x	x	x		
585	Vacuolar protein-sorting-associated protein 25 (Fragment) OS=Homo sapiens GN=VPS25 PE=1 SV=1	x	x	x		x
586	60 kDa heat shock protein, mitochondrial OS=Homo sapiens GN=HSPD1 PE=1 SV=2	x	x	x		
587	Acidic leucine-rich nuclear phosphoprotein 32 family member A OS=Homo sapiens GN=ANP32A PE=1 SV=1	x	x	x		
588	Heterogeneous nuclear ribonucleoproteins A2/B1 OS=Homo sapiens GN=HNRNPA2B1 PE=1 SV=2	x	x		x	
589	Glyoxalase domain-containing protein 4 OS=Homo sapiens GN=GLOD4 PE=1 SV=1	x	x	x		
590	Ubiquitin-like domain-containing CTD phosphatase 1 OS=Homo sapiens GN=UBLCP1 PE=1 SV=2	x	x	x		
591	Fatty acid synthase OS=Homo sapiens GN=FASN PE=1 SV=3	x	x		x	
592	182 kDa tankyrase-1-binding protein OS=Homo sapiens GN=TNKS1BP1 PE=1 SV=4	x	x		x	
593	15 kDa selenoprotein OS=Homo sapiens GN=SEP15 PE=1 SV=3	x	x	x		
594	Isoform 2 of NudC domain-containing protein 1 OS=Homo sapiens GN=NUDCD1	x	x		x	
595	Isoform 2 of Elongation of very long chain fatty acids protein 1 OS=Homo sapiens GN=ELOVL1	x	x		x	
596	Relaxin-3 (Fragment) OS=Homo sapiens GN=RLN3 PE=4 SV=1	x	x		x	
597	14 kDa phosphohistidine phosphatase OS=Homo sapiens GN=PHPT1 PE=1 SV=1	x	x	x		
598	Isoform 2 of Guanine nucleotide-binding protein subunit alpha-13 OS=Homo sapiens GN=GNA13	x	x	x		
599	Ataxin-10 OS=Homo sapiens GN=ATXN10 PE=1 SV=1	x	x		x	
600	Isoform 3 of Phosphatidylinositol-binding clathrin assembly protein OS=Homo sapiens GN=PICALM	x	x		x	x
601	Procollagen galactosyltransferase 1 OS=Homo sapiens GN=COLGALT1 PE=1 SV=1	x	x		x	
602	26S proteasome non-ATPase regulatory subunit 3 OS=Homo sapiens GN=PSMD3 PE=1 SV=2	x	x	x		
603	Isoform 3 of NSFL1 cofactor p47 OS=Homo sapiens GN=NSFL1C	x	x		x	
604	Isoform 2 of Asparagine synthetase [glutamine-hydrolyzing] OS=Homo sapiens GN=ASNS	x	x	x		
605	Lon protease homolog, mitochondrial OS=Homo sapiens GN=LONP1 PE=1 SV=2	x	x	x		
606	Isoform 2 of Vesicle-associated membrane protein 7 OS=Homo sapiens GN=VAMP7	x	x		x	
607	EH domain-containing protein 1 OS=Homo sapiens GN=EHD1 PE=1 SV=2	x	x	x		
608	Zinc finger CCCH domain-containing protein 4 (Fragment) OS=Homo sapiens GN=ZC3H4 PE=1 SV=1	x	x	x		
609	Isoform 2 of Stromal interaction molecule 1 OS=Homo sapiens GN=STIM1	x	x		x	
610	DnaJ homolog subfamily C member 7 OS=Homo sapiens GN=DNAJC7 PE=1 SV=2	x	x		x	
611	Translocon-associated protein subunit alpha OS=Homo sapiens GN=SSR1 PE=1 SV=3	x	x		x	
612	Isoform 2 of Putative ATP-dependent RNA helicase DHX30 OS=Homo sapiens GN=DHX30	x	x	x		x
613	Isoform 2 of Nuclear mitotic apparatus protein 1 OS=Homo sapiens GN=NUMA1	x	x	x		
614	N-terminal kinase-like protein OS=Homo sapiens GN=SCYL1 PE=1 SV=1	x	x	x		
615	Plastin-3 OS=Homo sapiens GN=PLS3 PE=1 SV=4	x	x		x	
616	Hemoglobin subunit alpha OS=Homo sapiens GN=HBA1 PE=1 SV=2	x	x		x	
617	Isoform 2 of Arf-GAP domain and FG repeat-containing protein 1 OS=Homo sapiens GN=AGFG1	x	x		x	
618	Mitochondrial translocator assembly and maintenance protein 41 homolog (Fragment) OS=Homo sapiens GN=TAMM	x	x		x	
619	2'-deoxynucleoside 5'-phosphate N-hydrolase 1 (Fragment) OS=Homo sapiens GN=DNPH1 PE=1 SV=1	x	x	x		
620	Proliferating cell nuclear antigen OS=Homo sapiens GN=PCNA PE=1 SV=1	x	x	x		
621	Isoform 2 of Presequence protease, mitochondrial OS=Homo sapiens GN=PITRM1	x	x	x		
622	Exocyst complex component 7 OS=Homo sapiens GN=EXOC7 PE=1 SV=1	x	x	x		

	A	B	C	D	E	F
622	Exocyst complex component 7 OS=Homo sapiens GN=EXOC7 PE=1 SV=1	x	x	x		
623	UDP-N-acetylhexosamine pyrophosphorylase-like protein 1 OS=Homo sapiens GN=UAP1L1 PE=1 SV=2	x	x		x	
624	Isoform 2 of MAP kinase-activated protein kinase 2 OS=Homo sapiens GN=MAPKAPK2	x	x	x		
625	Cation-dependent mannose-6-phosphate receptor OS=Homo sapiens GN=M6PR PE=1 SV=1	x	x		x	
626	Translocon-associated protein subunit delta OS=Homo sapiens GN=SSR4 PE=1 SV=1	x	x		x	
627	TRMT1-like protein OS=Homo sapiens GN=TRMT1L PE=1 SV=2	x	x	x		
628	NADH dehydrogenase [ubiquinone] iron-sulfur protein 8, mitochondrial (Fragment) OS=Homo sapiens GN=NDUFS8 F	x	x		x	
629	Isoform 2 of Actin-related protein 2/3 complex subunit 1A OS=Homo sapiens GN=ARPC1A	x	x	x		x
630	Isoform 2 of General transcription factor II-I OS=Homo sapiens GN=GTF2I	x	x	x		
631	Isoform 2 of AP-1 complex subunit gamma-1 OS=Homo sapiens GN=AP1G1	x	x	x		
632	Isoform 2 of Probable ATP-dependent RNA helicase DDX47 OS=Homo sapiens GN=DDX47	x	x		x	
633	Acyl-protein thioesterase 2 OS=Homo sapiens GN=LYPLA2 PE=1 SV=1	x	x	x		
634	Thioredoxin domain-containing protein 5 OS=Homo sapiens GN=TXNDC5 PE=1 SV=2	x	x		x	
635	Tyrosine--tRNA ligase, mitochondrial OS=Homo sapiens GN=YARS2 PE=1 SV=2	x	x		x	
636	Lipoma-preferred partner OS=Homo sapiens GN=LPP PE=1 SV=1	x	x	x		
637	Ras-related protein Rab-18 OS=Homo sapiens GN=RAB18 PE=1 SV=1	x	x		x	
638	Protein DJ-1 OS=Homo sapiens GN=PARK7 PE=1 SV=2	x	x	x		
639	Nucleosome assembly protein 1-like 1 (Fragment) OS=Homo sapiens GN=NAP1L1 PE=1 SV=1	x	x		x	
640	Isoform 2 of N-terminal Xaa-Pro-Lys N-methyltransferase 1 OS=Homo sapiens GN=NTMT1	x	x		x	
641	Isoform 2 of Nuclear protein localization protein 4 homolog OS=Homo sapiens GN=NPLOC4	x	x		x	
642	Replication protein A 14 kDa subunit OS=Homo sapiens GN=RPA3 PE=1 SV=1	x	x	x		
643	Acetyl-CoA acetyltransferase, mitochondrial OS=Homo sapiens GN=ACAT1 PE=1 SV=1	x	x		x	
644	Junctional adhesion molecule A OS=Homo sapiens GN=F11R PE=1 SV=1	x	x	x		
645	Tensin-3 OS=Homo sapiens GN=TNS3 PE=1 SV=2	x	x		x	
646	Isoform 1 of Cat eye syndrome critical region protein 5 OS=Homo sapiens GN=CECR5	x	x	x		
647	Rab-like protein 6 OS=Homo sapiens GN=RABL6 PE=1 SV=1	x	x		x	
648	Isoform 2 of Protein phosphatase Slingshot homolog 3 OS=Homo sapiens GN=SSH3	x	x	x		x
649	Eukaryotic translation initiation factor 4 gamma 2 (Fragment) OS=Homo sapiens GN=EIF4G2 PE=1 SV=1	x	x		x	
650	Isoform 3 of Leucine-rich repeat flightless-interacting protein 1 OS=Homo sapiens GN=LRRFIP1	x	x		x	
651	Four and a half LIM domains protein 1 (Fragment) OS=Homo sapiens GN=FHL1 PE=1 SV=1	x	x	x		x
652	UBX domain-containing protein 4 OS=Homo sapiens GN=UBXN4 PE=1 SV=2	x	x		x	
653	Ubiquitin-conjugating enzyme E2 N OS=Homo sapiens GN=UBE2N PE=1 SV=1	x	x	x		
654	Complement C3 OS=Homo sapiens GN=C3 PE=1 SV=2	x	x		x	
655	Proteasome activator complex subunit 2 OS=Homo sapiens GN=PSME2 PE=1 SV=4	x	x	x		
656	Peptidyl-prolyl cis-trans isomerase (Fragment) OS=Homo sapiens GN=PPIL3 PE=1 SV=1	x	x		x	
657	Isoform 10 of Merlin OS=Homo sapiens GN=NF2	x	x		x	
658	Proteasome assembly chaperone 2 OS=Homo sapiens GN=PSMG2 PE=1 SV=1	x	x		x	
659	Proteasome subunit beta type-6 OS=Homo sapiens GN=PSMB6 PE=1 SV=4	x	x	x		
660	Isoform 3 of Carbamoyl-phosphate synthase [ammonia], mitochondrial OS=Homo sapiens GN=CPS1	x	x	x		x

	A	B	C	D	E	F
660	Isoform 3 of Carbamoyl-phosphate synthase [ammonia], mitochondrial OS=Homo sapiens GN=CPS1	x	x	x		x
661	Long-chain-fatty-acid--CoA ligase 3 OS=Homo sapiens GN=ACSL3 PE=1 SV=3	x	x		x	
662	Serine/threonine-protein phosphatase 4 regulatory subunit 3A (Fragment) OS=Homo sapiens GN=SMEK1 PE=1 SV=1	x	x	x		
663	NADPH--cytochrome P450 reductase OS=Homo sapiens GN=POR PE=1 SV=2	x	x	x		
664	Protein Dr1 OS=Homo sapiens GN=DR1 PE=1 SV=1	x	x		x	
665	Lamina-associated polypeptide 2, isoform alpha OS=Homo sapiens GN=TMPO PE=1 SV=2	x	x	x		
666	Isoform 2 of Adenylyl cyclase-associated protein 1 OS=Homo sapiens GN=CAP1	x	x	x		
667	Glutathione S-transferase omega-1 OS=Homo sapiens GN=GSTO1 PE=1 SV=2	x	x		x	
668	28S ribosomal protein S5, mitochondrial OS=Homo sapiens GN=MRPS5 PE=1 SV=2	x	x	x		
669	PHD finger protein 6 OS=Homo sapiens GN=PHF6 PE=1 SV=1	x	x		x	
670	Vacuolar ATPase assembly integral membrane protein VMA21 OS=Homo sapiens GN=VMA21 PE=1 SV=1	x	x		x	
671	Isoform 2 of UPF0687 protein C20orf27 OS=Homo sapiens GN=C20orf27	x	x		x	
672	Four and a half LIM domains protein 3 OS=Homo sapiens GN=FHL3 PE=1 SV=4	x	x	x		
673	Isoform 4 of Poly(rC)-binding protein 2 OS=Homo sapiens GN=PCBP2	x	x		x	
674	RAD50-interacting protein 1 OS=Homo sapiens GN=RINT1 PE=1 SV=1	x	x		x	x
675	Isoform 2 of Receptor-type tyrosine-protein phosphatase F OS=Homo sapiens GN=PTPRF	x	x	x		x
676	Switch-associated protein 70 OS=Homo sapiens GN=SWAP70 PE=1 SV=1	x	x		x	
677	Isoform 2 of Peroxisomal acyl-coenzyme A oxidase 1 OS=Homo sapiens GN=ACOX1	x	x	x		
678	Tumor necrosis factor alpha-induced protein 8 (Fragment) OS=Homo sapiens GN=TNFAIP8 PE=4 SV=1	x	x	x		
679	Alpha-2-macroglobulin OS=Homo sapiens GN=A2M PE=1 SV=3	x	x		x	
680	Isoform 2 of Charged multivesicular body protein 5 OS=Homo sapiens GN=CHMP5	x	x		x	
681	Isoform 2 of Poly(U)-binding-splicing factor PUF60 OS=Homo sapiens GN=PUF60	x	x	x		
682	AFG3-like protein 2 OS=Homo sapiens GN=AFG3L2 PE=1 SV=2	x	x	x		
683	Isoform 4 of Histidine--tRNA ligase, cytoplasmic OS=Homo sapiens GN=HARS	x	x		x	
684	Ras-related protein Rap-2b OS=Homo sapiens GN=RAP2B PE=1 SV=1	x	x	x		
685	Isochorismatase domain-containing protein 1 OS=Homo sapiens GN=ISOC1 PE=1 SV=3	x	x	x		
686	Isoform 2 of Electron transfer flavoprotein subunit alpha, mitochondrial OS=Homo sapiens GN=ETFA	x	x	x		
687	D-tyrosyl-tRNA(Tyr) deacylase 1 OS=Homo sapiens GN=DTD1 PE=1 SV=2	x	x		x	
688	Mitochondrial-processing peptidase subunit alpha OS=Homo sapiens GN=PMPCA PE=1 SV=2	x	x	x		
689	Integrin beta-5 OS=Homo sapiens GN=ITGB5 PE=1 SV=1	x	x	x		
690	GDP-L-fucose synthase OS=Homo sapiens GN=TSTA3 PE=1 SV=1	x	x	x		
691	Sn1-specific diacylglycerol lipase beta OS=Homo sapiens GN=DAGLB PE=1 SV=1	x	x		x	
692	Acid phosphatase 1, soluble, isoform CRA_d OS=Homo sapiens GN=ACP1 PE=1 SV=1	x	x	x		
693	Translin OS=Homo sapiens GN=TSN PE=1 SV=1	x	x	x		
694	Isoform 3 of NADH-cytochrome b5 reductase 3 OS=Homo sapiens GN=CYB5R3	x	x	x		
695	RNA-binding protein 4 OS=Homo sapiens GN=RBM4 PE=1 SV=1	x	x	x		
696	Unconventional myosin-Ie OS=Homo sapiens GN=MYO1E PE=1 SV=2	x	x		x	
697	Isoform 2 of Protein FAM98A OS=Homo sapiens GN=FAM98A	x	x		x	
698	Capping protein (Actin filament) muscle Z-line, beta, isoform CRA_a OS=Homo sapiens GN=CAPZB PE=1 SV=1	x	x	x		

	A	B	C	D	E	F
698	Capping protein (Actin filament) muscle Z-line, beta, isoform CRA_a OS=Homo sapiens GN=CAPZB PE=1 SV=1	x	x	x		
699	Ribosome biogenesis protein BRX1 homolog OS=Homo sapiens GN=BRIX1 PE=1 SV=2	x	x	x		x
700	Isoform 2 of Perilipin-3 OS=Homo sapiens GN=PLIN3	x	x		x	
701	Phenylalanine--tRNA ligase alpha subunit OS=Homo sapiens GN=FARSA PE=1 SV=1	x	x		x	
702	Nuclear receptor-binding protein OS=Homo sapiens GN=NRBP1 PE=1 SV=1	x	x	x		x
703	Chloride intracellular channel protein 4 OS=Homo sapiens GN=CLIC4 PE=1 SV=4	x	x		x	
704	Adenylyl cyclase-associated protein 2 OS=Homo sapiens GN=CAP2 PE=1 SV=1	x	x	x		
705	Isoform 4 of Plectin OS=Homo sapiens GN=PLEC	x	x	x		
706	Isoform 2 of 5-formyltetrahydrofolate cyclo-ligase OS=Homo sapiens GN=MTHFS	x	x	x		x
707	Negative elongation factor C/D OS=Homo sapiens GN=TH1L PE=1 SV=1	x	x	x		
708	Isoform 2 of WD repeat-containing protein 44 OS=Homo sapiens GN=WDR44	x	x		x	
709	Fragile X mental retardation syndrome-related protein 1 OS=Homo sapiens GN=FXR1 PE=1 SV=3	x	x	x		
710	Beta-hexosaminidase subunit beta OS=Homo sapiens GN=HEXB PE=1 SV=1	x	x		x	
711	UPF0587 protein C1orf123 OS=Homo sapiens GN=C1orf123 PE=1 SV=1	x	x	x		
712	Mitochondrial import receptor subunit TOM22 homolog OS=Homo sapiens GN=TOMM22 PE=1 SV=3	x	x	x		
713	Lamin-B2 OS=Homo sapiens GN=LMNB2 PE=1 SV=3	x	x		x	
714	Spermidine synthase OS=Homo sapiens GN=SRM PE=1 SV=1	x	x	x		
715	NADH-cytochrome b5 reductase 1 (Fragment) OS=Homo sapiens GN=CYB5R1 PE=1 SV=1	x	x		x	
716	Voltage-dependent anion-selective channel protein 1 OS=Homo sapiens GN=VDAC1 PE=1 SV=2	x	x		x	
717	Synaptonemal complex protein SC65 OS=Homo sapiens GN=LEPREL4 PE=1 SV=1	x	x		x	
718	Twinfilin-2 OS=Homo sapiens GN=TWF2 PE=1 SV=2	x	x		x	
719	Ras-related protein Rab-7a OS=Homo sapiens GN=RAB7A PE=1 SV=1	x	x	x		
720	Dynamin-like 120 kDa protein, mitochondrial OS=Homo sapiens GN=OPA1 PE=1 SV=1	x	x	x		
721	Isoform 2 of Interferon-induced, double-stranded RNA-activated protein kinase OS=Homo sapiens GN=EIF2AK2	x	x		x	
722	Brefeldin A-inhibited guanine nucleotide-exchange protein 1 OS=Homo sapiens GN=ARFGEF1 PE=1 SV=2	x	x	x		
723	Isoform 2 of Phosphotriesterase-related protein OS=Homo sapiens GN=PTER	x	x	x		
724	Proteasome subunit alpha type OS=Homo sapiens GN=PSMA6 PE=1 SV=1	x	x	x		
725	Ras-related protein Rab-1B OS=Homo sapiens GN=RAB1B PE=1 SV=1	x	x	x		
726	NADH dehydrogenase [ubiquinone] 1 alpha subcomplex subunit 8 OS=Homo sapiens GN=NDUFA8 PE=1 SV=3	x	x		x	
727	Alcohol dehydrogenase [NADP(+)] OS=Homo sapiens GN=AKR1A1 PE=1 SV=3	x	x	x		
728	Isoform Ex1A-2-3 of AMP deaminase 2 OS=Homo sapiens GN=AMPD2	x	x	x		
729	Isoform 3 of Beta-galactosidase OS=Homo sapiens GN=GLB1	x	x	x		
730	Isoform 2 of Splicing factor U2AF 35 kDa subunit OS=Homo sapiens GN=U2AF1	x	x	x		
731	Isoform B of AP-2 complex subunit alpha-1 OS=Homo sapiens GN=AP2A1	x	x		x	
732	Torsin-1A-interacting protein 2, isoform IFRG15 OS=Homo sapiens GN=TOR1AIP2 PE=2 SV=1	x	x	x		
733	Mitochondrial fission 1 protein OS=Homo sapiens GN=FIS1 PE=1 SV=2	x	x	x		
734	CAAX prenyl protease 2 OS=Homo sapiens GN=RCE1 PE=1 SV=1	x	x	x		x
735	Importin-9 OS=Homo sapiens GN=IPO9 PE=1 SV=3	x	x	x		
736	Signal peptidase complex subunit 2 OS=Homo sapiens GN=SPCS2 PE=1 SV=1	x	x		x	

	A	B	C	D	E	F
736	Signal peptidase complex subunit 2 OS=Homo sapiens GN=SPCS2 PE=1 SV=1	x	x		x	
737	Isoform 2 of Acetyl-CoA carboxylase 1 OS=Homo sapiens GN=ACACA	x	x		x	
738	Ras-related protein Rab-32 OS=Homo sapiens GN=RAB32 PE=1 SV=3	x	x		x	
739	Far upstream element-binding protein 1 OS=Homo sapiens GN=FUBP1 PE=1 SV=3	x	x	x		
740	Isoform 2 of Cytosol aminopeptidase OS=Homo sapiens GN=LAP3	x	x	x		
741	Isoform 2 of Serine/threonine-protein kinase PAK 4 OS=Homo sapiens GN=PAK4	x	x		x	
742	ADP-ribosylation factor GTPase-activating protein 2 (Fragment) OS=Homo sapiens GN=ARFGAP2 PE=1 SV=1	x	x		x	
743	Isoform 2 of Mediator of DNA damage checkpoint protein 1 OS=Homo sapiens GN=MDC1	x	x	x		
744	Isoform 2 of Cytosolic Fe-S cluster assembly factor NUBP1 OS=Homo sapiens GN=NUBP1	x	x	x		
745	Isoform 2 of VIP36-like protein OS=Homo sapiens GN=LMAN2L	x	x		x	
746	Hydroxyacyl-coenzyme A dehydrogenase, mitochondrial OS=Homo sapiens GN=HADH PE=1 SV=1	x	x	x		
747	Mitochondrial glutamate carrier 1 OS=Homo sapiens GN=SLC25A22 PE=1 SV=1	x	x		x	x
748	Coatomer subunit zeta-1 OS=Homo sapiens GN=COPZ1 PE=1 SV=1	x	x		x	
749	Nucleolar protein 56 OS=Homo sapiens GN=NOP56 PE=1 SV=4	x	x	x		
750	Alanine--tRNA ligase, mitochondrial OS=Homo sapiens GN=AARS2 PE=1 SV=1	x	x	x		
751	Serine/threonine-protein phosphatase PP1-alpha catalytic subunit OS=Homo sapiens GN=PPP1CA PE=1 SV=1	x	x	x		
752	Rab11 family-interacting protein 5 OS=Homo sapiens GN=RAB11FIP5 PE=1 SV=1	x	x		x	
753	Protein RCC2 OS=Homo sapiens GN=RCC2 PE=1 SV=2	x	x	x		
754	Isoform 2 of Serine protease HTRA2, mitochondrial OS=Homo sapiens GN=HTRA2	x	x		x	
755	Isoform 3 of Leucine-rich repeat-containing protein 41 OS=Homo sapiens GN=LRRC41	x	x	x		
756	SRSF protein kinase 1 (Fragment) OS=Homo sapiens GN=SRPK1 PE=1 SV=1	x	x		x	
757	Isoform 2 of Beta-glucuronidase OS=Homo sapiens GN=GUSB	x	x	x		
758	Peptidyl-prolyl cis-trans isomerase FKBP4 OS=Homo sapiens GN=FKBP4 PE=1 SV=3	x	x		x	
759	Aconitate hydratase, mitochondrial OS=Homo sapiens GN=ACO2 PE=1 SV=1	x	x	x		
760	Isoform 2 of Replication protein A 32 kDa subunit OS=Homo sapiens GN=RPA2	x	x	x		
761	Isoform Long of Ubiquitin fusion degradation protein 1 homolog OS=Homo sapiens GN=UFD1L	x	x		x	
762	Isoform 3 of L-lactate dehydrogenase A chain OS=Homo sapiens GN=LDHA	x	x		x	
763	Glutaredoxin-1 OS=Homo sapiens GN=GLRX PE=1 SV=2	x	x		x	x
764	Glycogen phosphorylase, brain form OS=Homo sapiens GN=PYGB PE=1 SV=5	x	x		x	
765	Zinc finger protein ZPR1 (Fragment) OS=Homo sapiens GN=ZPR1 PE=1 SV=1	x	x		x	
766	Prolyl 3-hydroxylase 3 OS=Homo sapiens GN=LEPREL2 PE=1 SV=1	x	x		x	
767	DnaJ homolog subfamily C member 3 OS=Homo sapiens GN=DNAJC3 PE=1 SV=1	x	x		x	
768	Isoform 2 of Transgelin-2 OS=Homo sapiens GN=TAGLN2	x	x	x		
769	Isoform 2 of Thymidylate synthase OS=Homo sapiens GN=TYMS	x	x	x		x
770	Very-long-chain enoyl-CoA reductase OS=Homo sapiens GN=TECR PE=1 SV=1	x	x		x	
771	Isoform 2 of Sulfatase-modifying factor 1 OS=Homo sapiens GN=SUMF1	x	x	x		x
772	Glutamyl-tRNA(Gln) amidotransferase subunit A, mitochondrial OS=Homo sapiens GN=QRSL1 PE=4 SV=1	x	x	x		x
773	45 kDa calcium-binding protein (Fragment) OS=Homo sapiens GN=SDF4 PE=1 SV=1	x	x		x	
774	Ran GTPase-activating protein 1 OS=Homo sapiens GN=RANGAP1 PE=1 SV=1	x	x	x		

	A	B	C	D	E	F
774	Ran GTPase-activating protein 1 OS=Homo sapiens GN=RANGAP1 PE=1 SV=1	x	x	x		
775	DCC-interacting protein 13-alpha OS=Homo sapiens GN=APPL1 PE=1 SV=1	x	x	x		
776	Tyrosine-protein phosphatase non-receptor type OS=Homo sapiens GN=PTPN1 PE=1 SV=1	x	x		x	
777	Isoform 2 of Small ubiquitin-related modifier 3 OS=Homo sapiens GN=SUMO3	x	x		x	
778	Isoform 3 of Glutaminase kidney isoform, mitochondrial OS=Homo sapiens GN=GLS	x	x		x	
779	Src substrate cortactin OS=Homo sapiens GN=CTTN PE=1 SV=2	x	x	x		
780	Activator of 90 kDa heat shock protein ATPase homolog 1 OS=Homo sapiens GN=AHSA1 PE=1 SV=1	x	x	x		
781	Glyoxylate reductase/hydroxypyruvate reductase OS=Homo sapiens GN=GRHPR PE=1 SV=1	x	x		x	
782	Ras-related protein Ral-A OS=Homo sapiens GN=RALA PE=1 SV=1	x	x		x	
783	Apoptosis inhibitor 5 OS=Homo sapiens GN=API5 PE=1 SV=1	x	x		x	
784	Annexin A2 OS=Homo sapiens GN=ANXA2 PE=1 SV=2	x	x		x	
785	NAD(P) transhydrogenase, mitochondrial OS=Homo sapiens GN=NNT PE=1 SV=3	x	x		x	
786	Small acidic protein (Fragment) OS=Homo sapiens GN=C11orf58 PE=1 SV=1	x	x		x	
787	Poly [ADP-ribose] polymerase 1 OS=Homo sapiens GN=PARP1 PE=1 SV=4	x	x	x		
788	Unconventional myosin-IXb OS=Homo sapiens GN=MYO9B PE=1 SV=1	x	x		x	
789	Catenin beta-1 OS=Homo sapiens GN=CTNNB1 PE=1 SV=1	x	x		x	
790	Serine/threonine-protein phosphatase (Fragment) OS=Homo sapiens GN=PPP4C PE=1 SV=1	x	x	x		
791	tRNA methyltransferase 112 homolog OS=Homo sapiens GN=TRMT112 PE=1 SV=1	x	x	x		
792	Pleckstrin-2 OS=Homo sapiens GN=PLEK2 PE=1 SV=1	x	x	x		x
793	Prohibitin OS=Homo sapiens GN=PHB PE=1 SV=1	x	x		x	
794	Isoform 2 of RRP12-like protein OS=Homo sapiens GN=RRP12	x	x		x	
795	NEDD8 OS=Homo sapiens GN=NEDD8 PE=1 SV=1	x	x	x		
796	Isoform 2 of 5'-nucleotidase domain-containing protein 2 OS=Homo sapiens GN=NT5DC2	x	x	x		x
797	Isoform 2 of Tripeptidyl-peptidase 1 OS=Homo sapiens GN=TPP1	x	x		x	
798	Calnexin OS=Homo sapiens GN=CANX PE=1 SV=2	x	x		x	
799	Isoform 4 of Beta-catenin-like protein 1 OS=Homo sapiens GN=CTNNBL1	x	x		x	
800	ADP-ribosylation factor 5 OS=Homo sapiens GN=ARF5 PE=1 SV=2	x	x	x		
801	Isoform 2 of Probable 28S rRNA (cytosine(4447)-C(5))-methyltransferase OS=Homo sapiens GN=NOP2	x	x		x	
802	Serine-threonine kinase receptor-associated protein OS=Homo sapiens GN=STRAP PE=1 SV=1	x	x		x	
803	ADP-ribosylation factor-like protein 3 OS=Homo sapiens GN=ARL3 PE=1 SV=2	x	x		x	
804	Leucine-rich repeat-containing protein 47 OS=Homo sapiens GN=LRRC47 PE=1 SV=1	x	x	x		
805	Tricarboxylate transport protein, mitochondrial OS=Homo sapiens GN=SLC25A1 PE=1 SV=2	x	x	x		
806	Negative elongation factor B OS=Homo sapiens GN=NELFB PE=1 SV=1	x	x	x		
807	Isoform 2 of Negative elongation factor E OS=Homo sapiens GN=NELFE	x	x	x		
808	Retinoid-inducible serine carboxypeptidase (Fragment) OS=Homo sapiens GN=SCPEP1 PE=1 SV=1	x	x		x	x
809	60S ribosomal protein L3 OS=Homo sapiens GN=RPL3 PE=1 SV=2	x	x	x		
810	Macrophage migration inhibitory factor OS=Homo sapiens GN=MIF PE=1 SV=4	x	x		x	
811	Ribosyldihydronicotinamide dehydrogenase [quinone] OS=Homo sapiens GN=NQO2 PE=1 SV=1	x	x		x	
812	Lipoamide acyltransferase component of branched-chain alpha-keto acid dehydrogenase complex, mitochondrial OS	x	x	x		

	A	B	C	D	E	F
812	Lipoamide acyltransferase component of branched-chain alpha-keto acid dehydrogenase complex, mitochondrial OS	x	x	x		
813	Putative deoxyribonuclease TATDN1 OS=Homo sapiens GN=TATDN1 PE=1 SV=1	x	x	x		x
814	Isoform 3 of Basic leucine zipper and W2 domain-containing protein 1 OS=Homo sapiens GN=BZW1	x	x	x		
815	Neurofilament light polypeptide OS=Homo sapiens GN=NEFL PE=1 SV=3	x	x		x	
816	Uroporphyrinogen decarboxylase OS=Homo sapiens GN=UROD PE=1 SV=2	x	x	x		
817	Bax inhibitor 1 (Fragment) OS=Homo sapiens GN=TMBIM6 PE=4 SV=1	x	x	x		
818	Integrin-linked protein kinase OS=Homo sapiens GN=ILK PE=1 SV=2	x	x		x	
819	Isoform 2 of Myb-binding protein 1A OS=Homo sapiens GN=MYBBP1A	x	x		x	
820	PLEKHA5 protein OS=Homo sapiens GN=PLEKHA5 PE=1 SV=1	x	x	x		
821	Isoform Long of Glucose-6-phosphate 1-dehydrogenase OS=Homo sapiens GN=G6PD	x	x		x	
822	Plexin-B2 OS=Homo sapiens GN=PLXNB2 PE=1 SV=3	x	x		x	
823	Signal recognition particle subunit SRP72 OS=Homo sapiens GN=SRP72 PE=1 SV=3	x	x	x		
824	Isoform 2 of Protein TFG OS=Homo sapiens GN=TFG	x	x	x		
825	Putative adenosylhomocysteinase 2 OS=Homo sapiens GN=AHCYL1 PE=1 SV=2	x	x	x		
826	39S ribosomal protein L12, mitochondrial OS=Homo sapiens GN=MRPL12 PE=1 SV=1	x	x		x	
827	Nuclear pore complex protein Nup107 OS=Homo sapiens GN=NUP107 PE=1 SV=1	x	x	x		
828	Splicing factor 3A subunit 1 OS=Homo sapiens GN=SF3A1 PE=1 SV=1	x	x	x		
829	Alpha-actinin-4 OS=Homo sapiens GN=ACTN4 PE=1 SV=2	x	x		x	
830	Proteasomal ubiquitin receptor ADRM1 OS=Homo sapiens GN=ADRM1 PE=1 SV=2	x	x		x	
831	Spartin OS=Homo sapiens GN=SPG20 PE=1 SV=1	x	x		x	
832	Cysteine-rich with EGF-like domain protein 1 OS=Homo sapiens GN=CRELD1 PE=4 SV=1	x	x		x	x
833	Heme-binding protein 1 OS=Homo sapiens GN=HEBP1 PE=1 SV=1	x	x		x	
834	Signal recognition particle 9 kDa protein OS=Homo sapiens GN=SRP9 PE=1 SV=2	x	x	x		
835	Inositol 1,4,5-trisphosphate receptor type 2 OS=Homo sapiens GN=ITPR2 PE=1 SV=2	x	x		x	
836	EBNA1 binding protein 2, isoform CRA_d OS=Homo sapiens GN=EBNA1BP2 PE=1 SV=1	x	x	x		
837	RNA-binding motif protein, X chromosome, N-terminally processed (Fragment) OS=Homo sapiens GN=RBMX PE=1 S	x	x		x	
838	Golgi SNAP receptor complex member 2 (Fragment) OS=Homo sapiens GN=GOSR2 PE=1 SV=1	x	x		x	x
839	Endothelial differentiation-related factor 1 OS=Homo sapiens GN=EDF1 PE=1 SV=1	x	x	x		
840	Protein NipSnap homolog 2 OS=Homo sapiens GN=GBAS PE=1 SV=1	x	x	x		
841	THO complex subunit 2 OS=Homo sapiens GN=THOC2 PE=1 SV=2	x	x	x		x
842	Isoform 4 of Non-specific lipid-transfer protein OS=Homo sapiens GN=SCP2	x	x	x		
843	Rho GTPase-activating protein 35 OS=Homo sapiens GN=ARHGAP35 PE=1 SV=3	x	x		x	
844	Isoform 2 of Flotillin-1 OS=Homo sapiens GN=FLOT1	x	x	x		
845	Isoform 4 of Alpha-methylacyl-CoA racemase OS=Homo sapiens GN=AMACR	x	x	x		
846	Ragulator complex protein LAMTOR3 OS=Homo sapiens GN=LAMTOR3 PE=1 SV=1	x	x	x		
847	Isoform 2 of Alpha-aminoadipic semialdehyde dehydrogenase OS=Homo sapiens GN=ALDH7A1	x	x	x		
848	SH3 and PX domain-containing protein 2B OS=Homo sapiens GN=SH3PXD2B PE=1 SV=3	x	x		x	
849	Sorbitol dehydrogenase OS=Homo sapiens GN=SORD PE=1 SV=1	x	x		x	
850	Isoform 4 of Methyltransferase-like protein 13 OS=Homo sapiens GN=METTL13	x	x	x		x

	A	B	C	D	E	F
850	Isoform 4 of Methyltransferase-like protein 13 OS=Homo sapiens GN=METTL13	x	x	x		x
851	Prefoldin subunit 2 OS=Homo sapiens GN=PFDN2 PE=1 SV=1	x	x		x	
852	Isoform 2 of Yorkie homolog OS=Homo sapiens GN=YAP1	x	x		x	
853	Isoform 2 of Triosephosphate isomerase OS=Homo sapiens GN=TPI1	x	x		x	
854	Isoform 2 of Septin-2 OS=Homo sapiens GN=SEPT2	x	x		x	
855	Transmembrane emp24 domain-containing protein 2 OS=Homo sapiens GN=TMED2 PE=1 SV=1	x	x	x		
856	Isoform Beta-2 of Serine/threonine-protein phosphatase 2A 56 kDa regulatory subunit beta isoform OS=Homo sapie	x	x	x		
857	Isoform 2 of Collagen type IV alpha-3-binding protein OS=Homo sapiens GN=COL4A3BP	x	x		x	
858	Prolow-density lipoprotein receptor-related protein 1 OS=Homo sapiens GN=LRP1 PE=1 SV=2	x	x		x	
859	DNA repair protein RAD50 (Fragment) OS=Homo sapiens GN=RAD50 PE=1 SV=1	x	x		x	
860	Trophoblast glycoprotein OS=Homo sapiens GN=TPBG PE=1 SV=1	x	x		x	
861	Mitochondrial pyruvate carrier 2 (Fragment) OS=Homo sapiens GN=MPC2 PE=1 SV=1	x	x		x	
862	Elongator complex protein 3 OS=Homo sapiens GN=ELP3 PE=1 SV=1	x	x	x		
863	Casein kinase 2, beta polypeptide, isoform CRA_d OS=Homo sapiens GN=CSNK2B PE=1 SV=2	x	x	x		
864	Survival motor neuron protein (Fragment) OS=Homo sapiens GN=SMN1 PE=4 SV=1	x	x	x		
865	Platelet-activating factor acetylhydrolase IB subunit gamma OS=Homo sapiens GN=PAFAH1B3 PE=1 SV=1	x	x		x	
866	Isoform 3 of Dynactin subunit 4 OS=Homo sapiens GN=DCTN4	x	x		x	
867	F-box-like/WD repeat-containing protein TBL1XR1 OS=Homo sapiens GN=TBL1XR1 PE=1 SV=1	x	x	x		
868	Tubulin-specific chaperone A OS=Homo sapiens GN=TBCA PE=1 SV=1	x	x		x	
869	Proteasome subunit alpha type-2 OS=Homo sapiens GN=PSMA2 PE=1 SV=2	x	x	x		
870	NudC domain-containing protein 2 OS=Homo sapiens GN=NUDCD2 PE=1 SV=1	x	x		x	
871	Glutathione S-transferase Mu 3 OS=Homo sapiens GN=GSTM3 PE=1 SV=3	x	x	x		
872	Isoform 2 of 26S proteasome non-ATPase regulatory subunit 1 OS=Homo sapiens GN=PSMD1	x	x	x		
873	3-ketoacyl-CoA thiolase, mitochondrial OS=Homo sapiens GN=ACAA2 PE=1 SV=2	x	x		x	x
874	Rho guanine nucleotide exchange factor 2 OS=Homo sapiens GN=ARHGEF2 PE=1 SV=1	x	x		x	
875	Isoform 2 of Lipase maturation factor 2 OS=Homo sapiens GN=LMF2	x	x	x		
876	Spectrin beta chain, non-erythrocytic 1 OS=Homo sapiens GN=SPTBN1 PE=1 SV=2	x	x	x		
877	ELKS/Rab6-interacting/CAST family member 1 OS=Homo sapiens GN=ERC1 PE=1 SV=1	x	x		x	
878	Phosphoserine phosphatase (Fragment) OS=Homo sapiens GN=PSPH PE=1 SV=1	x	x		x	
879	Thioredoxin OS=Homo sapiens GN=TXN PE=1 SV=3	x	x		x	
880	S-methyl-5'-thioadenosine phosphorylase OS=Homo sapiens GN=MTAP PE=1 SV=1	x	x		x	
881	Alpha-soluble NSF attachment protein OS=Homo sapiens GN=NAPA PE=1 SV=3	x	x		x	
882	Importin-8 (Fragment) OS=Homo sapiens GN=IPO8 PE=1 SV=1	x	x	x		x
883	Polyribonucleotide nucleotidyltransferase 1, mitochondrial OS=Homo sapiens GN=PNPT1 PE=1 SV=2	x	x	x		
884	Acidic leucine-rich nuclear phosphoprotein 32 family member E OS=Homo sapiens GN=ANP32E PE=1 SV=1	x	x	x		
885	COMM domain-containing protein 4 (Fragment) OS=Homo sapiens GN=COMMD4 PE=1 SV=1	x	x	x		
886	Protein NipSnap homolog 3A OS=Homo sapiens GN=NIPSNAP3A PE=1 SV=2	x	x	x		
887	Gamma-enolase OS=Homo sapiens GN=ENO2 PE=1 SV=3	x	x		x	
888	Isoform 2 of Basigin OS=Homo sapiens GN=BSG	x	x		x	

	A	B	C	D	E	F
888	Isoform 2 of Basigin OS=Homo sapiens GN=BSG	x	x		x	
889	Signal peptidase complex catalytic subunit SEC11A OS=Homo sapiens GN=SEC11A PE=1 SV=1	x	x		x	
890	Archain 1, isoform CRA_a OS=Homo sapiens GN=ARCN1 PE=1 SV=1	x	x		x	
891	Iron-sulfur protein NUBPL OS=Homo sapiens GN=NUBPL PE=1 SV=3	x	x	x		x
892	Hematological and neurological expressed 1 protein OS=Homo sapiens GN=HN1 PE=1 SV=3	x	x		x	x
893	Ragulator complex protein LAMTOR1 (Fragment) OS=Homo sapiens GN=LAMTOR1 PE=1 SV=1	x	x	x		
894	Isoform 2 of Septin-10 OS=Homo sapiens GN=SEPT10	x	x		x	
895	Transcription elongation factor B polypeptide 1 (Fragment) OS=Homo sapiens GN=TCEB1 PE=1 SV=1	x	x	x		
896	Isoform 2 of Protein flightless-1 homolog OS=Homo sapiens GN=FLII	x	x		x	
897	Spliceosome-associated protein CWC15 homolog OS=Homo sapiens GN=CWC15 PE=1 SV=2	x	x		x	
898	Sorting nexin-6 OS=Homo sapiens GN=SNX6 PE=1 SV=1	x	x	x		
899	Isoform 2 of Zinc finger protein 280D OS=Homo sapiens GN=ZNF280D	x	x		x	
900	Puromycin-sensitive aminopeptidase OS=Homo sapiens GN=NPEPPS PE=1 SV=1	x	x	x		
901	Coiled-coil domain-containing protein 104 OS=Homo sapiens GN=CCDC104 PE=1 SV=1	x	x		x	
902	Isoform 4 of Protein phosphatase methylesterase 1 OS=Homo sapiens GN=PPME1	x	x		x	
903	Isoform 2 of NADH dehydrogenase [ubiquinone] complex I, assembly factor 7 OS=Homo sapiens GN=NDUFAF7	x	x		x	
904	Calpain-7 OS=Homo sapiens GN=CAPN7 PE=1 SV=1	x	x	x		x
905	Transcriptional activator protein Pur-beta OS=Homo sapiens GN=PURB PE=1 SV=3	x	x		x	
906	Isoform 2 of A-kinase anchor protein 12 OS=Homo sapiens GN=AKAP12	x	x		x	
907	Solute carrier family 35 member F6 OS=Homo sapiens GN=SLC35F6 PE=1 SV=1	x	x	x		
908	UDP-glucose 4-epimerase OS=Homo sapiens GN=GALE PE=1 SV=2	x	x	x		
909	Phosphoglucomutase-2 OS=Homo sapiens GN=PGM2 PE=1 SV=4	x	x	x		
910	Isoform 2 of Eukaryotic translation initiation factor 2D OS=Homo sapiens GN=EIF2D	x	x	x		
911	Ragulator complex protein LAMTOR5 OS=Homo sapiens GN=LAMTOR5 PE=1 SV=1	x	x	x		
912	Isoform 2 of Ester hydrolase C11orf54 OS=Homo sapiens GN=C11orf54	x	x		x	
913	Isoform GN-1 of Glycogenin-1 OS=Homo sapiens GN=GYG1	x	x	x		
914	PC4 and SFRS1-interacting protein OS=Homo sapiens GN=PSIP1 PE=1 SV=1	x	x		x	
915	Glycylpeptide N-tetradecanoyltransferase 2 OS=Homo sapiens GN=NMT2 PE=1 SV=1	x	x	x		
916	Isoform 2 of AP-2 complex subunit alpha-2 OS=Homo sapiens GN=AP2A2	x	x		x	
917	Anamorsin OS=Homo sapiens GN=CIAPIN1 PE=1 SV=1	x	x	x		x
918	ATP-dependent RNA helicase DDX1 OS=Homo sapiens GN=DDX1 PE=1 SV=2	x	x	x		
919	WASH complex subunit FAM21A OS=Homo sapiens GN=FAM21A PE=4 SV=2	x	x		x	
920	Protein S100-A10 OS=Homo sapiens GN=S100A10 PE=1 SV=2	x	x		x	
921	Isoform 3 of Chitinase domain-containing protein 1 OS=Homo sapiens GN=CHID1	x	x	x		
922	Caldesmon OS=Homo sapiens GN=CALD1 PE=1 SV=1	x	x		x	
923	Anoctamin (Fragment) OS=Homo sapiens GN=ANO10 PE=3 SV=1	x	x	x		
924	ADP-ribose pyrophosphatase, mitochondrial (Fragment) OS=Homo sapiens GN=NUDT9 PE=1 SV=1	x	x	x		x
925	Isoform 3 of Synembryn-A OS=Homo sapiens GN=RIC8A	x	x		x	
926	Isoform 2 of Signal transducing adapter molecule 1 OS=Homo sapiens GN=STAM	x	x	x		

	A	B	C	D	E	F
926	Isoform 2 of Signal transducing adapter molecule 1 OS=Homo sapiens GN=STAM	x	x	x		
927	Dihydrolipoyl dehydrogenase, mitochondrial OS=Homo sapiens GN=DLD PE=1 SV=1	x	x	x		
928	ATP synthase subunit delta, mitochondrial OS=Homo sapiens GN=ATP5D PE=1 SV=2	x	x		x	
929	Isoform 2 of Tubulin alpha-1A chain OS=Homo sapiens GN=TUBA1A	x	x	x		x
930	Cadherin-6 OS=Homo sapiens GN=CDH6 PE=1 SV=1	x	x		x	
931	Fructose-2,6-bisphosphatase TIGAR OS=Homo sapiens GN=TIGAR PE=1 SV=1	x	x		x	
932	NAD-dependent protein deacetylase sirtuin-3, mitochondrial OS=Homo sapiens GN=SIRT3 PE=1 SV=2	x	x	x		
933	WW domain-binding protein 2 OS=Homo sapiens GN=WBP2 PE=1 SV=2	x	x		x	
934	NEDD8-conjugating enzyme Ubc12 OS=Homo sapiens GN=UBE2M PE=1 SV=1	x	x		x	
935	Ketosamine-3-kinase OS=Homo sapiens GN=FN3KRP PE=1 SV=2	x	x	x		
936	Heat shock factor-binding protein 1 OS=Homo sapiens GN=HSBP1 PE=1 SV=1	x	x	x		
937	Polyadenylate-binding protein 1 OS=Homo sapiens GN=PABPC1 PE=1 SV=2	x	x		x	
938	Eukaryotic translation initiation factor 5B OS=Homo sapiens GN=EIF5B PE=1 SV=4	x	x		x	
939	Destrin OS=Homo sapiens GN=DSTN PE=1 SV=3	x	x		x	
940	Transmembrane protein 87B (Fragment) OS=Homo sapiens GN=TMEM87B PE=4 SV=1	x	x		x	
941	Isoform 2 of TSC22 domain family protein 2 OS=Homo sapiens GN=TSC22D2	x	x	x		
942	Acyl-CoA dehydrogenase family member 9, mitochondrial OS=Homo sapiens GN=ACAD9 PE=1 SV=1	x	x		x	
943	HIV Tat-specific factor 1 OS=Homo sapiens GN=HTATSF1 PE=1 SV=1	x	x	x		
944	Ribonuclease UK114 OS=Homo sapiens GN=HRSP12 PE=1 SV=1	x	x	x		
945	Isoform 3 of Serine hydroxymethyltransferase, mitochondrial OS=Homo sapiens GN=SHMT2	x	x	x		
946	SCY1-like protein 2 OS=Homo sapiens GN=SCYL2 PE=1 SV=1	x	x	x		
947	Calcium/calmodulin-dependent protein kinase type 1 OS=Homo sapiens GN=CAMK1 PE=1 SV=1	x	x	x		
948	Emerin OS=Homo sapiens GN=EMD PE=1 SV=1	x	x		x	
949	Synaptic vesicle membrane protein VAT-1 homolog OS=Homo sapiens GN=VAT1 PE=1 SV=2	x	x	x		
950	Ubiquilin-2 OS=Homo sapiens GN=UBQLN2 PE=1 SV=2	x	x		x	
951	Phosphoglucomutase-1 OS=Homo sapiens GN=PGM1 PE=1 SV=3	x	x	x		
952	Alpha-centractin OS=Homo sapiens GN=ACTR1A PE=1 SV=1	x	x		x	
953	Isoform 1 of Histone-arginine methyltransferase CARM1 OS=Homo sapiens GN=CARM1	x	x		x	
954	Isoform Beta-1 of DNA topoisomerase 2-beta OS=Homo sapiens GN=TOP2B	x	x	x		
955	Tumor susceptibility gene 101 protein (Fragment) OS=Homo sapiens GN=TSG101 PE=4 SV=1	x	x		x	
956	Cytochrome b-c1 complex subunit 6, mitochondrial OS=Homo sapiens GN=UQCRH PE=1 SV=2	x	x		x	
957	Ras-related protein Rab-27B OS=Homo sapiens GN=RAB27B PE=1 SV=4	x	x	x		x
958	Protein QIL1 OS=Homo sapiens GN=QIL1 PE=1 SV=1	x	x		x	
959	5'-3' exoribonuclease 2 OS=Homo sapiens GN=XRN2 PE=1 SV=1	x	x	x		
960	Mitochondrial carrier homolog 2 OS=Homo sapiens GN=MTCH2 PE=1 SV=1	x	x		x	
961	Isoform 2 of Liprin-alpha-1 OS=Homo sapiens GN=PPFIA1	x	x	x		
962	E3 ubiquitin-protein ligase ARIH1 (Fragment) OS=Homo sapiens GN=ARIH1 PE=1 SV=1	x	x	x		
963	Isoform 2 of Protein PRRC2A OS=Homo sapiens GN=PRRC2A	x	x	x		
964	Carboxypeptidase OS=Homo sapiens GN=CTSA PE=1 SV=1	x	x	x		

	A	B	C	D	E	F
964	Carboxypeptidase OS=Homo sapiens GN=CTSA PE=1 SV=1	x	x	x		
965	ATPase, H+ transporting, lysosomal 50/57kDa, V1 subunit H, isoform CRA_c OS=Homo sapiens GN=ATP6V1H PE=1 SV	x	x	x		
966	Isoform 2 of Protein LZIC OS=Homo sapiens GN=LZIC	x	x	x		
967	UPF0568 protein C14orf166 OS=Homo sapiens GN=C14orf166 PE=1 SV=1	x	x	x		
968	Isoform 2 of Septin-11 OS=Homo sapiens GN=SEPT11	x	x		x	
969	YLP motif-containing protein 1 (Fragment) OS=Homo sapiens GN=YLPM1 PE=1 SV=1	x	x	x		
970	Bis(5'-nucleosyl)-tetraphosphatase [asymmetrical] OS=Homo sapiens GN=NUDT2 PE=1 SV=3	x	x		x	
971	Estradiol 17-beta-dehydrogenase 12 OS=Homo sapiens GN=HSD17B12 PE=1 SV=2	x	x		x	
972	U6 snRNA-associated Sm-like protein LSm4 OS=Homo sapiens GN=LSM4 PE=1 SV=1	x	x	x		
973	Isoform 2 of Protein bicaudal D homolog 2 OS=Homo sapiens GN=BICD2	x	x		x	
974	Isoform 4 of Selenide, water dikinase 1 OS=Homo sapiens GN=SEPHS1	x	x	x		
975	Isoform 2 of Spectrin beta chain, non-erythrocytic 1 OS=Homo sapiens GN=SPTBN1	x	x	x		
976	Vesicular integral-membrane protein VIP36 OS=Homo sapiens GN=LMAN2 PE=1 SV=1	x	x	x		
977	Isoform 2 of Beta-1-syntrophin OS=Homo sapiens GN=SNTB1	x	x	x		
978	Cdc42-interacting protein 4 OS=Homo sapiens GN=TRIP10 PE=1 SV=1	x	x	x		
979	Protein lin-7 homolog B OS=Homo sapiens GN=LIN7B PE=1 SV=1	x	x	x		
980	Dihydropyrimidinase-related protein 2 OS=Homo sapiens GN=DPYSL2 PE=1 SV=1	x	x	x		x
981	Deoxycytidylate deaminase (Fragment) OS=Homo sapiens GN=DCTD PE=1 SV=1	x	x	x		
982	Zinc finger CCCH domain-containing protein 11A (Fragment) OS=Homo sapiens GN=ZC3H11A PE=1 SV=1	x	x	x		
983	Isoform 2 of Mitochondrial import inner membrane translocase subunit TIM50 OS=Homo sapiens GN=TIMM50	x	x	x		
984	Cyclin-dependent kinase 1 OS=Homo sapiens GN=CDK1 PE=1 SV=3	x	x	x		
985	39S ribosomal protein L4, mitochondrial (Fragment) OS=Homo sapiens GN=MRPL4 PE=1 SV=1	x	x		x	
986	Protein kinase C and casein kinase substrate in neurons protein 3 OS=Homo sapiens GN=PACSIN3 PE=1 SV=2	x	x	x		
987	MAGUK p55 subfamily member 6 OS=Homo sapiens GN=MPP6 PE=1 SV=1	x	x		x	
988	Adaptin ear-binding coat-associated protein 2 OS=Homo sapiens GN=NECAP2 PE=1 SV=1	x	x	x		
989	Isoform 2 of Phosphatidylinositol 5-phosphate 4-kinase type-2 alpha OS=Homo sapiens GN=PIP4K2A	x	x		x	
990	Protein disulfide-isomerase A4 OS=Homo sapiens GN=PDIA4 PE=1 SV=2	x	x	x		
991	Microsomal glutathione S-transferase 1 (Fragment) OS=Homo sapiens GN=MGST1 PE=1 SV=1	x	x		x	
992	Sorting nexin-8 OS=Homo sapiens GN=SNX8 PE=1 SV=1	x	x		x	
993	Isoform 2 of Cdc42 effector protein 4 OS=Homo sapiens GN=CDC42EP4	x	x		x	
994	Protein ERGIC-53 OS=Homo sapiens GN=LMAN1 PE=1 SV=2	x	x		x	
995	Isoform 2 of Serine hydroxymethyltransferase, cytosolic OS=Homo sapiens GN=SHMT1	x	x	x		
996	Isoform 2 of Transportin-2 OS=Homo sapiens GN=TNPO2	x	x		x	
997	Isoform 3 of Metaxin-1 OS=Homo sapiens GN=MTX1	x	x	x		
998	UPF0489 protein C5orf22 OS=Homo sapiens GN=C5orf22 PE=2 SV=1	x	x	x		
999	Neuroplastin OS=Homo sapiens GN=NPTN PE=1 SV=1	x	x	x		
1000	Dolichyl-diphosphooligosaccharide--protein glycosyltransferase subunit DAD1 OS=Homo sapiens GN=DAD1 PE=1 SV=	x	x		x	
1001	COP9 signalosome complex subunit 1 OS=Homo sapiens GN=GPS1 PE=1 SV=2	x	x		x	
1002	Isoform 2 of Putative RNA-binding protein Luc7-like 1 OS=Homo sapiens GN=LUC7L	x	x	x		

	A	B	C	D	E	F
1002	Isoform 2 of Putative RNA-binding protein Luc7-like 1 OS=Homo sapiens GN=LUC7L	x	x	x		
1003	Tyrosine--tRNA ligase, cytoplasmic OS=Homo sapiens GN=YARS PE=1 SV=4	x	x	x		
1004	Isoform 2 of Heterogeneous nuclear ribonucleoprotein R OS=Homo sapiens GN=HNRNPR	x	x		x	
1005	Vacuolar protein sorting-associated protein 35 OS=Homo sapiens GN=VPS35 PE=1 SV=2	x	x	x		
1006	Mitotic checkpoint protein BUB3 (Fragment) OS=Homo sapiens GN=BUB3 PE=1 SV=1	x	x	x		
1007	AP-3 complex subunit mu-2 (Fragment) OS=Homo sapiens GN=AP3M2 PE=4 SV=1	x	x	x		
1008	Isoform 2 of Cyclin-dependent-like kinase 5 OS=Homo sapiens GN=CDK5	x	x	x		
1009	Phosphatidylserine decarboxylase alpha chain OS=Homo sapiens GN=PISD PE=4 SV=1	x	x	x		
1010	Matrix metalloproteinase-14 OS=Homo sapiens GN=MMP14 PE=1 SV=3	x	x	x		
1011	Isoform 4 of Perilipin-3 OS=Homo sapiens GN=PLIN3	x	x		x	
1012	Non-POU domain-containing octamer-binding protein OS=Homo sapiens GN=NONO PE=1 SV=4	x	x	x		
1013	Isoform 3 of Calumenin OS=Homo sapiens GN=CALU	x	x		x	
1014	Adenylyl cyclase-associated protein 1 OS=Homo sapiens GN=CAP1 PE=1 SV=5	x	x	x		
1015	Protein transport protein Sec23A OS=Homo sapiens GN=SEC23A PE=1 SV=1	x	x	x		
1016	Cancer-related nucleoside-triphosphatase OS=Homo sapiens GN=NTPCR PE=1 SV=1	x	x	x		
1017	Haloacid dehalogenase-like hydrolase domain-containing protein 2 (Fragment) OS=Homo sapiens GN=HDHD2 PE=1 S	x	x	x		
1018	Isoform 2 of Vacuolar protein sorting-associated protein 52 homolog OS=Homo sapiens GN=VPS52	x	x	x		
1019	NAD-dependent malic enzyme, mitochondrial OS=Homo sapiens GN=ME2 PE=1 SV=1	x	x	x		
1020	Protein transport protein Sec61 subunit beta OS=Homo sapiens GN=SEC61B PE=1 SV=2	x	x		x	
1021	1,4-alpha-glucan-branching enzyme OS=Homo sapiens GN=GBE1 PE=1 SV=3	x	x	x		
1022	Isoform 3 of Lanosterol synthase OS=Homo sapiens GN=LSS	x	x		x	
1023	Calpastatin OS=Homo sapiens GN=CAST PE=1 SV=1	x	x		x	
1024	Amyloid beta A4 protein OS=Homo sapiens GN=APP PE=1 SV=1	x	x		x	
1025	Isoform 3 of Protein scribble homolog OS=Homo sapiens GN=SCRIB	x	x	x		
1026	Isoform 1 of 1-phosphatidylinositol 4,5-bisphosphate phosphodiesterase beta-4 OS=Homo sapiens GN=PLCB4	x	x	x		
1027	Serine/arginine-rich-splicing factor 11 (Fragment) OS=Homo sapiens GN=SRSF11 PE=1 SV=1	x	x	x		
1028	Protein-L-isoaspartate O-methyltransferase OS=Homo sapiens GN=PCMT1 PE=1 SV=1	x	x		x	
1029	Isoform BIN1-13 of Myc box-dependent-interacting protein 1 OS=Homo sapiens GN=BIN1	x	x	x		
1030	Alpha-adducin OS=Homo sapiens GN=ADD1 PE=1 SV=1	x	x	x		
1031	Serine/threonine-protein kinase VRK1 (Fragment) OS=Homo sapiens GN=VRK1 PE=1 SV=1	x	x	x		x
1032	Isoform 4 of Protein-methionine sulfoxide oxidase MICAL1 OS=Homo sapiens GN=MICAL1	x	x		x	
1033	Isoform 2 of Farnesyl pyrophosphate synthase OS=Homo sapiens GN=FDPS	x	x		x	
1034	Isoform 3 of Spectrin alpha chain, non-erythrocytic 1 OS=Homo sapiens GN=SPTAN1	x	x	x		
1035	Spectrin alpha chain, non-erythrocytic 1 OS=Homo sapiens GN=SPTAN1 PE=1 SV=3	x	x	x		
1036	Isoform 2 of Tyrosine-protein phosphatase non-receptor type 13 OS=Homo sapiens GN=PTPN13	x	x		x	x
1037	Nuclear export mediator factor NEMF (Fragment) OS=Homo sapiens GN=NEMF PE=1 SV=2	x	x	x		x
1038	Protein cornichon homolog 4 OS=Homo sapiens GN=CNIH4 PE=1 SV=1	x	x		x	
1039	Isoform F of Constitutive coactivator of PPAR-gamma-like protein 1 OS=Homo sapiens GN=FAM120A	x	x	x		
1040	Isoform 1 of RNA demethylase ALKBH5 OS=Homo sapiens GN=ALKBH5	x	x		x	x

	A	B	C	D	E	F
1040	Isoform 1 of RNA demethylase ALKBH5 OS=Homo sapiens GN=ALKBH5	x	x		x	x
1041	Density-regulated protein OS=Homo sapiens GN=DENR PE=1 SV=1	x	x		x	
1042	Protein kinase C delta-binding protein OS=Homo sapiens GN=PRKCDBP PE=1 SV=1	x	x		x	
1043	Isoform 2 of GDP-mannose 4,6 dehydratase OS=Homo sapiens GN=GMDS	x	x	x		
1044	Parathymosin OS=Homo sapiens GN=PTMS PE=1 SV=2	x	x		x	x
1045	Phosphofurin acidic cluster sorting protein 1 OS=Homo sapiens GN=PACS1 PE=1 SV=1	x	x	x		x
1046	Oxysterol-binding protein 1 OS=Homo sapiens GN=OSBP PE=1 SV=1	x	x		x	
1047	Isoform 2 of Epsin-1 OS=Homo sapiens GN=EPN1	x	x		x	
1048	Ferritin light chain OS=Homo sapiens GN=FTL PE=1 SV=2	x	x		x	x
1049	Isoform 3 of Protein YIPF5 OS=Homo sapiens GN=YIPF5	x	x		x	
1050	Isoform 2 of Ankycorbin OS=Homo sapiens GN=RAI14	x	x		x	
1051	ER membrane protein complex subunit 2 OS=Homo sapiens GN=EMC2 PE=1 SV=1	x	x	x		
1052	UPF0556 protein C19orf10 (Fragment) OS=Homo sapiens GN=C19orf10 PE=1 SV=1	x	x		x	
1053	Cleavage and polyadenylation specificity factor subunit 5 OS=Homo sapiens GN=NUDT21 PE=1 SV=1	x	x	x		
1054	Acyl carrier protein (Fragment) OS=Homo sapiens GN=NDUFAB1 PE=1 SV=1	x	x	x		
1055	Ras suppressor protein 1 OS=Homo sapiens GN=RSU1 PE=1 SV=3	x	x		x	
1056	Proteasome subunit beta type-1 OS=Homo sapiens GN=PSMB1 PE=1 SV=2	x	x	x		
1057	Isoform 2 of NAD-dependent protein deacylase sirtuin-5, mitochondrial OS=Homo sapiens GN=SIRT5	x	x	x		
1058	14-3-3 protein gamma OS=Homo sapiens GN=YWHAG PE=1 SV=2	x	x	x		
1059	BRCA1-A complex subunit BRE (Fragment) OS=Homo sapiens GN=BRE PE=1 SV=1	x	x	x		
1060	Peptidyl-prolyl cis-trans isomerase F, mitochondrial OS=Homo sapiens GN=PPIF PE=1 SV=1	x	x	x		
1061	Alpha-endosulfine OS=Homo sapiens GN=ENSA PE=1 SV=1	x	x		x	
1062	ATP-binding cassette sub-family F member 1 OS=Homo sapiens GN=ABCF1 PE=1 SV=2	x	x		x	
1063	Myristoylated alanine-rich C-kinase substrate OS=Homo sapiens GN=MARCKS PE=1 SV=4	x	x		x	
1064	Isoform 2 of Peptidyl-prolyl cis-trans isomerase NIMA-interacting 4 OS=Homo sapiens GN=PIN4	x	x	x		
1065	F-box only protein 17 OS=Homo sapiens GN=FBXO17 PE=4 SV=1	x	x	x		
1066	WD repeat-containing protein 11 (Fragment) OS=Homo sapiens GN=WDR11 PE=1 SV=1	x	x	x		
1067	Death-associated protein 1 OS=Homo sapiens GN=DAP PE=1 SV=3	x	x		x	x
1068	Activated RNA polymerase II transcriptional coactivator p15 OS=Homo sapiens GN=SUB1 PE=1 SV=3	x	x		x	
1069	Synapse-associated protein 1 OS=Homo sapiens GN=SYAP1 PE=1 SV=1	x	x		x	
1070	Cob(I)yrinic acid a,c-diamide adenosyltransferase, mitochondrial OS=Homo sapiens GN=MMAB PE=1 SV=1	x	x		x	
1071	Survival of motor neuron-related-splicing factor 30 OS=Homo sapiens GN=SMNDC1 PE=1 SV=1	x	x		x	
1072	Isoform 2 of Serine/arginine-rich splicing factor 3 OS=Homo sapiens GN=SRSF3	x	x		x	
1073	Isoform 2 of Ankyrin repeat and FYVE domain-containing protein 1 OS=Homo sapiens GN=ANKFY1	x	x	x		
1074	Isoform 2 of Cytoskeleton-associated protein 5 OS=Homo sapiens GN=CKAP5	x	x		x	
1075	Isoform 2 of NADH dehydrogenase [ubiquinone] iron-sulfur protein 2, mitochondrial OS=Homo sapiens GN=NDUFS2	x	x		x	
1076	Splicing factor 3B subunit 2 OS=Homo sapiens GN=SF3B2 PE=1 SV=1	x	x	x		
1077	Nucleoplasmin-3 OS=Homo sapiens GN=NPM3 PE=1 SV=3	x	x		x	
1078	OCIA domain-containing protein 2 OS=Homo sapiens GN=OCIAD2 PE=1 SV=1	x	x	x		

	A	B	C	D	E	F
1078	OCIA domain-containing protein 2 OS=Homo sapiens GN=OCIAD2 PE=1 SV=1	x	x	x		
1079	Gem-associated protein 5 OS=Homo sapiens GN=GEMIN5 PE=1 SV=3	x	x		x	
1080	Signal peptidase complex subunit 1 OS=Homo sapiens GN=SPCS1 PE=1 SV=4	x	x		x	
1081	Isoform 2 of Liprin-beta-1 OS=Homo sapiens GN=PPFIBP1	x	x		x	
1082	UTP--glucose-1-phosphate uridylyltransferase OS=Homo sapiens GN=UGP2 PE=1 SV=5	x	x	x		
1083	Cytoplasmic dynein 1 light intermediate chain 1 OS=Homo sapiens GN=DYNC1LI1 PE=1 SV=3	x	x		x	
1084	Interferon-induced guanylate-binding protein 1 OS=Homo sapiens GN=GBP1 PE=1 SV=2	x	x	x		
1085	Methylosome subunit pICln OS=Homo sapiens GN=CLNS1A PE=1 SV=1	x	x		x	
1086	Syntaxin-binding protein 3 OS=Homo sapiens GN=STXBP3 PE=1 SV=2	x	x	x		
1087	Raft-linking protein, isoform CRA_c OS=Homo sapiens GN=RFTN1 PE=1 SV=1	x	x		x	
1088	Pachytene checkpoint protein 2 homolog OS=Homo sapiens GN=TRIP13 PE=1 SV=2	x	x		x	
1089	Pyridoxal-dependent decarboxylase domain-containing protein 1 OS=Homo sapiens GN=PDXDC1 PE=1 SV=1	x	x		x	
1090	Vacuolar protein sorting-associated protein 28 homolog OS=Homo sapiens GN=VPS28 PE=1 SV=1	x	x		x	
1091	Isoform 2 of Xaa-Pro dipeptidase OS=Homo sapiens GN=PEPD	x	x	x		
1092	Eukaryotic translation initiation factor 6 OS=Homo sapiens GN=EIF6 PE=1 SV=1	x	x		x	
1093	Arginine--tRNA ligase, cytoplasmic OS=Homo sapiens GN=RARS PE=1 SV=2	x	x		x	
1094	Tight junction protein 1 (Zona occludens 1), isoform CRA_a OS=Homo sapiens GN=TJP1 PE=1 SV=1	x	x	x		
1095	Neural Wiskott-Aldrich syndrome protein OS=Homo sapiens GN=WASL PE=1 SV=2	x	x	x		
1096	Isoform 2 of General vesicular transport factor p115 OS=Homo sapiens GN=USO1	x	x		x	
1097	Kinectin OS=Homo sapiens GN=KTN1 PE=1 SV=1	x	x	x		
1098	Profilin-1 OS=Homo sapiens GN=PFN1 PE=1 SV=2	x	x		x	
1099	UPF0364 protein C6orf211 OS=Homo sapiens GN=C6orf211 PE=1 SV=1	x	x	x		
1100	Zinc fingers and homeoboxes protein 2 OS=Homo sapiens GN=ZHX2 PE=1 SV=1	x	x	x		x
1101	Isoform 2 of Phostensin OS=Homo sapiens GN=PPP1R18	x	x		x	
1102	Isoform 2 of Testis-expressed sequence 10 protein OS=Homo sapiens GN=TEX10	x	x	x		
1103	Pterin-4-alpha-carbinolamine dehydratase OS=Homo sapiens GN=PCBD1 PE=1 SV=2	x	x	x		
1104	Isoform 2 of Opioid growth factor receptor OS=Homo sapiens GN=OGFR	x	x		x	
1105	Isoform B of Ras-related C3 botulinum toxin substrate 1 OS=Homo sapiens GN=RAC1	x	x		x	
1106	WW domain-binding protein 11 OS=Homo sapiens GN=WBP11 PE=1 SV=1	x	x		x	
1107	Armadillo repeat-containing protein 10 OS=Homo sapiens GN=ARMC10 PE=1 SV=1	x	x	x		
1108	Signal recognition particle 14 kDa protein OS=Homo sapiens GN=SRP14 PE=1 SV=2	x	x	x		
1109	Isoform 2 of Leucine zipper protein 1 OS=Homo sapiens GN=LUZP1	x	x		x	
1110	Heterogeneous nuclear ribonucleoprotein H2 OS=Homo sapiens GN=HNRNPH2 PE=1 SV=1	x	x	x		
1111	Isoform 2 of Probable Xaa-Pro aminopeptidase 3 OS=Homo sapiens GN=XPNPEP3	x	x	x		
1112	Isoform 2 of Utrophin OS=Homo sapiens GN=UTRN	x	x	x		
1113	Isoform 2 of Treacle protein OS=Homo sapiens GN=TCOF1	x	x	x		
1114	Heterogeneous nuclear ribonucleoprotein L OS=Homo sapiens GN=HNRNPL PE=1 SV=2	x	x		x	
1115	UPF0554 protein C2orf43 OS=Homo sapiens GN=C2orf43 PE=1 SV=1	x	x	x		
1116	Peroxiredoxin-6 OS=Homo sapiens GN=PRDX6 PE=1 SV=3	x	x	x		

	A	B	C	D	E	F
1116	Peroxiredoxin-6 OS=Homo sapiens GN=PRDX6 PE=1 SV=3	x	x	x		
1117	FAS-associated factor 2 OS=Homo sapiens GN=FAF2 PE=1 SV=2	x	x	x		
1118	Pyrroline-5-carboxylate reductase 2 OS=Homo sapiens GN=PYCR2 PE=1 SV=1	x	x	x		
1119	Ankyrin repeat and MYND domain containing 2, isoform CRA_c OS=Homo sapiens GN=ANKMY2 PE=1 SV=1	x	x		x	
1120	Tumor suppressor p53-binding protein 1 OS=Homo sapiens GN=TP53BP1 PE=1 SV=2	x	x	x		
1121	Isoform 2 of Polymerase delta-interacting protein 3 OS=Homo sapiens GN=POLDIP3	x	x		x	
1122	Actin-related protein 2/3 complex subunit 1B OS=Homo sapiens GN=ARPC1B PE=1 SV=3	x	x		x	
1123	Isoform 2 of Ubiquitin-like modifier-activating enzyme 5 OS=Homo sapiens GN=UBA5	x	x	x		
1124	Small nuclear ribonucleoprotein E OS=Homo sapiens GN=SNRPE PE=1 SV=1	x	x	x		
1125	Unconventional myosin-Id OS=Homo sapiens GN=MYO1D PE=1 SV=1	x	x	x		x
1126	Isoform 2 of Mucosa-associated lymphoid tissue lymphoma translocation protein 1 OS=Homo sapiens GN=MALT1	x	x		x	
1127	Probable ATP-dependent RNA helicase DDX6 OS=Homo sapiens GN=DDX6 PE=1 SV=2	x	x		x	
1128	Isoform 2 of Prolyl 4-hydroxylase subunit alpha-1 OS=Homo sapiens GN=P4HA1	x	x	x		
1129	RNA polymerase II-associated factor 1 homolog OS=Homo sapiens GN=PAF1 PE=1 SV=1	x	x	x		
1130	Calcineurin B homologous protein 1 OS=Homo sapiens GN=CHP1 PE=1 SV=3	x	x	x		x
1131	Trifunctional purine biosynthetic protein adenosine-3 OS=Homo sapiens GN=GART PE=1 SV=1	x	x	x		
1132	Isoform 2 of Ubiquitin conjugation factor E4 B OS=Homo sapiens GN=UBE4B	x	x	x		
1133	Branched-chain-amino-acid aminotransferase (Fragment) OS=Homo sapiens GN=BCAT2 PE=1 SV=1	x	x	x		
1134	Isoform 2 of Phosphatidylglycerophosphatase and protein-tyrosine phosphatase 1 OS=Homo sapiens GN=PTPMT1	x	x		x	
1135	Glutamate--cysteine ligase catalytic subunit OS=Homo sapiens GN=GCLC PE=1 SV=2	x	x	x		x
1136	Peptidyl-prolyl cis-trans isomerase FKBP9 OS=Homo sapiens GN=FKBP9 PE=1 SV=2	x	x		x	
1137	Cleavage stimulation factor subunit 3 OS=Homo sapiens GN=CSTF3 PE=1 SV=1	x	x	x		
1138	Isoform 2 of Canalicular multispecific organic anion transporter 2 OS=Homo sapiens GN=ABCC3	x	x	x		x
1139	Acyl-protein thioesterase 1 (Fragment) OS=Homo sapiens GN=LYPLA1 PE=1 SV=1	x	x	x		
1140	NACHT, LRR and PYD domains-containing protein 14 OS=Homo sapiens GN=NLRP14 PE=2 SV=1	x	x		x	
1141	EH domain-containing protein 2 OS=Homo sapiens GN=EHD2 PE=1 SV=2	x	x		x	
1142	Isoform B of Peptidyl-prolyl cis-trans isomerase E OS=Homo sapiens GN=PPIE	x	x		x	
1143	Malate dehydrogenase, mitochondrial OS=Homo sapiens GN=MDH2 PE=1 SV=3	x	x	x		
1144	Hexokinase-2 OS=Homo sapiens GN=HK2 PE=1 SV=2	x	x		x	
1145	Ubiquitin-associated protein 2-like OS=Homo sapiens GN=UBAP2L PE=1 SV=1	x	x		x	
1146	Isoform 2 of Secernin-1 OS=Homo sapiens GN=SCRN1	x	x		x	
1147	Isoform 2 of Chloride channel CLIC-like protein 1 OS=Homo sapiens GN=CLCC1	x	x		x	
1148	Calpain small subunit 1 OS=Homo sapiens GN=CAPNS1 PE=1 SV=1	x	x	x		
1149	Uncharacterized protein FLJ45252 OS=Homo sapiens PE=1 SV=2	x	x	x		
1150	Isoform 2 of Phosphatidylinositol 3,4,5-trisphosphate 5-phosphatase 2 OS=Homo sapiens GN=INPPL1	x	x	x		
1151	Peptidyl-prolyl cis-trans isomerase B OS=Homo sapiens GN=PPIB PE=1 SV=2	x	x	x		
1152	Isoform 2 of Kinesin light chain 2 OS=Homo sapiens GN=KLC2	x	x	x		
1153	Neuropilin-1 (Fragment) OS=Homo sapiens GN=NRP1 PE=4 SV=1	x	x	x		
1154	Rab GDP dissociation inhibitor beta OS=Homo sapiens GN=GDI2 PE=1 SV=2	x	x		x	

1154	Rab GDP dissociation inhibitor beta OS=Homo sapiens GN=GDI2 PE=1 SV=2	x	x		x	
1155	NF-kappa-B inhibitor epsilon OS=Homo sapiens GN=NFKBIE PE=1 SV=3	x	x	x		
1156	Eukaryotic translation elongation factor 1 epsilon-1 OS=Homo sapiens GN=EEF1E1 PE=1 SV=1	x	x	x		
1157	Isocitrate dehydrogenase [NAD] subunit alpha, mitochondrial OS=Homo sapiens GN=IDH3A PE=1 SV=1	x	x	x		
1158	Isoform 2 of FAD-dependent oxidoreductase domain-containing protein 1 OS=Homo sapiens GN=FOXRED1	x	x		x	
1159	Isoform 2 of Splicing factor 1 OS=Homo sapiens GN=SF1	x	x	x		
1160	39S ribosomal protein L24, mitochondrial OS=Homo sapiens GN=MRPL24 PE=1 SV=1	x	x	x		
1161	Isoform 2 of General transcription factor 3C polypeptide 1 OS=Homo sapiens GN=GTF3C1	x	x	x		
1162	Exportin-T OS=Homo sapiens GN=XPOT PE=1 SV=2	x	x		x	
1163	Isoform 2 of Myosin light chain kinase, smooth muscle OS=Homo sapiens GN=MYLK	x	x	x		
1164	Endothelial protein C receptor OS=Homo sapiens GN=PROCR PE=1 SV=1	x	x	x		
1165	Isoform 2 of Mitochondrial ribonuclease P protein 3 OS=Homo sapiens GN=KIAA0391	x	x	x		x
1166	Monocarboxylate transporter 1 OS=Homo sapiens GN=SLC16A1 PE=1 SV=3	x	x		x	
1167	Isoform 2 of LisH domain-containing protein ARMC9 OS=Homo sapiens GN=ARMC9	x	x	x		
1168	UDP-glucose 6-dehydrogenase OS=Homo sapiens GN=UGDH PE=1 SV=1	x	x	x		
1169	Cytochrome c oxidase subunit 5A, mitochondrial OS=Homo sapiens GN=COX5A PE=1 SV=2	x	x	x		
1170	ATP-dependent Clp protease proteolytic subunit OS=Homo sapiens GN=CLPP PE=1 SV=1	x	x		x	
1171	Proteasome subunit alpha type-4 OS=Homo sapiens GN=PSMA4 PE=1 SV=1	x	x	x		
1172	Golgi-specific brefeldin A-resistance guanine nucleotide exchange factor 1 OS=Homo sapiens GN=GBF1 PE=1 SV=2	x	x		x	
1173	Guanylate kinase OS=Homo sapiens GN=GUK1 PE=1 SV=1	x	x	x		
1174	Vacuolar protein sorting-associated protein 18 homolog OS=Homo sapiens GN=VPS18 PE=1 SV=2	x	x	x		
1175	Calpain-2 catalytic subunit OS=Homo sapiens GN=CAPN2 PE=1 SV=6	x	x	x		
1176	Fascin OS=Homo sapiens GN=FSCN1 PE=1 SV=3	x	x	x		
1177	Isoform 2 of Oxysterol-binding protein-related protein 8 OS=Homo sapiens GN=OSBPL8	x	x		x	
1178	Mitochondrial import receptor subunit TOM34 OS=Homo sapiens GN=TOMM34 PE=1 SV=2	x	x	x		
1179	Crk-like protein OS=Homo sapiens GN=CRKL PE=1 SV=1	x	x		x	
1180	28S ribosomal protein S23, mitochondrial OS=Homo sapiens GN=MRPS23 PE=1 SV=1	x	x	x		
1181	Protein FAM49A OS=Homo sapiens GN=FAM49A PE=1 SV=1	x	x	x		
1182	Quinone oxidoreductase OS=Homo sapiens GN=CRYZ PE=1 SV=1	x	x	x		
1183	Thyroid receptor-interacting protein 6 OS=Homo sapiens GN=TRIP6 PE=1 SV=3	x	x		x	
1184	Protein kish-A OS=Homo sapiens GN=TMEM167A PE=1 SV=1	x	x		x	x
1185	Isoform 2 of Gelsolin OS=Homo sapiens GN=GSN	x	x	x		
1186	Nuclear pore complex protein Nup205 OS=Homo sapiens GN=NUP205 PE=1 SV=3	x	x	x		
1187	Isoform 2 of Cyclin-G-associated kinase OS=Homo sapiens GN=GAK	x	x	x		x
1188	Synemin OS=Homo sapiens GN=SYNM PE=1 SV=2	x	x		x	
1189	Serum paraoxonase/arylesterase 2 OS=Homo sapiens GN=PON2 PE=1 SV=1	x	x	x		
1190	NADH dehydrogenase [ubiquinone] iron-sulfur protein 7, mitochondrial OS=Homo sapiens GN=NDUFS7 PE=1 SV=1	x	x		x	
1191	Isoform 2 of Ethylmalonyl-CoA decarboxylase OS=Homo sapiens GN=ECHDC1	x	x	x		
1192	Cyclin-dependent kinase 6 OS=Homo sapiens GN=CDK6 PE=1 SV=1	x	x		x	

	A	B	C	D	E
1192	Cyclin-dependent kinase 6 OS=Homo sapiens GN=CDK6 PE=1 SV=1	x	x		x
1193	Isoform 2 of Exocyst complex component 3 OS=Homo sapiens GN=EXOC3	x	x	x	
1194	Annexin A6 OS=Homo sapiens GN=ANXA6 PE=1 SV=3	x	x		x
1195	PDZ and LIM domain protein 1 OS=Homo sapiens GN=PDLIM1 PE=1 SV=4	x	x		x
1196	Isoform 5 of Minor histocompatibility antigen H13 OS=Homo sapiens GN=HM13	x	x		x
1197	Isoform 2 of Protein arginine N-methyltransferase 5 OS=Homo sapiens GN=PRMT5	x	x	x	
1198	Ras-related protein Rab-2A OS=Homo sapiens GN=RAB2A PE=1 SV=1	x	x	x	
1199	Rho-related GTP-binding protein RhoC OS=Homo sapiens GN=RHOC PE=1 SV=1	x	x		x
1200	Inositol 1,4,5-trisphosphate receptor type 3 OS=Homo sapiens GN=ITPR3 PE=1 SV=2	x	x		x
1201	BET1 homolog (Fragment) OS=Homo sapiens GN=BET1 PE=1 SV=1	x	x	x	
1202	Peroxisomal biogenesis factor 3 OS=Homo sapiens GN=PEX3 PE=1 SV=1	x	x		x
1203	Chromosome 1 open reading frame 41, isoform CRA_b OS=Homo sapiens GN=HSPB11 PE=1 SV=1	x	x		x
1204	Uncharacterized protein (Fragment) OS=Homo sapiens PE=3 SV=1	x	x		x
1205	GTP-binding protein SAR1a OS=Homo sapiens GN=SAR1A PE=1 SV=1	x	x		x
1206	Isoform 2 of Receptor-interacting serine/threonine-protein kinase 2 OS=Homo sapiens GN=RIPK2	x	x	x	
1207	Isoform 2 of ATP-dependent RNA helicase DDX3Y OS=Homo sapiens GN=DDX3Y	x	x	x	
1208	ATPase ASNA1 OS=Homo sapiens GN=ASNA1 PE=1 SV=2	x	x	x	
1209	Isoform 2 of Rhotekin OS=Homo sapiens GN=RTKN	x	x		x
1210	Hydroxysteroid dehydrogenase-like protein 2 OS=Homo sapiens GN=HSDL2 PE=1 SV=1	x	x	x	
1211	Isoform 2 of Ubiquitin-like modifier-activating enzyme 1 OS=Homo sapiens GN=UBA1	x	x		x
1212	Vacuolar protein sorting-associated protein 37A (Fragment) OS=Homo sapiens GN=VPS37A PE=4 SV=1	x	x		x
1213	Eukaryotic translation initiation factor 1 OS=Homo sapiens GN=EIF1 PE=1 SV=1	x	x	x	
1214	Nuclear migration protein nudC OS=Homo sapiens GN=NUDC PE=1 SV=1	x	x	x	
1215	tRNA (guanine-N(7)-)-methyltransferase OS=Homo sapiens GN=METTL1 PE=1 SV=1	x	x	x	
1216	Gamma-glutamylcyclotransferase OS=Homo sapiens GN=GGCT PE=1 SV=1	x	x		x
1217	SEC23-interacting protein OS=Homo sapiens GN=SEC23IP PE=1 SV=1	x	x	x	
1218	Glutamate-rich WD repeat-containing protein 1 (Fragment) OS=Homo sapiens GN=GRWD1 PE=1 SV=1	x	x	x	
1219	Cytochrome b5 type B OS=Homo sapiens GN=CYB5B PE=1 SV=1	x	x	x	
1220	Pre-mRNA-splicing factor ATP-dependent RNA helicase PRP16 OS=Homo sapiens GN=DHX38 PE=1 SV=2	x	x	x	
1221	Isoform 2 of Nucleoporin NDC1 OS=Homo sapiens GN=NDC1	x	x	x	
1222	40S ribosomal protein S3 OS=Homo sapiens GN=RPS3 PE=1 SV=2	x	x	x	
1223	Glyceraldehyde-3-phosphate dehydrogenase OS=Homo sapiens GN=GAPDH PE=1 SV=3	x	x		x
1224	HLA class I histocompatibility antigen, B-44 alpha chain OS=Homo sapiens GN=HLA-B PE=1 SV=1	x	x		x
1225	Fumarylacetoacetate hydrolase domain-containing protein 2A OS=Homo sapiens GN=FAHD2A PE=1 SV=1	x	x		x
1226	Leucine-rich PPR motif-containing protein, mitochondrial OS=Homo sapiens GN=LRPPRC PE=1 SV=3	x	x	x	
1227	28S ribosomal protein S18b, mitochondrial OS=Homo sapiens GN=MRPS18B PE=1 SV=1	x	x	x	
1228	ATP-dependent RNA helicase SUPV3L1, mitochondrial OS=Homo sapiens GN=SUPV3L1 PE=1 SV=1	x	x	x	
1229	Obg-like ATPase 1 OS=Homo sapiens GN=OLA1 PE=1 SV=1	x	x		x
1230	Isoform 2 of G protein-regulated inducer of neurite outgrowth 1 OS=Homo sapiens GN=GPRIN1	x	x	x	

	A	B	C	D	E	F
1230	Isoform 2 of G protein-regulated inducer of neurite outgrowth 1 OS=Homo sapiens GN=GPRIN1	x	x	x		
1231	SRA stem-loop-interacting RNA-binding protein, mitochondrial OS=Homo sapiens GN=SLIRP PE=1 SV=1	x	x	x		
1232	Leupaxin OS=Homo sapiens GN=LPXN PE=1 SV=1	x	x		x	
1233	Ras GTPase-activating protein-binding protein 1 OS=Homo sapiens GN=G3BP1 PE=1 SV=1	x	x	x		
1234	Protein FAM3C (Fragment) OS=Homo sapiens GN=FAM3C PE=1 SV=1	x	x	x		x
1235	Synaptojanin-2-binding protein OS=Homo sapiens GN=SYNJ2BP PE=1 SV=2	x	x	x		
1236	Hexokinase-1 OS=Homo sapiens GN=HK1 PE=1 SV=1	x	x		x	
1237	Golgin subfamily A member 4 (Fragment) OS=Homo sapiens GN=GOLGA4 PE=1 SV=1	x	x		x	
1238	Nuclear pore complex protein Nup93 OS=Homo sapiens GN=NUP93 PE=1 SV=2	x	x	x		
1239	Isoform 2 of Coiled-coil domain-containing protein 51 OS=Homo sapiens GN=CCDC51	x	x	x		
1240	S-adenosylmethionine synthase isoform type-2 OS=Homo sapiens GN=MAT2A PE=1 SV=1	x	x	x		
1241	Chloride intracellular channel protein 1 OS=Homo sapiens GN=CLIC1 PE=1 SV=4	x	x		x	
1242	Isoform 2 of NEDD8-activating enzyme E1 catalytic subunit OS=Homo sapiens GN=UBA3	x	x	x		
1243	S-phase kinase-associated protein 1 OS=Homo sapiens GN=SKP1 PE=1 SV=2	x	x	x		
1244	Isoform 2 of Heat shock protein 75 kDa, mitochondrial OS=Homo sapiens GN=TRAP1	x	x	x		
1245	CD82 antigen (Fragment) OS=Homo sapiens GN=CD82 PE=4 SV=1	x	x		x	x
1246	Adenosylhomocysteinase OS=Homo sapiens GN=AHCY PE=1 SV=4	x	x		x	
1247	ADP-sugar pyrophosphatase OS=Homo sapiens GN=NUDT5 PE=1 SV=1	x	x		x	
1248	Isoform 2 of Filamin-C OS=Homo sapiens GN=FLNC	x	x	x		
1249	Pre-rRNA-processing protein TSR1 homolog OS=Homo sapiens GN=TSR1 PE=1 SV=1	x	x	x		
1250	S-formylglutathione hydrolase OS=Homo sapiens GN=ESD PE=1 SV=1	x	x	x		
1251	Isoform 2 of Inositol hexakisphosphate and diphosphoinositol-pentakisphosphate kinase 2 OS=Homo sapiens GN=PPI	x	x		x	
1252	Coiled-coil domain-containing protein 43 OS=Homo sapiens GN=CCDC43 PE=1 SV=1	x	x		x	x
1253	Isoform 2 of Probable asparagine--tRNA ligase, mitochondrial OS=Homo sapiens GN=NARS2	x	x		x	x
1254	Sulfatase-modifying factor 2 OS=Homo sapiens GN=SUMF2 PE=1 SV=1	x	x		x	
1255	Isoform 2 of Eukaryotic peptide chain release factor GTP-binding subunit ERF3A OS=Homo sapiens GN=GSPT1	x	x		x	
1256	Cartilage-associated protein OS=Homo sapiens GN=CRTAP PE=1 SV=1	x	x	x		
1257	Axin interactor, dorsalization-associated protein OS=Homo sapiens GN=AIDA PE=1 SV=1	x	x		x	
1258	Deoxyhypusine hydroxylase (Fragment) OS=Homo sapiens GN=DOHH PE=1 SV=1	x	x	x		
1259	Isoform 3 of Transmembrane protein 87A OS=Homo sapiens GN=TMEM87A	x	x		x	
1260	Acetyl-CoA acetyltransferase, cytosolic OS=Homo sapiens GN=ACAT2 PE=1 SV=2	x	x		x	
1261	Ubiquitin-conjugating enzyme E2 K OS=Homo sapiens GN=UBE2K PE=1 SV=3	x	x	x		
1262	U6 snRNA-associated Sm-like protein LSm2 OS=Homo sapiens GN=LSM2 PE=1 SV=1	x	x	x		
1263	Ubiquinol-cytochrome-c reductase complex assembly factor 2 OS=Homo sapiens GN=UQCC2 PE=1 SV=1	x	x	x		
1264	Proline-, glutamic acid- and leucine-rich protein 1 OS=Homo sapiens GN=PELP1 PE=1 SV=1	x	x	x		
1265	Diaphanous homolog 2 (Drosophila), isoform CRA_a OS=Homo sapiens GN=DIAPH2 PE=1 SV=1	x	x		x	
1266	Oral-facial-digital syndrome 1 protein OS=Homo sapiens GN=OFD1 PE=1 SV=1	x	x		x	
1267	Pyridoxal kinase OS=Homo sapiens GN=PDXK PE=1 SV=1	x	x		x	
1268	Isoform B of Histone acetyltransferase type B catalytic subunit OS=Homo sapiens GN=HAT1	x	x	x		

1268	Isoform B of Histone acetyltransferase type B catalytic subunit OS=Homo sapiens GN=HAT1	x	x	x		
1269	ATP-dependent RNA helicase DHX36 (Fragment) OS=Homo sapiens GN=DHX36 PE=1 SV=1	x	x	x		
1270	U6 snRNA-associated Sm-like protein LSm3 OS=Homo sapiens GN=LSM3 PE=1 SV=2	x	x	x		
1271	Guanine nucleotide-binding protein G(I)/G(S)/G(O) subunit gamma-12 OS=Homo sapiens GN=GNG12 PE=1 SV=3	x	x		x	
1272	Transmembrane emp24 domain-containing protein 9 OS=Homo sapiens GN=TMED9 PE=1 SV=2	x	x	x		
1273	Cullin-associated NEDD8-dissociated protein 1 OS=Homo sapiens GN=CAND1 PE=1 SV=2	x	x		x	
1274	Myosin phosphatase Rho-interacting protein (Fragment) OS=Homo sapiens GN=MPRIP PE=1 SV=1	x	x		x	
1275	Tubulin beta-6 chain OS=Homo sapiens GN=TUBB6 PE=1 SV=1	x	x	x		
1276	Rho GTPase-activating protein SYDE1 OS=Homo sapiens GN=SYDE1 PE=1 SV=1	x	x		x	x
1277	Probable ATP-dependent RNA helicase DDX17 OS=Homo sapiens GN=DDX17 PE=1 SV=2	x	x	x		
1278	DnaJ homolog subfamily A member 2 OS=Homo sapiens GN=DNAJA2 PE=1 SV=1	x	x	x		
1279	Transmembrane protein 109 OS=Homo sapiens GN=TMEM109 PE=1 SV=1	x	x		x	
1280	Isoform 2 of Membrane-associated progesterone receptor component 2 OS=Homo sapiens GN=PGRMC2	x	x	x		
1281	TraB domain-containing protein OS=Homo sapiens GN=TRABD PE=1 SV=1	x	x		x	
1282	Spermatogenesis-associated protein 22 OS=Homo sapiens GN=SPATA22 PE=1 SV=1	x	x		x	
1283	Isoform 2 of Reticulon-3 OS=Homo sapiens GN=RTN3	x	x		x	
1284	Nuclear fragile X mental retardation-interacting protein 2 OS=Homo sapiens GN=NUFIP2 PE=1 SV=1	x	x		x	
1285	Interleukin enhancer-binding factor 2 OS=Homo sapiens GN=ILF2 PE=1 SV=2	x	x	x		
1286	39S ribosomal protein L23, mitochondrial (Fragment) OS=Homo sapiens GN=MRPL23 PE=1 SV=1	x	x	x		
1287	Isocitrate dehydrogenase [NAD] subunit beta, mitochondrial OS=Homo sapiens GN=IDH3B PE=1 SV=2	x	x	x		
1288	WD repeat-containing protein 18 OS=Homo sapiens GN=WDR18 PE=1 SV=1	x	x	x		
1289	Isoform 2 of Serine/threonine-protein kinase N2 OS=Homo sapiens GN=PKN2	x	x	x		
1290	Lys-63-specific deubiquitinase BRCC36 (Fragment) OS=Homo sapiens GN=BRCC3 PE=1 SV=1	x	x	x		
1291	Isoform 2 of Putative pre-mRNA-splicing factor ATP-dependent RNA helicase DHX32 OS=Homo sapiens GN=DHX32	x	x		x	x
1292	DNA fragmentation factor subunit alpha OS=Homo sapiens GN=DFFA PE=1 SV=1	x	x	x		
1293	Isoform 2 of Coatomer subunit gamma-2 OS=Homo sapiens GN=COPG2	x	x	x		
1294	ATP-dependent 6-phosphofructokinase, liver type OS=Homo sapiens GN=PFKL PE=1 SV=6	x	x	x		
1295	Isoform 2 of Ubiquitin/ISG15-conjugating enzyme E2 L6 OS=Homo sapiens GN=UBE2L6	x	x		x	
1296	Prelamin-A/C OS=Homo sapiens GN=LMNA PE=1 SV=1	x	x		x	

786 cell line RNA sequencing data tables (349 out of the total 17,000 genes)

786_rnaseq_de

	baseMean	log2FoldChange	lfcSE	stat	pvalue	padj	ensemblid	symbol	entrezid
ENSG00000147642.16	52.5030719476877	3.72894587171267	0.573566500366001	6.5013313527432	7.96122543916221e-11	1.393612513125 34e-06	ENSG00000147642	SYBU	55638
ENSG00000265972.5	2733.60216120767	2.0950636527304	0.382056147123161	5.48365382550704	4.16629671947358e-08	0.000364655120371925	ENSG00000265972	TXNIP	10628
ENSG00000115165.9	21.1387544985696	3.81263300576385	0.825045459564989	4.62111870511243	3.81676298206691e-06	0.0222708120003604	ENSG00000115165	CYTIP	9595
ENSG00000169213.6	112.974487914343	-2.09201101027518	0.479838898769368	-4.35981954701987	1.30169742305591e-05	0.0389161857010064	ENSG00000169213	RAB3B	5865
ENSG00000104881.15	120.855455989846	-2.12601491536623	0.487703558043552	-4.35923601602344	1.30517291286644e-05	0.0389161857010064	ENSG00000104881	PPP1R13L	10848
ENSG00000125848.9	48.8431737689577	2.49035177578429	0.57634128633669	4.32096716793158	1.55346789396644e-05	0.0389161857010064	ENSG00000125848	FLRT3	23767
ENSG00000197172.10	117.360953594011	1.57511748283998	0.364561661142274	4.32057906995677	1.55620279866921e-05	0.0389161857010064	ENSG00000197172	MAGEA6	4105
ENSG00000179094.15	118.616348070615	-2.862615096917	0.706395021748833	-4.05242818646992	5.06887855873903e-05	0.110913398963408	ENSG00000179094	PER1	5187
ENSG00000166473.17	56.8329777216605	-3.20858007022575	0.807888383189261	-3.97156356866947	7.14024414910891e-05	0.138877748700168	ENSG00000166473	PKD1L2	114780
ENSG00000137752.23	80.713956587946	1.64674027763004	0.420221404446715	3.91874440522187	8.90114426081197e-05	0.149081417861969	ENSG00000137752	CASP1	834
ENSG00000166922.8	521.033458179774	-1.55955353929795	0.399744874209272	-3.90137219991343	9.56489543794428e-05	0.149081417861969	ENSG00000166922	SCG5	6447
ENSG00000057294.14	11.2309687014053	5.74783417112454	1.49039930427512	3.85657330531302	0.000114987625649284	0.149081417861969	ENSG00000057294	PKP2	5318
ENSG00000105877.17	36.7026119364163	1.99927067360901	0.519496564946957	3.84847717677044	0.00011885436788694	0.149081417861969	ENSG00000105877	DNAH11	8701
ENSG00000139329.4	267.332757465964	1.8808703897817	0.488829566347177	3.84770177433552	0.000119231068270069	0.149081417861969	ENSG00000139329	LUM	4060
ENSG00000205336.11	674.183128809868	-1.61807027822035	0.423541474632778	-3.82033490255769	0.000133270589531165	0.151513722681963	ENSG00000205336	ADGRG1	9289
ENSG00000103485.17	453.308697914739	-2.57926828095871	0.676821506062323	-3.8108544983516	0.000138487264376544	0.151513722681963	ENSG00000103485	QPRT	23475
ENSG00000073849.14	11.5272356957513	4.32642193597919	1.14540619070226	3.77719447572272	0.000158604885470015	0.161517716202903	ENSG00000073849	ST6GAL1	6480
ENSG00000151632.17	6.6693960899868	-6.42813035309671	1.70874301797189	-3.76190584861981	0.000168623527745851	0.161517716202903	ENSG00000151632	AKR1C2	1646
ENSG00000112137.17	288.313877074 19	-2.66384251310836	0.709947582959815	-3.7521678741445	0.000175312002733799	0.161517716202903	ENSG00000112137	PHACTR1	221692
ENSG00000118596.11	44.5334222983833	1.85282885253006	0.49706098788542	3.72756844268206	0.000193336066611758	0.169217392301941	ENSG00000118596	SLC16A7	9194
ENSG00000078114.18	120.088004520083	2.18755065065365	0.59320988738599	3.68765035305329	0.000226334360706647	0.182455644605237	ENSG00000078114	NEBL	10529
ENSG00000214145.6	134.991635537925	-2.01126264390582	0.548706682324864	-3.66546045217478	0.00024689396443178	0.182455644605237	ENSG00000214145	LINC00887	100131551
ENSG00000162631.18	469.088841484565	1.00078167750977	0.273046324001544	3.6652450135315	0.000247101901353621	0.182455644605237	ENSG00000162631	NTNG1	22854
ENSG00000109472.13	1423.77074912771	1.7750043415906	0.484695386356759	3.66210282076858	0.000250153411626718	0.182455644605237	ENSG00000109472	CPE	1363
ENSG00000233725.7	10.1506341891561	-6.01589801133236	1.65100065434658	-3.64378899275075	0.000268653692755166	0.184804123933707	ENSG00000233725	NA	NA
ENSG00000184163.3	37.2298524317138	-3.11307932747367	0.859796622426498	-3.62071593010915	0.000293788942168536	0.184804123933707	ENSG00000184163	C1QTNF12	388581
ENSG00000213626.11	39.1899698741111	2.47170901985254	0.684357953448116	3.61171957949624	0.000304173379088446	0.184804123933707	ENSG00000213626	LBH	81606
ENSG00000095303.15	139.402377661005	-2.6753536183505	0.74092255369949	-3.61084121033845	0.000305205486711397	0.184804123933707	ENSG00000095303	PTGS1	5742
ENSG00000110921.13	173.640986994291	-1.39843230053718	0.387373946384718	-3.61003189189274	0.000306159359844473	0.184804123933707	ENSG00000110921	MVK	4598
ENSG00000135821.18	20.6883699745668	3.5136117406612	0.979811691826415	3.58600715828534	0.000335779744807555	0.195927481095209	ENSG00000135821	GLUL	2752
ENSG00000106258.14	53.3087482282362	2.30493972796828	0.644984631674038	3.57363511435286	0.000352059445915795	0.198800019379226	ENSG00000106258	CYP3A5	1577
ENSG00000143365.17	407.444764143875	-2.37876455383213	0.667329017699862	-3.56460530074237	0.000364404135836938	0.19934044993205	ENSG00000143365	RORC	6097
ENSG00000007516.13	106.004983837745	-1.74857506131645	0.49216045581914	-3.55285566046984	0.000381073496286573	0.202142168257468	ENSG00000007516	BAIAP3	8938
ENSG00000099860.8	1735.45012565317	-1.99985469933807	0.564582106079675	-3.54218576501581	0.000396825909023053	0.204306986395546	ENSG00000099860	GADD45B	4616
ENSG00000142619.4	25.7002492593326	-3.8810375395182	1.112330110212	-3.48910589031749	0.000484639124504668	0.240100838180041	ENSG00000142619	PADI3	51702
ENSG00000204177.10	49.6823208853992	1.8781829444902	0.539071428294425	3.48410775624411	0.000493780644072065	0.240100838180041	ENSG00000204177	BMS1P1	399761
ENSG00000136859.9	29.1701546303095	-2.91625981005262	0.841028854667438	-3.46749079281682	0.000525341738725611	0.241522381791777	ENSG00000136859	ANGPTL2	23452
ENSG00000055163.19	196.475315845495	1.13585700514275	0.32835119920867	3.45927472742654	0.000541632142536284	0.241522381791777	ENSG00000055163	CYFIP2	26999
ENSG00000245685.6	14.7239754984694	2.77765945957189	0.804978834506001	3.45059937044988	0.000559343209406334	0.241522381791777	ENSG00000245685	NA	NA
ENSG00000105855.9	367.84743021226	1.91587778587709	0.555611159417792	3.44823489125863	0.000564263093521415	0.241522381791777	ENSG00000105855	ITGB8	3696
ENSG00000131650.13	12.3541290665319	-3.96920247466067	1.15131029082649	-3.44755232910434	0.000565690811394622	0.241522381791777	ENSG00000131650	KREMEN2	79412
ENSG00000035664.11	92.7698159872779	1.63009599522836	0.47379196680754	3.4405310968274	0.000580573717552561	0.241974831565656	ENSG00000035664	DAPK2	23604
ENSG00000196482.16	12.0021872444129	4.38095438186128	1.27743613069994	3.42948995771777	0.000604716810536014	0.242650122180893	ENSG00000196482	ESRRG	2104
ENSG00000224417.2	9.27044800199835	-5.88210474592614	1.71631773801199	-3.42716538765099	0.000609917473633778	0.242650122180893	ENSG00000224417	NA	NA
ENSG00000261305.1	39.5968679541167	-2.82573512991159	0.826707334522512	-3.41805982832325	0.000630692415651158	0.2453393496883	ENSG00000261305	NA	NA
ENSG00000214274.9	98.3771772583372	-2.1556890628146	0.633483175218217	-3.40291446899443	0.000666711481610286	0.253712706208436	ENSG00000214274	ANG	283
ENSG00000064042.17	83.8831770970911	1.62164573942691	0.477895851302836	3.3933036560288	0.000690550430069714	0.255720692882448	ENSG00000064042	LIMCH1	22998
ENSG00000185885.15	105.151243213318	-2.20780236132899	0.651440628407164	-3.38910756414946	0.000701204984767639	0.255720692882448	ENSG00000185885	IFITM1	8519
ENSG00000184304.14	70.901115561012	1.66565844987427	0.495313487804572	3.36283685158088	0.00077145941963023	0.275599941645453	ENSG00000184304	PRKD1	5587
ENSG00000155465.18	317.374118479188	-2.41949179139169	0.721025414230044	-3.3556262284809 7	0.000791855103543328	0.277228471750519	ENSG00000155465	SLC7A7	9056
ENSG00000234182.1	5.06590136662587	-6.031266900649	1.80690042445876	-3.33790773360165	0.000844117742114448	0.289731001484577	ENSG00000234182	NA	NA
ENSG00000250786.1	787.647871231721	-2.06171480967277	0.619362847078774	-3.32876732822586	0.000872312450456728	0.290017197733785	ENSG00000250786	SNHG18	100505806
ENSG00000241135.5	32.7111514857305	-2.93591775037645	0.882470772847823	-3.32692916378629	0.000878086916874642	0.290017197733785	ENSG00000241135	LINC00881	100498859
ENSG00000261716.1	20.9394757833627	2.08413643808147	0.628627570485 28	3.31537548770345	0.000915201018263435	0.292592379582612	ENSG00000261716	NA	NA
ENSG00000100628.11	30.2996134871397	-3.34874217248521	1.01044621382319	-3.3141221439335	0.000919313389148453	0.292592379582612	ENSG00000100628	ASB2	51676
ENSG00000152229.18	42.2462795866364	-2.37360546809056	0.718764898995818	-3.3023391534655	0.000958820609398906	0.29971704942014	ENSG00000152229	PSTPIP2	9050

ENSG00000152229.18	42.2462795866364	-2.37360546809056	0.718764898995818	-3.3023391534655	0.000958820609398906	0.29971704942014	ENSG00000152229	PSTPIP2	9050
ENSG00000254109.5	45.4169764827005	-1.68847644967433	0.51262519473978	-3.29378358106538	0.000988485745061858	0.303569174865049	ENSG00000254109	RBPMS-AS1	100128750
ENSG00000120451.10	271.091003467868	1.28421479552264	0.391434905065065	3.28078763264399	0.00103517655017014	0.307820501545226	ENSG00000120451	SNX19	399979
ENSG00000171425.9	374.270561670176	-1.45421329093014	0.443862422492669	-3.2762703424261	0.00105187821423151	0.307820501545226	ENSG00000171425	ZNF581	51545
ENSG00000188372.14	239.019065345422	-1.57439240553738	0.480670167328975	-3.27541110838245	0.00105508312440523	0.307820501545226	ENSG00000188372	ZP3	7784
ENSG00000120278.16	33.246094414043	2.45161714095516	0.753604545487084	3.25318783656033	0.00114118034287494	0.327481342656162	ENSG00000120278	PLEKHG1	57480
ENSG00000041982.15	2674.11529879155	1.71676872876425	0.530448290902368	3.23644878908702	0.00121026940242014	0.33997112198746	ENSG00000041982	TNC	3371
ENSG00000254682.1	499.163359479469	-1.77639781327001	0.55008392813567	-3.22932142244281	0.0012408434860462	0.33997112198746	ENSG00000254682	NA	NA
ENSG00000186480.12	916.783954961874	-1.63771015141963	0.507214381601616	-3.22883224692541	0.0012429678267465	0.33997112198746	ENSG00000186480	INSIG1	3638
ENSG00000128242.12	972.158132336752	-2.19177588848312	0.683336259717543	-3.20746317397103	0.00133911203962366	0.357672307313122	ENSG00000128242	GAL3ST1	9514
ENSG00000181126.13	75.5692951189948	-1.97288459949836	0.615479656818645	-3.20544241818813	0.00134855025893551	0.357672307313122	ENSG00000181126	HLA-V	352962
ENSG00000095596.11	4.2213221113249	-5.77210958378498	1.81260062669886	-3.18443539010425	0.00145036684023618	0.378935396094541	ENSG00000095596	CYP26A1	1592
ENSG00000163931.15	9835.08612885077	-1.60352772908743	0.507639289671027	-3.1587935798401	0.00158423656195058	0.404224784044906	ENSG00000163931	TKT	7086
ENSG00000100302.6	122.928696122901	-2.44881928917836	0.775675239265877	-3.15701619081718	0.00159392495834424	0.404224784044906	ENSG00000100302	RASD2	23551
ENSG00000110013.12	166.913853923485	1.14860490592918	0.364466172140657	3.15147191626306	0.00162449784004731	0.404224784044906	ENSG00000110013	SIAE	54414
ENSG00000082497.11	40.8875104809548	1.59732527275515	0.50728367411236	3.14878115395717	0.00163952925833695	0.404224784044906	ENSG00000082497	SERTAD4	56256
ENSG00000198203.9	126.161963520435	-1.3223378306311	0.421556226192671	-3.13680061749753	0.00170802236524466	0.410723382367051	ENSG00000198203	SULT1C2	6819
ENSG00000127415.12	80.3279109252316	2.45356585364566	0.782392275641479	3.13597913736303	0.00171281387676634	0.410723382367051	ENSG00000127415	IDUA	3425
ENSG00000226608.3	712.297838982405	-1.10512205776147	0.352879334782158	-3.13172789912362	0.00173780852979126	0.411085652891839	ENSG00000226608	NA	NA
ENSG00000148926.9	17638.5564906988	-1.81525690411557	0.582400493734339	-3.11685330566288	0.0018279250434436	0.418918354784134	ENSG00000148926	ADM	133
ENSG00000131435.12	19.4615070550051	-3.63312159752086	1.16638057334202	-3.11486806326935	0.00184027203547527	0.418918354784134	ENSG00000131435	PDLIM4	8572
ENSG00000076706.16	109.805046786313	-1.63315247928486	0.525837432665469	-3.10581251510835	0.00189756987011158	0.418918354784134	ENSG00000076706	MCAM	4162
ENSG00000182054.9	3188.20482232501	-1.7513160163295	0.564216337514177	-3.10397962605167	0.0019093647882531	0.418918354784134	ENSG00000182054	IDH2	3418
ENSG00000274750.2	57.7850601396865	1.49248244622011	0.481428060261456	3.10011519770902	0.0019344539006726	0.418918354784134	ENSG00000274750	HIST1H3E	8353
ENSG00000163545.8	245.081229838122	-1.98773925989655	0.641327842798966	-3.09941207483118	0.00193905121913939	0.418918354784134	ENSG00000163545	NUAK2	81788
ENSG00000178078.11	117.839532817398	-1.38063742645618	0.445801896163182	-3.09697522226511	0.00195506214549901	0.418918354784134	ENSG00000178078	STAP2	55620
ENSG00000127863.15	110.007956185936	-2.14422088216035	0.692607133110069	-3.09586889833488	0.00196237104211934	0.418918354784134	ENSG00000127863	TNFRSF19	55504
ENSG00000116176.6	6.67704265682018	-4.40383332832852	1.42890444473124	-3.08196488895156	0.00205639091576827	0.429574031297902	ENSG00000116176	TPSG1	25823
ENSG00000168386.18	60.3660034177616	1.60748076341814	0.521736442154668	3.0810206716241	0.00206292326373574	0.429574031297902	ENSG00000168386	FILIP1L	11259
ENSG00000172893.15	2017.34419516505	-1.44866832489786	0.470695260671881	-3.07772022779664	0.00208590646445711	0.429574031297902	ENSG00000172893	DHCR7	1717
ENSG00000283175.1	9.08079779085977	3.47041293684237	1.12897594316582	3.07394764064753	0.00211246504184033	0.4299848902025	ENSG00000283175	LOC10192913	101929130
ENSG00000162745.10	245.310273994757	-1.89547546303722	0.617401007744701	-3.07008806150347	0.00213995664097607	0.430574034486046	ENSG00000162745	OLFML2B	25903
ENSG00000125827.8	683.726611532301	1.16495603605007	0.381429774572799	3.05418222097323	0.00225674959989115	0.44891365620562	ENSG00000125827	TMX4	56255
ENSG00000141564.13	237.298658315311	-1.0483653283325	0.344386136649033	-3.04415659275187	0.00233333651773363	0.457697875570374	ENSG00000141564	RPTOR	57521
ENSG00000104419.14	9004.64639354505	-0.998147871246512	0.328164825614987	-3.04160529507074	0.0023532024450919	0.457697875570374	ENSG00000104419	NDRG1	10397
ENSG00000198846.5	226.539583419361	-1.13341226741145	0.373921182437544	-3.03115287564851	0.00243621865123345	0.458258916739194	ENSG00000198846	TOX	9760
ENSG00000112379.8	48.3579947100862	1.86631041699245	0.617458412531647	3.02256861209547	0.00250639256987298	0.458258916739194	ENSG00000112379	ARFGEF3	57221
ENSG00000136943.10	119.964982617263	-1.50632918771548	0.498961301174667	-3.01892989329883	0.00253669224606067	0.458258916739194	ENSG00000136943	CTSV	1515
ENSG00000116337.15	2962.47267710146	-1.72488391102569	0.57264034682894	-3.01215923847738	0.0025939648662722	0.458258916739194	ENSG00000116337	AMPD2	271
ENSG00000104808.7	35.1545531501886	-2.11710180853847	0.703179378464623	-3.01075639214721	0.00260597833923575	0.458258916739194	ENSG00000104808	DHDH	27294
ENSG00000169418.9	23.1439469301654	-3.43156558165989	1.13994693934499	-3.01028535909896	0.0026100234907554	0.458258916739194	ENSG00000169418	NPR1	4881
ENSG00000238120.1	12.7416014172386	-2.64779020049574	0.879983732619196	-3.00890812221588	0.00262188391929141	0.458258916739194	ENSG00000238120	LINC01589	100506737
ENSG00000112473.17	520.091118840958	-1.32130594300672	0.439359234530154	-3.00734760797668	0.00263538221622061	0.458258916739194	ENSG00000112473	SLC39A7	7922
ENSG00000141738.13	6.28438027531305	-4.38228778193958	1.46045804362392	-3.00062559213653	0.0026942562047521	0.458258916739194	ENSG00000141738	GRB7	2886
ENSG00000167608.11	15.6068893633054	-2.73445196784466	0.911927512238493	-2.99854092693447	0.00271275718610638	0.458258916739194	ENSG00000167608	TMC4	147798
ENSG00000250510.7	3.96618163508067	5.19880938921899	1.73490845411934	2.99659003728699	0.00273017600697772	0.458258916739194	ENSG00000250510	GPR162	27239
ENSG00000101194.17	655.250520607565	-1.53002123015427	0.510748959473057	-2.99564238316375	0.00273867410486104	0.458258916739194	ENSG00000101194	SLC17A9	63910
ENSG00000271447.5	53.461617360818	2.25908432897732	0.754319845175171	2.99486264802261	0.00274568450185943	0.458258916739194	ENSG00000271447	MMP28	79148
ENSG00000169583.12	187.498237889946	-2.00370945878631	0.669209293202249	-2.99414470052906	0.0027521538744288	0.458258916739194	ENSG00000169583	CLIC3	9022
ENSG00000273329.1	77.7533388073728	1.2002196962231	0.40114873334356	2.99195683909885	0.00277195450153266	0.458258916739194	ENSG00000273329	NA	NA
ENSG00000119280.16	2239.39742716139	-1.26408157529538	0.422539771658608	-2.99162743978738	0.00277494688228247	0.458258916739194	ENSG00000119280	C1orf198	84886
ENSG00000234545.7	137.277339084721	1.02888280938733	0.344677415051993	2.98506013001207	0.00283522584504256	0.461619234247376	ENSG00000234545	FAM133B	257415
ENSG00000173237.4	115.61527847974	-1.46499342970736	0.491002050176365	-2.98368088113104	0.00284803640666762	0.461619234247376	ENSG00000173237	C11orf86	254439
ENSG00000146166.16	9.46315674212769	-4.95678843492279	1.6655345364847	-2.97609465690496	0.00291944735989649	0.468708056723463	ENSG00000146166	LGSN	51557
ENSG00000213700.3	21.9428494529073	2.0189129591888	0.67919675745553	2.97250087993976	0.00295384363477327	0.468708056723463	ENSG00000213700	NA	NA
ENSG00000113273.16	66.9498462379914	1.2326846150726	0.415144742581429	2.96928875314088	0.00298489965126071	0.468708056723463	ENSG00000113273	ARSB	411
ENSG00000118762.7	192.355586732304	0.982830324909947	0.331158667131779	2.96785324516011	0.0029988747416754	0.468708056723463	ENSG00000118762	PKD2	5311
ENSG00000169432.15	976.382139010015	1.18906356103824	0.401250287829061	2.96339615722543	0.00304264703600261	0.471341029780758	ENSG00000169432	SCN9A	6335
ENSG00000138613.13	59.573089018272	-1.39388492968763	0.47178950272404	-2.95446363609101	0.00313213063162625	0.480946900935241	ENSG00000138613	APH1B	83464
ENSG00000135549.14	96.3243689365625	-1.37270607281947	0.466773265616511	-2.94084124763746	0.00327322240649283	0.498241375875278	ENSG00000135549	PKIB	5570
ENSG00000271755.1	21.5557076320303	-3.08505256771335	1.05032130581207	-2.93724648889999	0.00331140789217235	0.499708578900664	ENSG00000271755	NA	NA
ENSG00000166897.14	10.8803695828437	-2.71890969478692	0.927928931920527	-2.9300839765386	0.00338870411916367	0.50700227013641	ENSG00000166897	ELFN2	114794
ENSG00000129354.11	61.6494329857803	-2.69799473771661	0.922774452030432	-2.92378568975339	0.00345802736808001	0.512764766573948	ENSG00000129354	AP1M2	10053
ENSG00000130045.15	25.9230334920432	-2.44214204611089	0.836611330922285	-2.91908793946008	0.00351057174341657	0.512764766573948	ENSG00000130045	NXNL2	158046
ENSG00000112902.11	275.791235380321	-1.57351243431714	0.539513783554438	-2.91653796859552	0.00353939641515806	0.512764766573948	ENSG00000112902	SEMA5A	9037

ENSG00000132823.10	2248.53972084174	-1.27685515148784	0.460063592139529	-2.77538838826566	0.00551358203808137	0.533233445174665	ENSG00000132823	OSER1	51526
ENSG00000019549.10	762.386334130145	-1.56566207528593	0.564574003475171	-2.77317422631697	0.00555123911443108	0.533925498341297	ENSG00000019549	SNAI2	6591
ENSG00000105613.9	87.5402121456363	-1.35033727648468	0.488389151212987	-2.76487975445587	0.0056943782387396	0.536523830859162	ENSG00000105613	MAST1	22983
ENSG00000066468.22	45.6083921956277	-2.52833008976009	0.914521386810747	-2.76464840103659	0.00569841803780454	0.536523830859162	ENSG00000066468	FGFR2	2263
ENSG00000067715.13	6.33777004011237	4.00740752432651	1.44975569858516	2.76419504902612	0.00570634178207938	0.536523830859162	ENSG00000067715	SYT1	6857
ENSG00000166407.13	18.4984497235476	-1.97741247586738	0.715734189192175	-2.76277493198868	0.00573122712833909	0.536523830859162	ENSG00000166407	LMO1	4004
ENSG00000153294.11	85.9276968875491	1.53082818314255	0.55472495707645	2.75961656964277	0.00578692374153624	0.536523830859162	ENSG00000153294	ADGRF4	221393
ENSG00000164674.15	673.768373545133	-1.69270087729527	0.613488727131643	-2.75913933286023	0.00579538195636638	0.536523830859162	ENSG00000164674	SYTL3	94120
ENSG00000180573.9	1109.13942106897	1.0795292002799	0.3913838336449	2.75823656339201	0.00581141250994038	0.536523830859162	ENSG00000180573	HIST1H2AC	8334
ENSG00000087086.14	162089.080203713	-1.05102918323505	0.381318980755813	-2.75629915183295	0.0058459503236691	0.536523830859162	ENSG00000087086	FTL	2512
ENSG00000125731.12	13.0678379689642	-3.27988184803536	1.19034966072967	-2.75539360932386	0.00586215659777339	0.536523830859162	ENSG00000125731	SH2D3A	10045
ENSG00000229656.6	58.8356124621463	-1.2553621449194	0.455809977345647	-2.75413485292676	0.00588475152956065	0.536523830859162	ENSG00000229656	NA	NA
ENSG00000162366.7	1959.1490180602	-3.24373907469034	1.17850910862485	-2.75240899790355	0.00591585857044933	0.53656530712806	ENSG00000162366	PDZK1IP1	10158
ENSG00000125846.15	515.660681666319	-1.25396496743522	0.457622613071531	-2.74017264797887	0.00614069184410925	0.547747401733416	ENSG00000125846	ZNF133	7692
ENSG00000273319.1	110.636157318515	1.25476688751387	0.458042768751779	2.73940988290953	0.00615495858185328	0.547747401733416	ENSG00000273319	NA	NA
ENSG00000153823.18	31.271145393144	1.47565633286842	0.538688134222154	2.73935184222912	0.00615604539429263	0.547747401733416	ENSG00000153823	PID1	55022
ENSG00000107317.12	10.795029014333	-2.28370478824311	0.833961221510518	-2.73838246831998	0.00617422249617071	0.547747401733416	ENSG00000107317	PTGDS	5730
ENSG00000117228.9	892.712580828779	1.15079032661622	0.420419086047341	2.73724567891438	0.00619560043091781	0.547747401733416	ENSG00000117228	GBP1	2633
ENSG00000205808.5	88.5204538614972	1.38702234123353	0.507339990338357	2.73391092294635	0.00625869736082059	0.54953522915451	ENSG00000205808	PLPP6	403313
ENSG00000085563.14	79.238731801725	1.09261218014834	0.399804686736563	2.73286486225779	0.00627860873069992	0.54953522915451	ENSG00000085563	ABCB1	5243
ENSG00000187193.8	5115.48613694713	-1.53634956576059	0.563088669045532	-2.72843274996955	0.00636360641771874	0.5518409823346	ENSG00000187193	MT1X	4501
ENSG00000224897.6	83.4004553622649	1.35510158761162	0.496700795282326	2.72820498876265	0.00636800219546353	0.5518409823346	ENSG00000224897	POT1-AS1	401398
ENSG00000134013.15	11426.8212605188	-1.80116908724862	0.662682502782426	-2.71799704939544	0.00656784238331151	0.562480595901652	ENSG00000134013	LOXL2	4017
ENSG00000229989.3	68.6123702824262	1.78999503283583	0.658684493883979	2.71753024316847	0.00657711442244678	0.562480595901652	ENSG00000229989	NA	NA
ENSG00000162105.18	92.1388071988381	-1.12378954928194	0.413610409550683	-2.71702433819966	0.00658717635874543	0.562480595901652	ENSG00000162105	SHANK2	22941
ENSG00000213064.9	352.510042585917	0.836743314527442	0.308249178458416	2.71450298330745	0.006637502498457	0.564028966133733	ENSG00000213064	SFT2D2	375035
ENSG00000132879.13	173.187784722296	-1.03691379705394	0.382458403501024	-2.71118058215489	0.00670441020795675	0.566652943768623	ENSG00000132879	FBXO44	93611
ENSG00000269190.5	530.85580492555	-1.35163825356069	0.498803317436888	-2.70976195688937	0.00673315123129813	0.566652943768623	ENSG00000269190	FBXO17	115290
ENSG00000143320.8	264.896033089435	-1.92859701553463	0.712525809834733	-2.70670478025485	0.00679546573640549	0.567052348907224	ENSG00000143320	CRABP2	1382
ENSG00000173432.10	40.2536244242186	-2.41017086408236	0.890560666183469	-2.70635225156668	0.0068026845627259	0.567052348907224	ENSG00000173432	SAA1	6288
ENSG00000277268.1	35.3079482522316	-1.51622019963961	0.561655766547432	-2.69955422866929	0.0069432439070432	0.573251828443144	ENSG00000277268	LHX1-DT	102723471
ENSG00000186184.17	625.05002409366	-0.987515922309469	0.365985465931946	-2.6982380838399	0.00697075669816819	0.573251828443144	ENSG00000186184	POLR1D	51082
ENSG00000130762.14	170.360665367845	-1.48335887176065	0.54982217276639	-2.69788841780832	0.00697808258729535	0.573251828443144	ENSG00000130762	ARHGEF16	27237
ENSG00000141480.17	373.673460225973	-1.2703811476659	0.471241120887796	-2.69581980722005	0.00702156389601852	0.573251828443144	ENSG00000141480	ARRB2	409
ENSG00000100031.18	922.970673671464	-1.81378950512219	0.673043078516598	-2.69490848805669	0.00704079652186666	0.573251828443144	ENSG00000100031	GGT1	2678
ENSG00000228035.1	30.7050268780759	-5.27966242074207	1.963141988188606	-2.68939407819586	0.00715818599274191	0.578848018328666	ENSG00000228035	NA	NA
ENSG00000283415.1	3.51077210402352	5.01455286342597	1.86615132699121	2.68710944868063	0.00720733321759307	0.578848018328666	ENSG00000283415	NA	NA
ENSG00000188641.13	559.128196839923	0.959115333668766	0.357053586626435	2.68619436855632	0.00722710332864309	0.578848018328666	ENSG00000188641	DPYD	1806
ENSG00000163817.15	3.77253084889243	5.14868392540446	1.917370732816372	2.68528346515528	0.0072468315260511	0.578848018328666	ENSG00000163817	SLC6A20	54716
ENSG00000167261.13	2.91084609740027	-5.25878498100684	1.959314139372126	-2.68399276835432	0.00727486798242253	0.578848018328666	ENSG00000167261	DPEP2	64174
ENSG00000092421.16	495.266320519154	-1.66173530129645	0.619993558615123	-2.68024607385965	0.00735680568531692	0.582718929961415	ENSG00000092421	SEMA6A	57556
ENSG00000226674.9	60.8984121477477	1.16187964591723	0.434443996282427	2.67440603589769	0.00748617517700046	0.590295029159428	ENSG00000226674	TEX41	401014
ENSG00000100417.11	1019.61932403043	-1.22310908628188	0.45816046140022	-2.6696085527412	0.00759397216977371	0.596109788483806	ENSG00000100417	PMM1	5372
ENSG00000160180.15	28.0405351798203	1.61828652691812	0.606820285983249	2.66682997305531	0.00765703987088472	0.596576132845472	ENSG00000160180	TFF3	7033
ENSG00000112539.14	3.37546535925789	4.9982670464953	1.87486801383057	2.66593008661088	0.00767756574422001	0.596576132845472	ENSG00000112539	C6orf118	168090
ENSG00000146733.13	1520.61830480524	0.925367798998988	0.347248845584005	2.66485493261381	0.0077021540144574	0.596576132845472	ENSG00000146733	PSPH	5723
ENSG00000171766.15	23.7497459939706	1.54150217242714	0.578861915243582	2.66298772096361	0.00774502402884573	0.597253945484337	ENSG00000171766	GATM	2628
ENSG00000135678.11	45.009513355628	-1.32914963184358	0.499799585580816	-2.65936521395667	0.00782880479713075	0.601066789358657	ENSG00000135678	CPM	1368
ENSG00000137171.14	655.254425304256	-1.1342617464057	0.427304456273855	-2.65445803279609	0.00794359199878506	0.605281233983656	ENSG00000137171	KLC4	89953
ENSG00000075618.17	3306.53297245442	-0.993601267407861	0.374456548922377	-2.65344876533012	0.007967386503201	0.605281233983656	ENSG00000075618	FSCN1	6624
ENSG00000105854.12	2463.48326007244	0.831103405458928	0.3133490877661	2.65232431785251	0.00799397164623383	0.605281233983656	ENSG00000105854	PON2	5445
ENSG00000257354.2	23.8584552845284	2.51606924670126	0.949352239032019	2.65030106134968	0.00804200731379577	0.605281233983656	ENSG00000257354	NA	NA
ENSG00000182557.7	40.6080009766014	-1.53006458195543	0.577555082260552	-2.6492097965215	0.00806802300138415	0.605281233983656	ENSG00000182557	SPNS3	201305
ENSG00000167925.15	379.546059135122	-0.831504848824019	0.314108125387878	-2.64719305747736	0.00811630029886715	0.605281233983656	ENSG00000167925	GHDC	84514
ENSG00000090020.10	84.9121816551583	1.37131896187687	0.518104498637259	2.64679995152286	0.00812574064473916	0.605281233983656	ENSG00000090020	SLC9A1	6548
ENSG00000171914.16	47.934995128561	-1.40499606255966	0.531292459836057	-2.64448711166201	0.0081814822355699	0.606851044634115	ENSG00000171914	TLN2	83660
ENSG00000263272.1	9.19332121407555	2.66282817524598	1.00890025508076	2.63933739914937	0.00830682614582221	0.61079934559964	ENSG00000263272	NA	NA

ENSG00000263272.1	9.19332121407555	2.66282817524598	1.00890025508076	2.63933739914937	0.00830682614582221	0.61079934559964	ENSG00000263272	NA	NA
ENSG00000154639.18	1342.75466110611	0.777649206898302	0.294684244341856	2.63892359985209	0.00831697219981086	0.61079934559964	ENSG00000154639	CXADR	1525
ENSG00000131370.15	35.279712228408	-1.88996159071379	0.71645100950981	-2.6379495117285	0.00834089990329114	0.61079934559964	ENSG00000131370	SH3BP5	9467
ENSG00000215424.9	54.6993143091856	1.19021043033143	0.451692181513508	2.63500339178626	0.00841364424086526	0.61079934559964	ENSG00000215424	MCM3AP-AS1	114044
ENSG00000112511.17	474.215160401311	-0.909833407368125	0.345343403724657	-2.63457589621007	0.00842424678938677	0.61079934559964	ENSG00000112511	PHF1	5252
ENSG00000196305.17	12259.7184388917	0.719944654770923	0.27359737459156	2.63140191255743	0.00850334091470678	0.61079934559964	ENSG00000196305	IARS	3376
ENSG00000145476.15	131.02751244167	1.37444452095477	0.522406245204743	2.63098792093515	0.00851370618768713	0.61079934559964	ENSG00000145476	CYP4V2	285440
ENSG00000144619.14	26.8762540804218	2.2705603539784	0.863124920990453	2.6306277327422	0.00852273355180061	0.61079934559964	ENSG00000144619	CNTN4	152330
ENSG00000198246.8	462.21240167196	-1.85446463036689	0.706455597627532	-2.62502645119478	0.00866422360978239	0.61079934559964	ENSG00000198246	SLC29A3	55315
ENSG00000167513.8	41.709880664622	-1.66496948666986	0.634294996886627	-2.62491347849533	0.00866709880675486	0.61079934559964	ENSG00000167513	CDT1	81620
ENSG00000188707.5	204.589326785463	-1.64370056719637	0.626333282900372	-2.62432256447376	0.00868215168744606	0.61079934559964	ENSG00000188707	ZBED6CL	113763
ENSG00000168528.11	4211.31841591761	-0.850071492419193	0.324073612138795	-2.62308148697748	0.00871384285750233	0.61079934559964	ENSG00000168528	SERINC2	347735
ENSG00000141391.13	256.112444213755	-1.02397410948046	0.390401360056153	-2.62287536429991	0.0087191162413922	0.61079934559964	ENSG00000141391	PRELID3A	10650
ENSG00000243477.5	205.798580032211	-0.920192335678034	0.35097858306379	-2.62179055954189	0.00874691660658859	0.61079934559964	ENSG00000243477	NAT6	24142
ENSG00000111674.8	2368.88080780109	-0.852938775326257	0.325380893363046	-2.62135482667872	0.00875810544104597	0.61079934559964	ENSG00000111674	ENO2	2026
ENSG00000179406.7	37.890779728446	1.48945355192854	0.568858346673655	2.61832064280674	0.00883637304543074	0.613700713995034	ENSG00000179406	LINC00174	285908
ENSG00000113645.14	67.1599324636497	-1.52226932818927	0.581735130027574	-2.61677393991509	0.0088765106272132	0.613700713995034	ENSG00000113645	WWC1	23286
ENSG00000008517.16	2937.32046525997	-1.13359537528343	0.433415770125334	-2.61549175969213	0.00890990711408273	0.613700713995034	ENSG00000008517	IL32	9235
ENSG00000135924.15	110.17030896874	-1.12793981527423	0.431443048686445	-2.61434230707463	0.0089399418491136	0.613700713995034	ENSG00000135924	DNAJB2	3300
ENSG00000080561.13	40.3717722926391	-1.45506750472684	0.556931967908344	-2.6126485613523	0.00898436354121646	0.614340952300758	ENSG00000080561	MID2	11043
ENSG00000185950.8	543.417862363231	-1.30432020323165	0.499775480098801	-2.60981231607001	0.00905919098912399	0.615219312143148	ENSG00000185950	IRS2	8660
ENSG00000233426.3	17.0064468080671	-1.73834696513436	0.666455048460475	-2.6083484087186	0.00909802993120396	0.615219312143148	ENSG00000233426	NA	NA
ENSG00000259518.1	8.4170146727389	-2.46730343785859	0.946562020257453	-2.60659458657291	0.00914475628625897	0.615219312143148	ENSG00000259518	LINC01583	101929690
ENSG00000102312.21	1813.30909924382	-1.16500486194528	0.447170815899304	-2.60527928148071	0.0091799398607424	0.615219312143148	ENSG00000102312	PORCN	64840
ENSG00000100065.14	1865.64324915036	-1.55424026361182	0.596655424086527	-2.60492103292507	0.00918954369383027	0.615219312143148	ENSG00000100065	CARD10	29775
ENSG00000225764.1	20.9983557226499	-2.25244347858607	0.864917100904832	-2.60423048200767	0.00920808110719822	0.615219312143148	ENSG00000225764	P3H2-AS1	101929152
ENSG00000103145.10	3279.49882455562	-1.00012757130118	0.384455801345947	-2.60141105375396	0.00928411369092283	0.616263066885895	ENSG00000103145	HCFC1R1	54985
ENSG00000101224.17	1345.83347691621	-1.67314276439142	0.643258701019438	-2.60104179195682	0.009294113090995 5	0.616263066885895	ENSG00000101224	CDC25B	994
ENSG00000135476.11	120.834255166814	-1.44281246962862	0.555304557291939	-2.5982363203803	0.00937039805451256	0.616463378069207	ENSG00000135476	ESPL1	9700
ENSG00000171368.11	131.572081338396	1.60630584940332	0.618261291507088	2.59810192141861	0.00937406654389103	0.616463378069207	ENSG00000171368	TPPP	11076
ENSG00000182931.9	40.6729586963812	1.57139532637009	0.605399872603999	2.59563207308099	0.0094417108397411	0.616463378069207	ENSG00000182931	WFDC10B	280664
ENSG00000149260.15	152.602679261623	0.885908851639438	0.341706072459878	2.59260494044471	0.00952521166767362	0.616463378069207	ENSG00000149260	CAPN5	726
ENSG00000145850.8	43.4152787528612	-2.23885808282179	0.863948586822135	-2.59142513451754	0.00955793352378304	0.616463378069207	ENSG00000145850	TIMD4	91937
ENSG00000008083.13	237.435630554096	-0.817348519209769	0.31541341481399	-2.59135623540865	0.00955984753097767	0.616463378069207	ENSG00000008083	JARID2	3720
ENSG00000232519.2	27.7495124173516	-1.95482371853568	0.754409310385054	-2.591197764431	0.0095642511287329 6	0.616463378069207	ENSG00000232519	NA	NA
ENSG00000233783.7	11.1655014413879	2.1792317955616	0.84118388362591	2.59067231075334	0.00957886540044697	0.616463378069207	ENSG00000233783	NA	NA
ENSG00000214050.7	93.5005399121042	-1.42076991884997	0.548711808222204	-2.58928256611278	0.00961761393117272	0.616689860312009	ENSG00000214050	FBXO16	157574
ENSG00000198125.12	5.43566417890594	-3.95092721562647	1.52799365557041	-2.58569608664479	0.00971825773044283	0.620868983837232	ENSG00000198125	MB	4151
ENSG00000162729.13	2536.85766109378	-1.41282902682905	0.546834981228739	-2.58364785598467	0.00977615537181411	0.62229672648584	ENSG00000162729	IGSF8	93185
ENSG00000142530.10	9.67355284956939	-2.60946679371663	1.01087820113436	-2.58138595805945	0.00984044977583008	0.624119830890962	ENSG00000142530	FAM71E1	112703
ENSG00000197043.13	1460.01121460855	-0.891911639596173	0.345955635488389	-2.57810987335718	0.00993424048690236	0.625724435307797	ENSG00000197043	ANXA6	309
ENSG00000182621.17	52.5284983300797	1.13432525296882	0.440246831739769	2.57656653311096	0.00997869993246741	0.625724435307797	ENSG00000182621	PLCB1	23236
ENSG00000167508.11	987.826012418621	-0.982756483245091	0.381608499069986	-2.57530030290247	0.0100153088537743	0.625724435307797	ENSG00000167508	MVD	4597
ENSG00000163520.13	24.9706446003504	-1.89922664083874	0.737695926376896	-2.57453860449868	0.0100373884595904	0.625724435307797	ENSG00000163520	FBLN2	2199
ENSG00000174827.13	212.645166717512	-3.3168661827278	1.28845643966633	-2.57429438870807	0.0100444767964291	0.625724435307797	ENSG00000174827	PDZK1	5174
ENSG00000169499.14	98.4109647111536	-1.35683790827037	0.528052217226994	-2.56951465026632	0.0101841085559311	0.629785132534118	ENSG00000169499	PLEKHA2	59339
ENSG00000066056.13	20.305899584267	-1.79971051894672	0.700681491842243	-2.56851442474225	0.0102135461277492	0.629785132534118	ENSG00000066056	TIE1	7075
ENSG00000158089.14	525.848301076732	-1.64544548225064	0.640884214382213	-2.56746139992976	0.0102446194617066	0.629785132534118	ENSG00000158089	GALNT14	79623
ENSG00000090975.12	32.7820510677985	-1.2866194160094	0.501552283181042	-2.56527476626994	0.0103094129876349	0.629785132534118	ENSG00000090975	PITPNM2	57605
ENSG00000128849.10	240.047880454651	-1.91309742263038	0.745855953820585	-2.56469603032107	0.010318501446116	0.629785132534118	ENSG00000128849	CGNL1	84952
ENSG00000134107.4	5431.22098062415	-1.11422234797297	0.434439919019052	-2.56473288755057	0.0103255260232672	0.629785132534118	ENSG00000134107	BHLHE40	8553
ENSG00000157514.16	4426.96745900617	-1.00358074087232	0.392756615433244	-2.55522300945914	0.0106119784183548	0.64291403624678	ENSG00000157514	TSC22D3	1831
ENSG00000128422.15	28.5925140442345	-2.14990603407 53	0.841744505263635	-2.55410759515674	0.0106460353204571	0.64291403624678	ENSG00000128422	KRT17	3872
ENSG00000108828.15	8901.37640850401	-1.07238383082103	0.41989282661405	-2.55394653790246	0.0106509608975473	0.64291403624678	ENSG00000108828	VAT1	10493
ENSG00000106538.9	160.151351860688	-4.38330873504076	1.71711946635703	-2.55271040886875	0.0106888326638121	0.642982872096323	ENSG00000106538	RARRES2	5919
ENSG00000006704.10	299.397932061768	-1.35363908946122	0.530602307778164	-2.55113683001009	0.0107372162180893	0.643681403759085	ENSG00000006704	GTF2IRD1	9569
ENSG00000143333.6	15.5045097619001	1.86282598830832	0.730570074367916	2.54982520317442	0.0107776941056552	0.643902850919776	ENSG00000143333	RGS16	6004

ENSG00000143333.6	15.5045097619001	1.86282598830832	0.730570074367916	2.54982520317442	0.0107776941056552	0.643902850919776	ENSG00000143333	RGS16	6004
ENSG00000055955.15	55.9632932290205	1.20862410029263	0.474496931449607	2.54716947610226	0.0108600676781556	0.646617294918752	ENSG00000055955	ITIH4	3700
ENSG00000116117.17	4.31519454628466	4.32241314216918	1.69850218787808	2.54483813622232	0.0109328403600019	0.648743628819772	ENSG00000116117	PARD3B	117583
ENSG00000178127.12	46.1534795861606	-1.43718441891998	0.5655144242358	-2.54137535194102	0.011041730956148	0.650651660676901	ENSG00000178127	NDUFV2	4729
ENSG00000163482.11	200.448783239257	1.14881930357977	0.452157635583513	2.5407495377076	0.0110615127722588	0.650651660676901	ENSG00000163482	STK36	27148
ENSG00000184254.16	145.956533995519	-1.48764635678454	0.585623918056344	-2.54027595341727	0.0110765035636513	0.650651660676901	ENSG00000184254	ALDH1A3	220
ENSG00000197608.11	133.244048159847	-1.07887585878143	0.425648093468489	-2.53466625444031	0.0112554503208472	0.651261175317774	ENSG00000197608	ZNF841	284371
ENSG00000165272.15	11.0848380727396	-3.80340025401437	1.50202012607045	-2.53218994073317	0.0113352570155034	0.651261175317774	ENSG00000165272	AQP3	360
ENSG00000279319.1	3.00203078998969	4.82759098614074	1.90705173061083	2.53144207293971	0.0113594578917935	0.651261175317774	ENSG00000279319	NA	NA
ENSG00000120820.12	34.4723685715696	-1.69857977575393	0.671086281028319	-2.53109000105196	0.0113708667510524	0.651261175317774	ENSG00000120820	GLT8D2	83468
ENSG00000149090.11	8.08483142855431	-4.69028373773541	1.85340747871327	-2.530627393924	0.0113858729590259	0.651261175317774	ENSG00000149090	PAMR1	25891
ENSG00000148672.8	1218.88267156804	1.12806792895018	0.446092192006366	2.52877756922067	0.0114460540532271	0.651261175317774	ENSG00000148672	GLUD1	2746
ENSG00000196415.9	49.6221931048637	-1.94719959718319	0.770037329684863	-2.52870805364732	0.0114483211257226	0.651261175317774	ENSG00000196415	PRTN3	5657
ENSG00000273055.1	5.94158272158439	3.31032832802189	1.30951021907357	2.52791332194707	0.011474267604193	0.651261175317774	ENSG00000273055	NA	NA
ENSG00000167900.11	1111.4103083886	-1.732903253652	0.68559708416897	-2.52758258992962	0.0114850807461263	0.651261175317774	ENSG00000167900	TK1	7083
ENSG00000186469.8	260.88360639022	1.18294905156203	0.468089484610644	2.52718569943097	0.0114980688492731	0.651261175317774	ENSG00000186469	GNG2	54331
ENSG00000198743.6	165.293161141108	-0.82980398652952	0.328375261363342	-2.52699908965236	0.0115041800933218	0.651261175317774	ENSG00000198743	SLC5A3	6526
ENSG00000226380.9	32.4889308120541	1.42676498632497	0.565075974756691	2.52490824254084	0.0115728501498032	0.651261175317774	ENSG00000226380	NA	NA
ENSG00000154928.16	82.8997905786869	-1.3014825695633	0.51548847659913	-2.5247558939623	0.0115778679485519	0.651261175317774	ENSG00000154928	EPHB1	2047
ENSG00000149927.17	65.4453309825476	-1.948762286721 08	0.772138667390433	-2.52385014379248	0.0116077398856981	0.651261175317774	ENSG00000149927	DOC2A	8448
ENSG00000107938.17	244.176134221745	0.788314429777529	0.312827701599827	2.51996362772869	0.0117366961451024	0.655045992311897	ENSG00000107938	EDRF1	26098
ENSG00000138617.14	363.272391798032	-0.817249860327223	0.324792640634254	-2.5162203759645	0.0118620985829903	0.655045992311897	ENSG00000138617	PARP16	54956
ENSG00000246851.1	6.04365852384886	3.26046131942306	1.29582828649386	2.51612142859216	0.0118654294704103	0.655045992311897	ENSG00000246851	NA	NA
ENSG00000249784.1	20.0808884546785	-2.68574671630693	1.06802545355914	-2.5146841841239	0.0119139053556343	0.655045992311897	ENSG00000249784	SCARNA22	677770
ENSG00000158747.14	506.875518628956	1.51710308309511	0.603400353810782	2.51425620405064	0.0119283743081244	0.655045992311897	ENSG00000158747	NBL1	4681
ENSG00000198682.12	1197.09056176673	-1.1821458255964	0.470263907285134	-2.5137923776056	0.0119440727281033	0.655045992311897	ENSG00000198682	PAPSS2	9060
ENSG00000172366.19	568.967048171006	-0.989196601525258	0.39391602379375	-2.5111865011188	0.0120326108238596	0.655045992311897	ENSG00000172366	MCRIP2	84331
ENSG00000213085.9	28.5119938894789	-1.56833169531086	0.624543281570382	-2.5111657455787	0.0120333183498533	0.655045992311897	ENSG00000213085	CFAP45	25790
ENSG00000084207.16	73.0512240349145	-1.83396965088885	0.73045389469987	-2.51072608989564	0.0120483142354698	0.655045992311897	ENSG00000084207	GSTP1	2950
ENSG00000196366.3	2.43814493029951	-4.99037409867893	1.98800166703854	-2.51024643561437	0.012064693294942	0.655045992311897	ENSG00000196366	NA	NA
ENSG00000171227.6	120.545103755829	-1.85385046078909	0.738703780368134	-2.50959926029514	0.0120868240797911	0.655045992311897	ENSG00000171227	TMEM37	140738
ENSG00000225174.1	35.4286629871386	1.67630192802735	0.668318245844275	2.50823905893772	0.0121334547929862	0.655543599232171	ENSG00000225174	OSTM1-AS1	100287366
ENSG00000165757.8	2101.60636552318	-1.28479248179251	0.513486923704631	-2.5020938654546	0.0123461186865394	0.664980946485763	ENSG00000165757	JCAD	57608
ENSG00000129675.15	414.807627855839	0.840551484051111	0.336244288688862	2.49982382549522	0.0124255080911227	0.665328853384929	ENSG00000129675	ARHGEF6	9459
ENSG00000129128.12	1508.13561848247	1.05384367433903	0.421678684795916	2.49916278042147	0.0124487114578317	0.665328853384929	ENSG00000129128	SPCS3	60559
ENSG00000140553.17	1221.47482012919	-0.861093681605891	0.344623039098826	-2.49865384466928	0.0124666017657959	0.665328853384929	ENSG00000140553	UNC45A	55898
ENSG00000132840.9	124.367829527996	-0.932295706042298	0.373442107732878	-2.49649326291069	0.0125428051317958	0.667361105872598	ENSG00000132840	BHMT2	23743
ENSG00000131115.15	171.588500240966	-0.753364985705715	0.303009709746418	-2.48627341459186	0.0129088745047765	0.681452660326024	ENSG00000131115	ZNF227	7770
ENSG00000119899.12	1439.84908453604	-0.957340475921437	0.385106680427246	-2.48590981298829	0.0129220708734647	0.681452660326024	ENSG00000119899	SLC17A5	26503
ENSG00000187051.8	1564.4500010725	-0.859445757755628	0.345735910698155	-2.48584463216483	0.0129244377736784	0.681452660326024	ENSG00000187051	RPS19BP1	91582
ENSG00000117407.16	79.5735222689223	-1.59094174734788	0.640598876419941	-2.48352253790865	0.0130090102018164	0.683056187431561	ENSG00000117407	ARTN	9048
ENSG00000159399.9	2192.90273251701	-1.45072070245313	0.58429202553923	-2.48286924866772	0.0130328915511078	0.683056187431561	ENSG00000159399	HK2	3099
ENSG00000161048.11	117.663721029399	0.91868136192564	0.370342902952689	2.48062364527882	0.0131152768123079	0.685322151043135	ENSG00000161048	NAPEPLD	222236
ENSG00000119912.15	581.279868012174	0.807864398647742	0.326402015985146	2.47505946373967	0.013321399399017	0.692872500130491	ENSG00000119912	IDE	3416
ENSG00000173511.9	185.457797414701	-0.906115552621027	0.366169988529364	-2.4745762378294	0.013339434704767	0.692872500130491	ENSG00000173511	VEGFB	7423
ENSG00000141337.12	135.081857179732	1.28955710259956	0.521342581720548	2.47353112485792	0.0133785149982351	0.692872500130491	ENSG00000141337	ARSG	22901
ENSG00000137817.16	614.276369869442	-0.765164680973571	0.309694401298106	-2.47070879475486	0.0134845574917932	0.695581716326953	ENSG00000137817	PARP6	56965
ENSG00000102893.15	875.431162383389	0.651297034223904	0.263897636184532	2.46799116369682	0.0135873673660384	0.695581716326953	ENSG00000102893	PHKB	5257
ENSG00000130164.13	808.728968204379	-1.40855567506554	0.570809608912954	-2.4676453463143	0.0136004994191278	0.695581716326953	ENSG00000130164	LDLR	3949
ENSG00000196110.7	87.3310289517442	-1.12935355429868	0.457687822712192	-2.46751934016137	0.0136052871571895	0.695581716326953	ENSG00000196110	ZNF699	374879
ENSG00000111816.7	58.2241460341368	1.17601145025529	0.476719686448936	2.46688249653658	0.0136295074950097	0.695581716326953	ENSG00000111816	FRK	2444
ENSG00000233929.1	14.2392654937451	-1.73635083762798	0.705664651400828	-2.46058922489758	0.0138709077019937	0.702627462498644	ENSG00000233929	NA	NA
ENSG00000111846.17	287.153888122716	-1.15239492214317	0.468514418935599	-2.45967866850555	0.013906146057573	0.702627462498644	ENSG00000111846	GCNT2	2651
ENSG00000147485.12	2.367327472083	-4.93967299221928	2.00875575933763	-2.45907097926534	0.013929707465026	0.702627462498644	ENSG00000147485	PXDNL	137902
ENSG00000125652.7	531.641501757023	-0.877368198277565	0.356840208820947	-2.45871450747246	0.0139435450304595	0.702627462498644	ENSG00000125652	ALKBH7	84266
ENSG00000116663.10	59.0425736194347	-1.09619491678646	0.445963409813003	-2.45803779562567	0.0139698471004287	0.702627462498644	ENSG00000116663	FBXO6	26270
ENSG00000079215.13	55.4553048327681	-1.13220284888306	0.460798424614519	-2.45704800277954	0.0140083967101986	0.702627462498644	ENSG00000079215	SLC1A3	6507

6450 cell line RNA sequencing data tables (200 out of the total 17,000 genes)

	baseMean	log2FoldChange	lfcSE	stat	pvalue	padj	ensemblid	symbol	entrezid
ENSG00000129757.13	1865.31474984336	-6.57088969135161	0.433591933857127	-15.1545478092699	7.07003417303091e-52	1.185786131500074e-47	ENSG00000129757	CDKN1C	1028
ENSG00000265972.5	4890.83585478183	6.41756700627986	0.471682779802908	13.6056843308154	3.70484288814103e-42	3.106881245995078e-38	ENSG00000265972	TXNIP	10628
ENSG00000120875.8	1635.74246574226	-5.66865052247013	0.437868181123233	-12.9460206675186	2.47452397276422e-38	1.383423869040005e-34	ENSG00000120875	DUSP4	1846
ENSG00000182022.17	795.285149917611	-3.89731598405332	0.316969849081639	-12.2955416590728	9.571301398603039e-35	4.0132466764344e-31	ENSG00000182022	CHST15	51363
ENSG00000170525.20	5368.05761618643	-3.71722536121712	0.311705821777591	-11.9254280847839	8.72344506069415e-33	2.926192411159259e-29	ENSG00000170525	PFKFB3	5209
ENSG00000087116.14	213.737043073242	-6.2715791832607	0.53269068360164	-11.7733975388065	5.35245670621817e-32	1.496190064611526e-28	ENSG00000087116	ADAMTS2	9509
ENSG00000120594.16	297.66163613072	7.11021367561593	0.607417279714225	11.7056493337844	1.19242888025764e-31	2.801498365877316e-28	ENSG00000120594	PLXDC2	84898
ENSG00000120738.7	1314.56018016233	6.37989435392578	0.545477294723605	11.6959851778221	1.336273964167570e-31	2.801498365877316e-28	ENSG00000120738	EGR1	1958
ENSG00000055118.14	312.584939985776	-7.22143155670854	0.625839281761703	-11.5387956096022	8.40944070263862e-31	1.567145994057172e-27	ENSG00000055118	KCNH2	3757
ENSG00000145147.19	343.440404355672	4.7175747014331	0.414169054480909	11.3904567480199	4.66537716834688e-30	7.824770586751139e-27	ENSG00000145147	SLIT2	9353
ENSG00000148344.10	749.348909185163	-6.47739963669811	0.569607687883867	-11.3716857663247	5.7859197828514e-30	8.821949690725784e-27	ENSG00000148344	PTGES	9536
ENSG00000197046.11	401.434024212097	5.33618735997891	0.475956367855841	11.2115053403281	3.580514821560005e-29	5.004366215600043e-26	ENSG00000197046	SIGLEC15	284266
ENSG00000130513.6	3344.97863092395	-4.79131500465636	0.433742050965919	-11.0464618175396	2.28025692296148e-28	2.941882239377768e-25	ENSG00000130513	GDF15	9518
ENSG00000137959.15	360.462664350892	6.59831162036229	0.604013288763612	10.9241166429777	8.8396313363077e-28	1.058987834089666e-24	ENSG00000137959	IFI44L	10964
ENSG00000147872.9	54150.2541012738	-3.25821262333791	0.299106809060882	-10.8931409270416	1.242786943958250e-27	1.389601508271184e-24	ENSG00000147872	PLIN2	123
ENSG00000182492.15	188.806532542939	-6.47750636873341	0.610930324770695	-10.6026924938857	2.895226177768540e-26	3.034920840845870e-23	ENSG00000182492	BGN	633
ENSG00000123636.17	227.935962274764	5.22733628949516	0.493538990183823	10.5915366231717	3.261926717076854e-26	3.218178521122160e-23	ENSG00000123636	BAZ2B	29994
ENSG00000197415.11	327.604967358261	4.55673512038786	0.43178370601162	10.5532817865648	4.905319207711840e-26	4.570667430652390e-23	ENSG00000197415	VEPH1	79674
ENSG00000100321.14	149.666054800615	-6.6951302580753	0.639684931197642	-10.4662935322557	1.233797211527e-25	1.089118254296950e-22	ENSG00000100321	SYNGR1	9145
ENSG00000183671.12	220.391625678979	4.60126394080764	0.44327742019164	10.3800999807714	3.054551274512240e-25	2.561546698805960e-22	ENSG00000183671	GPR1	2825
ENSG00000072786.12	954.806961515027	-3.42875087499027	0.331764860674596	-10.3348825671845	4.900119082750 3e-25	3.913561774089 9e-22	ENSG00000072786	STK10	6793
ENSG00000153132.12	200.433827382071	6.59750984411698	0.645059902773383	10.227747556082	1.489432583233350e-24	1.135489240272260e-21	ENSG00000153132	CLGN	1047
ENSG00000154358.20	448.765457473767	-4.49891985503891	0.445126444636333	-10.1070603853126	5.140350741392410e-24	3.748433158027540e-21	ENSG00000154358	OBSCN	84033
ENSG00000152377.13	158.371968963798	7.38304543204323	0.730945783459512	10.100674947619	5.486352884551410e-24	3.834046274154010e-21	ENSG00000152377	SPOCK1	6695
ENSG00000128510.10	414.499255855459	-5.36317576875384	0.532522936065187	-10.0712577910397	7.402527389509170e-24	4.966207575073910e-21	ENSG00000128510	CPA4	51200
ENSG00000189056.13	124.025738814039	6.15739938465008	0.61531994866831	10.0068255514486	1.422436206347590e-23	9.175807712639180e-21	ENSG00000189056	RELN	5649
ENSG00000136167.13	321.757087558435	4.74002931680904	0.47521020278789	9.97459500869501	1.969030886460220e-23	1.223132815841140e-20	ENSG00000136167	LCP1	3936
ENSG00000177409.11	152.237834822531	4.92799057036021	0.495967876765139	9.93610836754618	2.899334177399690e-23	1.736701172262410e-20	ENSG00000177409	SAMD9L	219285
ENSG00000183691.4	980.63596093413	-3.37003133425659	0.339410794410685	-9.92906351168924	3.1116412502286e-23	1.799601622375590e-20	ENSG00000183691	NOG	9241
ENSG00000197989.13	878.813038486359	-3.79512837413568	0.382930219219553	-9.9107570613531	3.738028594385590e-23	2.089807186178420e-20	ENSG00000197989	SNHG12	85028
ENSG00000156103.15	126.6894999419	6.89254633859176	0.701787382478966	9.8214167291592	9.105476344160640e-23	4.926356427234270e-20	ENSG00000156103	MMP16	4325
ENSG00000103196.11	181.337902031186	-4.90882411375589	0.505245920233473	-9.71571252171128	2.584351266122680e-22	1.354523107356550e-19	ENSG00000103196	CRISPLD2	83716
ENSG00000170425.3	445.986293292758	-3.13194245150703	0.323770468688046	-9.67334193324675	3.913841999023610e-22	1.989180545685580e-19	ENSG00000170425	ADORA2B	136
ENSG00000198157.10	94.0940946664831	5.30856081705945	0.549758936221457	9.65616103222564	4.628857852349930e-22	2.283388349988620e-19	ENSG00000198157	HMGN5	79366
ENSG00000152463.14	141.974300992662	6.44552071293676	0.66931436464067	9.6300349334309	5.9709176539706e-22	2.861263739782710e-19	ENSG00000152463	OLAH	55301
ENSG00000134202.10	2981.4368884322	-3.53341193937372	0.368419136688438	-9.59073942557394	8.745597551718570e-22	4.074476726039550e-19	ENSG00000134202	GSTM3	2947
ENSG00000225742.5	102.713149030893	-5.59039380122216	0.583548992631622	-9.57999049233423	9.705387039105890e-22	4.399425714050920e-19	ENSG00000225742	LINC02036	100505920
ENSG00000157557.11	1107.55410043373	-2.9310498346714	0.306545293001247	-9.56155550775161	1.159999185032010e-21	5.119870087199170e-19	ENSG00000157557	ETS2	2114
ENSG00000245532.8	8480.27695779131	4.22694931622468	0.444637111120938	9.50651488709178	1.971571704894190e-21	8.478769408956830e-19	ENSG00000245532	NEAT1	283131
ENSG00000132170.20	960.740788363664	-3.3486137547165	0.353930931440968	-9.46120685491715	3.044092250000690e-21	1.276387880425290e-18	ENSG00000132170	PPARG	5468
ENSG00000162545.5	363.137382330392	3.39597229840194	0.360021563445529	9.43269138076431	3.996988992788 6e-21	1.635060960659770e-18	ENSG00000162545	CAMK2N1	55450
ENSG00000151632.17	112.145618581499	-5.17395162220909	0.550146186158378	-9.40468506805134	5.218625197779970e-21	2.083970956468e-18	ENSG00000151632	AKR1C2	1646
ENSG00000136286.14	124.619007737417	-7.00340925146629	0.757383698798977	-9.24684444961248	2.312179049657150e-20	9.018573725779020e-18	ENSG00000136286	MYO1G	64005
ENSG00000198681.6	203.93371714968	3.59981189601397	0.389490792331253	9.24235429152947	2.411321787471990e-20	9.191520231700030e-18	ENSG00000198681	MAGEA1	4100
ENSG00000254300.1	81.3613135319218	5.63941543494025	0.611437963337904	9.22320132716995	2.883597179261140e-20	1.074748708679280e-17	ENSG00000254300	LINC01111	101926978
ENSG00000241104.5	298.929147224432	-4.73438766098199	0.515282395595168	-9.18794762144671	4.004077786082540e-20	1.4599215788734e-17	ENSG00000241104	LOC284344	284344
ENSG00000170345.9	434.783762644951	4.47898357417551	0.489992418164697	9.14092424317885	6.192083475553380e-20	2.209651575574070e-17	ENSG00000170345	FOS	2353
ENSG00000111335.12	143.132289084365	6.43540220713133	0.706158316581931	9.11325697937125	7.994516099286190e-20	2.754024532288080e-17	ENSG00000111335	OAS2	4939
ENSG00000154646.8	76.6148256270018	5.1776024801659	0.568183025122283	9.11256100805121	8.045981521709760e-20	2.754024532288080e-17	ENSG00000154646	TMPRSS15	5651
ENSG00000099860.8	5919.75927695014	-3.13566318481902	0.344500335462982	-9.1020613393741	8.8633354239496e-20	2.973117234609650e-17	ENSG00000099860	GADD45B	4616
ENSG00000178927.17	213.277108144913	3.48701373936158	0.387685567279185	8.99443784774806	2.374442174095690e-19	7.808655714496660e-17	ENSG00000178927	CYBC1	79415
ENSG00000106789.12	351.838650439163	-4.85466568031435	0.540378047991465	-8.98383214928638	2.614965443914450e-19	8.434269312564060e-17	ENSG00000106789	CORO2A	7464
ENSG00000197696.9	97.741003481519	-5.92227747362889	0.65970370518846	-8.97717782551646	2.778006864562560e-19	8.791081345744020e-17	ENSG00000197696	NMB	4828
ENSG00000137501.17	223.669630690906	4.24659205373337	0.476180741933422	8.91802561458295	4.746746458196290e-19	1.474304288830890e-16	ENSG00000137501	SYTL2	54843
ENSG00000114698.14	96.1612140414701	5.3262298080692	0.59942628897033	8.8855459062671	6.3607655818382e-19	1.939686551610730e-16	ENSG00000114698	PLSCR4	57088
ENSG00000246223.8	90.4395833368072	8.10431433828573	0.919671494624049	8.81218390007693	1.227310699813170e-18	3.675795545940450e-16	ENSG00000246223	LINC01550	388011
ENSG00000205336.11	1794.94151723729	-4.46914290555798	0.507603820506921	-8.80439178155681	1.315640673222140e-18	3.871214977417840e-16	ENSG00000205336	ADGRG1	9289

ENSG00000205336.11	1794.94151723729	-4.46914290555798	0.507603820506921	-8.80439178155681	1.31564067322214e-18	3.87121497741784e-16	ENSG00000205336	ADGRG1	9289
ENSG00000230590.9	553.05078628887	3.99233482443499	0.454911919425857	8.77606115371455	1.69299791406851e-18	4.89568293357879e-16	ENSG00000230590	FTX	100302692
ENSG00000239467.5	63.988129331875	6.52722143113399	0.751515513696517	8.68541142820621	3.77373990808388e-18	1.07276552098954e-15	ENSG00000239467	ERICH2	285141
ENSG00000126790.11	650.158837964822	2.9618427646636	0.342232619154349	8.65447242282824	4.95196893291812e-18	1.38424038238171e-15	ENSG00000126790	L3HYPDH	112849
ENSG00000126368.5	3288.04619176519	-2.93927673364315	0.342323626648722	-8.58625144404454	8.98529028641213e-18	2.47051292924105e-15	ENSG00000126368	NR1D1	9572
ENSG00000258289.8	239.353303682094	3.94466311785749	0.461432526740034	8.54873223984895	1.24447847510279e-17	3.36651499748775e-15	ENSG00000258289	CHURC1	91612
ENSG00000169760.17	83.0159165850453	6.49605085840681	0.76514847681672	8.48992196316277	2.06775899495494e-17	5.50483394656894e-15	ENSG00000169760	NLGN1	22871
ENSG00000170627.10	250.953106214241	-10.5202680314362	1.24117402644812	-8.47606202455117	2.32944599089643e-17	6.10460439989296e-15	ENSG00000170627	GTSF1	121355
ENSG00000128294.15	1976.44440056507	-3.11348535476067	0.37022845786968	-8.40963272428023	4.11296575458195e-17	1.05836864993564e-14	ENSG00000128294	TPST2	8459
ENSG00000155850.7	131.634856505977	3.95770497414434	0.470697932237892	8.40816307674813	4.16481820270406e-17	1.05836864993564e-14	ENSG00000155850	SLC26A2	1836
ENSG00000217801.9	792.388690886207	-2.90834209849908	0.346406787272905	-8.39574224683954	4.62960238370892e-17	1.15892076387412e-14	ENSG00000217801	LOC1002881	100288175
ENSG00000108828.15	15812.423337938	-3.34947849461204	0.399977406681223	-8.37416923721778	5.56147897118405e-17	1.37172243095145e-14	ENSG00000108828	VAT1	10493
ENSG00000183421.11	766.658490077675	-3.15122317357531	0.377151016396114	-8.35533522801286	6.52471515908322e-17	1.58597858910353e-14	ENSG00000183421	RIPK4	54101
ENSG00000162775.14	454.699533334702	-2.71859827532284	0.326325060724178	-8.33095156495104	8.01951374681431e-17	1.92147549373671e-14	ENSG00000162775	RBM15	64783
ENSG00000171345.13	892.456689649215	-4.35572955251283	0.523868205099113	-8.31455222919807	9.20993362046979e-17	2.17561981242985e-14	ENSG00000171345	KRT19	3880
ENSG00000248370.1	110.86841284314	-10.3043608830693	1.24294287989953	-8.29029318217919	1.12969662939575e-16	2.63156553725354e-14	ENSG00000248370	NA	NA
ENSG00000187134.13	279.143014147407	-3.56271154391796	0.430913919531139	-8.26780334177743	1.3644972527265e-16	3.13497916749711e-14	ENSG00000187134	AKR1C1	1645
ENSG00000197183.14	1465.27438849675	-2.51841260569034	0.305057571320965	-8.25553220916652	1.51226834669986e-16	3.4275357717365e-14	ENSG00000197183	NOL4L	140688
ENSG00000186480.12	1534.2100072489	-3.01465952444689	0.365365633315358	-8.25107577056885	1.56974979314727e-16	3.51037913742214e-14	ENSG00000186480	INSIG1	3638
ENSG00000107890.16	77.3548042140058	4.99342158977475	0.6053500914609	8.24881611519056	1.59971367405742e-16	3.53031549227514e-14	ENSG00000107890	ANKRD26	22852
ENSG00000185909.14	124.771610981229	-3.78794932503755	0.460025640044702	-8.23421347703459	1.80741140324067e-16	3.92420591935856e-14	ENSG00000185909	KLHDC8B	200942
ENSG00000179542.15	72.4335797420405	4.06783882308013	0.494086238434652	8.23305428616617	1.82499440561631e-16	3.92420591935856e-14	ENSG00000179542	SLITRK4	139065
ENSG00000173432.10	1120.73767454795	-4.06665637495852	0.495943674757581	-8.19983514649384	2.40716907324807e-16	5.11051135398945e-14	ENSG00000173432	SAA1	6288
ENSG00000248323.5	519.123866048489	3.44726559251539	0.421301672562498	8.18241610945423	2.78208423131182e-16	5.83263959094523e-14	ENSG00000248323	LUCAT1	100505994
ENSG00000123689.5	3259.38978885063	2.94789562562921	0.360678535956254	8.17319394350305	3.00330606531868e-16	6.21869744784258e-14	ENSG00000123689	G0S2	50486
ENSG00000123933.16	74.1356134517739	4.05225864769099	0.497233246937672	8.14961323010433	3.65090047785904e-16	7.46742717251852e-14	ENSG00000123933	MXD4	10608
ENSG00000187325.4	253.846225361258	3.93249627603955	0.484318880762059	8.11964272351287	4.67558044293435e-16	9.44805243239698e-14	ENSG00000187325	TAF9B	51616
ENSG00000127914.16	506.972378198614	3.66250935315158	0.45202389284459	8.10246850028962	5.38550895668234e-16	1.07530662168424e-13	ENSG00000127914	AKAP9	10142
ENSG00000124216.3	365.180959603502	-2.94464871271999	0.363738148645285	-8.09551795347041	5.70212025858157e-16	1.12512895266977e-13	ENSG00000124216	SNAI1	6615
ENSG00000185946.15	118.085936568533	3.53467135220785	0.437366509202692	8.08171471256787	6.38623650729342e-16	1.24546463605029e-13	ENSG00000185946	RNPC3	55599
ENSG00000205413.7	154.5023641666	5.12839782980555	0.635456266710123	8.07041821517668	7.00577791422943e-16	1.35058513997076e-13	ENSG00000205413	SAMD9	54809
ENSG00000239911.2	83.0297887116242	-3.87535173818659	0.481373455293011	-8.05061370870081	8.2379897554616e-16	1.55910508101175e-13	ENSG00000239911	NA	NA
ENSG00000088827.12	63.3572647892341	-5.59923544520825	0.695591276997523	-8.04960560945646	8.30612582285296e-16	1.55910508101175e-13	ENSG00000088827	SIGLEC1	6614
ENSG00000163931.15	12528.3846610063	-3.25844201634793	0.404839668565318	-8.04872217165696	8.36629246905899e-16	1.55910508101175e-13	ENSG00000163931	TKT	7086
ENSG00000227467.3	76.0798345981885	5.61875480156112	0.699824771699257	8.02880239280201	9.8428747117542e-16	1.79487287671528e-13	ENSG00000227467	LINC01537	101928555
ENSG00000109472.13	1836.06237687941	3.29519819406866	0.410423788586901	8.0287699828855	9.84547487823789e-16	1.79487287671528e-13	ENSG00000109472	CPE	1363
ENSG00000108691.9	50.201370776972	5.57807232521399	0.698257104179872	7.98856508845068	1.36518383925324e-15	2.46202831741456e-13	ENSG00000108691	CCL2	6347
ENSG00000075213.10	58.3994236484615	6.20679268275901	0.779557288833583	7.96194554481808	1.69355011632636e-15	3.02172580330061e-13	ENSG00000075213	SEMA3A	10371
ENSG00000224848.1	68.1669159937059	-4.98207614467971	0.628344057617479	-7.9288983229514	2.21098472182384e-15	3.90343534257153e-13	ENSG00000224848	NA	NA
ENSG00000116183.10	47.9986101439218	6.1773929686211	0.779488864524009	7.92492779533585	2.28278937802324e-15	3.98822327585476e-13	ENSG00000116183	PAPPA2	60676
ENSG00000049323.15	619.175955102522	-2.63461700422385	0.333920464508989	-7.88995369929754	3.02298669735433e-15	5.22696215340482e-13	ENSG00000049323	LTBP1	4052
ENSG00000067715.13	55.7132236681354	7.39451843532886	0.937839879639921	7.88462785157733	3.15474265280977e-15	5.39911671152301e-13	ENSG00000067715	SYT1	6857
ENSG00000133107.14	165.680614807496	-3.86124053578494	0.490995968430591	-7.86409824937448	3.71765686473578e-15	6.29823645811601e-13	ENSG00000133107	TRPC4	7223
ENSG00000121671.11	425.304172333665	-3.00207846014184	0.382398941612854	-7.85064531685127	4.13901976645896e-15	6.94196395230497e-13	ENSG00000121671	CRY2	1408
ENSG00000183668.17	72.5278291921274	-5.17317158496928	0.659073381089626	-7.84915873315446	4.18837236351151e-15	6.95518626542723e-13	ENSG00000183668	PSG9	5678
ENSG00000198846.5	271.390613157468	-3.98522995516655	0.509490839103821	-7.82198549865283	5.19966002015153e-15	8.54987233901779e-13	ENSG00000198846	TOX	9760
ENSG00000019549.10	224.392829988961	-3.85619932768357	0.49389400828247	-7.8077467290879	5.82194288609575e-15	9.48015787238815e-13	ENSG00000019549	SNAI2	6591
ENSG00000165474.6	1771.47052365791	-2.78422697312403	0.356926612679012	-7.80055864208679	6.16337180298024e-15	9.9396222961139e-13	ENSG00000165474	GJB2	2706
ENSG00000072163.19	158.346471293037	-3.98783870102133	0.511476877833999	-7.79671354433268	6.35402545874947e-15	1.01494966661091e-12	ENSG00000072163	LIMS2	55679
ENSG00000136869.14	140.177929009359	3.23767607179664	0.417403503731066	7.75670554476869	8.71639885075242e-15	1.37916454268698e-12	ENSG00000136869	TLR4	7099
ENSG00000244242.1	61.6571602739308	-4.62033643644789	0.596338515565792	-7.74784173057182	9.34675336992283e-15	1.4650817525266e-12	ENSG00000244242	IFITM10	402778
ENSG00000116337.15	3926.07894849259	-3.12913846664761	0.404911341038505	-7.72795955436093	1.09284052056251e-14	1.69714085285875e-12	ENSG00000116337	AMPD2	271
ENSG00000157227.12	1339.46436353217	-2.79013411198199	0.361595109771828	-7.71618320209752	1.19864988284423e-14	1.84438126927187e-12	ENSG00000157227	MMP14	4323
ENSG00000250337.5	158.533996212619	3.12576909985429	0.405695341041889	7.70472022633248	1.31130256431156e-14	1.99937878260305e-12	ENSG00000250337	PURPL	643401
ENSG00000197872.11	757.433228996248	-3.3042321337074	0.42936982915496	-7.6955386926241	1.4089928483249e-14	2.12897550018965e-12	ENSG00000197872	FAM49A	81553
ENSG00000167996.15	29789.9991705919	-2.97675312500488	0.386995964575416	-7.69194874750378	1.44910670785986e-14	2.17003729502014e-12	ENSG00000167996	FTH1	2495
ENSG00000084207.16	1157.06397968887	-3.25417410419184	0.423344278014358	-7.68682671100488	1.50829204199483e-14	2.22887171834496e-12	ENSG00000084207	GSTP1	2950
ENSG00000187187.13	67.9837200422747	4.62721782749869	0.602011545381294	7.68626094133787	1.51497362205656e-14	2.22887171834496e-12	ENSG00000187187	ZNF546	339327

ENSG00000187187.13	67.9837200422747	4.62721782749869	0.602011545381294	7.68626094133787	1.51497362205656e-14	2.22887171834496e-12	ENSG00000187187	ZNF546	339327
ENSG00000148926.9	24344.3622745058	-2.39584111707686	0.31224283616784	-7.67300587735189	1.68011787560912e-14	2.45034234867097e-12	ENSG00000148926	ADM	133
ENSG00000145423.4	105.318788529399	6.69823935402902	0.87342191873699	7.66896182742357	1.73394025643617e-14	2.50703844663341e-12	ENSG00000145423	SFRP2	6423
ENSG00000165006.13	2990.74359907745	-2.43323128136103	0.317748740190334	-7.65772125454694	1.8926110954507e-14	2.71306609341018e-12	ENSG00000165006	UBAP1	51271
ENSG00000113552.15	6199.83276544904	-2.82812292031337	0.369839984875931	-7.64688253289356	2.0591026518482e-14	2.92671776922017e-12	ENSG00000113552	GNPDA1	10007
ENSG00000196912.12	110.788482497701	3.53729096105244	0.462917430992467	7.64129999051601	2.15039374369796e-14	3.03079024111783e-12	ENSG00000196912	ANKRD36B	57730
ENSG00000121207.11	50.8980796974381	5.4499052617096	0.714090024891438	7.63195825699728	2.31214310868885e-14	3.23160535157746e-12	ENSG00000121207	LRAT	9227
ENSG00000187957.7	106.397175738047	-3.7030682289405	0.48604635986602	-7.61875519438364	2.56133698319907e-14	3.55030941175328e-12	ENSG00000187957	DNER	92737
ENSG00000158639.12	53.3211632809483	9.18126082330659	1.20546705334332	7.61635151939049	2.60946444369614e-14	3.58737193849768e-12	ENSG00000158639	PAGE5	90737
ENSG00000088826.17	5151.19508351597	-3.23286520127786	0.424640674149635	-7.61317883370487	2.67436274807351e-14	3.64670016347064e-12	ENSG00000088826	SMOX	54498
ENSG00000183696.13	9219.0641033238	-2.98513715132757	0.392257823843963	-7.61014049910968	2.73798119877952e-14	3.70334037628468e-12	ENSG00000183696	UPP1	7378
ENSG00000167191.11	119.14351895424	-4.1139055053744	0.540717668502587	-7.60823206825674	2.77870578506041e-14	3.72835627416266e-12	ENSG00000167191	GPRC5B	51704
ENSG00000249867.5	102.611487147581	3.95730546863316	0.520596717553672	7.60147986954062	2.92763318615005e-14	3.89700506334195e-12	ENSG00000249867	NA	NA
ENSG00000162409.10	44.8202330957779	5.01077082460094	0.659625228895306	7.59639050342666	3.04504722615429e-14	4.02138047850864e-12	ENSG00000162409	PRKAA2	5563
ENSG00000233452.6	245.819325189437	3.01395006008006	0.397143420010926	7.58907212914956	3.22204376091041e-14	4.22188421546793e-12	ENSG00000233452	NA	NA
ENSG00000108848.15	488.815225588833	3.0961548995214	0.408283299185053	7.58334936966911	3.36746453995059e-14	4.37822598946134e-12	ENSG00000108848	LUC7L3	51747
ENSG00000164318.17	509.12963907659	-3.24546769456408	0.428083669641652	-7.58138636141121	3.41881818495765e-14	4.41080143062383e-12	ENSG00000164318	EGFLAM	133584
ENSG00000232453.6	109.279487889265	-4.14844549618609	0.547834933862718	-7.57243695091861	3.66287004166759e-14	4.68959208693502e-12	ENSG00000232453	LOC105378753	105378753
ENSG00000104892.16	91.7792332428386	-4.37471382688685	0.579216897655081	-7.55280766945435	4.25973818625856e-14	5.4124491560552e-12	ENSG00000104892	KLC3	147700
ENSG00000132965.9	153.180584964217	3.46659620588762	0.459692584403865	7.54111839846871	4.65957815854454e-14	5.87597329888038e-12	ENSG00000132965	ALOX5AP	241
ENSG00000006704.10	672.498722188956	-2.52960330595368	0.335664491215156	-7.53610635666625	4.84211709008852e-14	6.06059610708691e-12	ENSG00000006704	GTF2IRD1	9569
ENSG00000134070.4	420.904967715609	-2.61071842286997	0.346816045160956	-7.5276748561571	5.16518150095539e-14	6.41706845437213e-12	ENSG00000134070	IRAK2	3656
ENSG00000023445.13	382.349094411315	3.78077748494174	0.503282115011875	7.51224287962732	5.81228235093694e-14	7.16791173455253e-12	ENSG00000023445	BIRC3	330
ENSG00000172927.7	1665.71029209746	-3.35354431898923	0.448759778779309	-7.47291641891649	7.84366715448263e-14	9.60248069452428e-12	ENSG00000172927	MYEOV	26579
ENSG00000174501.14	139.18718324367	3.43523873609438	0.459948389407237	7.46874826656438	8.0961250635302e-14	9.8397253308354e-12	ENSG00000174501	ANKRD36C	400986
ENSG00000165300.7	66.2138889176771	3.87459723910058	0.519144139787982	7.46343248848569	8.42970783781453e-14	1.01714431550954e-11	ENSG00000165300	SLITRK5	26050
ENSG00000169583.12	78.8898216014326	-7.34999216302496	0.98618462568011	-7.45295756152772	9.12706495849819e-14	1.08245527695871e-11	ENSG00000169583	CLIC3	9022
ENSG00000114200.9	167.590148328749	2.82345217872135	0.378850319679037	7.45268522173449	9.14593210289368e-14	1.08245527695871e-11	ENSG00000114200	BCHE	590
ENSG00000113719.15	1609.7611262773	-2.85358916252218	0.382907910683645	-7.45241631970301	9.16459869592993e-14	1.08245527695871e-11	ENSG00000113719	ERGIC1	57222
ENSG00000145979.17	1190.76069839181	-2.38309277334956	0.319837305795636	-7.45095312575034	9.26682856490659e-14	1.08687586496932e-11	ENSG00000145979	TBC1D7	51256
ENSG00000109072.13	64.9042505766997	-5.45000804698406	0.731785988077877	-7.44754359303756	9.50941328988377e-14	1.1075824979023e-11	ENSG00000109072	VTN	7448
ENSG00000219507.4	245.721173453771	-3.13093367949625	0.422363692384126	-7.41288547276163	1.235806034535E-13	1.42944405594627e-11	ENSG00000219507	NA	NA
ENSG00000013588.7	425.264517840706	-2.5231759376433	0.340473101305264	-7.41079376893583	1.25545688007968e-13	1.43982944631653e-11	ENSG00000013588	GPRC5A	9052
ENSG00000198947.15	104.283360746456	3.57413455903528	0.482332234556971	7.41010926279512	1.26195402223068e-13	1.43982944631653e-11	ENSG00000198947	DMD	1756
ENSG00000170873.18	334.69852289884	-2.90411833511312	0.392100556363002	-7.40656519860818	1.296125350512E-13	1.46882529586401e-11	ENSG00000170873	MTSS1	9788
ENSG00000115282.19	179.440561048888	2.88271174085273	0.389842277397242	7.39455905116032	1.41878294605818e-13	1.59703540746898e-11	ENSG00000115282	TTC31	64427
ENSG00000138696.10	43.7360068009388	8.89571971379664	1.20361394240861	7.39084136562509	1.459026058689E-13	1.63138567042213e-11	ENSG00000138696	BMPR1B	658
ENSG00000116667.12	152.744365877649	3.62805026235784	0.491288243213359	7.38476915024045	1.52718125594348e-13	1.69628371024398e-11	ENSG00000116667	C1orf21	81563
ENSG00000006042.11	45.1959880906436	8.94204796749022	1.2114315725964	7.38138923383448	1.56646308809386e-13	1.72846834957304e-11	ENSG00000006042	TMEM98	26022
ENSG00000215252.11	116.23077949935	3.5842413711066	0.485718498824482	7.37925646188286	1.591759557586865e-13	1.73842768168752e-11	ENSG00000215252	GOLGA8B	440270
ENSG00000125375.14	209.027414605325	2.94679649451655	0.399355311982051	7.37888393143247	1.59621907333578e-13	1.73842768168752e-11	ENSG00000125375	ATP5S	27109
ENSG00000143365.17	57.9972544791644	-5.64429935272086	0.765201392785508	-7.37622723368853	1.628379968663777e-13	1.76201218286637e-11	ENSG00000143365	RORC	6097
ENSG00000047365.11	42.9383369466778	5.17550696439794	0.70242494285687	7.36805692484148	1.7313286400439e-13	1.86140025325745e-11	ENSG00000047365	ARAP2	116984
ENSG00000167106.11	318.50444653729	-2.91687095227074	0.396469540001877	-7.35711235787983	1.87931161951872e-13	2.00763149570497e-11	ENSG00000167106	FAM102A	399665
ENSG00000164256.10	101.686433345586	-3.39828259183803	0.463547427466031	-7.33103538167528	2.28381354480826e-13	2.42431144136229e-11	ENSG00000164256	PRDM9	56979
ENSG00000129317.14	110.45992459767	3.29679431044558	0.451954812186144	7.29452197775858	2.99721300935244e-13	3.16158846495969e-11	ENSG00000129317	PUS7L	83448
ENSG00000185955.4	77.3553037261775	-3.71025997153799	0.508760532822035	-7.29274330883651	3.03706404753421e-13	3.18360238782774e-11	ENSG00000185955	C7orf61	402573
ENSG00000136235.15	338.917913186287	-3.19952042245089	0.439821915398519	-7.27458162140881	3.47495720914229e-13	3.61999890134997e-11	ENSG00000136235	GPNMB	10457
ENSG00000135976.17	175.425830521519	3.4924678085211	0.480511796763875	7.26822490528221	3.64242003545937e-13	3.7710289404151e-11	ENSG00000135976	ANKRD36	375248
ENSG00000185129.5	204.658971892259	3.20115426030863	0.441219849278294	7.25523628536835	4.0096126101761e-13	4.12571918391862e-11	ENSG00000185129	PURA	5813
ENSG00000100815.12	315.14241057875	3.37255757594515	0.466568435334941	7.22843064495791	4.88607245152494e-13	4.99690287542539e-11	ENSG00000100815	TRIP11	9321
ENSG00000132879.13	110.233827957496	-3.50036442390408	0.484621982375996	-7.22287587274221	5.08994715402514e-13	5.17385416165513e-11	ENSG00000132879	FBXO44	93611
ENSG00000075340.22	39.6750583282169	7.33052278004866	1.0175332144385	7.20420982433858	5.83814070787505e-13	5.898632286294E-11	ENSG00000075340	ADD2	119
ENSG00000133739.15	85.2209727773856	3.7382529006725	0.519955165903869	7.18956776624014	6.49967543025089e-13	6.52769798300407e-11	ENSG00000133739	LRRCC1	85444
ENSG00000115380.19	1030.68330337103	-4.16143978259418	0.578890298452755	-7.18865006671693	6.54350408710781e-13	6.53259824696263e-11	ENSG00000115380	EFEMP1	2202
ENSG00000163453.11	1538.24574225604	2.81163988251772	0.391497884019986	7.18174988239318	6.88247492458911e-13	6.8303473038585e-11	ENSG00000163453	IGFBP7	3490
ENSG00000135919.12	3964.7676077623	-2.90443095930267	0.405160593738218	-7.16859192179801	7.57730492346071e-13	7.47567989272553e-11	ENSG00000135919	SERPINE2	5270
ENSG00000169031.19	54.2254918882886	3.83502407702455	0.535332161626703	7.16382155215771	7.84585217912401e-13	7.69535864024959e-11	ENSG00000169031	COL4A3	1285

ENSG00000205336.11	1794.94151723729	-4.46914290555798	0.507603820506921	-8.80439178155681	1.31564067322214e-18	3.87121497741784e-16	ENSG00000205336	ADGRG1	9289
ENSG00000230590.9	553.05078628887	3.99233482443499	0.454911919425857	8.77606115371455	1.69299791406851e-18	4.89568293357879e-16	ENSG00000230590	FTX	100302692
ENSG00000239467.5	63.988129331875	6.52722143113399	0.751515513696517	8.68541142820621	3.77373990808388e-18	1.07276552098954e-15	ENSG00000239467	ERICH2	285141
ENSG00000126790.11	650.158837964822	2.9618427646636	0.342232619154349	8.65447242282824	4.95196893291812e-18	1.38424038238171e-15	ENSG00000126790	L3HYPDH	112849
ENSG00000126368.5	3288.04619176519	-2.93927673364315	0.342323626648722	-8.58625144404454	8.98529028641213e-18	2.47051292924105e-15	ENSG00000126368	NR1D1	9572
ENSG00000258289.8	239.353303682094	3.94466311785749	0.461432526740034	8.54873223984895	1.24447847510279e-17	3.36651499748775e-15	ENSG00000258289	CHURC1	91612
ENSG00000169760.17	83.0159165850453	6.49605085840681	0.76514847681672	8.48992196316277	2.06775899495494e-17	5.50483394656894e-15	ENSG00000169760	NLGN1	22871
ENSG00000170627.10	250.953106214241	-10.5202680314362	1.24117402644812	-8.47606202455117	2.32944599089643e-17	6.10460439989296e-15	ENSG00000170627	GTSF1	121355
ENSG00000128294.15	1976.44440056507	-3.11348535476067	0.37022845786968	-8.40963272428023	4.11296575458195e-17	1.05836864993564e-14	ENSG00000128294	TPST2	8459
ENSG00000155850.7	131.634856505977	3.95770497414434	0.470697932237892	8.40816307674813	4.16481820270406e-17	1.05836864993564e-14	ENSG00000155850	SLC26A2	1836
ENSG00000217801.9	792.388690886207	-2.90834209849908	0.346406787272905	-8.39574224683954	4.62960238370892e-17	1.15892076387412e-14	ENSG00000217801	LOC100288175	100288175
ENSG00000108828.15	15812.423337938	-3.34947849461204	0.399977406681223	-8.37416923721778	5.56147897118405e-17	1.37172243095145e-14	ENSG00000108828	VAT1	10493
ENSG00000183421.11	766.658490077675	-3.15122317357531	0.377151016396114	-8.35533522801286	6.52471515908322e-17	1.58597858910353e-14	ENSG00000183421	RIPK4	54101
ENSG00000162775.14	454.699533334702	-2.71859827532284	0.326325060724178	-8.33095156495104	8.01951374681431e-17	1.92147549373671e-14	ENSG00000162775	RBM15	64783
ENSG00000171345.13	892.456689649215	-4.35572955251283	0.523868205099113	-8.31455222919807	9.20993362046979e-17	2.17561981242985e-14	ENSG00000171345	KRT19	3880
ENSG00000248370.1	110.86841284314	-10.3043608830693	1.24294287989953	-8.29029318217919	1.12969662939575e-16	2.63156553725354e-14	ENSG00000248370	NA	NA
ENSG00000187134.13	279.143014147407	-3.56271154391796	0.430913919531139	-8.26780334177743	1.3644972527265e-16	3.13497916749711e-14	ENSG00000187134	AKR1C1	1645
ENSG00000197183.14	1465.27438849675	-2.51841260569034	0.305057571320965	-8.25553220916652	1.51226834669986e-16	3.4275357717365e-14	ENSG00000197183	NOL4L	140688
ENSG00000186480.12	1534.2100072489	-3.01465952444689	0.365365633315358	-8.25107577056885	1.56974979314727e-16	3.51037913742214e-14	ENSG00000186480	INSIG1	3638
ENSG00000107890.16	77.3548042140058	4.99342158977475	0.6053500914609	8.24881611519056	1.59971367405742e-16	3.53031549227514e-14	ENSG00000107890	ANKRD26	22852
ENSG00000185909.14	124.771610981229	-3.78794932503755	0.460025640044702	-8.23421347703459	1.80741140324067e-16	3.92420591935856e-14	ENSG00000185909	KLHDC8B	200942
ENSG00000179542.15	72.4335797420405	4.06783882308013	0.494086238434652	8.23305428616617	1.82499440561631e-16	3.92420591935856e-14	ENSG00000179542	SLITRK4	139065
ENSG00000173432.10	1120.73767454795	-4.06665637495852	0.495943674757581	-8.19983514649384	2.40716907324807e-16	5.11051135398945e-14	ENSG00000173432	SAA1	6288
ENSG00000248323.5	519.123866048489	3.44726559251539	0.421301672562498	8.18241610945423	2.78208423131182e-16	5.83263959094523e-14	ENSG00000248323	LUCAT1	100505994
ENSG00000123689.5	3259.38978885063	2.94789562562921	0.360678535956254	8.17319394350305	3.00330606531868e-16	6.21869744784258e-14	ENSG00000123689	G0S2	50486
ENSG00000123933.16	74.1356134517739	4.05225864769099	0.497233246937672	8.14961323010433	3.65090047785904e-16	7.46742717251852e-14	ENSG00000123933	MXD4	10608
ENSG00000187325.4	253.846225361258	3.93249627603955	0.484318880762059	8.11964272351287	4.67558044293435e-16	9.44805243239698e-14	ENSG00000187325	TAF9B	51616
ENSG00000127914.16	506.972378198614	3.66250935315158	0.45202389284459	8.10246850028962	5.38550895668234e-16	1.07530662168424e-13	ENSG00000127914	AKAP9	10142
ENSG00000124216.3	365.180959603502	-2.94464871271999	0.363738148645285	-8.09551795347041	5.70212025858157e-16	1.12512895266977e-13	ENSG00000124216	SNAI1	6615
ENSG00000185946.15	118.085936568533	3.53467135220785	0.437366509202692	8.08171471256787	6.38623650729342e-16	1.24546463605029e-13	ENSG00000185946	RNPC3	55599
ENSG00000205413.7	154.5023641666	5.12839782980555	0.635456266710123	8.07041821517668	7.00577791422943e-16	1.35058513997076e-13	ENSG00000205413	SAMD9	54809
ENSG00000239911.2	83.0297887116242	-3.87535173818659	0.481373455293011	-8.05061370870081	8.2379897554616e-16	1.55910508101175e-13	ENSG00000239911	NA	NA
ENSG00000088827.12	63.3572647892341	-5.59923544520825	0.695591276997523	-8.04960560945646	8.30612582285296e-16	1.55910508101175e-13	ENSG00000088827	SIGLEC1	6614
ENSG00000163931.15	12528.3846610063	-3.25844201634793	0.404839668565318	-8.04872217165696	8.36629246905899e-16	1.55910508101175e-13	ENSG00000163931	TKT	7086
ENSG00000227467.3	76.0798345981885	5.61875480156112	0.699824771699257	8.02880239280201	9.8428747117542e-16	1.79487287671528e-13	ENSG00000227467	LINC01537	101928555
ENSG00000109472.13	1836.06237687941	3.29519819406866	0.410423788586901	8.0287699828855	9.84547487823789e-16	1.79487287671528e-13	ENSG00000109472	CPE	1363
ENSG00000108691.9	50.201370776972	5.57807232521399	0.698257104179872	7.98856508845068	1.36518383925324e-15	2.46202831741456e-13	ENSG00000108691	CCL2	6347
ENSG00000075213.10	58.3994236484615	6.20679268275901	0.779557288833583	7.96194554481808	1.69355011632636e-15	3.02172580330061e-13	ENSG00000075213	SEMA3A	10371
ENSG00000224848.1	68.1669159937059	-4.98207614467971	0.628344057617479	-7.9288983229514	2.21098472182384e-15	3.90343534257153e-13	ENSG00000224848	NA	NA
ENSG00000116183.10	47.9986101439218	6.1773929686211	0.779488864524009	7.92492779533585	2.28278937802324e-15	3.98822327585476e-13	ENSG00000116183	PAPPA2	60676
ENSG00000049323.15	619.175955102522	-2.63461700422385	0.333920464508989	-7.88995369929754	3.02298669735433e-15	5.22696215340482e-13	ENSG00000049323	LTBP1	4052
ENSG00000067715.13	55.7132236681354	7.39451843532886	0.937839879639921	7.88462785157733	3.15474265280977e-15	5.39911671152301e-13	ENSG00000067715	SYT1	6857
ENSG00000133107.14	165.680614807496	-3.86124053578494	0.490995968430591	-7.86409824937448	3.71765686473578e-15	6.29823645811601e-13	ENSG00000133107	TRPC4	7223
ENSG00000121671.11	425.304172333665	-3.00207846014184	0.382398941612854	-7.85064531685127	4.13901976645896e-15	6.94196395230497e-13	ENSG00000121671	CRY2	1408
ENSG00000183668.17	72.5278291921274	-5.17317158496928	0.659073381089626	-7.84915873315446	4.18837236351151e-15	6.95518626542723e-13	ENSG00000183668	PSG9	5678
ENSG00000198846.5	271.390613157468	-3.98522995516655	0.509490839103821	-7.82198549865283	5.19966002015153e-15	8.54987233901779e-13	ENSG00000198846	TOX	9760
ENSG00000019549.10	224.392829988961	-3.85619932768357	0.49389400828247	-7.8077467290879	5.82194288609575e-15	9.48015787238815e-13	ENSG00000019549	SNAI2	6591
ENSG00000165474.6	1771.47052365791	-2.78422697312403	0.356926612679012	-7.80055864208679	6.16337180298024e-15	9.9396222961139e-13	ENSG00000165474	GJB2	2706
ENSG00000072163.19	158.346471293037	-3.98783870102133	0.511476877833999	-7.79671354433268	6.35402545874947e-15	1.01494966661091e-12	ENSG00000072163	LIMS2	55679
ENSG00000136869.14	140.177929009359	3.23767607179664	0.417403503731066	7.75670554476869	8.71639885075242e-15	1.37916454268698e-12	ENSG00000136869	TLR4	7099
ENSG00000244242.1	61.6571602739308	-4.62033643644789	0.596338515565792	-7.74784173057182	9.34675336992283e-15	1.4650817525266e-12	ENSG00000244242	IFITM10	402778
ENSG00000116337.15	3926.07894849259	-3.12913846664761	0.404911341038505	-7.72795955436093	1.09284052056251e-14	1.69714085285875e-12	ENSG00000116337	AMPD2	271
ENSG00000157227.12	1339.46436353217	-2.79013411198199	0.361595109771828	-7.71618320209752	1.19864988284423e-14	1.84438126927187e-12	ENSG00000157227	MMP14	4323
ENSG00000250337.5	158.533996212619	3.12576909985429	0.405695341041889	7.70472022633248	1.31130256431156e-14	1.99937878260305e-12	ENSG00000250337	PURPL	643401
ENSG00000197872.11	757.433228996248	-3.3042321337074	0.42936982915496	-7.6955386926241	1.4089928483249e-14	2.12897550018965e-12	ENSG00000197872	FAM49A	81553
ENSG00000167996.15	29789.9991705919	-2.97675312500488	0.386995964575416	-7.69194874750378	1.44910670785986e-14	2.17003729502014e-12	ENSG00000167996	FTH1	2495
ENSG00000084207.16	1157.06397968887	-3.25417410419184	0.423344278014358	-7.68682671100488	1.50829204199483e-14	2.22887171834496e-12	ENSG00000084207	GSTP1	2950
ENSG00000187187.13	67.9837200422747	4.62721782749869	0.602011545381294	7.68626094133787	1.51497362205656e-14	2.22887171834496e-12	ENSG00000187187	ZNF546	339327

ENSG00000187187.13	67.9837200422747	4.62721782749869	0.602011545381294	7.68626094133787	1.51497362205656e-14	2.22887171834496e-12	ENSG00000187187	ZNF546	339327
ENSG00000148926.9	24344.3622745058	-2.39584111707686	0.31224283616784	-7.67300587735189	1.68011787560912e-14	2.45034234867097e-12	ENSG00000148926	ADM	133
ENSG00000145423.4	105.318788529399	6.69823935402902	0.87342191873699	7.66896182742357	1.73394025643617e-14	2.50703844663341e-12	ENSG00000145423	SFRP2	6423
ENSG00000165006.13	2990.74359907745	-2.43323128136103	0.317748740190334	-7.65772125454694	1.89261109545O7e-14	2.71306609341018e-12	ENSG00000165006	UBAP1	51271
ENSG00000113552.15	6199.83276544904	-2.82812292031337	0.369839984875931	-7.64688253289356	2.0591026518482e-14	2.92671776922017e-12	ENSG00000113552	GNPDA1	10007
ENSG00000196912.12	110.788482497701	3.53729096105244	0.462917430992467	7.64129999051601	2.15039374369796e-14	3.03079024111783e-12	ENSG00000196912	ANKRD36B	57730
ENSG00000121207.11	50.8980796974381	5.4499052617096	0.714090024891438	7.63195825699728	2.31214310868885e-14	3.23160535157746e-12	ENSG00000121207	LRAT	9227
ENSG00000187957.7	106.397175738047	-3.7030682289405	0.48604635986602	-7.61875519438364	2.56133698319907e-14	3.55030941175328e-12	ENSG00000187957	DNER	92737
ENSG00000158639.12	53.3211632809483	9.18126082330659	1.20546705334332	7.61635151939049	2.60946444369614e-14	3.58737193849768e-12	ENSG00000158639	PAGE5	90737
ENSG00000088826.17	5151.19508351597	-3.23286520127786	0.424640674149635	-7.61317838370487	2.67436274807351e-14	3.64670016347064e-12	ENSG00000088826	SMOX	54498
ENSG00000183696.13	9219.0641033238	-2.98513715132757	0.392257823843963	-7.61014049910968	2.73798119877952e-14	3.70334037628468e-12	ENSG00000183696	UPP1	7378
ENSG00000167191.11	119.14351895424	-4.1139055053744	0.540717668502587	-7.60823206825674	2.77870578506041e-14	3.72835627416266e-12	ENSG00000167191	GPRC5B	51704
ENSG00000249867.5	102.611487147581	3.95730546863316	0.520596717553672	7.60147986954062	2.92763318615005e-14	3.89700506334195e-12	ENSG00000249867	NA	NA
ENSG00000162409.10	44.8202330957779	5.01077082460094	0.659625228895306	7.59639050342666	3.04504722615429e-14	4.02138047850864e-12	ENSG00000162409	PRKAA2	5563
ENSG00000233452.6	245.819325189437	3.01395006008006	0.397143420010926	7.58907212914956	3.22204376091041e-14	4.22188421546793e-12	ENSG00000233452	NA	NA
ENSG00000108848.15	488.815225588833	3.0961548995214	0.408283299185053	7.58334936966911	3.36746453995059e-14	4.37822598946134e-12	ENSG00000108848	LUC7L3	51747
ENSG00000164318.17	509.12963907659	-3.24546769456408	0.428083669641652	-7.58138636141121	3.41881818495765e-14	4.41080143062383e-12	ENSG00000164318	EGFLAM	133584
ENSG00000232453.6	109.279487889265	-4.14844549618609	0.547834933862718	-7.57243695091861	3.66287004166759e-14	4.68959208693502e-12	ENSG00000232453	LOC1053787	105378753
ENSG00000104892.16	91.7792332428386	-4.37471382688685	0.579216897655081	-7.55280766945435	4.25973818625856e-14	5.4124491560552e-12	ENSG00000104892	KLC3	147700
ENSG00000132965.9	153.180584964217	3.46659620588762	0.459692584403865	7.54111839846871	4.65957815854454e-14	5.87597329888038e-12	ENSG00000132965	ALOX5AP	241
ENSG00000006704.10	672.498722188956	-2.52960330595368	0.335664491215156	-7.53610635666625	4.84211709008852e-14	6.06059610708691e-12	ENSG00000006704	GTF2IRD1	9569
ENSG00000134070.4	420.904967715609	-2.61071842286997	0.346816045160956	-7.5276748561571	5.16518150095539e-14	6.41706845437213e-12	ENSG00000134070	IRAK2	3656
ENSG00000023445.13	382.349094411315	3.78077748494174	0.503282115011875	7.51224287962732	5.81228235093694e-14	7.16791173455253e-12	ENSG00000023445	BIRC3	330
ENSG00000172927.7	1665.71029209746	-3.35354431898923	0.448759778779309	-7.47291641891649	7.84366715448263e-14	9.60248069452428e-12	ENSG00000172927	MYEOV	26579
ENSG00000174501.14	139.18718324367	3.43523873609438	0.459948389407237	7.46874826656438	8.0961250635302e-14	9.8397253308354e-12	ENSG00000174501	ANKRD36C	400986
ENSG00000165300.7	66.2138889176771	3.87459723910058	0.519144139787982	7.46343248848569	8.42970783781453e-14	1.01714431550954e-11	ENSG00000165300	SLITRK5	26050
ENSG00000169583.12	78.8898216014326	-7.34999216302496	0.98618462568011	-7.45295756152772	9.12706495849819e-14	1.08245527695871e-11	ENSG00000169583	CLIC3	9022
ENSG00000114200.9	167.590148328749	2.82345217872135	0.378850319679037	7.45268522173449	9.14593210289368e-14	1.08245527695871e-11	ENSG00000114200	BCHE	590
ENSG00000113719.15	1609.7611262773	-2.85358916252218	0.382907910683645	-7.45241631970301	9.16459869592993e-14	1.08245527695871e-11	ENSG00000113719	ERGIC1	57222
ENSG00000145979.17	1190.76069839181	-2.38309277334956	0.319837305795636	-7.45095312575034	9.26682856490659e-14	1.08687586496932e-11	ENSG00000145979	TBC1D7	51256
ENSG00000109072.13	64.9042505766997	-5.45000804698406	0.731785988077877	-7.44754359303756	9.50941328988377e-14	1.1075824979023e-11	ENSG00000109072	VTN	7448
ENSG00000219507.4	245.721173453771	-3.13093367949625	0.422363692384126	-7.41288547276163	1.235806034535E-13	1.42944405594627e-11	ENSG00000219507	NA	NA
ENSG00000013588.7	425.264517840706	-2.5231759376433	0.340473101305264	-7.41079376893583	1.25545688007968e-13	1.43982944631653e-11	ENSG00000013588	GPRC5A	9052
ENSG00000198947.15	104.283360746456	3.57413455903528	0.482332234556971	7.41010926279512	1.26195402223068e-13	1.43982944631653e-11	ENSG00000198947	DMD	1756
ENSG00000170873.18	334.69852289884	-2.90411833511312	0.392100556363002	-7.40656519860818	1.296125350512E-13	1.46882529586401e-11	ENSG00000170873	MTSS1	9788
ENSG00000115282.19	179.440561048888	2.88271174085273	0.389842277397242	7.39455905116032	1.41878294605818e-13	1.59703540746898e-11	ENSG00000115282	TTC31	64427
ENSG00000138696.10	43.7360068009388	8.89571971379664	1.20361394240861	7.39084136562509	1.459026058689E-13	1.63138567042213e-11	ENSG00000138696	BMPR1B	658
ENSG00000116667.12	152.744365877649	3.62805026235784	0.491288243213359	7.38476915024045	1.52718125594348e-13	1.69628371024398e-11	ENSG00000116667	C1orf21	81563
ENSG00000006042.11	45.1959880906436	8.94204796749022	1.2114315725964	7.38138923383448	1.56646308809386e-13	1.72846834957304e-11	ENSG00000006042	TMEM98	26022
ENSG00000215252.11	116.23077949935	3.5842413711066	0.485718498824482	7.37925646188286	1.59175955758865e-13	1.73842768168752e-11	ENSG00000215252	GOLGA8B	440270
ENSG00000125375.14	209.027414605325	2.94679649451655	0.399355311982051	7.37888393143247	1.59621907333578e-13	1.73842768168752e-11	ENSG00000125375	ATP5S	27109
ENSG00000143365.17	57.9972544791644	-5.64429935272086	0.765201392785508	-7.37622723368853	1.62837996866377e-13	1.76201218286637e-11	ENSG00000143365	RORC	6097
ENSG00000047365.11	42.9383369466778	5.17550696439794	0.70242494285687	7.36805692484148	1.7313286400439e-13	1.86140025325745e-11	ENSG00000047365	ARAP2	116984
ENSG00000167106.11	318.50444653729	-2.91687095227074	0.396469540001877	-7.35711235787983	1.87931161951872e-13	2.00763149570497e-11	ENSG00000167106	FAM102A	399665
ENSG00000164256.10	101.686433345586	-3.39828259183803	0.463547427466031	-7.33103538167528	2.28381354480826e-13	2.42431144136229e-11	ENSG00000164256	PRDM9	56979
ENSG00000129317.14	110.45992459767	3.29679431044558	0.451954812186144	7.29452197775858	2.99721300935244e-13	3.16158846495969e-11	ENSG00000129317	PUS7L	83448
ENSG00000185955.4	77.3553037261775	-3.71025997153799	0.508760532822035	-7.29274330883651	3.03706404753421e-13	3.18360238782774e-11	ENSG00000185955	C7orf61	402573
ENSG00000136235.15	338.917913186287	-3.19952042245089	0.439821915398519	-7.27458162140881	3.47495720914229e-13	3.61999890134997e-11	ENSG00000136235	GPNMB	10457
ENSG00000135976.17	175.425830521519	3.4924678085211	0.480511796763875	7.26822490528221	3.64242003545937e-13	3.7710289404151e-11	ENSG00000135976	ANKRD36	375248
ENSG00000185129.5	204.658971892259	3.20115426030863	0.441219849278294	7.25523628536835	4.0096126101761e-13	4.12571918391862e-11	ENSG00000185129	PURA	5813
ENSG00000100815.12	315.14241057875	3.37255757594515	0.466568435334941	7.22843064495791	4.88607245152494e-13	4.99690287542539e-11	ENSG00000100815	TRIP11	9321
ENSG00000132879.13	110.233827957496	-3.50036442390408	0.484621982375996	-7.22287587274221	5.08994715402514e-13	5.17385416165513e-11	ENSG00000132879	FBXO44	93611
ENSG00000075340.22	39.6750583282169	7.33052278004866	1.0175332144385	7.20420982433858	5.83814070787505e-13	5.898632286294E-11	ENSG00000075340	ADD2	119
ENSG00000133739.15	85.2209727773856	3.7382529006725	0.519955165903869	7.18956776624014	6.49967543025089e-13	6.52769798300407e-11	ENSG00000133739	LRRCC1	85444
ENSG00000115380.19	1030.68330337103	-4.16143978259418	0.578890298452755	-7.18865006671693	6.54350408710781e-13	6.53259824696263e-11	ENSG00000115380	EFEMP1	2202
ENSG00000163453.11	1538.24574225604	2.81163988251772	0.391497884019986	7.18174988239318	6.88247492458911e-13	6.8303473038585e-11	ENSG00000163453	IGFBP7	3490
ENSG00000135919.12	3964.7676077623	-2.90443095930267	0.405160593738218	-7.16859192179801	7.57730492346071e-13	7.47567989272253e-11	ENSG00000135919	SERPINE2	5270
ENSG00000169031.19	54.2254918882886	3.83502407702455	0.535332161626703	7.16382155215771	7.84585217912401e-13	7.69535864024959e-11	ENSG00000169031	COL4A3	1285
ENSG00000065618.18	154.527223204034	3.07655781985552	0.429949831407513	7.15562048200806	8.32952942428476e-13	8.08878685447659e-11	ENSG00000065618	COL17A1	1308

ENSG00000185955.4	77.3553037261775	-3.71025997153799	0.508760532822035	-7.29274330883651	3.03706404753421e-13	3.18360238782774e-11	ENSG00000185955	C7orf61	402573
ENSG00000136235.15	338.917913186287	-3.19952042245089	0.439821915398519	-7.27458162140881	3.47495720914229e-13	3.61999890134997e-11	ENSG00000136235	GPNMB	10457
ENSG00000135976.17	175.425830521519	3.4924678085211	0.480511796763875	7.26822490528221	3.64242003545937e-13	3.7710289404151e-11	ENSG00000135976	ANKRD36	375248
ENSG00000185129.5	204.658971892259	3.20115426030863	0.441219849278294	7.25523628536835	4.0096126101761e-13	4.12571918391862e-11	ENSG00000185129	PURA	5813
ENSG00000100815.12	315.14241057875	3.37255757594515	0.466568435334941	7.22843064495791	4.88607245152494e-13	4.99690287542539e-11	ENSG00000100815	TRIP11	9321
ENSG00000132879.13	110.233827957496	-3.50036442390408	0.484621982375996	-7.22287587274221	5.08994715402514e-13	5.17385416165513e-11	ENSG00000132879	FBXO44	93611
ENSG00000075340.22	39.6750583282169	7.33052278004866	1.0175332144385	7.20420982433858	5.83814070787505e-13	5.898632286294E-11	ENSG00000075340	ADD2	119
ENSG00000133739.15	85.2209727773856	3.7382529006725	0.519955165903869	7.18956776624014	6.49967543025089e-13	6.52769798300407e-11	ENSG00000133739	LRRCC1	85444
ENSG00000115380.19	1030.68330337103	-4.16143978259418	0.578890298452755	-7.18865006671693	6.54350408710781e-13	6.53259824696263e-11	ENSG00000115380	EFEMP1	2202
ENSG00000163453.11	1538.24574225604	2.81163988251772	0.391497884019986	7.18174988239318	6.88247492458911e-13	6.8303473038585e-11	ENSG00000163453	IGFBP7	3490
ENSG00000135919.12	3964.7676077623	-2.90443095930267	0.405160593738218	-7.16859192179801	7.57730492346071e-13	7.47567989272253e-11	ENSG00000135919	SERPINE2	5270
ENSG00000169031.19	54.2254918882886	3.83502407702455	0.535332161626703	7.16382155215771	7.84585217912401e-13	7.69535864024959e-11	ENSG00000169031	COL4A3	1285
ENSG00000065618.18	154.527223204034	3.07655781985552	0.429949831407513	7.15562048200806	8.32952942428476e-13	8.08878685447659e-11	ENSG00000065618	COL17A1	1308
ENSG00000164761.8	114.823172791342	3.89233068998651	0.543971710096716	7.15539175611627	8.34343027560487e-13	8.08878685447659e-11	ENSG00000164761	TNFRSF11B	4982
ENSG00000198707.14	113.696662173163	3.23661039584287	0.452392415809301	7.15443115918021	8.40205974279763e-13	8.09881298886218e-11	ENSG00000198707	CEP290	80184
ENSG00000267534.3	686.808253511664	-2.79211622061706	0.391981524511878	-7.12308118117044	1.05540612822211e-12	1.0107847148876e-10	ENSG00000267534	S1PR2	9294
ENSG00000136160.15	39.7463227972166	7.91165792270863	1.11081445311116	7.12239375401508	1.06068512890662e-12	1.0107847148876e-10	ENSG00000136160	EDNRB	1910
ENSG00000153956.15	38.5071826775154	5.22844573597945	0.734561011070799	7.1177828079355	1.09677016553102e-12	1.03926718736081e-10	ENSG00000153956	CACNA2D1	781
ENSG00000165025.14	77.7874540032704	4.78598633945742	0.672547033917495	7.11621061144186	1.10934738848818e-12	1.04527946065863e-10	ENSG00000165025	SYK	6850
ENSG00000141447.17	39.9835431668147	8.75878534337878	1.231317496797	7.11334433739699	1.13264219496433e-12	1.06126675385149e-10	ENSG00000141447	OSBPL1A	114876
ENSG00000136783.9	396.314173714613	2.5788649486108	0.362961009492221	7.1050743224971	1.20257805930232e-12	1.12053551170103e-10	ENSG00000136783	NIPSNAP3A	25934
ENSG00000169239.12	317.997051695632	-2.32025216841009	0.326950640674131	-7.09664359007224	1.27823134088174e-12	1.1844472955397e-10	ENSG00000169239	CA5B	11238
ENSG00000132357.13	36.402748840597	8.62895512864573	1.21650049695782	7.09326066879932	1.30988393311388e-12	1.20710842451571e-10	ENSG00000132357	CARD6	84674
ENSG00000165912.15	157.340925135937	-2.89413470026329	0.408659484780786	-7.08202013668119	1.42068006830221e-12	1.30086820830347e-10	ENSG00000165912	PACSIN3	29763
ENSG00000140297.12	425.314213377337	-2.9267495064948	0.413301458005193	-7.08139168107658	1.42713898359073e-12	1.30086820830347e-10	ENSG00000140297	GCNT3	9245
ENSG00000160867.14	193.997374761967	-3.39528066596834	0.479783370988373	-7.076695173853	1.47632778896268e-12	1.33843079332335e-10	ENSG00000160867	FGFR4	2264
ENSG00000168243.10	115.133029386057	-2.99194225111354	0.423032910510922	-7.07259926302187	1.52058138061699e-12	1.37113929654345e-10	ENSG00000168243	GNG4	2786
ENSG00000111331.12	964.254913769934	3.44413967331545	0.487085219164287	7.07091806075477	1.53912006175782e-12	1.38043431421402e-10	ENSG00000111331	OAS3	4940
ENSG00000214114.8	137.022209505342	2.98020035968319	0.421613776735556	7.06855545081588	1.56554793272008e-12	1.39666861316922e-10	ENSG00000214114	MYCBP	26292
ENSG00000166016.5	512.521619054105	-2.34398196408373	0.332067009315988	-7.05876193155112	1.67992595793739e-12	1.49077873896963e-10	ENSG00000166016	ABTB2	25841
ENSG00000150756.13	70.5048325878336	3.61698954705102	0.512921338953382	7.05174316676218	1.76690114411027e-12	1.55970873626408e-10	ENSG00000150756	FAM173B	134145
ENSG00000166046.10	95.3086707446312	-2.87508815067688	0.408046129983252	-7.04598803766351	1.84150075476133e-12	1.61704977271502e-10	ENSG00000166046	TCP11L2	255394
ENSG00000248475.5	55.9252684580606	5.04658662598399	0.716413427677029	7.04423790931383	1.86479291173536e-12	1.62897430810549e-10	ENSG00000248475	NA	NA
ENSG00000253352.9	199.366704886654	3.0259609992454	0.429697380155975	7.04207458315668	1.89398393418994e-12	1.64590147897584e-10	ENSG00000253352	NA	NA
ENSG00000105514.7	320.21885426076	-2.49577765950329	0.354902120906478	-7.03229851974022	2.03158553865552e-12	1.75637900280054e-10	ENSG00000105514	RAB3D	9545
ENSG00000158528.11	128.319996662366	3.35188125631777	0.476943913509595	7.02783107483841	2.09768635769101e-12	1.804225414933E-10	ENSG00000158528	PPP1R9A	55607
ENSG00000116212.14	788.18094115894	-2.34553862590116	0.333947695970418	-7.023670635263	2.1611392539378e-12	1.84931773301249e-10	ENSG00000116212	LRRC42	115353
ENSG00000077684.15	2116.20440230818	-2.2401996498664	0.319799577292636	-7.00501129123285	2.46965916344361e-12	2.10259510097849e-10	ENSG00000077684	JADE1	79960
ENSG00000198910.13	371.377883931241	-4.11930768533154	0.588390398425269	-7.00097706617274	2.54183554280623e-12	2.15311443050233e-10	ENSG00000198910	L1CAM	3897
ENSG00000036672.15	138.057906918693	-2.92973703770972	0.418537235003765	-6.99994359565971	2.56065576698628e-12	2.15815670974341e-10	ENSG00000036672	USP2	9099
ENSG00000105855.9	35.9106299554001	7.7649609310894	1.11051263955514	6.99223102422317	2.70548877637368e-12	2.26882288786696e-10	ENSG00000105855	ITGB8	3696
ENSG00000198074.9	51.4518290061411	-3.78906734640162	0.542058301786722	-6.99014724783694	2.74597887537818e-12	2.29132127849664e-10	ENSG00000198074	AKR1B10	57016
ENSG00000169242.11	1696.51555803738	-2.4926622587735	0.357118121745906	-6.97993774885237	2.95310885579134e-12	2.45195751135309e-10	ENSG00000169242	EFNA1	1942
ENSG00000196586.13	500.700671382185	3.07221817485666	0.440474014404224	6.97480004356688	3.06306156830944e-12	2.5307225922998e-10	ENSG00000196586	MYO6	4646
ENSG00000106366.8	31007.359683443	-3.79206841034501	0.544066743237444	-6.96985885919157	3.17259110620112e-12	2.60836755064731e-10	ENSG00000106366	SERPINE1	5054
ENSG00000247345.2	40.7238508252218	5.50992589715277	0.790743940168123	6.96802797626408	3.21414322656983e-12	2.62963952175752e-10	ENSG00000247345	NA	NA
ENSG00000144136.10	1959.23486226043	-2.39824088484346	0.34445224210457	-6.96247720784293	3.34340702927176e-12	2.72025421015915e-10	ENSG00000144136	SLC20A1	6574
ENSG00000280128.1	40.1920637552244	8.76431921533876	1.25889911551396	6.96189163002204	3.35733735692191e-12	2.72025421015915e-10	ENSG00000280128	NA	NA
ENSG00000068028.17	1770.16293093169	-2.24746605067679	0.322899403440865	-6.96026696465667	3.39628523747366e-12	2.73858153860135e-10	ENSG00000068028	RASSF1	11186
ENSG00000162745.10	54.7266710237024	-5.17685260675896	0.744127136234349	-6.95694640697609	3.47727160115517e-12	2.79046886576911e-10	ENSG00000162745	OLFML2B	25903
ENSG00000092607.14	479.366316700438	-2.65977297341565	0.382451681118382	-6.95453335605121	3.53730940934013e-12	2.82513111492632e-10	ENSG00000092607	TBX15	6913
ENSG00000180626.9	109.932179343997	4.20170593671596	0.604822871584778	6.94700239378598	3.73129373635097e-12	2.96593642398476e-10	ENSG00000180626	ZNF594	84622
ENSG00000134107.4	7186.55033063756	-2.68816527185637	0.387454993853449	-6.93800651559841	3.97671381468924e-12	3.14610585377207e-10	ENSG00000134107	BHLHE40	8553
ENSG00000197646.7	137.78522207986	3.37665336027738	0.486866418601984	6.93548215950752	4.04837987569454e-12	3.18776653873938e-10	ENSG00000197646	PDCD1LG2	80380
ENSG00000136960.12	4170.59262715138	-7.11473167904477	1.0280378781045	-6.92069021052311	4.49448389212981e-12	3.5224992448038e-10	ENSG00000136960	ENPP2	5168
ENSG00000181722.16	958.434164275001	2.94857420057176	0.426568158899649	6.91231668153042	4.7680195683234e-12	3.71949879999628e-10	ENSG00000181722	ZBTB20	26137
ENSG00000206337.10	100.837489526406	3.26892568001885	0.473041659293011	6.91043931501605	4.83155093315514e-12	3.75160982642953e-10	ENSG00000206337	HCP5	10866
ENSG00000144369.12	51.943596717219	4.21788925544222	0.611123013694643	6.90186617247859	5.13237760427876e-12	3.96683120640384e-10	ENSG00000144369	FAM171B	165215

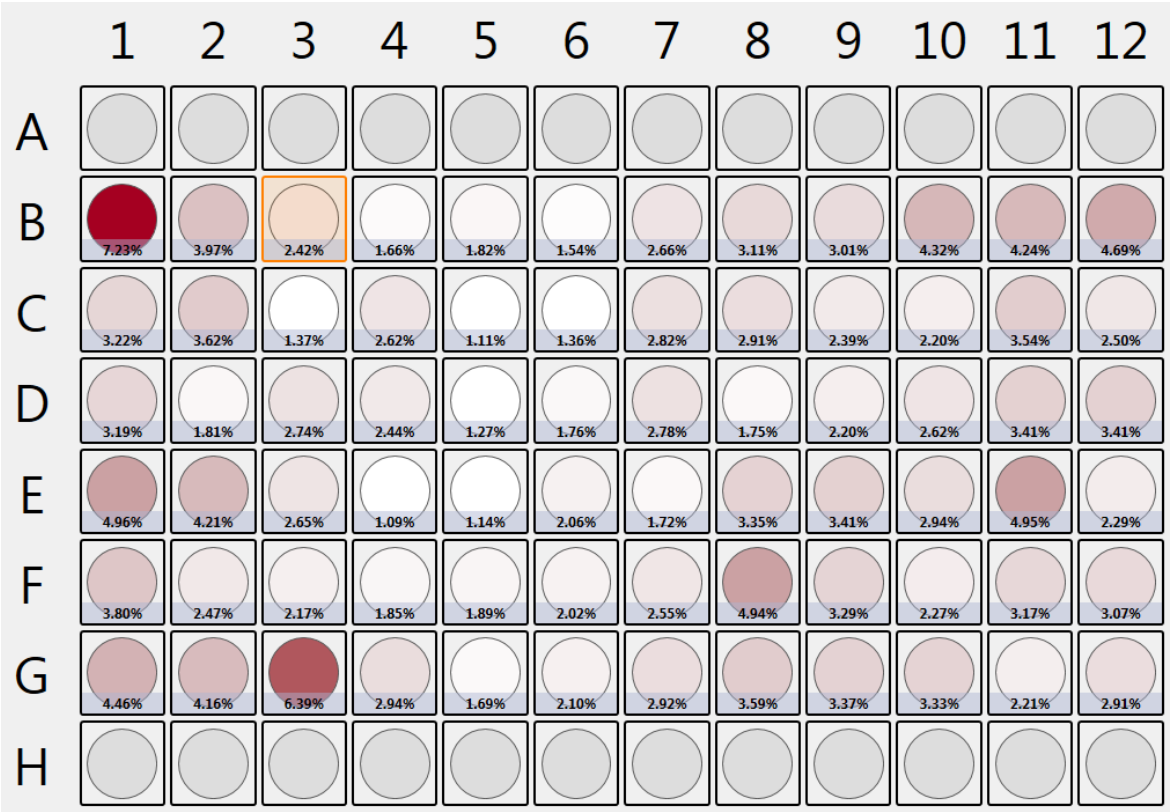


Figure S3.3: Invasion assay live/dead cells analysis with Carbonic anhydrase inhibitor shows no significant cell death: Live /Death cell analysis carried to determine the amount of cell death if any induced by the use of the carbonic anhydrase inhibitor Acetazolamide (5mM) – apart from wells B1 and G3 there is no notable cell death observed. Colour gradient denotes amount of cell death with dark red corresponding with high cell death and white corresponding with little to no cell death. Cells were plated at 50,000 cells per well and the test was carried out in triplicate.

Supplementary material chapter 4

Proteomic data lists (200 out of total number of both mouse and human proteins detected)

	A	B	C	D	E	F	G	H	I	J	K	L	M	N	O	P	Q	R	S	T
1	Intensity B3	Intensity C3	Intensity D26	Intensity E3	C: Species	N: Peptides	N: Razor + uni	N: Unique pe	N: Sequence	N: Unique +	N: Unique se	N: Mol. weig	N: Q-value	N: Score	N: Intensity	N: MS/MS co	T: Protein IDs	T: Majority protei	T: Protein names	T: Gene names
2	0	0	0	0	Mus musculus	2	2	0	27.5	27.5	0	11.799	0	31.201	0	0	G3UZW7	A0A023T778	Q9CQL1	P61327
3	9270800	8741400	24138000	17948000	Homo sapiens	5	5	1	22.2	22.2	3	34.081	0	34.83	60099000	1	A0A024QZP7	P06493-2	P06493	E5RIU6
4	0	0	194470000	54701000	Homo sapiens	9	7	7	33.9	28.9	28.9	43.024	0	54.606	249170000	7	A0A024QZX5	A0A087X1N8	P35237	C9JTJ8
5	0	0	30629000	0	Homo sapiens	28	1	1	27.2	1.3	1.3	141.44	0.0024969	8.3167	30629000	1	A0A024R4E5	Q00341-2	Q00341-2	H0Y394
6	0	0	0	0	Homo sapiens	13	13	0	47.4	47.4	0	22.591	0	86.614	0	0	A0A024R4M0	P46781	B5MCT8	C9JM19
7	0	0	0	0	Homo sapiens	5	5	0	10.3	10.3	0	58.311	0	34.038	0	0	A0A024R7W5	A0A087WXQ1	A0A087WY31	Q7Z739
8	0	0	0	0	Homo sapiens	6	6	0	44.9	44.9	0	25.898	0	66.588	0	0	A0A024RAS2	P257B7	C9JCK5	H7C402
9	0	0	0	0	Homo sapiens	4	4	0	4.5	4.5	0	118.7	0	30.778	0	0	A0A024RCR6	A0A0G2JK23	P46379-2	P46379
10	0	0	0	0	Mus musculus	1	1	0	3.5	3.5	0	32.502	0.0050694	6.1058	0	0	F6Y9J5	A0A067XG53	O70589-3	O70589-4
11	93948000	0	0	0	Mus musculus	3	3	3	30.8	30.8	30.8	11.778	0	23.364	93948000	2	A0A075B5P2	P01837	A0A075B5P2	P01837
12	104310000	0	0	0	Mus musculus	4	4	4	14.9	14.9	14.9	36.568	0	41.833	104310000	4	A0A075B5P3	P01867-2	P01867	A0A0A6YY53
13	2.042E+09	0	3759200	0	Mus musculus	8	8	8	28.2	28.2	28.2	36.198	0	70.953	2.046E+09	11	A0A075B5P5	P03987-2	P03987	A0A075B5P5
14	24182000	0	0	0	Mus musculus	1	1	1	5.1	5.1	5.1	49.943	0.0026543	10.36	24182000	1	A0A075B6A0	A0A075B6A0	P01872	P01872-2
15	0	0	0	0	Homo sapiens	3	2	0	4	3.1	0	109.97	0	14.109	0	0	E7EQB9	E7EQB9	E7EQS5	F8VX32
16	5144000	14204000	20864000	37529000	Homo sapiens	3	3	3	20.5	20.5	20.5	25.347	0	21.943	124040000	7	A0A087WNN8	Q61263	A0A087WSI5	A0A087WNN8
17	0	0	0	0	Mus musculus	1	1	0	19.6	19.6	0	5.4431	0	13.978	0	0	A0A087WPE4	A0A087WQE6	A0A087WNT1	P83940
18	9824500	0	0	3417600	Mus musculus	8	2	2	7.9	2.3	2.3	137.63	0	13.344	23685000	4	A0A087WQP8	A0A087WP48	A0A087WS04	A0A087WS29
19	0	0	0	0	Mus musculus	2	2	0	2.4	2.4	0	136.62	0	15.85	0	0	A0A0A6YXZ1	E9Q8N5	Q08EB5	Q08EB5
20	429430000	373390000	0	64985000	Mus musculus	2	2	2	33.3	33.3	33.3	12.032	0	24.787	867810000	5	A0A087WRP7	A0A087WN25	P0CW02	P0CW03
21	0	0	0	0	Mus musculus	2	2	0	2.9	2.9	0	94.9	0	14.27	0	0	A0A087WRV6	A0A087WNZ7	G5E870	A0A087WRV6
22	3303100	0	0	0	Mus musculus	4	2	2	6.3	3.4	3.4	59.111	0	12.797	3303100	2	F6UND7	A0A087WQ04	P08103-2	P08103
23	17164000	18184000	0	0	Mus musculus	1	1	1	9.2	9.2	9.2	23.177	0.0022995	6.9382	35349000	2	A0A087WQ89	A0A087WQ89		Z2100111C24Rik
24	21844000	35738000	5275100	30715000	Mus musculus	2	2	1	30.1	30.1	21.4	11.157	0	18.271	93571000	3	A0A087WQH8	A0A087WQH8		Sk35a4
25	1.656E+09	1.56E+09	5374000	66227000	Mus musculus	52	52	27	44.9	44.9	24.2	198.98	0	323.31	3.288E+09	55	A0A087WQM0	A0A087WQM0	A0A1D5RM59	E9QD56
26	0	0	0	0	Mus musculus	4	4	0	7.3	7.3	0	51.209	0	25.634	0	0	A0A087WQS2	Q9CQC6	A0A087WPF9	A0A087WQS2
27	9927700	5842800	6418500	18179000	Mus musculus	2	2	2	6.4	6.4	6.4	57.82	0.0003482	11.784	40368000	3	A0A087WQT6	Q99110	A0A087WQT6	Q89110
28	0	3462700	7374600	26640000	Mus musculus	1	1	1	8.9	8.9	8.9	25.388	0.0024257	7.7833	37477000	1	A0A087WRT7	A0A087WRT7	M54a44	M54a44
29	18206000	21802000	2728900	20061000	Mus musculus	54	1	1	28.7	0.4	0.4	288.69	0.0027624	6.4428	62798000	2	J3QQ16	A0A087WS16	J3QQ16	A0A087WS16
30	57166000	1803100	101710000	94566000	Mus musculus	1	1	1	0.6	0.6	0.6	135.87	0.008666	5.9853	255250000	3	A0A087WS76	A0A140LHL6	E9Q3S4	A0A087WS76
31	582410000	336890000	1.543E+09	3.985E+09	Mus musculus	66	66	39	46.3	46.3	28.9	253.01	0	323.31	6.447E+09	82	A0A087WSN6	B9EHT6	A0A087WR50	B7ZNJ1
32	100550000	30408000	83963000	125190000	Mus musculus	16	4	4	29.9	8.3	8.3	87.314	0	33.944	340110000	7	Q8C3V4	A0A087WSP5	P42225	Q99K94
33	0	0	0	0	Mus musculus	2	2	0	2.4	2.4	0	131.87	0.000348	11.77	0	0	A0A087WSS1	G3X9J4	E9QM90	Q148V7-2
34	0	0	16791000	31521000	Homo sapiens	2	1	1	10.7	6.2	6.2	40.368	0	12.001	48313000	2	E9PKG6	Q2L696	V9HW75	A0A087WSV8
35	0	0	49726000	0	Homo sapiens	6	3	3	25.1	14.7	14.7	53.166	0	17.332	49726000	3	E9PIR7	F8WB09	A0A087WSW9	A0A182DWI3
36	0	6147600	76020000	14706000	Homo sapiens	4	3	3	25.5	21.4	21.4	22.024	0	25.616	96874000	3	A0A087X2J2	A0A087WT12	P36969-2	P36969
37	0	0	28487000	0	Homo sapiens	3	1	1	9.2	3.5	3.5	41.669	0.0025502	8.744	28487000	1	A0A087WTA4	P30519-2	P30519	I3L159
38	0	0	0	0	Homo sapiens	1	1	0	6.5	6.5	0	29.127	0.0025633	8.8679	0	0	A0A087WTB2	P30519	O75487-2	O75487
39	0	0	6712800	0	Homo sapiens	2	2	1	7.1	7.1	5	57.495	0.0026455	10.242	6712800	1	A0A087WTA5	E7ERK9	Q9U1J0-3	Q9U1J0
40	0	0	0	0	Homo sapiens	3	3	0	6.3	6.3	0	80.282	0	18.688	0	0	H7BMX6	A0A087WTE4	A0A087WTF6	A0A087WX77
41	0	0	10373000	4754800	Homo sapiens	1	1	1	5.6	5.6	5.6	48.871	0.0029883	6.2832	15128000	1	A0A087WTL4	A0A087WX97	Q9BXK5-4	Q9BXK5
42	0	0	4881800	0	Homo sapiens	1	1	1	10.4	10.4	10.4	14.143	0.0023817	7.5302	4881800	1	F8W1I4	Q8TBL5	A0A087WTL9	F8VY40
43	0	0	76869000	19305000	Homo sapiens	2	2	2	37.5	37.5	37.5	8.6075	0	18.416	96174000	2	A0A087WTP2	A0A087X1D8	A0A087WVN4	P14324-2
44	0	0	78473000	21497000	Homo sapiens	2	2	2	25.9	7.3	7.3	73.027	0	21.27	99970000	2	A0A087WTP3	Q92945	M0R0I5	M0QH43
45	0	0	14929000	7076300	Homo sapiens	1	1	1	38.6	38.6	38.6	6.2591	0.0025047	8.3796	22005000	2	H0YHJ8	H0Y5I8	H0Y5I0	A0A087WUQ2
46	0	0	0	0	Homo sapiens	1	1	0	83.3	83.3	0	1.9022	0.0024768	8.1491	0	0	A0A087WUA8	F8WF88	C9J760	C9JOX3
47	0	0	0	0	Homo sapiens	2	2	0	12.6	12.6	0	22.994	0.0003476	11.753	0	0	B7Z7G7	A0A087WU65	Q9NRW7	A0A1B0GXJ6
48	0	0	0	0	Homo sapiens	2	2	0	4.4	4.4	0	65.702	0	13.618	0	0	A0A087WUB9	Q8WVM6	Q8WVM6-3	Q8WVM6-2
49	0	0	83051000	44444000	Homo sapiens	5	2	2	34.8	13.7	13.7	25.09	0	18.8	127490000	3	A0A087WUC6	E9PY68	Q15005	E9PUO1
50	0	0	10578000	0	Homo sapiens	1	1	1	1.6	1.6	1.6	117.44	0.0022663	6.7808	10578000	1	A0A087WUE9	Q92797	A0A087WUE9	Q92797
51	0	0	0	0	Homo sapiens	1	1	0	7.9	7.9	0	17.188	0.0022241	6.5582	0	0	A0A087X1F5	A0A087WYV9	A0A087WUM0	P57105
52	0	0	30648000	6469600	Homo sapiens	1	1	1	18.4	18.4	18.4	8.6918	0.0020195	10.85	37117000	2	H0YIW7	A0A087WUN7	H0YI40	G3V4X6
53	0	0	30520000	16470000	Homo sapiens	2	1	1	13.4	8.9	8.9	21.938	0.0025543	8.8051	46990000	1	A0A087WUQ6	P07203	A0A087WUQ6	P07203
54	0	0	0	0	Homo sapiens	4	4	0	29.8	29.8	0	15.197	0	30.573	0	0	E7ETK0	A0A087WU50	P62847-2	P62847-3
55	0	0	19446000	4037500	Homo sapiens	3	3	1	4.3	4.3	2	138.68	0	21.943	23483000	1	A0A087WUT6	O60841	A0A087WUT6	O60841
56	40234000	44983000	4500100	18427000	Homo sapiens	2	2	2	2.2	2.2	2.2	72.155	0.0023295	10.473	108140000	3	A0A087WUX3	J3QTJ6	Q5CZC0	A0A087WUX3
57	0	0	3040000	418560	Homo sapiens	2	2	1	6.2	6.2	3.1	93.533	0.0020148	10.827	3458500	1	A0A087WV29	Q9H0A0-2	Q9H0A0	A0A087WV29
58	0	0	29800000	9921300	Homo sapiens	5	5	3	7.9	7.9	4.9	99.31	0	30.435	39721000	3	A0A087WVM4	B7ZM99	Q6UB35	H0Y327
59	3085400	1844800	127490000	37455000	Homo sapiens	75	1	1	56.6	1.5	1.5	192.06	0.0023396	10.661	169870000	2	A0A087WVQ6	Q00610-2	Q00610	J3KS13
60	0	0	0	0	Homo sapiens	1	1	0	10.7	10.7	0	12.2	0.0010232	11.207	0	0	A0A087X0C7	E5RJK0	E5RJK0	E5RK44
61	0	0	0	0	Homo sapiens	3	3	0	7.9	7.9	0	44.26	0	21.328	0	0	A0A087WW40	Q9Y371-3	Q9Y371	Q9Y371-2
62	0	0	0	0	Homo sapiens	1	1	0	14.1	14.1	0	15.421	0.0086591	5.9759	0	0	H0Y8D1	A6XMV8	A0A0J9YTC8	A0A087WW55
63	0	0	0	0	Homo sapiens	1	1	0	2.8	2.8	0	77.12	0.0023516	7.2939	0	0	B4DGL8	A0A087WW65	O75027-3	O75027
64	0	0	0	0	Homo sapiens	2	2	0	1.5	1.5	0	218.2	0.0013578	11.056	0	0	A0A087WWE2	P24928-2	P24928	A0A087WWE2
65	0	0	0	0	Homo sapiens	1	1	0	1.1	1.1	0	121.12	0.0023824	7.5354	0	0	A0A087WWJ1	P52701-4	P52701-2	P52701-3
66	0	0	0	0	Homo sapiens	1	1	0	6.8	6.8	0	13.343	0.002234	6.6028	0	0	A6NKE1	A0A087WWM0	A0A087WWM0	O43617-2
67	0	0	4785300	0	Homo sapiens	1	1	1	5	5	5	24.986	0.0024993	6.5125	4785300	1	A0A087WWN7	Q9NRL2-2	Q9NRL2	A0A087WWN7
68	0	0	20923000	6719100	Homo sapiens	1	1	1	10.9	10.9	10.9	22.373	0.0025308	8.5847	27642000	1	Q8N1B9	C9J6X0	A0A087WXC5	E7ESZ7

0	0	20923000	6719100	Homo sapiens	1	1	1	10.9	10.9	10.9	22.373	0.0025308	8.5847	27642000	1	Q8N1B9	C9J6X0	A0A087WXC5	E7ESZ7
0	0	0	0	Homo sapiens	8	8	0	50.9	50.9	0	19.586	0	68.973	0	0	A0A087WXM6	J3QQT2	J3KRX5	A0A0A6YYL6
0	0	0	0	Homo sapiens	1	1	0	1.3	1.3	0	75.849	0.002745	6.3658	0	0	A0A087WXP3	E9PEE8	P18564-2	P18564
0	0	0	0	Homo sapiens	5	5	0	24.5	24.5	0	37.119	0	41.108	0	0	A0A087WXS7	O43681	K7ERW9	A0A087WXS7
0	0	0	0	Homo sapiens	2	2	0	1.5	1.5	0	212.2	0	13.772	0	0	A0A087WY00	G3V394	F8WE88	F8W6H6
0	0	0	0	Homo sapiens	1	1	0	12.1	12.1	0	11.523	0.0023135	7.0194	0	0	A0A087WY28	Q96CV9-3	Q96CV9-2	Q96CV9
0	0	0	0	Homo sapiens	2	2	0	8.6	8.6	0	31.102	0	12.112	0	0	A0A087WY55	Q9NP79	Q5TGM0	Q9NP79-2
0	0	0	0	Homo sapiens	11	11	0	29.7	29.7	0	49.526	0	87.824	0	0	A0A087WY71	E9PFW3	Q96CW1-2	Q96CW1
0	0	0	0	Homo sapiens	2	2	0	35.7	35.7	0	11.065	0	15.614	0	0	D6RFM0	D6RAH7	H9KV45	A0A0A0MQU3
7835000	11599000	18960000	21093000	Homo sapiens	2	2	1	3.2	3.2	1.7	72.046	0	15.788	59487000	2	A0A140T9S0	A0A0G2JLV0	A0A087WYD6	X5CMH5
0	0	103820000	9163000	Homo sapiens	8	8	3	41.9	41.9	21.6	23.764	0	73.315	112980000	3	A0A087WYR3	O43399	O43399-5	O43399-7
0	0	13987000	0	Homo sapiens	8	8	1	21.7	21.7	1.6	56.967	0	74.9	13987000	1	A0A087WYS1	E7EUC7	Q16851-2	Q16851
0	0	0	0	Homo sapiens	5	5	0	34.8	34.8	0	19.155	0	49.682	0	0	A0A087WYT3	Q15185-4	Q15185	Q15185-3
0	0	15371000	4282200	Homo sapiens	1	1	1	4.1	4.1	4.1	39.911	0.0027716	6.4948	19653000	1	B7Z385	A0A087X0J3	A0A087WZ15	E9PDI2
0	0	0	0	Homo sapiens	3	1	0	11.4	4.2	0	33.257	0.002445	7.9009	0	0	A0A087WZB5	Q9HBI1-3	Q9HBI1	Q9HBI1-2
0	0	0	0	Homo sapiens	1	1	0	6.9	6.9	0	13.956	0.0086387	5.9645	0	0	A0A087WZE9	Q15651-2	P05204	Q15651
0	0	6068300	1913700	Homo sapiens	1	1	1	3.8	3.8	3.8	44.756	0.0025031	8.3635	7982000	1	A0A087X028	Q9NZT2-2	Q9NZT2	A0A087X028
7935100	20793000	296660000	224290000	Homo sapiens	27	11	11	37.6	16.3	16.3	104.78	0	85.65	549680000	17	A0A087X054	Q9Y4L1	E9PJ21	A0A087WWI4
2598700	0	483010000	189500000	Homo sapiens	12	9	9	21.4	16.2	16.2	108.34	0	75.022	675110000	15	A0A087X0S5	P12109	A0A087X0S5	P12109
0	0	369150000	89393000	Homo sapiens	34	34	8	59.5	59.5	22.2	77.569	0	253.38	458550000	9	A0A087X0X3	P52272	P52272-2	M0QZM1
0	0	16645000	8757000	Homo sapiens	1	1	1	12.5	12.5	12.5	17.851	0.0026525	10.302	25402000	1	H0YJE4	A0A087X0Z7	H0YJ66	Q9Y394-2
0	0	0	0	Homo sapiens	1	1	0	8.3	8.3	0	23.685	0.0023276	7.096	0	0	A0A087X101	Q10570	A0A087X101	Q10570
0	0	60543000	36206000	Homo sapiens	7	7	3	8.2	8.2	4.1	139.38	0	50.059	96749000	3	J3KN36	A0A0G2JN29	A0A087X117	Q5JPE7-2
0	0	0	0	Homo sapiens	1	1	0	2.6	2.6	0	54.945	0.0029948	6.3052	0	0	A0A087X1A5	Q5JW30	O95793-2	O95793-3
0	0	0	0	Homo sapiens	2	2	0	7.2	7.2	0	56.399	0	13.44	0	0	A0A087X1B2	B9A018	Q53GS9-2	Q53GS9-3
0	0	21219000	12090000	Homo sapiens	1	1	1	15.7	15.7	15.7	17.981	0.0022676	6.7891	33309000	2	A0A087X1K9	B4DP64	E5RGR0	O75608-2
1118200	0	355740000	221080000	Homo sapiens	10	10	4	52.4	52.4	20.5	29.126	0	103.1	577940000	7	A0A087X1Z3	Q9UL46	H0YM70	H0YKU2
0	0	0	0	Homo sapiens	1	1	0	9.5	9.5	0	13.362	0.0023242	7.0788	0	0	F8W1W1	A0A087X256	Q2M389	F8W1W1
0	0	135220000	24862000	Homo sapiens	5	5	2	38.5	38.5	15.6	19.757	0	53.088	160080000	3	A0A087X271	B4DDF4	B4DUT8	Q99439
0	0	490480000	190280000	Homo sapiens	6	6	6	46.2	46.2	46.2	23.896	0	65.613	680760000	10	A0A087X2B5	P35613-2	P35613	I3L192
0	0	0	0	Homo sapiens	3	2	0	32.6	17.9	0	10.32	0.0006892	11.572	0	0	A0A087X2D0	P84103-2	P84103	A0A087X2D0
0	0	15091000	0	Homo sapiens	6	1	1	7.1	1.8	1.8	145.17	0.0086796	6.0039	15091000	1	A0A087X2D8	O60271-9	O60271-4	O60271-2
0	0	0	0	Homo sapiens	15	15	0	51.4	51.4	0	45.796	0	128.62	0	0	A0A087X2I1	P62333	H0YJC0	H0YJS8
0	0	0	0	Homo sapiens	1	1	0	8.2	8.2	0	32.585	0.002594	9.2714	0	0	A0A096LNW8	Q68E01-3	Q68E01-2	Q68E01
0	0	0	0	Homo sapiens	2	2	0	5.3	5.3	0	53.371	0	15.841	0	0	C9JFE4	A0A096LP07	A0A096LPJ3	A8K070
0	0	0	0	Homo sapiens	1	1	0	8.3	8.3	0	15.911	0.0040312	6.1757	0	0	A0A0G2JQ95	A0A096LP11	A0A140TA76	Q8ND56-3
0	0	28725000	1106400	Homo sapiens	4	4	2	30.8	30.8	13.6	30.376	0	23.696	29831000	2	A0A096LPI6	A0A0B4J2H4	H7C1F6	A0A0B4J2D5
0	10549000	0	0	Mus musculus	1	1	1	3.8	3.8	3.8	49.57	0.0023364	7.1492	10549000	1	A0A0A0MQ68	Q60759	A0A0A0MQ68	Q60759
0	0	0	0	Mus musculus	1	1	0	4.3	4.3	0	31.2	0.0024472	7.9207	0	0	D3Z0U5	D6RGM7	D3Z4J2	A0A0G2JFY0
17632000	22863000	2561300	45807000	Mus musculus	2	2	2	13.8	13.8	13.8	17.744	0	14.036	88864000	3	A0A0A0MQ90	P97352	A0A0A0MQ90	P97352
1.75E+09	994890000	711920000	7.007E+09	Mus musculus	15	4	4	44.6	12.1	12.1	45.854	0	43.588	1.047E+10	24	A0A0R4J0X5	A0A0A0MQA3	P07758	Q00896
0	0	0	0	Mus musculus	23	4	0	57.9	11.3	0	52.793	0	37.098	0	0	A0A0A0MQA5	P68368	A0A087WQS4	A0A087WRB4
156350000	0	0	0	Mus musculus	1	1	1	13.1	13.1	13.1	11.277	0	13.127	156350000	1	A0A0A0MQC1	A0A0A0MQC1		Ighv3-5
11117000	15697000	0	0	Mus musculus	1	1	1	2.2	2.2	2.2	76.259	0.0022962	6.9333	26814000	2	A0A0A0MQC7	A2A5Y6	P10637-2	P10637
11484000	9974900	0	0	Mus musculus	2	2	1	2.4	2.4	1.6	192.22	0	13.108	21459000	1	A0A0A0MQD5	Q4ACU6-2	Q4ACU6	Q4ACU6-6
2.50E+09	1.48E+09	1.74E+09	3.30E+09	Mus musculus	15	8	8	59.9	38.4	38.4	38.653	0	87.185	9.03E+09	30	A0A0A0MQF6	P16858	S4R1W1	A0A1D5RLD8
22541000	18840000	12709000	21957000	Mus musculus	9	1	1	35	5.4	5.4	42.736	0.0023888	7.5764	76046000	1	A0A0A0MQH5	A0A0A0MQH5		Macf1
0	0	0	0	Mus musculus	1	1	0	5.9	5.9	0	16.125	0.0063644	6.065	0	0	E0CY47	H3BKE1	A0A0A0MQM2	I1E4X4
15491000	13005000	4887500	13766000	Mus musculus	3	3	2	6.1	6.1	4	68.243	0	18.688	47149000	3	S4R2D5	A0A0A0MQN4	Q9D906	S4R2P7
0	0	8778800	0	Homo sapiens	1	1	1	3.7	3.7	3.7	29.109	0.0024046	7.6739	8778800	1	K7EML4	U3KQC1	K7EIR0	A0A0A0MQU0
0	0	0	0	Homo sapiens	4	4	0	15.8	15.8	0	35.71	0	23.097	0	0	H7C4T5	C9JP00	A0A0A0MQX8	Q9NR56-3
157410000	25684000	498270000	230940000	Homo sapiens	13	4	4	62.4	21.6	21.6	30.348	0	35.581	912300000	9	A0A0A0MR02	P45880	P45880-2	P45880-1
0	0	0	0	Homo sapiens	3	3	0	24.6	24.6	0	30.315	0	25.185	0	0	A0A0A0MRJ6	H7BYS8	P22061	P22061-2
5045400	5686000	16673000	3521400	Homo sapiens	3	1	1	8.4	3	3	51.462	0.002748	6.3746	30925000	1	A0A0A0MRK6	Q13505-3	Q13505	A0A0C4DFQ1
0	0	0	0	Homo sapiens	1	1	0	8.1	8.1	0	19.642	0.0026429	10.196	0	0	H0Y7N6	F6XFR5	J3QSX6	F8W8M4
0	0	3623400	1567800	Homo sapiens	2	2	1	3.7	3.7	2.1	74.543	0	15.976	5191200	1	A0A0A0MRM9	Q14978	Q14978-3	Q14978-2
0	0	0	0	Homo sapiens	1	1	0	3.2	3.2	0	55.57	0.0023357	10.58	0	0	A0A0A0MRN4	Q5BKZ1-3	Q5BKZ1	A0A0A0MRN4
0	0	0	0	Homo sapiens	1	1	0	5	5	0	33.454	0.0024791	8.1648	0	0	Q5T457	A0A0A0MRN9	Q9GZV1-2	Q9GZV1
0	0	0	0	Homo sapiens	1	1	0	3.8	3.8	0	43.294	0.0025276	8.5665	0	0	B6VEX4	A0A0A0MRT6	Q8IZP0-11	Q8IZP0-10
2302400	0	475900000	140930000	Homo sapiens	23	15	15	21.7	15.5	15.5	152.45	0	146.71	619130000	17	A0A0A0MRV0	Q9P2E9-2	Q9P2E9	Q9P2E9-3
0	0	40265000	11154000	Homo sapiens	6	2	2	23.7	9.7	9.7	35.503	0	16.991	51420000	2	A0A0A0MS41	Q9BWM7	S4R3N9	A0A0A0MS41
0	0	176450000	7017100	Homo sapiens	8	8	7	24.4	24.4	21.9	44.205	0	59.407	183470000	7	J3KNW4	A0A0A0MSG2	Q14192	C9J3S8
0	0	0	0	Homo sapiens	3	3	0	7.2	7.2	0	77.813	0	17.728	0	0	A0A0A0MSJ0	Q86XP3-2	Q86XP3	A0A0A0MSJ0
0	0	104890000	0	Homo sapiens	4	3	3	22.6	19.8	19.8	36.867	0	20.416	104890000	3	A0A0A0MSS8	P42330	S4R3Z2	P42330-2
0	0	81011000	125690000	Homo sapiens	4	4	4	9.8	9.8	9.8	47.606	0	31.842	206700000	7	A0A0G2JKZ1	A2AB90	A0A0G2JH37	A0A0A0MSV9
0	0	0	0	Homo sapiens	1	1	0	0.7	0.7	0	114.69	0.0071466	6.0464	0	0	H3BUD4	A0A0A0MT40	Q15111-2	Q15111
0	0	4823600	0	Homo sapiens	1	1	1	0.3	0.3	0.3	591.4	0.0025205	8.4856	4823600	1	A0A0A0MTR7	A0A0A0MTC1	Q63HN8	Q63HN8-4
0	0	0	0	Homo sapiens	1	1	0	5	5	0	30.742	0.0024638	8.0201	0	0	A0A0A0MTI6	Q9NYP7-3	Q9NYP7	Q9NYP7-2

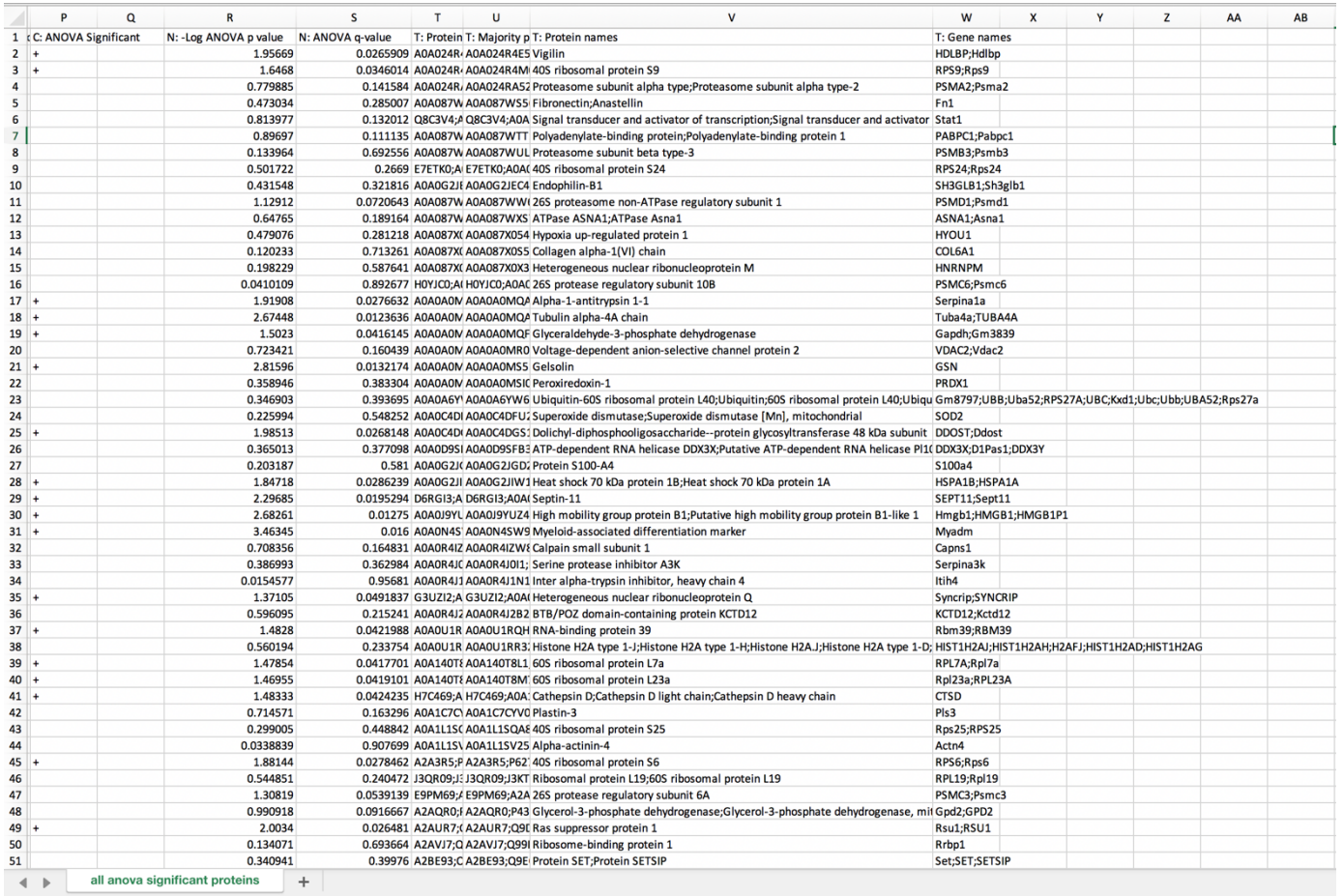
	A	B	C	D	E	F	G	H	I	J	K	L	M	N	O	P	Q	R	S	T
135	0	0	0	0	Homo sapiens	1	1	0	5	5	0	30.742	0.0024638	8.0201	0	0	A0A0A0MTI6	Q9NYP7-3	Q9NYP7	Q9NYP7-2
136	0	0	202280000	70510000	Homo sapiens	7	7	5	22.3	22.3	17.5	49.062	0	62.243	272790000	6	A0A0R4J2G3	A0A0A0MTJ9	Q6PIU2	Q6PIU2-2
137	0	0	0	0	Homo sapiens	2	2	0	4.1	4.1	0	82.358	0.0020094	10.716	0	0	Q5T2B5	A0A0A0MTN0	Q13617	Q13617-2
138	2453200	0	870450000	60467000	Homo sapiens	16	11	10	38.6	26.4	23.7	64.824	0	80.558	933370000	10	A0A0A0MTS2	P06744	P06744-2	K7EQ48
139	0	0	0	0	Mus musculus	1	1	0	4	4	0	22.283	0.0099062	5.929	0	0	A0A0A6YVS2	Q921L3	A0A0A6YVS2	Q921L3
140	86216000	100460000	1779900	45976000	Mus musculus	3	3	3	22	22	22	28.522	0	19.518	234440000	7	A0A0A6YVT1	A0A0A6YXN9	A0A0A6YY75	Q64735-2
141	51291000	50991000	6991500	25688000	Mus musculus	4	2	2	15.2	8.6	8.6	42.147	0	18.167	134960000	4	A0A0A6YVU8	Q9JKV1	D3YUD8	A0A0A6YVU8
142	37814000	48856000	6899500	45033000	Mus musculus	1	1	1	25.6	25.6	25.6	9.22	0.0026273	9.9052	138600000	3	A0A0A6YW87	Q9CX13	A0A0A6YW87	Q9CX13
143	0	0	0	0	Mus musculus	1	1	0	0.5	0.5	0	166.43	1	-2	0	0	E9QNQ4	A0A0A6YWG7	Q8CHG7	E9QNQ4
144	0	0	0	0	Mus musculus	1	1	0	5.7	5.7	0	39.312	0.0022516	6.6899	0	0	A0A0A6YWY4	A0A140T8R7	A0A0A6YWP7	A0A0A6YXM5
145	0	0	0	0	Mus musculus	2	2	0	26.1	26.1	0	15.738	0	19.203	0	0	A0A0A6YX02	Q9CQ22	A0A0A6YX02	Q9CQ22
146	0	0	0	0	Mus musculus	4	4	0	13.5	13.5	0	54.108	0	35.937	0	0	A0A0A6YX18	Q8BVE3	A0A0A6YWP6	A0A0A6YVU0
147	0	0	0	0	Mus musculus	3	3	0	24	24	0	14.996	0	21.999	0	0	A0A0A6YX26	P62900	A0A0A6YXL3	A0A0A6YX26
148	428980000	54481000	20301000	51961000	Mus musculus	15	15	8	55.3	55.3	36.3	43.165	0	128.33	1.046E+09	15	A0A0A6YX73	Q8K1M3	P12367	A0A0A6YY28
149	0	0	0	0	Mus musculus	1	1	0	5	5	0	36.221	0.0025332	8.5996	0	0	A0A0A6YXB0	Q9Z1K6	A0A0A6YXB0	Q9Z1K6
150	0	0	0	0	Mus musculus	1	1	0	1.6	1.6	0	70.147	0.0022378	6.6359	0	0	Q5FWX7	E9Q6C1	F6UHR6	E9PXZ2
151	10632000	0	0	0	Mus musculus	3	1	1	13.6	5.3	5.3	32.079	0.0022472	6.6666	10632000	1	A0A0A6YXR4	P47199	D3YWU6	D3Z4Q4
152	0	0	0	0	Mus musculus	1	1	0	4.6	4.6	0	29.541	0.0025982	9.2989	0	0	A0A0A6YXZ6	Q8BUN3	G3X8R5	Q3UA37
153	0	0	70858000	19711000	Homo sapiens	4	1	1	28.7	6.4	6.4	21.233	0.0025723	8.9097	90569000	1	A0A0A6YYA0	Q86XR7-2	Q9Y3B3-2	Q9Y3B3
154	0	0	7256200	46430000	Homo sapiens	1	1	1	1.1	1.1	1.1	71.964	0.0022708	6.8104	53686000	2	C9JR62	A0A0A6YYF7	E7ERF0	Q6ZP82
155	0	0	0	0	Homo sapiens	3	3	0	8.1	8.1	0	54.223	0	24.882	0	0	Q96HJ9-2	A0A0A6YYJ8	Q9Y383-3	Q9Y383-2
156	0	0	83368000	0	Homo sapiens	3	3	3	14	14	14	34.779	0	24.152	83368000	3	A0A0A6YYL2	P0DMN0	P0DMM9	P0DMM9-3
157	10207000	9454900	58090000	361970000	Mus musculus	5	5	5	22.5	22.5	22.5	32.976	0	44.55	439720000	5	A0A0B4J1G1	E9Q415	A0A0B4J1E6	P08101-2
158	30495000	40592000	9845200	29748000	Mus musculus	6	2	2	18	6.3	6.3	68.03	0	17.301	110680000	3	A0A0B4J1E7	O35343	D3YTN1	A0A0B4J1E7
159	0	0	0	0	Homo sapiens	4	4	0	28.5	28.5	0	15.763	0	27.991	0	0	A0A0B4J1Z1	C9JAB2	Q16629-3	Q16629-2
160	0	0	0	0	Homo sapiens	4	4	0	39.3	39.3	0	12.99	0	31.364	0	0	K7EM56	A0A0B4J2B4	S4R417	K7EQJ5
161	0	0	144240000	63145000	Homo sapiens	4	1	1	25	7.4	7.4	21.525	0	18.491	207390000	3	Q5W0H4	A0A0B4J2C3	P13693	J3KPG2
162	0	0	8469500	1441000	Homo sapiens	1	1	1	6.3	6.3	6.3	25.537	0.0024228	7.7679	9910400	1	H7C0D0	A0A0C4DFL7	Q16850-2	Q16850
163	0	0	9988400	3098300	Homo sapiens	1	1	1	28.6	28.6	28.6	7.5454	0.002425	7.7798	13087000	1	H0YJN8	G3V267	G3V5T0	A0A0C4DFM0
164	0	0	0	0	Homo sapiens	2	2	0	3.1	3.1	0	99.813	0.0023271	10.457	0	0	A0A0C4DFT3	Q12959-8	Q12959-9	Q12959-5
165	3259000	5982400	380920000	210530000	Homo sapiens	7	7	4	38.7	38.7	25.2	24.75	0	81.984	600690000	9	A0A0C4DFU2	P04179-4	P04179	A0A0C4DFU1
166	0	0	0	0	Homo sapiens	13	13	0	59.7	59.7	0	29.404	0	172.87	0	0	C9J9K3	A0A0C4DG17	P08865	F8WD59
167	24593000	24096000	4271600	14836000	Homo sapiens	1	1	1	2.5	2.5	2.5	33.746	0.0035012	6.2023	67797000	3	E9PFG0	A0A0C4DG85	P40394	P40394-2
168	0	0	30470000	0	Homo sapiens	1	1	1	6	6	6	23.577	0.0024992	8.3475	30470000	1	B5MC36	A0A0C4DG87	B5MC34	B5MCK8
169	0	0	0	0	Homo sapiens	2	2	0	5.5	5.5	0	53.964	0	15.151	0	0	D6RJA6	A0A0C4DG89	Q7L014	D6RJA6
170	0	0	31594000	10502000	Homo sapiens	2	2	2	7.6	7.6	7.6	47.713	0	17.788	42095000	2	H0Y7F0	H0Y9H6	E9PDE4	E7ES10
171	0	0	0	0	Homo sapiens	18	11	0	31.8	21.9	0	69.226	0	71.36	0	0	A0A0C4DGB6	P02768	A0A087WWT3	P02768-3
172	0	0	0	0	Homo sapiens	1	1	0	2.8	2.8	0	39.208	0.0022903	6.907	0	0	A0A0C4DGF0	E7ER77	Q7Z2K6-2	Q7Z2K6
173	0	0	0	0	Homo sapiens	1	1	0	17.4	17.4	0	7.8296	0.0024031	7.6443	0	0	E9PJ33	E9PJ75	E9PNM9	E9PJY1
174	0	0	0	0	Homo sapiens	6	6	0	5	5	0	217.1	0	39.849	0	0	F5GWX5	A0A0C4DGG9	Q14839	Q14839-2
175	9201100	0	300110000	145020000	Homo sapiens	7	3	3	33.5	17.7	17.7	33.786	0	29.82	454330000	5	A0A0C4DGQ5	P04632	K7EIV0	A0A075B7C0
176	0	0	19162000	0	Homo sapiens	2	2	2	23.2	23.2	23.2	13.61	0.0020141	10.796	19162000	2	J3KRS1	A0A0C4DGQ8	Q6IAN0	J3KRS1
177	0	0	138450000	24113000	Homo sapiens	11	11	2	34.4	34.4	11.2	48.799	0	95.917	162570000	2	A0A0C4DGS1	P39656	P39656-3	P39656-2
178	17751000	190810000	0	28837000	Homo sapiens	2	2	1	2.8	2.8	0.9	111.66	0.0020101	10.721	237400000	1	A0A0C4DGS5	Q08379-2	Q08379	A0A0C4DGS5
179	0	0	0	0	Homo sapiens	3	3	0	6.4	6.4	0	87.387	0	23.986	0	0	A0A0C4DGX4	Q13616	A0A0C4DGX4	Q13616
180	0	0	0	0	Homo sapiens	1	1	0	2.1	2.1	0	43.904	0.0032406	6.2203	0	0	A0A0C4DGZ5	P54577	A0A0C4DGZ5	P54577
181	255460000	265640000	0	4402400	Mus musculus	7	7	7	12.6	12.6	12.6	80.202	0	72.414	525500000	13	Q9DC42	A0A0D9SEG8	E9QMJ5	E9QJS7
182	0	0	0	0	Homo sapiens	1	1	0	2.3	2.3	0	86.823	0.0023433	7.1822	0	0	Q5QPR4	J3QR29	A0A0D9SEI3	Q5QPR3
183	0	0	0	0	Homo sapiens	1	1	0	2.8	2.8	0	46.56	0.0024775	8.1607	0	0	A0A0D9SFG6	Q15438-3	Q15438-2	Q15438
184	0	0	49035000	41366000	Homo sapiens	24	3	3	34.9	6.6	6.6	113.31	0	22.26	90402000	3	A0A0D9SFS3	Q02218	E9PCR7	E9PDF2
185	0	0	0	0	Homo sapiens	11	10	0	27	25.8	0	65.215	0	76.061	0	0	A0A1B0GWF2	A0A1B0GVQ5	A0A0D9SG72	A0A1B0GTP9
186	0	0	10958000	0	Homo sapiens	2	2	1	23.7	23.7	9.7	10.862	0	14.09	10958000	1	E5RG62	E5RK70	H0YBX2	G5EA19
187	135130000	96921000	0	8247000	Mus musculus	8	8	3	23.1	23.1	11.1	62.697	0	67.086	240300000	6	A0A0G2JDI9	P55096	A0A0G2JDI9	P55096
188	8706000	7195200	0	26391000	Mus musculus	2	2	1	5.2	5.2	3.4	43.282	0	13.812	42292000	1	A0A0G2JDK2	P17439	A0A0G2JDK2	P17439
189	0	0	0	0	Mus musculus	3	3	0	3.9	3.9	0	103.94	0	22.286	0	0	A0A0H2UH17	A0A0G2JDV6	Q80X50-2	Q80X50-3
190	44594000	27953000	0	102570000	Mus musculus	5	5	2	28.2	28.2	10.6	31.395	0	52.028	175120000	4	A0A0G2JDV8	Q9DAW9	A0A0G2JFC8	A0A0G2JFG3
191	0	0	0	0	Mus musculus	4	4	0	40.2	40.2	0	9.2327	0	37.363	0	0	A0A0G2JDW7	Q6ZWU9	A0A0G2JG29	A0A0G2JEX7
192	2247300	3568900	1373600	6360700	Mus musculus	1	1	1	4.7	4.7	4.7	35.25	0.0022747	6.8243	13551000	1	A0A0G2JEG3	Q8VE96	A0A0G2JEG3	Q8VE96
193	0	0	0	0	Mus musculus	5	5	0	9.7	9.7	0	63.915	0	33.706	0	0	A0A0G2JEP0	Q61584-2	Q61584-5	Q61584-6
194	4.278E+09	4.396E+09	124570000	860420000	Mus musculus	21	19	12	55.4	53.5	34.8	51.349	0	192.18	9.659E+09	39	A0A0G2JEU1	P47738	A0A0G2JF60	A0A0G2JFQ0
195	197310000	143810000	0	23640000	Mus musculus	9	9	6	15.5	15.5	11.2	94.457	0	90.111	364760000	9	A0A0G2JF67	Q8CGC03	A0A0G2JF67	Q8CGC03
196	0	0	0	0	Mus musculus	6	6	0	12.3	12.3	0	74.482	0	57.404	0	0	A0A0G2JF72	Q8JZN2	Q91WS0	A0A0G2JDJ7
197	26489000	21504000	0	34250000	Mus musculus	3	3	1	22.7	22.7	6.1	15.057	0	22.315	82244000	2	A0A0G2JFB4	A0A0G2JGT5	A0A0G2JH04	P63073
198	0	0	0	0	Mus musculus	1	1	0	3.5	3.5	0	22.211	0.0030038	6.3243	0	0	A0A0G2JFE3	E9PUE1	Q8BSI6	E9Q816
199	0	0	0	0	Mus musculus	1	1	0	3.7	3.7	0	51.96	0.0023269	7.0909	0	0	A0A0G2JG60	Q6P9Z1	Q99JR8-2	Q61466-2
200	0	968990	0	54558000	Mus musculus	3	3	2	41	41	30.8	9.0621	0	20.732	55527000	2	A0A0G2JGD2	P07091	A0A0G2JGD2	P07091
201	46775000	28587000	6395200	27679000	Mus musculus	3	3	1	25.4	25.4	9.5	20.008	0	25.518	109440000	1	D3YWR7	A0A0G2JGJ1	Q8BVI4	D3Z099
202	0	0	0	0	Mus musculus	4	1	0	26.2	4.9	0	20.586	0.0032415	6.2255	0	0	A0A0G2JGP4	Q9D091	P08556	A0A0G2JE25

Metabolomics data tables (45 metabolites detected)

	A	B	C	D	E	F	G	H	I	J	K	L	M
1	T: id	T: 1--C--1804	T: 2--B--1804	T: 3--B--1804	T: 4--B--180418B	T: 5--C--1804	T: 6--C--1804	T: 7--D--1804	T: 8--D--1804	T: 9--D--1804	T: 10--E--18(	T: 11--E--18(	T: 12--E--c18(
2	Propanoic acid, 2-[(trimethylsilyl)oxy]-, trimethylsilyl ester	1	0	0.3461	0.4777	0.5894	0	0.1599	0.1358	0.1229	0.5449	0.3301	0.3193
3	Lactic acid-2TMS ; Propanoic acid, 2-[(trimethylsilyl)oxy]-, trimethylsilyl	1	0.2124	0.302	0.3213	1.0425	1.7325	0.351	0.3531	0.3383	0.4775	0.4939	0.4962
4	Alanine-2TMS	1		0.50103107	0	0.9817	0.8903	0.32752138			0.6197	0	0.6929
5	Phosphoric acid, bis(trimethylsilyl)monomethyl ester	1	0	0	0	0.9187	0.859	0	0	0	0	0	0
6	Propanedioic acid, bis(trimethylsilyl) ester	1	0.9076	1.5796	0.7271	1.0717	0.8182	0.5069	0.5307	0.4901	0.6168	0	0.8442
7	Silanamine, 1,1,1-trimethyl-N-(trimethylsilyl)-N-[2-[(trimethylsilyl)oxy]	1	0.3691	0.4791	0.5406	1.1057	1.14	0.9201	0.8008	0.7628	1.1845	1.2091	1.1974
8	Glycerol, tris(trimethylsilyl) ether	1	0.6959	0.7773	0.8382	1.0066	1.1711	0.302	0.3021	0.2759	1.4243	1.5811	1.6005
9	Urea, N,N'-bis(trimethylsilyl)-	1	0.2051	0.2508	0.2941	0.9365	0	0.0994	0.1195	0.1141	0.4101	0.4356	0.4386
10	Phosphoric acid-3TMS ; Phosphoric acid, tris(trimethylsilyl) ester	1	0.1867	0.2128	0.222	0.4172	1.0629	1.2291	1.1759	1.2133	0	0.093	0.0923
11	Glycine, N,N-bis(trimethylsilyl)-, trimethylsilyl ester	1	0.6147	0.6549	0.6851	0.9688	1.0045	0.2579	0.2529	0	0.5053	0.5764	0.5689
12	Butanedioic acid, bis(trimethylsilyl) ester Succinic acid	1	1.0071	1.1429	1.1284	0.743	1.1784	0.9469	0.6754	0.9414	1.6121	1.8455	1.862
13	Propanoic acid, 2,3-bis[(trimethylsilyl)oxy]-, trimethylsilyl ester	1	0.1097	0.1379	0.135	0.4404	0.9799	0.4207	0.7159	0.0675	0.0368	0.0372	0.0362
14	Uracil, 1,3-bis(trimethylsilyl)-	1	0.4096	0	0	0.8191	1.0167	0	0	0	0.3563	0	0
15	L-Serine-3TMS	1	0	0	0.574	1.2802	0.9947	N.D	0	0	0.5843	0.5934	0.6477
16	Picolinic acid, trimethylsilyl ester	1	0.7873	1.0281	1.0762	0.9611	1.0513	0.701	0.6693	0.748	0.8487	0.878	0.8741
17	L-Threonine-3TMS	1	0.2474	0.2641	0.327	0.8541	1.0285	0.1417	0.1456	0.1426	0.7541	0.8087	0.8572
18	Propanedioic acid, [(trimethylsilyl)oxy]-, bis(trimethylsilyl) ester	1	2.0253	1.8284	0.779	0.3633	1.0263	0.4701	0.2131	0.9175	0.2396	0.6145	0.3389
19	Aminomalonic acid, tris(trimethylsilyl)-	1	0	0	0	0.7111	1.1195	0	0	3.00E-04	0	0	0.005
20	L-Aspartic acid-3TMS	1	0	0	0.5198	0.8872	1.2562	0	0	0	0.2334	0.4692	0.6589
21	L-Threonic acid, tris(trimethylsilyl) ether, trimethylsilyl ester	1	0.7113	0.8086	0.8498	1.0001	0.962	0.2516	0.2457	0.2485	0.5587	0.591	0.5736
22	L-Proline, 5-oxo-1-(trimethylsilyl)-, trimethylsilyl ester	1	0	0	0	0.9138	0.77996851	0	0	0	0	0	1.6083
23	Creatinine-3TMS	1	0.2815	0.2052	0.2786	0.9818	1.0556	0	0	0	0.9569	0.9466	0.944
24	L-Glutamic acid-3TMS	1	0.0726	0	0.1059	0.8781	1.132	0.0507	0.0381	0.0852	1.2898	1.2458	1.3077
25	L-Phenylalanine-2TMS	1	0	0	0	0	1.0724	0	0	0	0	0.1223	0.0832
26	Silanol, trimethyl-, pyrophosphate (4:1)	1	0.4856	1.2111	0.9769	0.6982	1.0873	0.4295	0.224	0.1915	0.142	0	0
27	Phosphoric acid, bis(trimethylsilyl) 2,3-bis[(trimethylsilyl)oxy]propyl est	1	0.4087	0.3654	0.1634	0.8378	0.8363	0	0	0	0.7383	0.6912	0.7758
28	Phosphoric acid, 2-[bis(trimethylsilyl)amino]ethyl bis(trimethylsilyl) est	1	0.1783	0.1686	0.1941	0.9758	1.0355	0.4352	0.4265	0.3717	0.2727	0.2763	0.263
29	Citric acid-4TMS ; 1,2,3-Propanetricarboxylic acid, 2-[(trimethylsilyl)oxy	1	0.3423	0.3187	0.5197	0.9766	1.0037	0.2946	0.2629	0.267	0.5945	0.6117	0.497
30	D-Glucose-5TMS-Methyloxime	1	0.64250412	0.7586		1.0402	0.9378	0.0849	0.0662	0.0546	0.9743	0.995	0.9895
31	Myristic acid-D3-TMS	1	0	0	0	0	0	0	0	0	0	0	0
32	D-Glucose, 2,3,4,5,6-pentakis-O-(trimethylsilyl)-	1	0	0	0	1.0134	0.9725	0	0	0	0	0.0526	0
33	Pantothenic acid tritms	1	0.042	0.2412	0.3462	1.1947	0.7813	0	0	0	3.902	5.3885	3.9573
34	Palmitic acid-TMS	1	1.005	0.9917	1.0566	0.9963	1.077	0.6237	0.581	0.5405	0.5753	0.5897	0.6252
35	Myo-Inositol, 1,2,3,4,5,6-hexakis-O-(trimethylsilyl)-	1	0	0	0	0	0	0.1291	0	0	0	0.5464	0
36	Methyl stearate	1	0.5247	0.714	0.788	0.9234	1.1111	0.2216	0.3521	0.1601	3.49	3.5653	3.6855
37	Oleic acid, trimethylsilyl ester	1	0.6899	0.7711	0.7863	0.8376	1.0233	0.3298	0.3487	0.3379	0.5584	0.663	0.667
38	Stearic acid-TMS	1	0.7801	0.8313	0.8317	0.97	1.0312	0.5892	0.577	0.5699	0.6153	0.6438	0.6302
39	Arachidonic acid, trimethylsilyl ester	1	0.7085	0.8039	0.839	1.0773	1.2826	0.1672	0.1909	0.1857	0.5418	0.6284	0.7302
40	Uridine, 2',3',5'-tris-O-(trimethylsilyl)-	1	0.501	0.6013	0.6524	0.8431	0.8968	0.0221	0.0193	0	0.488	0.5278	0.5271
41	2-Monopalmitoylglycerol trimethylsilyl ether	1	0.7779	0.6841	0.9685	0.8636	1.4609	0.453	0.4207	0.8594	0.7672	0.8168	0.5219
42	Hexadecanoic acid, 2,3-bis[(trimethylsilyl)oxy]propyl ester	1	1.0798	0.9165	1.1237	0.9178	1.0273	0.9142	0.874	0.8782	0.6371	0.6352	0.6243
43	cis-4,7,10,13,16,19-Docosahexaenoic acid, trimethylsilyl ester	1	0.0146	0.0199	0.0234	0.9313	0	0.1816	0.1833	0.1956	0	0.289	0
44	cis-5,8,11-Eicosatrienoic acid, trimethylsilyl ester	1	0.3628	0.1836	0.2206	1.0358	0.2153	0.2016	0.0465	0.0447	0.0843	0.211	0.5658
45	Maltose, octakis(trimethylsilyl) ether (isomer 2)	1	0	0	0	0.3747	0.184	0	0	0	0	0	0

LCM (top 200 significant proteins)

	P	Q	R	S	T	U	V	W	X	Y	Z	AA
1	ς	C: ANOVA Significant	N: -Log ANOVA p value	N: ANOVA q-value	T: Protein	T: Majority p	T: Protein names	T: Gene names				
2		+	1.95669	0.0265909	A0A024R	A0A024R4E5	Vigilin	HDLBP;Hdlbp				
3		+	1.6468	0.0346014	A0A024R	A0A024R4M	40S ribosomal protein S9	RPS9;Rps9				
4			0.779885	0.141584	A0A024R	A0A024RA52	Proteasome subunit alpha type;Proteasome subunit alpha type-2	PSMA2;Psma2				
5			0.473034	0.285007	A0A087W	A0A087WS5	Fibronectin;Anastellin	Fn1				
6			0.813977	0.132012	Q8C3V4	Q8C3V4	A0A Signal transducer and activator of transcription;Signal transducer and activator	Stat1				
7			0.89697	0.111135	A0A087W	A0A087WTT	Polyadenylate-binding protein;Polyadenylate-binding protein 1	PABPC1;Pabpc1				
8			0.133964	0.692556	A0A087W	A0A087WUL	Proteasome subunit beta type-3	PSMB3;Psmb3				
9			0.501722	0.2669	E7ETK0	A0A	40S ribosomal protein S24	RPS24;Rps24				
10			0.431548	0.321816	A0A0G2J	A0A0G2JEC4	Endophilin-B1	SH3GLB1;Sh3glb1				
11			1.12912	0.0720643	A0A087W	A0A087WWW	26S proteasome non-ATPase regulatory subunit 1	PSMD1;Psmd1				
12			0.64765	0.189164	A0A087W	A0A087WXS	ATPase ASNA1;ATPase Asna1	ASNA1;Asna1				
13			0.479076	0.281218	A0A087X	A0A087X054	Hypoxia up-regulated protein 1	HYOU1				
14			0.120233	0.713261	A0A087X	A0A087X0S5	Collagen alpha-1(VI) chain	COL6A1				
15			0.198229	0.587641	A0A087X	A0A087X0X3	Heterogeneous nuclear ribonucleoprotein M	HNRNPM				
16			0.0410109	0.892677	H0YJC0	A0A	26S protease regulatory subunit 10B	PSMC6;Psmc6				
17		+	1.91908	0.0276632	A0A0A0V	A0A0A0MQA	Alpha-1-antitrypsin 1-1	Serpina1a				
18		+	2.67448	0.0123636	A0A0A0V	A0A0A0MQA	Tubulin alpha-4A chain	Tuba4a;TUBA4A				
19		+	1.5023	0.0416145	A0A0A0V	A0A0A0MQF	Glyceraldehyde-3-phosphate dehydrogenase	Gapdh;Gm3839				
20			0.723421	0.160439	A0A0A0V	A0A0A0MR0	Voltage-dependent anion-selective channel protein 2	VDAC2;Vdac2				
21		+	2.81596	0.0132174	A0A0A0V	A0A0A0MS5	Gelsolin	GSN				
22			0.358946	0.383304	A0A0A0V	A0A0A0MSI	Peroxiredoxin-1	PRDX1				
23			0.346903	0.393695	A0A0A6Y	A0A0A6YW6	Ubiquitin-60S ribosomal protein L40;Ubiquitin;60S ribosomal protein L40;Ubiqu	Gm8797;UBB;Uba52;RPS27A;UBC;Kxd1;Ubc;Ubb;UBA52;Rps27a				
24			0.225994	0.548252	A0A0C4D	A0A0C4DFU	Superoxide dismutase;Superoxide dismutase [Mn], mitochondrial	SOD2				
25	+		1.98513	0.0268148	A0A0C4D	A0A0C4DGS	Dolichyl-diphosphooligosaccharide--protein glycosyltransferase 48 kDa subunit	DDOST;Ddost				
26			0.365013	0.377098	A0A0D9S	A0A0D95FB	ATP-dependent RNA helicase DDX3X;Putative ATP-dependent RNA helicase Pl1(	DDX3X;D1Pas1;DDX3Y				
27			0.203187	0.581	A0A0G2J	A0A0G2JGD	Protein S100-A4	S100a4				
28		+	1.84718	0.0286239	A0A0G2J	A0A0G2JIW1	Heat shock 70 kDa protein 1B;Heat shock 70 kDa protein 1A	HSPA1B;HSPA1A				
29		+	2.29685	0.0195294	D6RGI3	A0A	Septin-11	SEPT11;Sept11				
30		+	2.68261	0.01275	A0A0J9Y	A0A0J9YUZ4	High mobility group protein B1;Putative high mobility group protein B1-like 1	Hmgb1;HMGB1;HMGB1P1				
31		+	3.46345	0.016	A0A0N4S	A0A0N4SW9	Myeloid-associated differentiation marker	Myadm				
32			0.708356	0.164831	A0A0R4I	A0A0R4IZW	Calpain small subunit 1	Capns1				
33			0.386993	0.362984	A0A0R4J	A0A0R4J0I1	Serine protease inhibitor A3K	Serpina3k				
34			0.0154577	0.95681	A0A0R4J1	A0A0R4J1N1	Inter alpha-trypsin inhibitor, heavy chain 4	Itih4				
35		+	1.37105	0.0491837	G3UZI2	A0A	Heterogeneous nuclear ribonucleoprotein Q	Syncrip;SYNCRIP				
36			0.596095	0.215241	A0A0R4J	A0A0R4J2B2	BTB/POZ domain-containing protein KCTD12	KCTD12;Kctd12				
37		+	1.4828	0.0421988	A0A0U1R	A0A0U1RQH	RNA-binding protein 39	Rbm39;RBM39				
38			0.560194	0.233754	A0A0U1R	A0A0U1RR3	Histone H2A type 1-J;Histone H2A type 1-H;Histone H2A.J;Histone H2A type 1-D;	HIST1H2AJ;HIST1H2AH;H2AFJ;HIST1H2AD;HIST1H2AG				
39		+	1.47854	0.0417701	A0A140T	A0A140T8L1	60S ribosomal protein L7a	RPL7A;Rpl7a				



	P	Q	R	S	T	U	V	W	X	Y	Z	AA	AB
1	C: ANOVA Significant		N: -Log ANOVA p value	N: ANOVA q-value	T: Protein	T: Majority p	T: Protein names	T: Gene names					
2	+		1.95669	0.0265909	A0A024R4	A0A024R4E5	Vigilin	HDLBP;Hdlbp					
3	+		1.6468	0.0346014	A0A024R4	A0A024R4M	40S ribosomal protein S9	RPS9;Rps9					
4			0.779885	0.141584	A0A024R4	A0A024RA52	Proteasome subunit alpha type;Proteasome subunit alpha type-2	PSMA2;Psma2					
5			0.473034	0.285007	A0A087W	A0A087WS5	Fibronectin;Anastellin	Fn1					
6			0.813977	0.132012	Q8C3V4;A	Q8C3V4;A0A	Signal transducer and activator of transcription;Signal transducer and activator	Stat1					
7			0.89697	0.111135	A0A087W	A0A087WTT	Polyadenylate-binding protein;Polyadenylate-binding protein 1	PABPC1;Pabpc1					
8			0.133964	0.692556	A0A087W	A0A087WUL	Proteasome subunit beta type-3	PSMB3;Psmb3					
9			0.501722	0.2669	E7ETK0;A	E7ETK0;A0A	40S ribosomal protein S24	RPS24;Rps24					
10			0.431548	0.321816	A0A0G2JI	A0A0G2JEC4	Endophilin-B1	SH3GLB1;Sh3glb1					
11			1.12912	0.0720643	A0A087W	A0A087WW	26S proteasome non-ATPase regulatory subunit 1	PSMD1;Psmd1					
12			0.64765	0.189164	A0A087W	A0A087WXS	ATPase ASNA1;ATPase Asna1	ASNA1;Asna1					
13			0.479076	0.281218	A0A087X	A0A087X054	Hypoxia up-regulated protein 1	HYOU1					
14			0.120233	0.713261	A0A087X	A0A087X0S5	Collagen alpha-1(VI) chain	COL6A1					
15			0.198229	0.587641	A0A087X	A0A087X0X3	Heterogeneous nuclear ribonucleoprotein M	HNRNPM					
16			0.0410109	0.892677	H0YJC0;A	H0YJC0;A0A	26S protease regulatory subunit 10B	PSMC6;Psmc6					
17	+		1.91908	0.0276632	A0A0A0M	A0A0A0MQA	Alpha-1-antitrypsin 1-1	Serpina1a					
18	+		2.67448	0.0123636	A0A0A0M	A0A0A0MQA	Tubulin alpha-4A chain	Tuba4a;TUBA4A					
19	+		1.5023	0.0416145	A0A0A0M	A0A0A0MQF	Glyceraldehyde-3-phosphate dehydrogenase	Gapdh;Gm3839					
20			0.723421	0.160439	A0A0A0M	A0A0A0MR0	Voltage-dependent anion-selective channel protein 2	VDAC2;Vdac2					
21	+		2.81596	0.0132174	A0A0A0M	A0A0A0MS5	Gelsolin	GSN					
22			0.358946	0.383304	A0A0A0M	A0A0A0MSI	Peroxiredoxin-1	PRDX1					
23			0.346903	0.393695	A0A0A6Y	A0A0A6YW6	Ubiquitin-60S ribosomal protein L40;Ubiquitin;60S ribosomal protein L40;Ubiqu	Gm8797;UBB;Uba52;RPS27A;UBC;Kxd1;Ubc;Ubb;UBA52;Rps27a					
24			0.225994	0.548252	A0A0C4DI	A0A0C4DFU	Superoxide dismutase;Superoxide dismutase [Mn], mitochondrial	SOD2					
25	+		1.98513	0.0268148	A0A0C4DI	A0A0C4DGS	Dolichyl-diphosphooligosaccharide--protein glycosyltransferase 48 kDa subunit	DDOST;Ddost					
26			0.365013	0.377098	A0A0D9SI	A0A0D9SFB	ATP-dependent RNA helicase DDX3X;Putative ATP-dependent RNA helicase Pl1(	DDX3X;D1Pas1;DDX3Y					
27			0.203187	0.581	A0A0G2JI	A0A0G2JGD	Protein S100-A4	S100a4					
28	+		1.84718	0.0286239	A0A0G2JI	A0A0G2JIW1	Heat shock 70 kDa protein 1B;Heat shock 70 kDa protein 1A	HSPA1B;HSPA1A					
29	+		2.29685	0.0195294	D6RGI3;A	D6RGI3;A0A	Septin-11	SEPT11;Sept11					
30	+		2.68261	0.01275	A0A0J9YL	A0A0J9YUZ4	High mobility group protein B1;Putative high mobility group protein B1-like 1	Hmgb1;HMGB1;HMGB1P1					
31	+		3.46345	0.016	A0A0N4S	A0A0N4SW9	Myeloid-associated differentiation marker	Myadm					
32			0.708356	0.164831	A0A0R4IZ	A0A0R4IZW8	Calpain small subunit 1	Capns1					
33			0.386993	0.362984	A0A0R4J0	A0A0R4J0I1;	Serine protease inhibitor A3K	Serpina3k					
34			0.0154577	0.95681	A0A0R4J1	A0A0R4J1N1	Inter alpha-trypsin inhibitor, heavy chain 4	Itih4					
35	+		1.37105	0.0491837	G3UZI2;A	G3UZI2;A0A	Heterogeneous nuclear ribonucleoprotein Q	Syncrip;SYNCRIP					
36			0.596095	0.215241	A0A0R4J2	A0A0R4J2B2	BTB/POZ domain-containing protein KCTD12	KCTD12;Kctd12					
37	+		1.4828	0.0421988	A0A0U1R	A0A0U1RQH	RNA-binding protein 39	Rbm39;RBM39					
38			0.560194	0.233754	A0A0U1R	A0A0U1RR3	Histone H2A type 1-J;Histone H2A type 1-H;Histone H2A.J;Histone H2A type 1-D;	HIST1H2AJ;HIST1H2AH;H2AFJ;HIST1H2AD;HIST1H2AG					
39	+		1.47854	0.0417701	A0A140T8	A0A140T8L1	60S ribosomal protein L7a	RPL7A;Rpl7a					
40	+		1.46955	0.0419101	A0A140T8	A0A140T8M	60S ribosomal protein L23a	Rpl23a;RPL23A					
41	+		1.48333	0.0424235	H7C469;A	H7C469;A0A	Cathepsin D;Cathepsin D light chain;Cathepsin D heavy chain	CTSD					
42			0.714571	0.163296	A0A1C7C	A0A1C7CYV0	Plastin-3	Pls3					
43			0.299005	0.448842	A0A1L1S	A0A1L1SQA8	40S ribosomal protein S25	Rps25;RPS25					
44			0.0338839	0.907699	A0A1L1S	A0A1L1SV25	Alpha-actinin-4	Actn4					
45	+		1.88144	0.0278462	A2A3R5;P	A2A3R5;P62	40S ribosomal protein S6	RPS6;Rps6					
46			0.544851	0.240472	J3QR09;J	J3QR09;J3KT	Ribosomal protein L19;60S ribosomal protein L19	RPL19;Rpl19					
47			1.30819	0.0539139	E9PM69;A	E9PM69;A2A	26S protease regulatory subunit 6A	PSMC3;Psmc3					
48			0.990918	0.0916667	A2AQR0;A	A2AQR0;P43	Glycerol-3-phosphate dehydrogenase;Glycerol-3-phosphate dehydrogenase, mit	Gpd2;GPD2					
49	+		2.0034	0.026481	A2AUR7;(	A2AUR7;Q9(	Ras suppressor protein 1	Rsu1;RSU1					
50			0.134071	0.693664	A2AVJ7;Q	A2AVJ7;Q99	Ribosome-binding protein 1	Rrbp1					
51			0.340941	0.39976	A2BE93;C	A2BE93;Q9E	Protein SET;Protein SETSIP	Set;SET;SETSIP					

all anova significant proteins

51				0.340941	0.39976	A2BE93;C	A2BE93;Q9E	Protein SET;Protein SETSIP	Set;SET;SETSIP		
52		+		2.30647	0.0196	A3KGU5;E	A3KGU5;E9C	Spectrin alpha chain, non-erythrocytic 1	Sptan1		
53				0.129473	0.700099	B0QZ43;C	B0QZ43;O75	Erlin-1	ERLIN1;Erlin1		
54				0.260748	0.499048	B0YIW6;C	B0YIW6;Q5X	Coatomer subunit delta	ARCN1;Arcn1		
55				0.347986	0.393207	B2M1R6;I	B2M1R6;P61	Heterogeneous nuclear ribonucleoprotein K	Hnrnpk;HNRNPK		
56		+		2.37965	0.0180426	G3V4W0;	G3V4W0;B4I	Heterogeneous nuclear ribonucleoproteins C1/C2	HNRNPC		
57				1.18308	0.0686288	B2RXM2;.	B2RXM2;J3Q	Heterogeneous nuclear ribonucleoprotein A3	Gm6793;Gm9242;HNRNPA3;Hnrnpa3		
58		+		2.69966	0.0129333	H0YJH9;D	H0YJH9;D3YU	Polyadenylate-binding protein 2	PABPN1;Pabpn1;Gm20521		
59		+		1.56233	0.0370566	B4DGU4;(	B4DGU4;Q0Z	Catenin beta-1	CTNNB1;Ctnnb1		
60		+		1.76027	0.0306341	B4DJV2;O	B4DJV2;O75	Citrate synthase;Citrate synthase, mitochondrial	CS		
61				0.0576811	0.848551	B5MDF5;I	B5MDF5;P62	GTP-binding nuclear protein Ran;GTP-binding nuclear protein Ran, testis-specif	RAN;Ran;1700009N14Rik;Rasl2-9		
62		+		1.44276	0.0430919	B7FAU9;(	B7FAU9;Q8E	Filamin-A	Flna		
63		+		1.92222	0.0277447	B9EHJ3;P:	B9EHJ3;P394	Tight junction protein ZO-1	Tjp1;TJP1		
64				0.188047	0.60523	C9J3L8;C9	C9J3L8;C9J5\	Translocon-associated protein subunit alpha	SSR1;Ssr1		
65		+		1.92889	0.0274409	C9J9K3;P1	C9J9K3;P142	40S ribosomal protein SA	RPSA;Rpsa		
66				0.25283	0.510202	C9JXB8;C9	C9JXB8;C9JN	60S ribosomal protein L24	RPL24;Rpl24		
67		+		1.72029	0.0310677	F5GYN4;I	F5GYN4;D3Y	Ubiquitin thioesterase OTUB1	OTUB1;Otub1		
68				0.855563	0.122264	D3YXG6;C	D3YXG6;Q9C	Actin-related protein 2/3 complex subunit 2	Arpc2;ARPC2		
69				0.083071	0.792707	E5RI99;P(	E5RI99;P628	60S ribosomal protein L30	RPL30;Rpl30		
70				0.275939	0.477056	Q8BPI2;F!	Q8BPI2;F5G)	Transmembrane emp24 domain-containing protein 2	Tmed2;TMED2		
71				0.645569	0.189211	E7EQV9;E	E7EQV9;E9Q	Ribosomal protein L15;60S ribosomal protein L15	RPL15;Gm10020;Rpl15		
72				0.308803	0.436262	E7EU96;C	E7EU96;Q60	Casein kinase II subunit alpha;Casein kinase II subunit alpha 3	CSNK2A1;Csnk2a1;CSNK2A3		
73				0.0360645	0.90286	F8VZJ2;H(	F8VZJ2;H0YH	Nascent polypeptide-associated complex subunit alpha;Nascent polypeptide-as	NACA;Naca		
74				0.52192	0.25343	E9PGZ1;C	E9PGZ1;Q05	Caldesmon	CALD1		
75				1.18377	0.0687895	E9PK01;P:	E9PK01;P296	Elongation factor 1-delta	EEF1D		
76		+		1.97676	0.0264286	E9PKZ0;P(	E9PKZ0;P629	60S ribosomal protein L8	RPL8;Rpl8		
77				0.377531	0.368761	E9PV24;E	E9PV24;E9P\	Fibrinogen alpha chain;Fibrinopeptide A;Fibrinogen alpha chain	Fga		
78				0.819971	0.130602	E9PWQ3;	E9PWQ3;D3YWD1		Col6a3		
79		+		1.39589	0.0467435	E9PYL9;Q	E9PYL9;Q9C)	60S ribosomal protein L11	Gm10036;Rpl11;RPL11;Gm5093		
80				0.976485	0.0947354	E9PZ16	E9PZ16		Hspg2		
81				0.178783	0.618976	G3X9T8;G	G3X9T8;G3X	Ceruloplasmin	Cp		
82				1.05255	0.081417	E9Q9F5;E	E9Q9F5;E9Q	Septin-7	Sept7;SEPT7		
83				0.52662	0.251903	E9Q3T0;P	E9Q3T0;P47!	60S acidic ribosomal protein P1	Gm10073;Rplp1		
84		+		2.6907	0.0131613	E9Q456;E	E9Q456;E9Q453;F5H7S3;B7Z596		Tpm1;TPM1		
85				0.485948	0.277626	E9Q557;E	E9Q557;E9P2	Desmoplakin	Dsp		
86		+		2.44737	0.0158222	E9Q616;G	E9Q616		Ahnak		
87				0.868045	0.119783	G3X9V2;E	G3X9V2;E9Q	Catenin delta-1	Ctnnd1;CTNND1		
88				0.791136	0.139522	Q8VCQ8;(	Q8VCQ8;E9QA16;S4R1T7;E9Q0M9;D3Z6I7;E9QA15		Cald1		
89				0.401908	0.347702	E9QN08;(	E9QN08;Q80	Elongation factor 1-delta	Eef1d		
90				0.537212	0.244968	E9QN70;F	E9QN70;P02	Laminin subunit beta-1	Lamb1		
91				1.29008	0.0553615	E9QPX1;P	E9QPX1;P39(	Collagen alpha-1(XVIII) chain;Endostatin	Col18a1		
92				0.405942	0.343873	F2Z388;Q	F2Z388;Q6ZV	60S ribosomal protein L35	RPL35;Rpl35		
93				0.998192	0.0897282	F2Z456;Q	F2Z456;Q9D(	NADH-cytochrome b5 reductase;NADH-cytochrome b5 reductase 3;NADH-cytoch	Cyb5r3		
94				0.553581	0.235002	F5GXX5;P	F5GXX5;P61	Dolichyl-diphosphooligosaccharide--protein glycosyltransferase subunit DAD1	DAD1;Dad1		
95				0.410765	0.339873	F8W020;I	F8W020;F8V	Nucleosome assembly protein 1-like 1	NAP1L1		
96		+		1.71579	0.0311642	F6QA74;P	F6QA74;P28:	DNA-(apurinic or apyrimidinic site) lyase;DNA-(apurinic or apyrimidinic site) lya	Apex1;APEX1		
97				0.669746	0.180248	F6SVV1;P	F6SVV1;P62(	40S ribosomal protein S7	Gm9493;Rps7;RPS7		
98		+		2.07704	0.0244638	F6YVP7;P	F6YVP7;P622	40S ribosomal protein S18	Gm10260;Rps18;RPS18		
99				1.28392	0.0559065	F8VQJ3;P	F8VQJ3;P024	Laminin subunit gamma-1	Lamc1		
100		+		1.52785	0.0403457	F8W6I7;C	F8W6I7;Q5E	Heterogeneous nuclear ribonucleoprotein A1;Heterogeneous nuclear ribonucleo	HNRNPA1;Hnrnpa1;HNRNPA1L2		
101				1.09824	0.0756576	F8WCF6;I	F8WCF6;P59	Actin-related protein 2/3 complex subunit 4	ARPC4-TTLL3;Arpc4;ARPC4		

	O	P	Q	R	S	T	U	V	W	X	Y	Z	AA
101				1.09824	0.0756576	F8WCF6;F	F8WCF6;P59	Actin-related protein 2/3 complex subunit 4	ARPC4-TTLL3;Arpc4;ARPC4				
102		+		1.4003	0.0465053	F8WIT2;P	F8WIT2;P14	Annexin;Annexin A6	Anxa6				
103				0.0480317	0.875682	Q3T9X3;F	Q3T9X3;F8W	Dynamin-2	Dnm2;DNM2				
104		+		1.93766	0.0272527	F8WIX8;C	F8WIX8;Q64	Histone H2A;Histone H2A type 2-C;Histone H2A type 2-A	Hist1h2al;Hist2h2ac;HIST2H2AC;Hist2h2aa1;HIST2H2AA3				
105				0.00190433	0.993597	G3UVV4;I	G3UVV4;P17	Hexokinase;Hexokinase-1	Hk1				
106				0.699955	0.16884	G3UXZ5;F	G3UXZ5;P97	Proteasome activator complex subunit 1	Psme1				
107		+		2.27053	0.0195556	G3UYV7;F	G3UYV7;P62	40S ribosomal protein S28	Rps28;RPS28;Gm10263				
108				0.315422	0.427975	G3V5Z7;C	G3V5Z7;Q9C	Proteasome subunit alpha type;Proteasome subunit alpha type-6	PSMA6;Psma6				
109				0.319763	0.423898	G3X9V0;P	G3X9V0;P97	Proteasome activator complex subunit 2	Psme2				
110				0.748637	0.152184	G5E839;P	G5E839;P50	T-complex protein 1 subunit delta	Cct4;CCT4				
111				0.490652	0.274404	G8JLB6;P	G8JLB6;P319	Heterogeneous nuclear ribonucleoprotein H;Heterogeneous nuclear ribonucleop	HNRNPH1;Hnrnph1				
112				0.177044	0.621124	H0Y7A7;P	H0Y7A7;P62	Calmodulin;Calmodulin-like protein 3	CALM2;Calm1;CALM1;Calml3				
113		+		1.72738	0.0312923	H0YE29;Q	H0YE29;Q07	Rho GTPase-activating protein 1	ARHGAP1;Arhgap1				
114		+		1.51673	0.0407805	H3BK43;H	H3BK43;H3B	S-formylglutathione hydrolase	Esd				
115				1.1409	0.0706016	Q3U741;H	Q3U741;H3B	Probable ATP-dependent RNA helicase DDX17	Ddx17;DDX17				
116		+		1.98088	0.0269268	H7BWZ3;H	H7BWZ3;Q9	Actin-related protein 2/3 complex subunit 3	Arpc3;ARPC3				
117				0.165976	0.638706	J3KPX7;Q	J3KPX7;Q996	Prohibitin-2	PHB2;Phb2				
118				0.234255	0.535128	J3KTA4;Q	J3KTA4;Q8B1	Probable ATP-dependent RNA helicase DDX5	DDX5;Ddx5				
119				0.200888	0.58396	J3QRS3;P	J3QRS3;P191	Myosin regulatory light chain 12A;Myosin regulatory light chain 12B	MYL12A;Myl12b;MYL12B				
120		+		1.79527	0.030807	K7ERI7;K7	K7ERI7;K7EN	60S ribosomal protein L22	RPL22;Rpl22				
121		+		2.19904	0.0219661	M0QWP1	M0QWP1;Z4	Agrin;Agrin N-terminal 110 kDa subunit;Agrin C-terminal 110 kDa subunit;Agrin	Agrn				
122				0.918153	0.10555	M0QXS5;I	M0QXS5;P14	Heterogeneous nuclear ribonucleoprotein L	HNRNPL				
123				1.04237	0.0826232	M0R0F0;F	M0R0F0;P46	40S ribosomal protein S5;40S ribosomal protein S5, N-terminally processed	RPS5;Rps5				
124				0.653111	0.186904	M0R3D6;I	M0R3D6;M0	60S ribosomal protein L18a	RPL18A				
125		+		1.69881	0.0318832	M0R210;F	M0R210;P62	40S ribosomal protein S16	RPS16;Rps16;ZNF90				
126				0.867124	0.119835	O00151	O00151	PDZ and LIM domain protein 1	PDLIM1				
127				0.830392	0.128074	Q8BG32;(	Q8BG32;O0(	26S proteasome non-ATPase regulatory subunit 11	Psmd11;PSMD11				
128		+		2.0001	0.02625	O00299	O00299	Chloride intracellular channel protein 1	CLIC1				
129				0.553745	0.235455	O08529;C	O08529	Calpain-2 catalytic subunit	Capn2				
130				1.14465	0.07093	O75396;C	O75396;O08	Vesicle-trafficking protein SEC22b	SEC22B;Sec22b				
131		+		2.02451	0.0252468	O08553	O08553	Dihydropyrimidinase-related protein 2	Dpysl2				
132				1.13348	0.0718704	O08583;C	O08583;Q86	THO complex subunit 4;Aly/REF export factor 2	Alyref;ALYREF;Alyref2				
133				1.27424	0.0567593	O08709;C	O08709;Q6G	Peroxiredoxin-6	Prdx6				
134				1.03608	0.0834676	O09061;P	O09061;P20	Proteasome subunit beta type-1	Psmb1;PSMB1				
135		+		1.7639	0.0305902	Q8BH40;(	Q8BH40;O15	Syntaxin-7	Stx7;STX7				
136				0.159443	0.649802	O43143;C	O43143;O35	Pre-mRNA-splicing factor ATP-dependent RNA helicase DHX15	DHX15;Dhx15				
137		+		3.18666	0.0136	O35639;C	O35639;Q3T	Annexin A3;Annexin	Anxa3				
138				1.31865	0.0531068	Q8VHM5;	Q8VHM5;O4	Heterogeneous nuclear ribonucleoprotein R	Hnrnpr;HNRNPR				
139		+		2.51666	0.0142	O54724	O54724	Polymerase I and transcript release factor	Ptrf				
140		+		2.72905	0.0137778	P18077;O	P18077;O55	60S ribosomal protein L35a	RPL35A;Rpl35a				
141				0.877093	0.117125	O55143-2	O55143-2;O5	Sarcoplasmic/endoplasmic reticulum calcium ATPase 2	Atp2a2				
142		+		1.57321	0.0367949	O55222;A	O55222;A0A	Integrin-linked protein kinase	Ilk;ILK				
143		+		2.33561	0.0191667	O70400;S	O70400;S4R	PDZ and LIM domain protein 1	Pdlim1				
144				1.23864	0.0608507	O70435;P	O70435;P25	Proteasome subunit alpha type-3	Psma3;PSMA3				
145				0.122144	0.712913	O75131;E	O75131	Copine-3	CPNE3				
146		+		1.72617	0.031084	O75369-2	O75369-2;O7	Filamin-B	FLNB				
147				1.06726	0.0808182	O88322	O88322	Nidogen-2	Nid2				
148				0.286488	0.4641	O88342;A	O88342	WD repeat-containing protein 1	Wdr1				
149				0.679444	0.176621	P22626;O	P22626;O88	Heterogeneous nuclear ribonucleoproteins A2/B1	HNRNPA2B1;Hnrnpa2b1				
150				0.207662	0.575004	O89053;P	O89053;P31	Coronin-1A;Coronin	Coro1a;CORO1A				
151		+		1.44845	0.0434286	P00338;P(	P00338;P003	L-lactate dehydrogenase A chain	LDHA				

	N	O	P	Q	R	S	T	U	V	W	X	Y
151			+		1.44845	0.0434286	P00338;P(	P00338;P003	L-lactate dehydrogenase A chain	LDHA		
152					0.0660528	0.829515	P00491;G	P00491;G3V!	Purine nucleoside phosphorylase	PNP		
153			+		1.74832	0.030912	P00558;P(	P00558;P005	Phosphoglycerate kinase 1;Phosphoglycerate kinase	PGK1;Pgk1		
154			+		2.89924	0.0144444	P00920;A	P00920	Carbonic anhydrase 2	Ca2		
155					0.682367	0.175683	P01024;N	P01024	Complement C3;Complement C3 beta chain;C3-beta-c;Complement C3 alpha ch	C3		
156					0.624709	0.199354	P01027;P(	P01027	Complement C3;Complement C3 beta chain;C3-beta-c;Complement C3 alpha ch	C3		
157			+		1.75217	0.0310645	P01900;P(	P01900;P018	H-2 class I histocompatibility antigen, D-D alpha chain;H-2 class I histocompatit	H2-D1		
158			+		3.10917	0.012	P01942;A	P01942	Hemoglobin subunit alpha	Hba		
159			+		2.97463	0.0131765	P02088;A	P02088;A8D(	Hemoglobin subunit beta-1	Hbb-b1;Hbbt1		
160			+		1.4433	0.0433261	P02089	P02089	Hemoglobin subunit beta-2	Hbb-b2		
161			+		1.70985	0.0314963	P02463;A	P02463;A0A:	Collagen alpha-1(IV) chain;Arresten	Col4a1;COL4A1		
162					0.377697	0.369348	P02545;P(	P02545;P025	Prelamin-A/C;Lamin-A/C	LMNA		
163					1.05495	0.0816506	P02751-1	P02751-17;P	Fibronectin;Anastellin;Ugl-Y1;Ugl-Y2;Ugl-Y3	FN1		
164					0.0876784	0.784859	P02794;E!	P02794;E9PP	Ferritin heavy chain;Ferritin heavy chain, N-terminally processed;Ferritin	FTH1		
165					0.918867	0.105817	P04075;J3	P04075;J3KP	Fructose-bisphosphate aldolase A;Fructose-bisphosphate aldolase	ALDOA		
166			+		1.8309	0.0294414	P04083;Q	P04083;Q5T3	Annexin A1;Annexin	ANXA1		
167					1.25952	0.0586055	P04406;P(	P04406;P044	Glyceraldehyde-3-phosphate dehydrogenase	GAPDH		
168					0.459152	0.297247	Q5SRN7;(	Q5SRN7;Q5S	HLA class I histocompatibility antigen, A-3 alpha chain;HLA class I histocompati	HLA-A		
169			+		3.19811	0.0151111	P04792;F	P04792	Heat shock protein beta-1	HSPB1		
170					1.31352	0.0536232	P04843;B	P04843;B7Z4	Dolichyl-diphosphooligosaccharide--protein glycosyltransferase subunit 1	RPN1		
171					0.63728	0.193016	P05023-3	P05023-3;P0	Sodium/potassium-transporting ATPase subunit alpha-1	ATP1A1		
172					0.72997	0.158334	P05089;P(	P05089;P050	Arginase-1	ARG1		
173			+		2.26833	0.0194182	P05109	P05109	Protein S100-A8;Protein S100-A8, N-terminally processed	S100A8		
174					1.07542	0.0796322	P05202	P05202	Aspartate aminotransferase, mitochondrial	Got2		
175					0.271457	0.483104	P68363;P(	P68363;P052	Tubulin alpha-1B chain	TUBA1B;Tuba1b		
176					0.676838	0.176997	P05388;F	P05388;F8VV	60S acidic ribosomal protein P0;60S acidic ribosomal protein P0-like	RPLP0;RPLP0P6;Rplp0		
177					0.372175	0.372492	P05783;F	P05783;F8V2	Keratin, type I cytoskeletal 18	KRT18		
178			+		1.90563	0.02724	Q564E2;P	Q564E2;P06	L-lactate dehydrogenase;L-lactate dehydrogenase A chain	Ldha		
179			+		1.58251	0.0363871	P06702	P06702	Protein S100-A9	S100A9		
180			+		1.47258	0.0419545	P06733;P(	P06733;P067	Alpha-enolase	ENO1		
181			+		1.67819	0.0331799	P06745;A	P06745	Glucose-6-phosphate isomerase	Gpi		
182					0.34528	0.394815	P06748;Q	P06748;Q5S(	Nucleophosmin	NPM1;Npm1		
183			+		1.37378	0.0491487	P07195;A	P07195;A8M	L-lactate dehydrogenase B chain;L-lactate dehydrogenase	LDHB		
184					0.922087	0.105193	P07237;H	P07237;H7B2	Protein disulfide-isomerase	P4HB		
185					0.0399791	0.892675	P07355;P(	P07355;P073	Annexin A2;Annexin;Putative annexin A2-like protein	ANXA2;ANXA2P2		
186					0.633643	0.194736	P07356;B	P07356;B0V2	Annexin A2;Annexin	Anxa2		
187			+		1.97046	0.026186	P07384;E!	P07384	Calpain-1 catalytic subunit	CAPN1		
188			+		2.73704	0.0141538	Q5JP53;P!	Q5JP53;P990	Tubulin beta-5 chain;Tubulin beta chain	TUBB;Tubb5		
189			+		3.58442	0.012	P07724	P07724	Serum albumin	Alb		
190					0.956583	0.0986983	P07737;K	P07737;K7EJ	Profilin-1	PFN1		
191					0.837551	0.126259	P07900;P(	P07900;P079	Heat shock protein HSP 90-alpha	HSP90AA1		
192			+		1.86472	0.028381	P08122;P(	P08122;P085	Collagen alpha-2(IV) chain;Canstatin	Col4a2;COL4A2		
193			+		1.74784	0.0306667	P08228	P08228	Superoxide dismutase [Cu-Zn]	Sod1		
194					0.278848	0.473683	P11499;P(	P11499;P082	Heat shock protein HSP 90-beta	Hsp90ab1;HSP90AB1		
195			+		1.72815	0.0315349	P08249;A	P08249	Malate dehydrogenase, mitochondrial	Mdh2		
196					0.647619	0.188728	P08473;C!	P08473	Neprilysin	MME		
197			+		3.11299	0.0126154	P08670;B	P08670;B0YJ	Vimentin	VIM		
198					0.182495	0.61385	P63276;P(	P63276;P087	40S ribosomal protein S17	Rps17;RPS17		
199			+		2.51206	0.0140488	P08752;A	P08752;A0A(	Guanine nucleotide-binding protein G(i) subunit alpha-2	Gnai2		
200					0.69476	0.171152	P08758;D	P08758;D6RE	Annexin A5;Annexin	ANXA5		
201			+		1.5561	0.0373	P09055;P(	P09055;P090	Integrin beta-1	Itgb1		

References

1. Hanahan, D. & Weinberg, R. A. Hallmarks of cancer: The next generation. *Cell* (2011). doi:10.1016/j.cell.2011.02.013
2. Ashkenazi, R., Gentry, S. N. & Jackson, T. L. Pathways to Tumorigenesis—Modeling Mutation Acquisition in Stem Cells and Their Progeny. *Neoplasia* (2008). doi:10.1593/neo.08572
3. Fouad, Y. A. & Aanei, C. Revisiting the hallmarks of cancer. *American Journal of Cancer Research* (2017). doi:10.1016/j.jmwh.2009.11.004
4. Feitelson, M. A. *et al.* Sustained proliferation in cancer: Mechanisms and novel therapeutic targets. *Seminars in Cancer Biology* (2015). doi:10.1016/j.semcancer.2015.02.006
5. Rhind, N. & Russell, P. Signaling Pathways that Regulate Cell Division. *Cold Spring Harb. Perspect. Biol.* (2012). doi:10.1101/cshperspect.a005942
6. Lemmon, M. A. & Schlessinger, J. Cell signaling by receptor tyrosine kinases. *Cell* (2010). doi:10.1016/j.cell.2010.06.011
7. Vogelstein, B. *et al.* Cancer genome landscapes. *Science* (2013). doi:10.1126/science.1235122
8. Cheng, N., Chytil, A., Shyr, Y., Joly, A. & Moses, H. L. Transforming growth factor-beta signaling-deficient fibroblasts enhance hepatocyte growth factor signaling in mammary carcinoma cells to promote scattering and invasion. *Mol. Cancer Res.* (2008). doi:10.1158/1541-7786.MCR-07-2203
9. Giancotti, F. G. Deregulation of cell signaling in cancer. *FEBS Letters* (2014). doi:10.1016/j.febslet.2014.02.005
10. Seshacharyulu, P. *et al.* Targeting the EGFR signaling pathway in cancer therapy. *Expert Opin. Ther. Targets* (2012). doi:10.1517/14728222.2011.648617
11. Aykul, S. & Martinez-Hackert, E. Transforming growth factor-β family ligands can function as antagonists by competing for type II receptor binding. *J. Biol. Chem.* (2016). doi:10.1074/jbc.M115.713487
12. Yoko, K., Samy, L. & Rik, D. TGF-β signaling and epithelial–mesenchymal transition in cancer progression. *Curr. Opin. Oncol.* (2013). doi:10.1097/CCO.0b013e32835b6371
13. Pickup, M., Novitskiy, S. & Moses, H. L. The roles of TGFβ in the tumour microenvironment. *Nature Reviews Cancer* (2013). doi:10.1038/nrc3603
14. Fernández-Medarde, A. & Santos, E. Ras in cancer and developmental diseases. *Genes and Cancer* (2011). doi:10.1177/1947601911411084
15. Ratner, N. & Miller, S. J. A RASopathy gene commonly mutated in cancer: The neurofibromatosis type 1 tumour suppressor. *Nature Reviews Cancer* (2015). doi:10.1038/nrc3911
16. Csermely, P., Korcsmáros, T. & Nussinov, R. Intracellular and intercellular signaling networks in cancer initiation, development and precision anti-cancer therapy: RAS acts as contextual signaling hub. *Seminars in Cell and Developmental Biology* (2016). doi:10.1016/j.semcdb.2016.07.005
17. Hobbs, G. A., Der, C. J. & Rossman, K. L. RAS isoforms and mutations in cancer at a glance. *J. Cell Sci.* (2016). doi:10.1242/jcs.182873
18. Reuter, C. W., Morgan, M. a & Bergmann, L. Targeting the Ras signaling pathway: a rational, mechanism-based treatment for hematologic malignancies? *Blood* (2000).
19. Pylayeva-Gupta, Y., Grabocka, E. & Bar-Sagi, D. RAS oncogenes: Weaving a tumorigenic web. *Nature Reviews Cancer* (2011). doi:10.1038/nrc3106
20. Malumbres, M. & Barbacid, M. Cell cycle, CDKs and cancer: A changing paradigm.

Nature Reviews Cancer (2009). doi:10.1038/nrc2602
21. Weinberg, R. A. The retinoblastoma protein and cell cycle control. *Cell* (1995). doi:10.1016/0092-8674(95)90385-2
22. Dick, F. A. & Rubin, S. M. Molecular mechanisms underlying RB protein function. *Nature Reviews Molecular Cell Biology* (2013). doi:10.1038/nrm3567
23. Kruiswijk, F., Labuschagne, C. F. & Vousden, K. H. P53 in survival, death and metabolic health: A lifeguard with a licence to kill. *Nature Reviews Molecular Cell Biology* (2015). doi:10.1038/nrm4007
24. Feng, G. S. Conflicting Roles of Molecules in Hepatocarcinogenesis: Paradigm or Paradox. *Cancer Cell* (2012). doi:10.1016/j.ccr.2012.01.001
25. Shojaee, S. *et al.* PTEN opposes negative selection and enables oncogenic transformation of pre-B cells. *Nat. Med.* (2016). doi:10.1038/nm.4062
26. Lou, X., Zhang, J., Liu, S., Lou, X. & Liao, D. J. The other side of the coin: The tumor-suppressive aspect of oncogenes and the oncogenic aspect of tumor-suppressive genes, such as those along the CCND–CDK4/6–RB axis. *Cell Cycle* (2014). doi:10.4161/cc.29082
27. Fulda, S., Gorman, A. M., Hori, O. & Samali, A. Cellular stress responses: Cell survival and cell death. *International Journal of Cell Biology* (2010). doi:10.1155/2010/214074
28. Sancar, A. *et al.* MOLECULAR MECHANISMS OF MAMMALIAN DNA REPAIR AND THE DNA DAMAGE CHECKPOINTS. *Annu. Rev. Biochem.* (2004). doi:10.1146/annurev.biochem.73.011303.073723
29. Hoeijmakers, J. H. J. Genome maintenance mechanisms for preventing cancer. *Nature* (2001). doi:10.1038/35077232
30. Kraemer, K. H., Lee, M. M., Andrews, A. D. & Lambert, W. C. The Role of Sunlight and DNA Repair in Melanoma and Nonmelanoma Skin Cancer: The Xeroderma Pigmentosum Paradigm. *Arch. Dermatol.* (1994). doi:10.1001/archderm.1994.01690080084012
31. Ciccia, A. & Elledge, S. J. The DNA Damage Response: Making It Safe to Play with Knives. *Molecular Cell* (2010). doi:10.1016/j.molcel.2010.09.019
32. Torgovnick, A. & Schumacher, B. DNA repair mechanisms in cancer development and therapy. *Frontiers in Genetics* (2015). doi:10.3389/fgene.2015.00157
33. Kelley, M. R., Logsdon, D. & Fishel, M. L. Targeting DNA repair pathways for cancer treatment: What's new? *Future Oncology* (2014). doi:10.2217/fon.14.60
34. O'Connor, M. J. Targeting the DNA Damage Response in Cancer. *Molecular Cell* (2015). doi:10.1016/j.molcel.2015.10.040
35. O'Neil, N. J., Bailey, M. L. & Hieter, P. Synthetic lethality and cancer. *Nature Reviews Genetics* (2017). doi:10.1038/nrg.2017.47
36. Hung, R. J., Hall, J., Brennan, P. & Boffetta, P. Genetic polymorphisms in the base excision repair pathway and cancer risk: A huge review. *Am. J. Epidemiol.* (2005). doi:10.1093/aje/kwi318
37. Goode, E. L., Ulrich, C. M. & Potter, J. D. Polymorphisms in DNA repair genes and associations with cancer risk. *Cancer Epidemiol. Biomarkers Prev.* (2002). doi:Published December 2002
38. Srivastava, M. & Raghavan, S. C. DNA double-strand break repair inhibitors as cancer therapeutics. *Chemistry and Biology* (2015). doi:10.1016/j.chembiol.2014.11.013
39. Curtin, N. J. DNA repair dysregulation from cancer driver to therapeutic target. *Nature Reviews Cancer* (2012). doi:10.1038/nrc3399
40. Green, D. R. & Evan, G. I. A matter of life and death. *Cancer Cell* (2002).

doi:10.1016/S1535-6108(02)00024-7
41. Lopez, J. & Tait, S. W. G. Mitochondrial apoptosis: Killing cancer using the enemy within. *British Journal of Cancer* (2015). doi:10.1038/bjc.2015.85
42. Redza-Dutordoir, M. & Averill-Bates, D. A. Activation of apoptosis signalling pathways by reactive oxygen species. *Biochim. Biophys. Acta - Mol. Cell Res.* (2016). doi:10.1016/j.bbamcr.2016.09.012
43. Koff, J. L., Ramachandiran, S. & Bernal-Mizrachi, L. A time to kill: Targeting apoptosis in cancer. *International Journal of Molecular Sciences* (2015). doi:10.3390/ijms16022942
44. Juin, P., Geneste, O., Gautier, F., Depil, S. & Campone, M. Decoding and unlocking the BCL-2 dependency of cancer cells. *Nature Reviews Cancer* (2013). doi:10.1038/nrc3538
45. Choi, S. *et al.* Bcl-xL promotes metastasis independent of its anti-apoptotic activity. *Nat. Commun.* (2016). doi:10.1038/ncomms10384
46. Fortunato, A. *et al.* Natural selection in cancer biology: From molecular snowflakes to trait hallmarks. *Cold Spring Harb. Perspect. Med.* (2017). doi:10.1101/cshperspect.a029652
47. Lee, J., Giordano, S. & Zhang, J. Autophagy, mitochondria and oxidative stress: cross-talk and redox signalling. *Biochem J* (2012). doi:10.1042/bj20111451
48. Gozuacik, D. & Kimchi, A. Autophagy as a cell death and tumor suppressor mechanism. *Oncogene* (2004). doi:10.1038/sj.onc.1207521
49. Keulers, T. G., Schaaf, M. B. E. & Rouschop, K. M. A. Autophagy-Dependent Secretion: Contribution to Tumor Progression. *Front. Oncol.* (2016). doi:10.3389/fonc.2016.00251
50. Galluzzi, L. *et al.* Autophagy in malignant transformation and cancer progression. *EMBO J.* (2015). doi:10.15252/embj.201490784
51. Edinger, A. L. & Thompson, C. B. Defective autophagy leads to cancer. *Cancer Cell* (2003). doi:10.1016/S1535-6108(03)00306-4
52. Qu, X. *et al.* Promotion of tumorigenesis by heterozygous disruption of the beclin 1 autophagy gene. *J. Clin. Invest.* (2003). doi:10.1172/JCI20039
53. White, E. Deconvoluting the context-dependent role for autophagy in cancer. *Nature Reviews Cancer* (2012). doi:10.1038/nrc3262
54. Ozpolat, B. & Benbrook, D. M. Targeting autophagy in cancer management - strategies and developments. *Cancer Manag. Res.* (2015). doi:10.2147/CMAR.S34859
55. Yin, Z., Pascual, C. & Klionsky, D. Autophagy: machinery and regulation. *Microb. Cell* (2016). doi:10.15698/mic2016.12.546
56. Mowers, E. E., Sharifi, M. N. & Macleod, K. F. Autophagy in cancer metastasis. *Oncogene* (2017). doi:10.1038/onc.2016.333
57. Campisi, J. Aging, Cellular Senescence, and Cancer. *Annu. Rev. Physiol.* (2013). doi:10.1146/annurev-physiol-030212-183653
58. Bernadotte, A., Mikhelson, V. M. & Spivak, I. M. Markers of cellular senescence. Telomere shortening as a marker of cellular senescence. *Aging (Albany. NY).* (2016). doi:10.18632/aging.100871
59. Martínez, P. & Blasco, M. A. Telomeric and extra-telomeric roles for telomerase and the telomere-binding proteins. *Nature Reviews Cancer* (2011). doi:10.1038/nrc3025
60. Pérez-Mancera, P. A., Young, A. R. J. & Narita, M. Inside and out: The activities of senescence in cancer. *Nature Reviews Cancer* (2014). doi:10.1038/nrc3773
61. Jafri, M. A., Ansari, S. A., Alqahtani, M. H. & Shay, J. W. Roles of telomeres and telomerase in cancer, and advances in telomerase-targeted therapies. *Genome*

Medicine (2016). doi:10.1186/s13073-016-0324-x
62. Shay, J. W. & Wright, W. E. Role of telomeres and telomerase in cancer. *Seminars in Cancer Biology* (2011). doi:10.1016/j.semcancer.2011.10.001
63. Günes, C. & Rudolph, K. L. The role of telomeres in stem cells and cancer. *Cell* (2013). doi:10.1016/j.cell.2013.01.010
64. Ben-Porath, I. & Weinberg, R. A. When cells get stressed: An integrative view of cellular senescence. *Journal of Clinical Investigation* (2004). doi:10.1172/JCI200420663
65. Naylor, R. M., Baker, D. J. & Van Deursen, J. M. Senescent cells: A novel therapeutic target for aging and age-related diseases. *Clin. Pharmacol. Ther.* (2013). doi:10.1038/clpt.2012.193
66. He, S. & Sharpless, N. E. Senescence in Health and Disease. *Cell* (2017). doi:10.1016/j.cell.2017.05.015
67. Coppé, J.-P., Desprez, P.-Y., Krtolica, A. & Campisi, J. The Senescence-Associated Secretory Phenotype: The Dark Side of Tumor Suppression. *Annu. Rev. Pathol. Mech. Dis.* (2010). doi:10.1146/annurev-pathol-121808-102144
68. Tchkonia, T., Zhu, Y., van Jan, D., Campisi, J. & Kirkland, L. Cellular senescence and the senescent secretory phenotype: therapeutic opportunities. *J. Clin. Invest.* (2013). doi:10.1172/JCI64098
69. Jiang, W. G. *et al.* Tissue invasion and metastasis: Molecular, biological and clinical perspectives. *Seminars in Cancer Biology* (2015). doi:10.1016/j.semcancer.2015.03.008
70. Pickup, M. W., Mouw, J. K. & Weaver, V. M. The extracellular matrix modulates the hallmarks of cancer. *EMBO Rep.* (2014). doi:10.15252/embr.201439246
71. Micalizzi, D. S., Maheswaran, S. & Haber, D. A. A conduit to metastasis: circulating tumor cell biology. *Genes Dev.* (2017). doi:10.1101/gad.305805.117
72. Massagué, J. & Obenauf, A. C. Metastatic colonization by circulating tumour cells. *Nature* (2016). doi:10.1038/nature17038
73. Valastyan, S. & Weinberg, R. A. Tumor metastasis: Molecular insights and evolving paradigms. *Cell* (2011). doi:10.1016/j.cell.2011.09.024
74. Cheung, K. J. & Ewald, A. J. A collective route to metastasis: Seeding by tumor cell clusters. *Science* (2016). doi:10.1126/science.aaf6546
75. Clark, A. G. & Vignjevic, D. M. Modes of cancer cell invasion and the role of the microenvironment. *Current Opinion in Cell Biology* (2015). doi:10.1016/j.ceb.2015.06.004
76. Ye, X. & Weinberg, R. A. Epithelial-Mesenchymal Plasticity: A Central Regulator of Cancer Progression. *Trends in Cell Biology* (2015). doi:10.1016/j.tcb.2015.07.012
77. Kalluri, R. & Weinberg, R. A. The basics of epithelial-mesenchymal transition. *Journal of Clinical Investigation* (2009). doi:10.1172/JCI39104
78. Nieto, M. A., Huang, R. Y. Y. J., Jackson, R. A. A. & Thiery, J. P. P. EMT: 2016. *Cell* (2016). doi:10.1016/j.cell.2016.06.028
79. Craene, B. De & Berx, G. Regulatory networks defining EMT during cancer initiation and progression. *Nature Reviews Cancer* (2013). doi:10.1038/nrc3447
80. Rankin, E. B. & Giaccia, A. J. Hypoxic control of metastasis. *Science* (2016). doi:10.1126/science.aaf4405
81. Lamouille, S., Xu, J. & Derynck, R. Molecular mechanisms of epithelial-mesenchymal transition. *Nature Reviews Molecular Cell Biology* (2014). doi:10.1038/nrm3758
82. Diepenbruck, M. & Christofori, G. Epithelial-mesenchymal transition (EMT) and metastasis: Yes, no, maybe? *Current Opinion in Cell Biology* (2016).

doi:10.1016/j.ceb.2016.06.002
83. Fischer, K. R. *et al.* Epithelial-to-mesenchymal transition is not required for lung metastasis but contributes to chemoresistance. *Nature* (2015). doi:10.1038/nature15748
84. Zheng, X. *et al.* Epithelial-to-mesenchymal transition is dispensable for metastasis but induces chemoresistance in pancreatic cancer. *Nature* (2015). doi:10.1038/nature16064
85. Li, W. & Kang, Y. Probing the Fifty Shades of EMT in Metastasis. *Trends in Cancer* (2016). doi:10.1016/j.trecan.2016.01.001
86. Curran, S. & Murray, G. I. Matrix metalloproteinasesmolecular aspects of their roles in tumour invasion and metastasis. *European Journal of Cancer* (2000). doi:10.1016/S0959-8049(00)00156-8
87. Kessenbrock, K., Plaks, V. & Werb, Z. Matrix Metalloproteinases: Regulators of the Tumor Microenvironment. *Cell* (2010). doi:10.1016/j.cell.2010.03.015
88. Shuman Moss, L. A., Jensen-Taubman, S. & Stetler-Stevenson, W. G. Matrix metalloproteinases: changing roles in tumor progression and metastasis. *Am. J. Pathol.* (2012). doi:10.1016/j.ajpath.2012.08.044
89. Hadler-Olsen, E., Winberg, J. O. & Uhlin-Hansen, L. Matrix metalloproteinases in cancer: Their value as diagnostic and prognostic markers and therapeutic targets. *Tumor Biology* (2013). doi:10.1007/s13277-013-0842-8
90. Bockhorn, M., Jain, R. K. & Munn, L. L. Active versus passive mechanisms in metastasis: do cancer cells crawl into vessels, or are they pushed? *Lancet Oncol.* (2007). doi:10.1016/S1470-2045(07)70140-7
91. Reymond, N., D'Água, B. B. & Ridley, A. J. Crossing the endothelial barrier during metastasis. *Nature Reviews Cancer* (2013). doi:10.1038/nrc3628
92. Zervantonakis, I. K. *et al.* Three-dimensional microfluidic model for tumor cell intravasation and endothelial barrier function. *Proc. Natl. Acad. Sci.* (2012). doi:10.1073/pnas.1210182109
93. Alix-Panabières, C. & Pantel, K. Clinical applications of circulating tumor cells and circulating tumor DNA as liquid biopsy. *Cancer Discovery* (2016). doi:10.1158/2159-8290.CD-15-1483
94. Stegner, D., Dütting, S. & Nieswandt, B. Mechanistic explanation for platelet contribution to cancer metastasis. *Thromb. Res.* (2014). doi:10.1016/S0049-3848(14)50025-4
95. Zhang, C., Guan, Y., Sun, Y., Ai, D. & Guo, Q. Tumor heterogeneity and circulating tumor cells. *Cancer Letters* (2016). doi:10.1016/j.canlet.2016.02.024
96. Lorusso, G. & Rüegg, C. New insights into the mechanisms of organ-specific breast cancer metastasis. *Seminars in Cancer Biology* (2012). doi:10.1016/j.semcancer.2012.03.007
97. Friedl, P. & Alexander, S. Cancer invasion and the microenvironment: Plasticity and reciprocity. *Cell* (2011). doi:10.1016/j.cell.2011.11.016
98. Langley, R. R. & Fidler, I. J. The seed and soil hypothesis revisited-The role of tumor-stroma interactions in metastasis to different organs. *Int. J. Cancer* (2011). doi:10.1002/ijc.26031
99. Nguyen, D. X. & Massagué, J. Genetic determinants of cancer metastasis. *Nature Reviews Genetics* (2007). doi:10.1038/nrg2101
100. Croucher, P. I., McDonald, M. M. & Martin, T. J. Bone metastasis: The importance of the neighbourhood. *Nature Reviews Cancer* (2016). doi:10.1038/nrc.2016.44
101. Lu, X. & Kang, Y. Organotropism of breast cancer metastasis. *J. Mammary Gland Biol. Neoplasia* (2007). doi:10.1007/s10911-007-9047-3

102. Psaila, B., Kaplan, R. N., Port, E. R. & Lyden, D. Priming the 'soil' for breast cancer metastasis: the pre-metastatic niche. *Breast Dis.* (2007). doi:10.3233/BD-2007-26106
103. Peinado, H., Lavotshkin, S. & Lyden, D. The secreted factors responsible for pre-metastatic niche formation: Old sayings and new thoughts. *Seminars in Cancer Biology* (2011). doi:10.1016/j.semcancer.2011.01.002
104. Sceneay, J., Smyth, M. J. & Möller, A. The pre-metastatic niche: Finding common ground. *Cancer and Metastasis Reviews* (2013). doi:10.1007/s10555-013-9420-1
105. Peinado, H. *et al.* Melanoma exosomes educate bone marrow progenitor cells toward a pro-metastatic phenotype through MET. *Nat. Med.* (2012). doi:10.1038/nm.2753
106. Costa-Silva, B. *et al.* Pancreatic cancer exosomes initiate pre-metastatic niche formation in the liver. *Nat. Cell Biol.* (2015). doi:10.1038/ncb3169
107. Giancotti, F. G. XMechanisms governing metastatic dormancy and reactivation. *Cell* (2013). doi:10.1016/j.cell.2013.10.029
108. Sosa, M. S., Bragado, P. & Aguirre-Ghiso, J. A. Mechanisms of disseminated cancer cell dormancy: An awakening field. *Nature Reviews Cancer* (2014). doi:10.1038/nrc3793
109. Celià-terrassa, T. & Kang, Y. Distinctive properties of metastasis- initiating cells. *Genes Dev.* (2016). doi:10.1101/gad.277681.116.892
110. Cairns, R. A. & Mak, T. W. The current state of cancer metabolism. *Nature Reviews Cancer* (2016). doi:10.1038/nrc.2016.100
111. Pavlova, N. N. & Thompson, C. B. The Emerging Hallmarks of Cancer Metabolism. *Cell Metabolism* (2016). doi:10.1016/j.cmet.2015.12.006
112. Altman, B. J., Stine, Z. E. & Dang, C. V. From Krebs to clinic: Glutamine metabolism to cancer therapy. *Nature Reviews Cancer* (2016). doi:10.1038/nrc.2016.71
113. Deberardinis, R. J. & Cheng, T. Q's next: The diverse functions of glutamine in metabolism, cell biology and cancer. *Oncogene* (2010). doi:10.1038/onc.2009.358
114. Otto Warburg, B., Wind, F. & Negelein, N. THE METABOLISM OF TUMORS IN THE BODY. The Journal of General Physiology. *Biochem. Z. Biochem. Z. Biochem. Z.. Biol. Chem* (1923). doi:10.1097/00000441-193107000-00022
115. Cairns, R., Harris, I. & Mak, T. Regulation of cancer cell metabolism. *Nat. Rev. Cancer* (2011). doi:10.1038/nrc2981
116. Szablewski, L. Expression of glucose transporters in cancers. *Biochim. Biophys. Acta - Rev. Cancer* (2013). doi:10.1016/j.bbcan.2012.12.004
117. Younes, M., Juarez, D., Lechago, L. V & Lerner, S. P. Glut 1 expression in transitional cell carcinoma of the urinary bladder is associated with poor patient survival. *Anticancer Res* (2001).
118. Cho, H., Lee, Y. S., Kim, J., Chung, J. Y. & Kim, J. H. Overexpression of glucose transporter-1 (GLUT-1) predicts poor prognosis in epithelial ovarian cancer. *Cancer Invest.* (2013). doi:10.3109/07357907.2013.849722
119. Hay, N. Reprogramming glucose metabolism in cancer: Can it be exploited for cancer therapy? *Nature Reviews Cancer* (2016). doi:10.1038/nrc.2016.77
120. Mathupala, S. P., Ko, Y. H. & Pedersen, P. L. The pivotal roles of mitochondria in cancer: Warburg and beyond and encouraging prospects for effective therapies. *Biochimica et Biophysica Acta - Bioenergetics* (2010). doi:10.1016/j.bbabio.2010.03.025
121. Fruman, D. A. *et al.* The PI3K Pathway in Human Disease. *Cell* (2017). doi:10.1016/j.cell.2017.07.029
122. Reynolds, M. R. *et al.* Control of glutamine metabolism by the tumor suppressor Rb. *Oncogene* (2014). doi:10.1038/onc.2012.635

123. Ward, P. S. & Thompson, C. B. Signaling in control of cell growth and metabolism. *Cold Spring Harb. Perspect. Biol.* (2012). doi:10.1101/cshperspect.a006783
124. Röhrig, F. & Schulze, A. The multifaceted roles of fatty acid synthesis in cancer. *Nature Reviews Cancer* (2016). doi:10.1038/nrc.2016.89
125. Yang, M. & Vousden, K. H. Serine and one-carbon metabolism in cancer. *Nature Reviews Cancer* (2016). doi:10.1038/nrc.2016.81
126. Schug, Z. T., Vande Voorde, J. & Gottlieb, E. The metabolic fate of acetate in cancer. *Nature Reviews Cancer* (2016). doi:10.1038/nrc.2016.87
127. Vyas, S., Zaganjor, E. & Haigis, M. C. Mitochondria and Cancer. *Cell* (2016). doi:10.1016/j.cell.2016.07.002
128. De Berardinis, R. J. & Chandel, N. S. Fundamentals of cancer metabolism. *Science Advances* (2016). doi:10.1126/sciadv.1600200
129. Iqbal, M. A., Gupta, V., Gopinath, P., Mazurek, S. & Bamezai, R. N. K. Pyruvate kinase M2 and cancer: An updated assessment. *FEBS Letters* (2014). doi:10.1016/j.febslet.2014.04.011
130. Yang, W. & Lu, Z. Regulation and function of pyruvate kinase M2 in cancer. *Cancer Letters* (2013). doi:10.1016/j.canlet.2013.06.008
131. Sabharwal, S. S. & Schumacker, P. T. Mitochondrial ROS in cancer: Initiators, amplifiers or an Achilles' heel? *Nature Reviews Cancer* (2014). doi:10.1038/nrc3803
132. Vander Heiden, M. G. & DeBerardinis, R. J. Understanding the Intersections between Metabolism and Cancer Biology. *Cell* (2017). doi:10.1016/j.cell.2016.12.039
133. Her, Y. F. & Maher, L. J. Succinate dehydrogenase loss in familial paraganglioma: Biochemistry, genetics, and epigenetics. *International Journal of Endocrinology* (2015). doi:10.1155/2015/296167
134. Gentric, G., Mieulet, V. & Mechta-Grigoriou, F. Heterogeneity in Cancer Metabolism: New Concepts in an Old Field. *Antioxid. Redox Signal.* (2017). doi:10.1089/ars.2016.6750
135. Sullivan, L. B., Gui, D. Y. & Van Der Heiden, M. G. Altered metabolite levels in cancer: Implications for tumour biology and cancer therapy. *Nature Reviews Cancer* (2016). doi:10.1038/nrc.2016.85
136. Lu, C. *et al.* IDH mutation impairs histone demethylation and results in a block to cell differentiation. *Nature* (2012). doi:10.1038/nature10860
137. Terunuma, A. *et al.* MYC-driven accumulation of 2-hydroxyglutarate is associated with breast cancer prognosis. *J. Clin. Invest.* (2014). doi:10.1172/JCI71180
138. Lu, P., Weaver, V. M. & Werb, Z. The extracellular matrix: A dynamic niche in cancer progression. *Journal of Cell Biology* (2012). doi:10.1083/jcb.201102147
139. Bhowmick, N. A., Neilson, E. G. & Moses, H. L. Stromal fibroblasts in cancer initiation and progression. *Nature* (2004). doi:10.1038/nature03096
140. Bhowmick, N. A. *et al.* TGF-β Signaling in Fibroblasts Modulates the Oncogenic Potential of Adjacent Epithelia. *Science (80-.).* (2004). doi:10.1126/science.1090922
141. Trimboli, A. J. *et al.* Pten in stromal fibroblasts suppresses mammary epithelial tumours. *Nature* (2009). doi:10.1038/nature08486
142. Hill, R., Song, Y., Cardiff, R. D. & Van Dyke, T. Selective evolution of stromal mesenchyme with p53 loss in response to epithelial tumorigenesis. *Cell* (2005). doi:10.1016/j.cell.2005.09.030
143. Franco, O. E., Shaw, A. K., Strand, D. W. & Hayward, S. W. Cancer associated fibroblasts in cancer pathogenesis. *Seminars in Cell and Developmental Biology* (2010). doi:10.1016/j.semcdb.2009.10.010
144. Quail, D. F. & Joyce, J. A. Microenvironmental regulation of tumor progression and metastasis. *Nat Med* (2013). doi:10.1038/nm.3394

145. Raaijmakers, M. H. G. P. Myelodysplastic syndromes: Revisiting the role of the bone marrow microenvironment in disease pathogenesis. in *International Journal of Hematology* (2012). doi:10.1007/s12185-011-1001-x
146. Wiseman, D. H. Donor Cell Leukemia: A Review. *Biology of Blood and Marrow Transplantation* (2011). doi:10.1016/j.bbmt.2010.10.010
147. Heindl, A., Nawaz, S. & Yuan, Y. Mapping spatial heterogeneity in the tumor microenvironment: a new era for digital pathology. *Lab. Invest.* (2015). doi:10.1038/labinvest.2014.155
148. Zhou, Z. & Lu, Z. R. Molecular imaging of the tumor microenvironment. *Advanced Drug Delivery Reviews* (2017). doi:10.1016/j.addr.2016.07.012
149. Anderberg, C. & Pietras, K. On the origin of cancer-associated fibroblasts. *Cell Cycle* (2009). doi:10.4161/cc.8.10.8557
150. Meacham, C. E. & Morrison, S. J. Tumour heterogeneity and cancer cell plasticity. *Nature* (2013). doi:10.1038/nature12624
151. Zhang, J. *et al.* Identification of the haematopoietic stem cell niche and control of the niche size. *Nature* (2003). doi:10.1038/nature02041
152. Walkley, C. R. *et al.* A Microenvironment-Induced Myeloproliferative Syndrome Caused by Retinoic Acid Receptor γ Deficiency. *Cell* (2007). doi:10.1016/j.cell.2007.05.014
153. Aanei, C. M. *et al.* Intrinsic Growth Deficiencies of Mesenchymal Stromal Cells in Myelodysplastic Syndromes. *Stem Cells Dev.* (2012). doi:10.1089/scd.2011.0390
154. Poitz, D. M. *et al.* Regulation of the Hif-system by micro-RNA 17 and 20a - Role during monocyte-to-macrophage differentiation. *Mol. Immunol.* (2013). doi:10.1016/j.molimm.2013.06.014
155. Chang, C. H. *et al.* Metabolic Competition in the Tumor Microenvironment Is a Driver of Cancer Progression. *Cell* (2015). doi:10.1016/j.cell.2015.08.016
156. Sundstrom, A., Bar-Sagi, D. & Mishra, B. Simulating heterogeneous tumor cell populations. *PLoS One* (2016). doi:10.1371/journal.pone.0168984
157. Tabassum, D. P. & Polyak, K. Tumorigenesis: It takes a village. *Nature Reviews Cancer* (2015). doi:10.1038/nrc3971
158. Junttila, M. R. & De Sauvage, F. J. Influence of tumour micro-environment heterogeneity on therapeutic response. *Nature* (2013). doi:10.1038/nature12626
159. Burnet, M. Cancer--A Biological Approach: I. The Processes Of Control. II. The Significance of Somatic Mutation. *BMJ* (1957). doi:10.1136/bmj.1.5022.779
160. Marin-Acevedo, J. A. *et al.* Next generation of immune checkpoint therapy in cancer: New developments and challenges. *Journal of Hematology and Oncology* (2018). doi:10.1186/s13045-018-0582-8
161. Ribatti, D. The concept of immune surveillance against tumors. The first theories. *Oncotarget* (2015). doi:10.18632/oncotarget.12739
162. Mittal, D., Gubin, M. M., Schreiber, R. D. & Smyth, M. J. New insights into cancer immunoediting and its three component phases-elimination, equilibrium and escape. *Current Opinion in Immunology* (2014). doi:10.1016/j.coi.2014.01.004
163. Dunn, G. P., Bruce, A. T., Ikeda, H., Old, L. J. & Schreiber, R. D. Cancer immunoediting: From immunosurveillance to tumor escape. *Nature Immunology* (2002). doi:10.1038/ni1102-991
164. Greaves, M. Nothing in cancer makes sense except. *BMC Biology* (2018). doi:10.1186/s12915-018-0493-8
165. Malmberg, K. J. Effective immunotherapy against cancer: A question of overcoming immune suppression and immune escape? in *Cancer Immunology, Immunotherapy* (2004). doi:10.1007/s00262-004-0577-x

166. Rodríguez, J. A. HLA-mediated tumor escape mechanisms that may impair immunotherapy clinical outcomes via T-cell activation (Review). *Oncology Letters* (2017). doi:10.3892/ol.2017.6784
167. Welte, T. *et al.* Oncogenic mTOR signalling recruits myeloid-derived suppressor cells to promote tumour initiation. *Nat. Cell Biol.* (2016). doi:10.1038/ncb3355
168. Jin, P. *et al.* Interferon-γ and Tumor Necrosis Factor-α Polarize Bone Marrow Stromal Cells Uniformly to a Th1 Phenotype. *Sci. Rep.* (2016). doi:10.1038/srep26345
169. Buck, M. D. D. *et al.* Mitochondrial Dynamics Controls T Cell Fate through Metabolic Programming. *Cell* (2016). doi:10.1016/j.cell.2016.05.035
170. Zitvogel, L., Ayyoub, M., Routy, B. & Kroemer, G. Microbiome and Anticancer Immunosurveillance. *Cell* (2016). doi:10.1016/j.cell.2016.03.001
171. Donnem, T. *et al.* Non-angiogenic tumours and their influence on cancer biology. *Nat. Rev. Cancer* (2018). doi:10.1038/nrc.2018.14
172. Carmeliet, P. Angiogenesis in life, disease and medicine. *Nature* (2005). doi:10.1038/nature04478
173. Folkman, J. Tumor angiogenesis: therapeutic implications. *N. Engl. J. Med.* (1971). doi:10.1056/NEJM197111182852108
174. Welti, J., Loges, S., Dimmeler, S. & Carmeliet, P. Recent molecular discoveries in angiogenesis and antiangiogenic therapies in cancer. *Journal of Clinical Investigation* (2013). doi:10.1172/JCI70212
175. Ribatti, D., Nico, B. & Crivellato, E. The development of the vascular system: a historical overview. *Methods Mol. Biol.* (2015). doi:10.1007/978-1-4939-1462-3_1
176. Wicki, A. & Christofori, G. The angiogenic switch in tumorigenesis. in *Tumor Angiogenesis: Basic Mechanisms and Cancer Therapy* (2008). doi:10.1007/978-3-540-33177-3_4
177. Carmeliet, P. & Jain, R. K. Angiogenesis in cancer and other diseases. *Nature* (2000). doi:10.1038/35025220
178. Favaro, E., Lord, S., Harris, A. L. & Buffa, F. M. Gene expression and hypoxia in breast cancer. *Genome Medicine* (2011). doi:10.1186/gm271
179. Hashimoto, T. & Shibasaki, F. Hypoxia-Inducible Factor as an Angiogenic Master Switch. *Front. Pediatr.* (2015). doi:10.3389/fped.2015.00033
180. Fraisl, P., Mazzone, M., Schmidt, T. & Carmeliet, P. Regulation of Angiogenesis by Oxygen and Metabolism. *Developmental Cell* (2009). doi:10.1016/j.devcel.2009.01.003
181. Petrovic, P. Targeting angiogenesis in cancer treatments: Where do we stand? *J. Pharm. Pharm. Sci.* (2016). doi:10.18433/J30033
182. Ferrara, N., Gerber, H. P. & LeCouter, J. The biology of VEGF and its receptors. *Nature Medicine* (2003). doi:10.1038/nm0603-669
183. Sakurai, T. & Kudo, M. Signaling pathways governing tumor angiogenesis. *Oncology* (2011). doi:10.1159/000333256
184. Hicklin, D. J. & Ellis, L. M. Role of the vascular endothelial growth factor pathway in tumor growth and angiogenesis. *J. Clin. Oncol.* (2005). doi:10.1200/JCO.2005.06.081
185. Folkman, J. Role of angiogenesis in tumor growth and metastasis. *Semin. Oncol.* (2002). doi:10.1053/sonc.2002.37263
186. Cao, Y. *et al.* Forty-year journey of angiogenesis translational research. *Science Translational Medicine* (2011). doi:10.1126/scitranslmed.3003149
187. Perren, T. J. *et al.* A phase 3 trial of bevacizumab in ovarian cancer. *N. Engl. J. Med.* (2011). doi:10.1056/NEJMoa1103799
188. Cao, Y. & Langer, R. Optimizing the delivery of cancer drugs that block

angiogenesis. *Science Translational Medicine* (2010). doi:10.1126/scitranslmed.3000399
189. Miller, K. *et al.* Paclitaxel plus bevacizumab versus paclitaxel alone for metastatic breast cancer. *N. Engl. J. Med.* (2007). doi:10.1056/NEJMoa072113
190. Hurwitz, H. *et al.* Bevacizumab plus irinotecan, fluorouracil, and leucovorin for metastatic colorectal cancer. *N. Engl. J. Med.* (2004). doi:10.1056/NEJMoa032691
191. Cao, Y. VEGF-targeted cancer therapeutics—paradoxical effects in endocrine organs. *Nat. Rev. Endocrinol.* (2014). doi:10.1038/nrendo.2014.114
192. Cao, Y. Future options of anti-angiogenic cancer therapy. *Chinese Journal of Cancer* (2016). doi:10.1186/s40880-016-0084-4
193. Cao, Y. Off-tumor target—beneficial site for antiangiogenic cancer therapy? *Nat. Rev. Clin. Oncol.* (2010). doi:10.1038/nrclinonc.2010.118
194. Fidler, I. J. *Cancer metastasis*. *Br Med Bull* (1991). doi:https://doi.org/10.1016/0749-2081(92)90007-P
195. Lee, S. L. C. *et al.* Hypoxia-induced pathological angiogenesis mediates tumor cell dissemination, invasion, and metastasis in a zebrafish tumor model. *Proc. Natl. Acad. Sci.* (2009). doi:10.1073/pnas.0909228106
196. Rouhi, P. *et al.* Hypoxia-induced metastasis model in embryonic zebrafish. *Nat. Protoc.* (2010). doi:10.1038/nprot.2010.150
197. Stacker, S. A. *et al.* Lymphangiogenesis and lymphatic vessel remodelling in cancer. *Nature Reviews Cancer* (2014). doi:10.1038/nrc3677
198. Giuliani, N., Storti, P., Bolzoni, M., Palma, B. D. & Bonomini, S. Angiogenesis and multiple myeloma. *Cancer Microenvironment* (2011). doi:10.1007/s12307-011-0072-9
199. Kerbel, R. S. *et al.* Preclinical recapitulation of antiangiogenic drug clinical efficacies using models of early or late stage breast cancer metastatis. *Breast* (2013). doi:10.1016/j.breast.2013.07.011
200. Tannock, I. F. *et al.* Aflibercept versus placebo in combination with docetaxel and prednisone for treatment of men with metastatic castration-resistant prostate cancer (VENICE): A phase 3, double-blind randomised trial. *Lancet Oncol.* (2013). doi:10.1016/S1470-2045(13)70184-0
201. Garon, E. B. *et al.* Ramucirumab plus docetaxel versus placebo plus docetaxel for second-line treatment of stage IV non-small-cell lung cancer after disease progression on platinum-based therapy (REVEL): A multicentre, double-blind, randomised phase 3 trial. *Lancet* (2014). doi:10.1016/S0140-6736(14)60845-X
202. Cao, Y., Zhong, W. & Sun, Y. Improvement of antiangiogenic cancer therapy by understanding the mechanisms of angiogenic factor interplay and drug resistance. *Seminars in Cancer Biology* (2009). doi:10.1016/j.semcancer.2009.05.001
203. Motzer, R. J., Hutson, T. E., McCann, L., Deen, K. & Choueiri, T. K. Overall Survival in Renal-Cell Carcinoma with Pazopanib versus Sunitinib. *N. Engl. J. Med.* (2014). doi:10.1056/NEJMc1400731
204. Folkman, J. What is the evidence that tumors are angiogenesis dependent? *Journal of the National Cancer Institute* (1990). doi:10.1093/jnci/82.1.4
205. Pezzella, F. *et al.* Non-small-cell lung carcinoma tumor growth without morphological evidence of neo-angiogenesis. *Am.J.Pathol.* (1997).
206. Offersen, B. V., Pfeiffer, P., Hamilton-Dutoit, S. & Overgaard, J. Patterns of angiogenesis in nonsmall-cell lung carcinoma. *Cancer* (2001). doi:10.1002/1097-0142(20010415)91:8<1500::AID-CNCR1158>3.0.CO;2-M
207. Sardari Nia, P. *et al.* Different Growth Patterns of Non-Small Cell Lung Cancer Represent Distinct Biologic Subtypes. *Ann. Thorac. Surg.* (2008).

doi:10.1016/j.athoracsur.2007.08.054
208. Chuang, H.-Y., Lee, E., Liu, Y.-T., Lee, D. & Ideker, T. Network-based classification of breast cancer metastasis. *Mol. Syst. Biol.* (2007). doi:10.1038/msb4100180
209. Sardari Nia, P., Hendriks, J., Friedel, G., Van Schil, P. & Van Marck, E. Distinct angiogenic and non-angiogenic growth patterns of lung metastases from renal cell carcinoma. *Histopathology* (2007). doi:10.1111/j.1365-2559.2007.02800.x
210. Szabo, V. *et al.* Mechanism of tumour vascularization in experimental lung metastases. *J. Pathol.* (2015). doi:10.1002/path.4464
211. Bridgeman, V. L. *et al.* Vessel co-option is common in human lung metastases and mediates resistance to anti-angiogenic therapy in preclinical lung metastasis models. *J. Pathol.* (2017). doi:10.1002/path.4845
212. Zhao, C. *et al.* Distinct contributions of angiogenesis and vascular co-option during the initiation of primary microtumors and micrometastases. *Carcinogenesis* (2011). doi:10.1093/carcin/bgr076
213. Folkman, J. Angiogenesis in cancer, vascular, rheumatoid and other disease. *Nature Medicine* (1995). doi:10.1038/nm0195-27
214. Boehm, T., Folkman, J., Browder, T. & O'Reilly, M. S. Antiangiogenic therapy of experimental cancer does not induce acquired drug resistance. *Nature* (1997). doi:10.1038/37126
215. Ghosh, K. *et al.* Tumor-derived endothelial cells exhibit aberrant Rho-mediated mechanosensing and abnormal angiogenesis in vitro. *Proc. Natl. Acad. Sci.* (2008). doi:10.1073/pnas.0800835105
216. Casanovas, O., Hicklin, D. J., Bergers, G. & Hanahan, D. Drug resistance by evasion of antiangiogenic targeting of VEGF signaling in late-stage pancreatic islet tumors. *Cancer Cell* (2005). doi:10.1016/j.ccr.2005.09.005
217. Crawford, Y. *et al.* PDGF-C Mediates the Angiogenic and Tumorigenic Properties of Fibroblasts Associated with Tumors Refractory to Anti-VEGF Treatment. *Cancer Cell* (2009). doi:10.1016/j.ccr.2008.12.004
218. Blouw, B. *et al.* The hypoxic response of tumors is dependent on their microenvironment. *Cancer Cell* (2003). doi:10.1016/S1535-6108(03)00194-6
219. Yu, J. L., Rak, J. W., Coomber, B. L., Hicklin, D. J. & Kerbel, R. S. Effect of p53 status on tumor response to antiangiogenic therapy. *Science (80-.).* (2002). doi:10.1126/science.1068327
220. Farnsworth, R. H., Lackmann, M., Achen, M. G. & Stacker, S. A. Vascular remodeling in cancer. *Oncogene* (2014). doi:10.1038/onc.2013.304
221. Orimo, A. *et al.* Stromal fibroblasts present in invasive human breast carcinomas promote tumor growth and angiogenesis through elevated SDF-1/CXCL12 secretion. *Cell* (2005). doi:10.1016/j.cell.2005.02.034
222. Guo, W. & Giancotti, F. G. Integrin signalling during tumour progression. *Nature Reviews Molecular Cell Biology* (2004). doi:10.1038/nrm1490
223. Donnem, T. *et al.* Vessel co-option in primary human tumors and metastases: An obstacle to effective anti-angiogenic treatment? *Cancer Medicine* (2013). doi:10.1002/cam4.105
224. Rubenstein, J. L. *et al.* Anti-VEGF antibody treatment of glioblastoma prolongs survival but results in increased vascular cooption. *Neoplasia (New York, NY)* (2000). doi:10.1038/sj.neo.7900102
225. De Groot, J. F. *et al.* Tumor invasion after treatment of glioblastoma with bevacizumab: Radiographic and pathologic correlation in humans and mice. *Neuro. Oncol.* (2010). doi:10.1093/neuonc/nop027
226. Kuczynski, E. A. *et al.* Co-option of liver vessels and not sprouting angiogenesis

drives acquired sorafenib resistance in hepatocellular carcinoma. *J. Natl. Cancer Inst.* (2016). doi:10.1093/jnci/djw030
227. Jeong, H. S. *et al.* Investigation of the Lack of Angiogenesis in the Formation of Lymph Node Metastases. *J. Natl. Cancer Inst.* (2015). doi:10.1093/jnci/djv155
228. Frentzas, S. *et al.* Vessel co-option mediates resistance to anti-angiogenic therapy in liver metastases. *Nat. Med.* (2016). doi:10.1038/nm.4197
229. Küsters, B. *et al.* Vascular endothelial growth factor-A165 induces progression of melanoma brain metastases without induction of sprouting angiogenesis. *Cancer Res.* (2002).
230. Adighibe, O. *et al.* Why some tumours trigger neovascularisation and others don't: The story thus far. *Chin. J. Cancer* (2016). doi:10.1186/s40880-016-0082-6
231. Ribatti, D. & Djonov, V. Intussusceptive microvascular growth in tumors. *Cancer Letters* (2012). doi:10.1016/j.canlet.2011.10.040
232. Krishna Priya, S. *et al.* Tumour angiogenesis—Origin of blood vessels. *International Journal of Cancer* (2016). doi:10.1002/ijc.30067
233. Gianni-Barrera, R., Trani, M., Reginato, S. & Banfi, A. To sprout or to split? VEGF, Notch and vascular morphogenesis. *Biochem. Soc. Trans.* (2011). doi:10.1042/BST20110650
234. Kirschmann, D. A., Seftor, E. A., Hardy, K. M., Seftor, R. E. B. & Hendrix, M. J. C. Molecular Pathways: Vasculogenic Mimicry in Tumor Cells: Diagnostic and Therapeutic Implications. *Clin. Cancer Res.* (2012). doi:10.1158/1078-0432.CCR-11-3237
235. Yang, J. P. *et al.* Tumor vasculogenic mimicry predicts poor prognosis in cancer patients: a meta-analysis. *Angiogenesis* (2016). doi:10.1007/s10456-016-9500-2
236. Seftor, R. E. B. *et al.* Tumor cell vasculogenic mimicry: From controversy to therapeutic promise. *American Journal of Pathology* (2012). doi:10.1016/j.ajpath.2012.07.013
237. Hida, K., Maishi, N., Torii, C. & Hida, Y. Tumor angiogenesis—characteristics of tumor endothelial cells. *International Journal of Clinical Oncology* (2016). doi:10.1007/s10147-016-0957-1
238. Nia, P. S. *et al.* Prognostic value of nonangiogenic and angiogenic growth patterns in non-small-cell lung cancer. *Br. J. Cancer* (2004). doi:10.1038/sj.bjc.6602134
239. Trivella, M., Pezzella, F., Pastorino, U., Harris, A. L. & Altman, D. G. Microvessel density as a prognostic factor in non-small-cell lung carcinoma: a meta-analysis of individual patient data. *Lancet Oncol.* (2007). doi:10.1016/S1470-2045(07)70145-6
240. Passalidou, E. *et al.* Vascular phenotype in angiogenic and non-angiogenic lung non-small cell carcinomas. *Br. J. Cancer* (2002). doi:10.1038/sj.bjc.6600015
241. Hillen, F. & Griffioen, A. W. Tumour vascularization: Sprouting angiogenesis and beyond. *Cancer and Metastasis Reviews* (2007). doi:10.1007/s10555-007-9094-7
242. Jain, R. K. Antiangiogenesis Strategies Revisited: From Starving Tumors to Alleviating Hypoxia. *Cancer Cell* (2014). doi:10.1016/j.ccell.2014.10.006
243. Kazerounian, S., Yee, K. O. & Lawler, J. Thrombospondins in cancer. *Cell. Mol. Life Sci.* (2008). doi:10.1007/s00018-007-7486-z
244. Sakariassen, P. O. *et al.* Angiogenesis-independent tumor growth mediated by stem-like cancer cells. *Proc. Natl. Acad. Sci.* (2006). doi:10.1073/pnas.0607668103
245. Hu, J. *et al.* Gene expression signature for angiogenic and nonangiogenic non-small-cell lung cancer. *Oncogene* (2005). doi:10.1038/sj.onc.1208242
246. Lu, K. V. *et al.* VEGF Inhibits Tumor Cell Invasion and Mesenchymal Transition through a MET/VEGFR2 Complex. *Cancer Cell* (2012). doi:10.1016/j.ccr.2012.05.037

247. Sennino, B. *et al.* Suppression of tumor invasion and metastasis by concurrent inhibition of c-Met and VEGF signaling in pancreatic neuroendocrine tumors. *Cancer Discov.* (2012). doi:10.1158/2159-8290.CD-11-0240
248. Witsch, E., Sela, M. & Yarden, Y. Roles for Growth Factors in Cancer Progression. *Physiology* (2010). doi:10.1152/physiol.00045.2009
249. Dorai, T., Sawczuk, I., Pastorek, J., Wiernik, P. H. & Dutcher, J. P. Role of carbonic anhydrases in the progression of renal cell carcinoma subtypes: Proposal of a unified hypothesis. *Cancer Investigation* (2006). doi:10.1080/07357900601062321
250. Zhan, T., Rindtorff, N. & Boutros, M. Wnt signaling in cancer. *Oncogene* (2017). doi:10.1038/onc.2016.304
251. Wallez, Y., Vilgrain, I. & Huber, P. Angiogenesis: The VE-cadherin switch. *Trends in Cardiovascular Medicine* (2006). doi:10.1016/j.tcm.2005.11.008
252. Kienast, Y. *et al.* Real-time imaging reveals the single steps of brain metastasis formation. *Nat. Med.* (2010). doi:10.1038/nm.2072
253. Reymond, N. *et al.* Cdc42 promotes transendothelial migration of cancer cells through β1 integrin. *J. Cell Biol.* (2012). doi:10.1083/jcb.201205169
254. Auf, G. *et al.* Inositol-requiring enzyme 1 is a key regulator of angiogenesis and invasion in malignant glioma. *Proc. Natl. Acad. Sci.* (2010). doi:10.1073/pnas.0914072107
255. Goel, H. L. & Mercurio, A. M. VEGF targets the tumour cell. *Nature Reviews Cancer* (2013). doi:10.1038/nrc3627
256. Greenman, C. *et al.* Patterns of somatic mutation in human cancer genomes. *Nature* (2007). doi:10.1038/nature05610
257. Fidler, I. J. & Ellis, L. M. The implications of angiogenesis for the biology and therapy of cancer metastasis. *Cell* (1994). doi:10.1016/0092-8674(94)90187-2
258. Aalders, K. C., Tryfonidis, K., Senkus, E. & Cardoso, F. Anti-angiogenic treatment in breast cancer: Facts, successes, failures and future perspectives. *Cancer Treatment Reviews* (2017). doi:10.1016/j.ctrv.2016.12.009
259. Ferrara, N., Hillan, K. J., Gerber, H. P. & Novotny, W. Discovery and development of bevacizumab, an anti-VEGF antibody for treating cancer. *Nature Reviews Drug Discovery* (2004). doi:10.1038/nrd1381
260. Kerbel, R. S. Tumor angiogenesis. *N. Engl. J. Med.* (2008). doi:10.1056/NEJMra0706596
261. Comunanza, V. & Bussolino, F. Therapy for Cancer: Strategy of Combining Anti-Angiogenic and Target Therapies. *Front. Cell Dev. Biol.* (2017). doi:10.3389/fcell.2017.00101
262. Zhang, Y. *et al.* Function of the c-Met receptor tyrosine kinase in carcinogenesis and associated therapeutic opportunities. *Molecular Cancer* (2018). doi:10.1186/s12943-018-0796-y
263. Wilhelm, S. M. *et al.* BAY 43-9006 exhibits broad spectrum oral antitumor activity and targets the RAF/MEK/ERK pathway and receptor tyrosine kinases involved in tumor progression and angiogenesis. *Cancer Res.* (2004). doi:10.1158/0008-5472.CAN-04-1443
264. Beeram, M., Patnaik, A. & Rowinsky, E. K. Raf: A strategic target for therapeutic development against cancer. *Journal of Clinical Oncology* (2005). doi:10.1200/JCO.2005.08.036
265. Mendel, D. B. *et al.* In vivo antitumor activity of SU11248, a novel tyrosine kinase inhibitor targeting vascular endothelial growth factor and platelet-derived growth factor receptors: Determination of a pharmacokinetic/pharmacodynamic relationship. *Clin. Cancer Res.* (2003). doi:10.1158/1078-0432.ccr-08-1893

266. Aparicio-Gallego, G. *et al.* New Insights into Molecular Mechanisms of Sunitinib-Associated Side Effects. *Mol. Cancer Ther.* (2011). doi:10.1158/1535-7163.MCT-10-1124
267. Gotink, K. J. & Verheul, H. M. W. Anti-angiogenic tyrosine kinase inhibitors: What is their mechanism of action? *Angiogenesis* (2010). doi:10.1007/s10456-009-9160-6
268. Demetri, G. D. *et al.* Effi cacy and safety of regorafenib for advanced gastrointestinal stromal tumours after failure of imatinib and sunitinib (GRID): An international, multicentre, randomised, placebo-controlled, phase 3 trial. *Lancet* (2013). doi:10.1016/S0140-6736(12)61857-1
269. Tada, Y. *et al.* Targeting VEGFR2 with Ramucirumab strongly impacts effector/activated regulatory T cells and CD8+ T cells in the tumor microenvironment. *J. Immunother. Cancer* (2018). doi:10.1186/s40425-018-0403-1
270. Ebos, J. M. L. & Kerbel, R. S. Antiangiogenic therapy: Impact on invasion, disease progression, and metastasis. *Nature Reviews Clinical Oncology* (2011). doi:10.1038/nrclinonc.2011.21
271. Earl, H. M. *et al.* Efficacy of neoadjuvant bevacizumab added to docetaxel followed by fluorouracil, epirubicin, and cyclophosphamide, for women with HER2-negative early breast cancer (ARTemis): An open-label, randomised, phase 3 trial. *Lancet Oncol.* (2015). doi:10.1016/S1470-2045(15)70137-3
272. Leenders, W. P. J. *et al.* Antiangiogenic therapy of cerebral melanoma metastases results in sustained tumor progression via vessel co-option. *Clin. Cancer Res.* (2004). doi:10.1158/1078-0432.CCR-04-0823
273. Baker, G. J. *et al.* Mechanisms of Glioma Formation: Iterative Perivascular Glioma Growth and Invasion Leads to Tumor Progression, VEGF-Independent Vascularization, and Resistance to Antiangiogenic Therapy. *Neoplasia* (2014). doi:10.1016/j.neo.2014.06.003
274. Pàez-Ribes, M. *et al.* Antiangiogenic Therapy Elicits Malignant Progression of Tumors to Increased Local Invasion and Distant Metastasis. *Cancer Cell* (2009). doi:10.1016/j.ccr.2009.01.027
275. Depner, C. *et al.* EphrinB2 repression through ZEB2 mediates tumour invasion and anti-angiogenic resistance. *Nat. Commun.* (2016). doi:10.1038/ncomms12329
276. Jayson, G. C., Kerbel, R., Ellis, L. M. & Harris, A. L. Antiangiogenic therapy in oncology: current status and future directions. *The Lancet* (2016). doi:10.1016/S0140-6736(15)01088-0
277. Motz, G. T. *et al.* Tumor endothelium FasL establishes a selective immune barrier promoting tolerance in tumors. *Nat. Med.* (2014). doi:10.1038/nm.3541
278. Osada, T. *et al.* The effect of anti-VEGF therapy on immature myeloid cell and dendritic cells in cancer patients. *Cancer Immunol. Immunother.* (2008). doi:10.1007/s00262-007-0441-x
279. Page, D. B. *et al.* Pretreatment Serum VEGF Is Associated with Clinical Response and Overall Survival in Advanced Melanoma Patients Treated with Ipilimumab. *Cancer Immunol. Res.* (2014). doi:10.1158/2326-6066.cir-13-0163
280. Vasudev, N. S. & Reynolds, A. R. Anti-angiogenic therapy for cancer: Current progress, unresolved questions and future directions. *Angiogenesis* (2014). doi:10.1007/s10456-014-9420-y
281. Ferrara, N. & Kerbel, R. S. Angiogenesis as a therapeutic target. *Nature* (2005). doi:10.1038/nature04483
282. Zhang, A. *et al.* Metabolomics in diagnosis and biomarker discovery of colorectal cancer. *Cancer Letters* (2014). doi:10.1016/j.canlet.2013.11.011
283. Monteiro, M. S., Carvalho, M., Bastos, M. L. & Guedes de Pinho, P. Metabolomics

analysis for biomarker discovery: advances and challenges. *Curr. Med. Chem.* (2013). doi:CMC-EPUB-20121126-5 [pii]
284. Hernandez-Fernaud, J. R., Reid, S. E., Neilson, L. J. & Zanivan, S. Quantitative mass spectrometry-based proteomics in angiogenesis. *Proteomics - Clinical Applications* (2013). doi:10.1002/prca.201200055
285. Emmert-Buck, M. R. *et al.* Laser capture microdissection. *Science (80-.).* (1996). doi:10.1126/science.274.5289.998
286. Hu, P., Zhang, W., Xin, H. & Deng, G. Single Cell Isolation and Analysis. *Front. Cell Dev. Biol.* (2016). doi:10.3389/fcell.2016.00116
287. Yu, Z. *et al.* Optimizing 2D gas chromatography mass spectrometry for robust tissue, serum and urine metabolite profiling. *Talanta* (2017). doi:10.1016/j.talanta.2017.01.003
288. Hughes, C. S. *et al.* Ultrasensitive proteome analysis using paramagnetic bead technology. *Mol. Syst. Biol.* (2014). doi:10.15252/msb.20145625
289. Sielaff, M. *et al.* Evaluation of FASP, SP3, and iST Protocols for Proteomic Sample Preparation in the Low Microgram Range. *J. Proteome Res.* (2017). doi:10.1021/acs.jproteome.7b00433
290. Tyanova, S. *et al.* The Perseus computational platform for comprehensive analysis of (prote)omics data. *Nature Methods* (2016). doi:10.1038/nmeth.3901
291. Tyanova, S., Temu, T. & Cox, J. The MaxQuant computational platform for mass spectrometry-based shotgun proteomics. *Nat. Protoc.* (2016). doi:10.1038/nprot.2016.136
292. Potter, M., Badder, L., Hoade, Y., Johnston, I. G. & Morten, K. J. Monitoring intracellular oxygen concentration: Implications for hypoxia studies and real-time oxygen monitoring. in *Advances in Experimental Medicine and Biology* (2016). doi:10.1007/978-1-4939-3023-4_32
293. Marelli-Berg, F. M., Peek, E., Lidington, E. A., Stauss, H. J. & Lechler, R. I. Isolation of endothelial cells from murine tissue. *J. Immunol. Methods* (2000). doi:10.1016/S0022-1759(00)00258-1
294. Qiu, W. & Su, G. H. Development of orthotopic pancreatic tumor mouse models. *Methods Mol. Biol.* (2013). doi:10.1007/978-1-62703-287-2_11
295. Gómez-Cuadrado, L., Tracey, N., Ma, R., Qian, B. & Brunton, V. G. Mouse models of metastasis: progress and prospects. *Dis. Model. Mech.* (2017). doi:10.1242/dmm.030403
296. Kerbel, R. S. Therapeutic implications of intrinsic or induced angiogenic growth factor redundancy in tumors revealed. *Cancer Cell* (2005). doi:10.1016/j.ccr.2005.09.016
297. Eklund, L., Bry, M. & Alitalo, K. Mouse models for studying angiogenesis and lymphangiogenesis in cancer. *Molecular Oncology* (2013). doi:10.1016/j.molonc.2013.02.007
298. Winkler, F. The brain microenvironment: Friend or foe for metastatic tumor cells? *Neuro-Oncology* (2014). doi:10.1093/neuonc/nou308
299. Falletta, P. *et al.* Translation reprogramming is an evolutionarily conserved driver of phenotypic plasticity and therapeutic resistance in melanoma. *Genes Dev.* (2017). doi:10.1101/gad.290940.116
300. Wang, L. *et al.* Molecular link between glucose and glutamine consumption in cancer cells mediated by CtBP and SIRT4. *Oncogenesis* (2018). doi:10.1038/s41389-018-0036-8
301. Abdi, H. & Williams, L. J. Principal component analysis. *Wiley Interdisciplinary Reviews: Computational Statistics* (2010). doi:10.1002/wics.101

302. Lawler, P. R. & Lawler, J. Molecular basis for the regulation of angiogenesis by thrombospondin-1 and -2. *Cold Spring Harb. Perspect. Med.* (2012). doi:10.1101/cshperspect.a006627
303. Rolland T. Tasan M., C. B. P. S. Z. Q. et al. A proteome-scale map of the human interactome network. *Cell* (2014). doi:10.1016/j.cell.2014.10.050.A
304. Vaupel, P. & Mayer, A. Hypoxia in cancer: Significance and impact on clinical outcome. *Cancer and Metastasis Reviews* (2007). doi:10.1007/s10555-007-9055-1
305. Wu, C.-A., Chao, Y., Shiah, S.-G. & Lin, W.-W. Nutrient deprivation induces the Warburg effect through ROS/AMPK-dependent activation of pyruvate dehydrogenase kinase. *Biochim. Biophys. Acta* (2013). doi:10.1016/j.bbamcr.2013.01.025
306. Dmitriev, R. I., Zhdanov, A. V., Jasionek, G. & Papkovsky, D. B. Assessment of cellular oxygen gradients with a panel of phosphorescent oxygen-sensitive probes. *Anal. Chem.* (2012). doi:10.1021/ac3000144
307. Crossin, K. L. Oxygen levels and the regulation of cell adhesion in the nervous system: a control point for morphogenesis in development, disease and evolution? *Cell Adh. Migr.* (2012). doi:10.4161/cam.19582
308. Justus, C. R., Leffler, N., Ruiz-Echevarria, M. & Yang, L. V. In vitro cell migration and invasion assays. *J. Vis. Exp.* (2014). doi:10.3791/51046
309. Zhang, C. *et al.* Carbonic anhydrase 2 inhibits epithelial-mesenchymal transition and metastasis in hepatocellular carcinoma. *Carcinogenesis* (2018). doi:10.1093/carcin/bgx148
310. Benton, G., Arnaoutova, I., George, J., Kleinman, H. K. & Koblinski, J. Matrigel: From discovery and ECM mimicry to assays and models for cancer research. *Advanced Drug Delivery Reviews* (2014). doi:10.1016/j.addr.2014.06.005
311. Barkan, D., Green, J. E. & Chambers, A. F. Extracellular matrix: A gatekeeper in the transition from dormancy to metastatic growth. *Eur. J. Cancer* (2010). doi:10.1016/j.ejca.2010.02.027
312. Anjomshoaa, A. *et al.* Slow proliferation as a biological feature of colorectal cancer metastasis. *Br. J. Cancer* (2009). doi:10.1038/sj.bjc.6605229
313. Luo, W. & Yao, K. Molecular characterization and clinical implications of spindle cells in nasopharyngeal carcinoma: A novel molecule-morphology model of tumor progression proposed. *PLoS One* (2013). doi:10.1371/journal.pone.0083135
314. Swietach, P., Vaughan-Jones, R. D., Harris, A. L. & Hulikova, A. The chemistry, physiology and pathology of pH in cancer. *Philosophical Transactions of the Royal Society B: Biological Sciences* (2014). doi:10.1098/rstb.2013.0099
315. Wallert, M. A., Hastle, D., Wallert, C. H., Cottle, W. T. & Provost, J. J. You can never have too many kinases: The sodium hydrogen exchanger isoform 1 regulation by phosphorylation. *J. Cell Signal.* (2016). doi:10.4172/jcs.1000121
316. Allocati, N., Masulli, M., Di Ilio, C. & Federici, L. Glutathione transferases: Substrates, inihibitors and pro-drugs in cancer and neurodegenerative diseases. *Oncogenesis* (2018). doi:10.1038/s41389-017-0025-3
317. Huang, T., Sun, L., Yuan, X. & Qiu, H. Thrombospondin-1 is a multifaceted player in tumor progression. *Oncotarget* (2017). doi:10.18632/oncotarget.19165
318. Li, C., Zhang, G., Zhao, L., Ma, Z. & Chen, H. Metabolic reprogramming in cancer cells: Glycolysis, glutaminolysis, and Bcl-2 proteins as novel therapeutic targets for cancer. *World Journal of Surgical Oncology* (2016). doi:10.1186/s12957-016-0769-9
319. Roudier, E., Bachelet, C. & Perrin, A. Pyruvate reduces DNA damage during hypoxia and after reoxygenation in hepatocellular carcinoma cells. *FEBS J.* (2007). doi:10.1111/j.1742-4658.2007.06044.x
320. Wang, X. *et al.* Pyruvate protects mitochondria from oxidative stress in human

neuroblastoma SK-N-SH cells. *Brain Res.* (2007). doi:10.1016/j.brainres.2006.11.032
321. Lord-Fontaine, S. & Averill-Bates, D. A. Heat shock inactivates cellular antioxidant defenses against hydrogen peroxide: Protection by glucose. *Free Radic. Biol. Med.* (2002). doi:10.1016/S0891-5849(02)00769-4
322. Berggren, M. I. *et al.* Thioredoxin peroxidase-1 (peroxiredoxin-1) is increased in thioredoxin-1 transfected cells and results in enhanced protection against apoptosis caused by hydrogen peroxide but not by other agents including dexamethasone, etoposide, and doxorubicin. *Arch. Biochem. Biophys.* (2001). doi:10.1006/abbi.2001.2435
323. SPITZ, D. R., SIM, J. E., RIDNOUR, L. A., GALOFORO, S. S. & LEE, Y. J. Glucose Deprivation-Induced Oxidative Stress in Human Tumor Cells: A Fundamental Defect in Metabolism? TL - 899. *Ann. N. Y. Acad. Sci.* (2000). doi:10.1111/j.1749-6632.2000.tb06199.x
324. Ahmad, I. M. *et al.* Mitochondrial O2.- and H2O2 mediate glucose deprivation-induced cytotoxicity and oxidative stress in human cancer cells. *J. Biol. Chem.* (2005). doi:10.1074/jbc.M411662200
325. Lee, Y. J. *et al.* Glucose deprivation-induced cytotoxicity and alterations in mitogen-activated protein kinase activation are mediated by oxidative stress in multidrug-resistant human breast carcinoma cells. *J. Biol. Chem.* (1998). doi:10.1074/jbc.273.9.5294
326. Fantin, V. R., St-Pierre, J. & Leder, P. Attenuation of LDH-A expression uncovers a link between glycolysis, mitochondrial physiology, and tumor maintenance. *Cancer Cell* (2006). doi:10.1016/j.ccr.2006.04.023
327. Bonuccelli, G. *et al.* Ketones and lactate 'fuel' tumor growth and metastasis: Evidence that epithelial cancer cells use oxidative mitochondrial metabolism. *Cell Cycle* (2010). doi:10.4161/cc.9.17.12731
328. Wang, Z., Wei, D. & Xiao, H. Methods of cellular senescence induction using oxidative stress. *Methods Mol. Biol.* (2013). doi:10.1007/978-1-62703-556-9_11
329. Hecht, I. *et al.* The motility-proliferation-metabolism interplay during metastatic invasion. *Sci. Rep.* (2015). doi:10.1038/srep13538
330. Gao, C.-F. *et al.* Proliferation and invasion: Plasticity in tumor cells. *Proc. Natl. Acad. Sci.* (2005). doi:10.1073/pnas.0504367102
331. Leung, L. *et al.* Loss of canonical Smad4 signaling promotes KRAS driven malignant transformation of human pancreatic duct epithelial cells and metastasis. *PLoS One* (2013). doi:10.1371/journal.pone.0084366
332. Rhim, A. D. *et al.* EMT and dissemination precede pancreatic tumor formation. *Cell* (2012). doi:10.1016/j.cell.2011.11.025
333. Shi, Y. & Massagué, J. Mechanisms of TGF-beta signaling from cell membrane to the nucleus. *Cell* (2003). doi:10.1016/S0092-8674(03)00432-X
334. Ahmed, S., Bradshaw, A.-D., Gera, S., Dewan, M. & Xu, R. The TGF-β/Smad4 Signaling Pathway in Pancreatic Carcinogenesis and Its Clinical Significance. *J. Clin. Med.* (2017). doi:10.3390/jcm6010005
335. Kumar, S., Rao, N. & Ge, R. Emerging roles of ADAMTSS in angiogenesis and cancer. *Cancers* (2012). doi:10.3390/cancers4041252
336. Valiente, M. *et al.* Serpins promote cancer cell survival and vascular Co-option in brain metastasis. *Cell* (2014). doi:10.1016/j.cell.2014.01.040
337. Angiolini, F. & Cavallaro, U. The pleiotropic role of L1CAM in tumor vasculature. *International Journal of Molecular Sciences* (2017). doi:10.3390/ijms18020254
338. Napiwotzki, J. & Kadenbach, B. Extramitochondrial ATP/ADP-ratios regulate cytochrome c oxidase activity via binding to the cytosolic domain of subunit IV. *Biol.*

Chem. (1998). doi:10.1515/bchm.1998.379.3.335
339. Hao, Y. H. *et al.* HIF-1α regulates COXIV subunits, a potential mechanism of self-protective response to microwave induced mitochondrial damages in neurons. *Sci. Rep.* (2018). doi:10.1038/s41598-018-28427-5
340. Fukuda, R. *et al.* HIF-1 Regulates Cytochrome Oxidase Subunits to Optimize Efficiency of Respiration in Hypoxic Cells. *Cell* (2007). doi:10.1016/j.cell.2007.01.047
341. Tang, M. K. S. *et al.* Soluble E-cadherin promotes tumor angiogenesis and localizes to exosome surface. *Nat. Commun.* (2018). doi:10.1038/s41467-018-04695-7
342. Luo, W. *et al.* PRDX2 and PRDX4 are negative regulators of hypoxia-inducible factors under conditions of prolonged hypoxia. *Oncotarget* (2016). doi:10.18632/oncotarget.7142
343. Luo, W. *et al.* Hsp70 and CHIP selectively mediate ubiquitination and degradation of hypoxia-inducible factor (HIF)-1α but not HIF-2α. *J. Biol. Chem.* (2010). doi:10.1074/jbc.M109.068577
344. Weigele, B. A., Orchard, R. C., Jimenez, A., Cox, G. W. & Alto, N. M. A systematic exploration of the interactions between bacterial effector proteins and host cell membranes. *Nat. Commun.* (2017). doi:10.1038/s41467-017-00700-7
345. Lee, J. L. & Streuli, C. H. Integrins and epithelial cell polarity. *J. Cell Sci.* (2014). doi:10.1242/jcs.146142
346. Nikolova, S., Lee, Y. S., Lee, Y. S. & Kim, J. A. Rac1-NADPH oxidase-regulated generation of reactive oxygen species mediates glutamate-induced apoptosis in SH-SY5Y human neuroblastoma cells. *Free Radic. Res.* (2005). doi:10.1080/10715760500176866
347. Williamson, R. C. *et al.* Coronin-1C and RCC2 guide mesenchymal migration by trafficking Rac1 and controlling GEF exposure. *J. Cell Sci.* (2014). doi:10.1242/jcs.154864
348. Parri, M. & Chiarugi, P. Rac and Rho GTPases in cancer cell motility control. *Cell Communication and Signaling* (2010). doi:10.1186/1478-811X-8-23
349. Hanna, S. & El-Sibai, M. Signaling networks of Rho GTPases in cell motility. *Cellular Signalling* (2013). doi:10.1016/j.cellsig.2013.04.009
350. Migita, T. *et al.* ATP citrate lyase: Activation and therapeutic implications in non-small cell lung cancer. *Cancer Res.* (2008). doi:10.1158/0008-5472.CAN-08-1235
351. Khwairakpam, A. *et al.* ATP Citrate Lyase (ACLY): A Promising Target for Cancer Prevention and Treatment. *Curr. Drug Targets* (2015). doi:10.2174/1389450115666141224125117
352. Jang, J. Y., Choi, Y., Jeon, Y. K., Aung, K. C. Y. & Kim, C. W. Over-expression of adenine nucleotide translocase 1 (ANT1) induces apoptosis and tumor regression in vivo. *BMC Cancer* (2008). doi:10.1186/1471-2407-8-160
353. Lena, A. *et al.* The silencing of adenine nucleotide translocase isoform 1 induces oxidative stress and programmed cell death in ADF human glioblastoma cells. *FEBS J.* (2010). doi:10.1111/j.1742-4658.2010.07702.x
354. Lazebnik, Y. What are the hallmarks of cancer? *Nature Reviews Cancer* (2010). doi:10.1038/nrc2827
355. Sonnenschein, C. & Soto, A. M. The aging of the 2000 and 2011 Hallmarks of Cancer reviews: A critique. *J. Biosci.* (2013). doi:10.1007/s12038-013-9335-6
356. Horne, S. D., Pollick, S. A. & Heng, H. H. Q. Evolutionary mechanism unifies the hallmarks of cancer. *International Journal of Cancer* (2015). doi:10.1002/ijc.29031
357. Milsom, C. C., Lee, C. R., Hackl, C., Man, S. & Kerbel, R. S. Differential Post-Surgical Metastasis and Survival in SCID, NOD-SCID and NOD-SCID-IL-2Rγnull

Mice with Parental and Subline Variants of Human Breast Cancer: Implications for Host Defense Mechanisms Regulating Metastasis. *PLoS One* (2013). doi:10.1371/journal.pone.0071270